**The Dissertation Committee for Aaron Thomas Hill, Jr. Certifies that this is the approved version of the following dissertation:**

# Numerical Simulations of Riveted Connections under Quasi-Static and Dynamic Loadings

**Committee:**

Eric B. Williamson, Supervisor

Michael D. Engelhardt

Todd A. Helwig

Patricia Clayton

Eric M. Taleff

Charles K. Crane

# Numerical Simulations of Riveted Connections under Quasi-Static and Dynamic Loadings

**by**

**Aaron Thomas Hill, Jr., B.S.; M.S.; M.C.E.**

**Dissertation**

Presented to the Faculty of the Graduate School of

The University of Texas at Austin

in Partial Fulfillment

of the Requirements

for the Degree of

**Doctor of Philosophy**

**The University of Texas at Austin**

**May 2016**

# Dedication

*"But my life is worth nothing to me unless I use it for finishing*

*the work assigned me by the Lord Jesus…."*

-Acts of the Apostles 20:24

This dissertation is dedicated to my Lord and Savior Jesus Christ for blessing me with this once in a lifetime opportunity to pursue a doctoral degree. May I never be a fan; instead, let me always look for ways to be a committed and unquestioned active follower. I will continue to use this blessing to motivate, educate, and train tomorrow's leaders in a myriad of venues.

# Acknowledgements

First of all, I must thank the United States Army and the United States Military Academy for this opportunity to pursue a doctoral degree. I would like to thank the U.S Army Engineer Research and Development Center, and especially Dr. Kennan Crane and Chris Rabalais, for their expertise throughout this research endeavor. Thanks to fellow graduate student Michalis Hadjioannou for his LS-DYNA (2013) tutelage. Thanks also to the members of my dissertation committee for their guidance and expertise throughout my doctoral pursuit.

Dr. Eric Williamson's expertise, support, and patience over the past three years is greatly appreciated. I would recommend any potential graduate student to seek out his expertise as a supervisor. Not only did he provide educational guidance and motivation when needed, he genuinely cared about my development as a father, husband, and military officer. I hope to have the opportunity to work with Dr. Eric Williamson throughout the rest of my career.

Finally, I am forever grateful to my beautiful wife, Diana, and wonderful kids, Aaron III, Alyssa, and Amaya, for their support and encouragement over the last three years. Their unwavering confidence in me pushed me to cross the finish line. Thank God for blessing me with such a phenomenal team of professional experts, family members, and friends.

# Numerical Simulations of Riveted Connections under Quasi-Static and Dynamic Loadings

Aaron Thomas Hill, Jr., Ph.D.

The University of Texas at Austin, 2016

Supervisor: Eric B. Williamson

Despite years of concerted effort in the war against terrorism, there still exist terrorist networks and lone wolf actors that continue to threaten people and infrastructure around the world. Among the potential targets of terrorists are the more prominent, high value, and symbolic locations that make up the United States' critical transportation network. This is an urgent national security issue. While many organizations such as the Federal Highway Administration (FHWA) and the Association of State Highway and Transportation Officials (AASHTO) continue to sponsor experts from professional practice, academia, and other agencies to develop strategies to deter and disrupt such attacks, there is little known about the specific response of riveted connections under high rates of loading. A general lack of access and expertise with riveted connections, which have not been widely used in construction of bridges since the 1950s, and the expense and difficulty in replicating and collecting accurate data for close-in detonation testing on riveted steel connections make it a challenge to analyze and estimate the capacity and behavior of riveted connections.

This research focuses on numerical simulation of riveted steel connections under high rates of loading. Finite element modeling using LS-DYNA (2013) is first developed to match the physical testing of A502 Grade 2 riveted structural connections subjected to dynamic and quasi-static shear loadings completed at the U.S. Army Engineer Research and Development Center (ERDC). This initial modeling serves as validation for the LS-DYNA (2013) model parameters for response. Subsequent analyses expand on the validated modeling to serve as a numerical prediction of additional riveted connections subjected to dynamic loads. Results from the testing and numerical simulations can serve to expand the capabilities of existing anti-terrorist planning software and serve as an addition to existing bridge protection guidelines. The numerical simulation modeling will fill an important gap in the current knowledge base on the performance of riveted connections under high loading rates that will be of value to the U.S. Army Corps of Engineers and the Federal Highway Administration. Understanding the capacity and behavior of these connections will assist future researchers in developing mitigation strategies against blast loadings.

# Table of Contents

# List of Tables

# List of Figures

# Chapter 1: Introduction

*"Let us all take a moment to remember the 3000 people who died in the World Trade Center on September 11th. And let us all remember that it will likely happen again. Such is the nature of revenge that this war will never be won, but instead will be fought for as long as there are people with revenge in their hearts. May whatever god you worship forgive us all. May God teach us forgiveness, understanding and peace."*

-William Jefferson Clinton, 2007

## 1.1 Introduction

On September 11, 2001, as 19 al-Qaeda terrorists hijacked four planes to attack the World Trade Center and the Pentagon, the entire world was put on alert that no nation, no piece of infrastructure, and no group of people are immune to the threat of terrorist attack. While terrorism has been around for centuries, the U.S. was largely fortunate to avoid large-scale terrorist activity within its borders until the 1993 bombing of the World Trade Center's Tower One underground parking garage by al-Qaeda trained terrorists. The detonation of this 1,310-pound bomb resulted in 6 dead, 1,040 injured, and a crater 100 feet wide that went through four sublevels of reinforced concrete (Dusenberry, 2010). Two years later, in an act of domestic terrorism, two disgruntled militia movement sympathizers detonated an ammonium nitrate/fuel oil (ANFO) bomb that killed 168 people and injured over 680 others in downtown Oklahoma City (Dusenberry, 2010). These horrific events

within the U.S. are just a few of many examples of terrorism worldwide that demonstrate why engineers have invested in developing innovative approaches to protect society.

The trend of increasing terrorism demands the need for enhanced security for vulnerable infrastructure. Statistics from a declassified Canadian intelligence report reveal there were 190 explosive attacks against bridges and tunnels alone from 2002 through 2008 ('Terrorist Attack Methodology And Tactics Against Bridges And Tunnels: January 2002 - December 2008'). What makes this statistic even more concerning is that these numbers do not include attacks in active combat zones, such as those attacks conducted in Iraq or Afghanistan. With over 700,000 bridges in the U.S. carrying millions of people daily, terrorists have thousands of targets that would undoubtedly result in the closure of a critical transportation route, a significant economic impact for a region, and significant loss of life. To make matters worse, a large number of the nation's bridges have been weakened structurally from wear and age. The 2013 American Society of Civil Engineers (ASCE) Report Card for America's Infrastructure exposed the poor state of the U.S.'s bridges with one in nine rated as structurally deficient (Infrastructurereportcard.org, 2013). With an average age of 42 years, design and construction from the early 1900s make up a good portion of the nation's aging infrastructure inventory.

Most of the steel bridges designed and built prior to 1950 used hot-driven rivets to connect plates and other shapes. Today, high-strength bolts and nuts are almost exclusively used as the steel connector of choice. In fact, in today's literature, mention of the rivet as a structural connector is often merely a footnote. Ironically, the rivet serves as the structural connector for some of the U.S.'s most iconic bridges, such as the Golden Gate Bridge and

the Brooklyn Bridge. Furthermore, terrorists have had a long fascination with bridges and have taught tactics in bringing them down in their terrorist training camps (Weiser and Baker, 2011). As federal and local governments fight to prevent these attacks, private and academic organizations have collaborated to understand and develop technology to both prevent and to mitigate the effects of terrorism. To date, there has been little to no literature found that discusses the response of steel riveted connections subjected to blast loads. These riveted connections, responsible for holding together some of the world's most well-known bridges, are vital for maintaining strategic and commercial interests, potentially making them a prime target for terrorist activity.

While the risk of attack and severity of consequences associated with an attack will vary among bridges, there is little debate that the nation's older bridges are likely vulnerable and are under an elevated threat relative to other bridges. The research presented in this dissertation is designed to provide bridge engineers an understanding and techniques to predict and assess the response of steel riveted connections subjected to blast loads. This information will assist engineers and force protection experts in developing new techniques to implement blast-resistant design strategies. This chapter outlines the motivation and research approach for this endeavor.

## 1.2 MOTIVATION

With the United States and its allies bringing a decade and a half of conflict in Iraq and Afghanistan to a close, many Americans are under the misconception that terrorism is no longer a major concern. While the world did see a dip in terrorism worldwide as U.S. combat operations in those countries transitioned to support and training, the trend over the past few years has reversed. In fact, the former head of the Defense Intelligence Agency, Lt. Gen. Michael Flynn, contended as recently as 2014 that the core Al-Qa'ida ideology was stronger than ever (Baier, 2015). While the leadership losses suffered by Al-Qa'ida has significantly weakened it over the years, the Islamic State in Iraq and the Levant (ISIS) has grown to contain thousands of jihadists and has quickly emerged as the world's most dangerous terrorist organization.

The growth of fighters flocking to join ISIS and other extremist groups has likely contributed to the increase in terrorist attacks. Between 2001 and 2009, there were 380 international terrorist attacks and 91 homegrown terrorist attacks against U.S. interests (RAND Database of Worldwide Terrorism Incidents, 2009). More recently, 2013 alone saw 9,707 terrorist attacks tracked in 93 different countries, resulting in over 17,800 deaths and 32,500 injuries (U.S. Department of State, 2013). Statistics from 2014 were even worse with 13,463 terrorist attacks worldwide, resulting in over 32,700 deaths and 34,700 injuries. These numbers reflect a 35% increase in terrorist attacks and an 81% increase in fatalities from 2013 to 2014 alone (U.S. Department of State, 2014). As shown in Fig. 1-1, ISIS and other terrorist organizations have shown an extraordinary ability to inspire

terrorist attacks through brutality and effective recruiting, leading to a recent increasing trend in terrorist incidents worldwide. While the United States has led a bombing campaign against ISIS, there has been no indication that this campaign will put an end to these acts of terror.

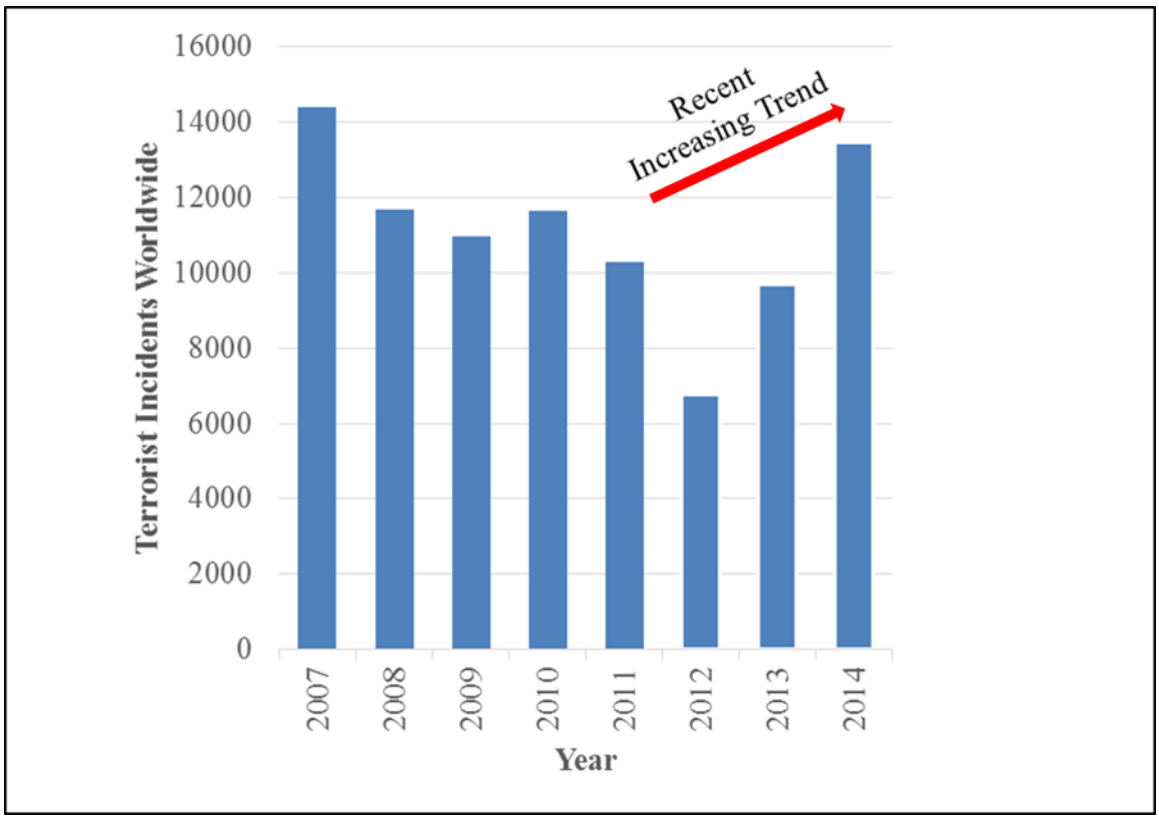


Fig. 1-1: Histogram of Terrorist Incidents Worldwide (data from the Jewish Virtual Library, A Project of the American-Israeli Cooperative Enterprise, at https://www.jewishvirtuallibrary.org)

While just over 60% of all terrorist attacks in 2014 occurred within Iraq, Pakistan, Afghanistan, India, and Nigeria, supporters of extreme organizations around the world

continue to present themselves as a serious and persistent threat within the U.S (U.S. Department of State, 2014). Prior to the 2015 Fourth of July holiday, FBI Director James Comey announced that authorities foiled attacks planned by Islamic State online recruits by arresting more than 10 people within the United States (Edwards and Hosenball, 2015). While fortunate that these attacks were thwarted, the Islamic State has persistently called for all followers to do whatever they can wherever they can to carry out violence on their behalf. The influence of ISIS revealed itself in San Bernardino, California, on December 2, 2015, when two extremist sympathizers killed 14 and wounded 21. This marked the 12th domestic terror attack or plot in 2015 and the 75th publically known Islamic terrorist attack or plot since the tragic events on September 11, 2001 (Walters, 2015).

This upward trend in terrorist incidents in the U.S. over the last four years is surprising considering enhancements made in border security limiting the travel of suspected terrorists into the U.S. However, with online recruitment of Islamic State recruits at an all-time high, the threat to the United States remains high. While testifying in front of the Senate Judiciary Committee, Comey revealed that the Islamic State's sophisticated social media propaganda campaign allows it to reach 21,000 English-language followers on Twitter. Furthermore, once the Islamic State adopts another recruit, it uses an encrypted mobile-messaging platform to issue kill orders (Edwards and Hosenball, 2015). Comey's testimony is supported with the fact that at least 62 of the 75 publically known Islamic terrorist plots or attacks actually involved an American citizen that was recruited and radicalized by jihadist terrorists (Inserra, 2015). As shown in Fig. 1-2, statistics collected from the open-source Global Terrorism Database (GTD) reveals a

steady to increasing trend in terrorism within the U.S. when both domestic and international terrorist incidents are included.

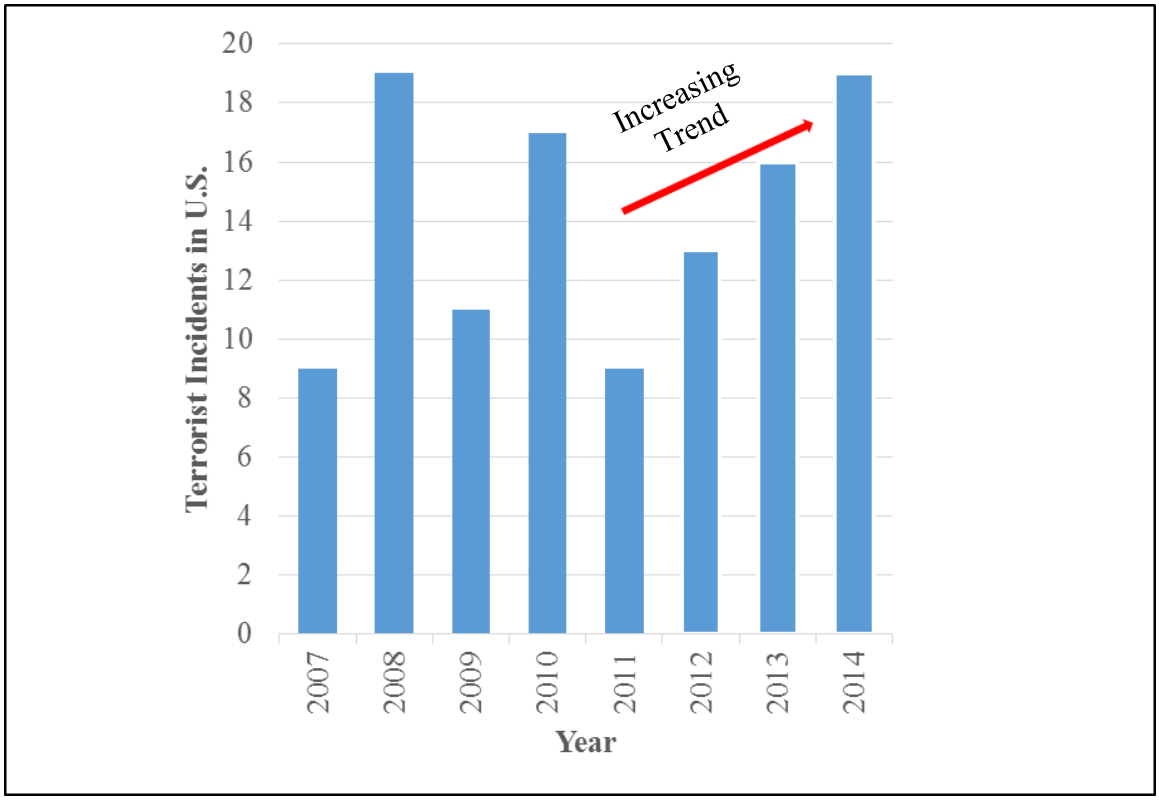


Fig. 1-2: Histogram of Terrorist Incidents in U.S. (data from the Global Terrorism Database, at http://www.start.umd.edu/gtd/)

Historical data from law enforcement and transit official surveys reveal transportation assets such as bridges have been among the most likely targets for terrorists (Boyd and Sullivan, 2008). Furthermore, transportation infrastructure can be readily attacked using explosives. As shown in Fig. 1-3, from 2001 until 2009, the preferred method of terrorist attacks against U.S. interests worldwide was bombings at

55.6 percent (RAND Database of Worldwide Terrorism Incidents). More recently, bombing/explosion was cited as the most common tactic used by terrorists in 2013 and 2014, accounting for 57% and 54% of all attacks, respectively (U.S. Department of State, 2014).

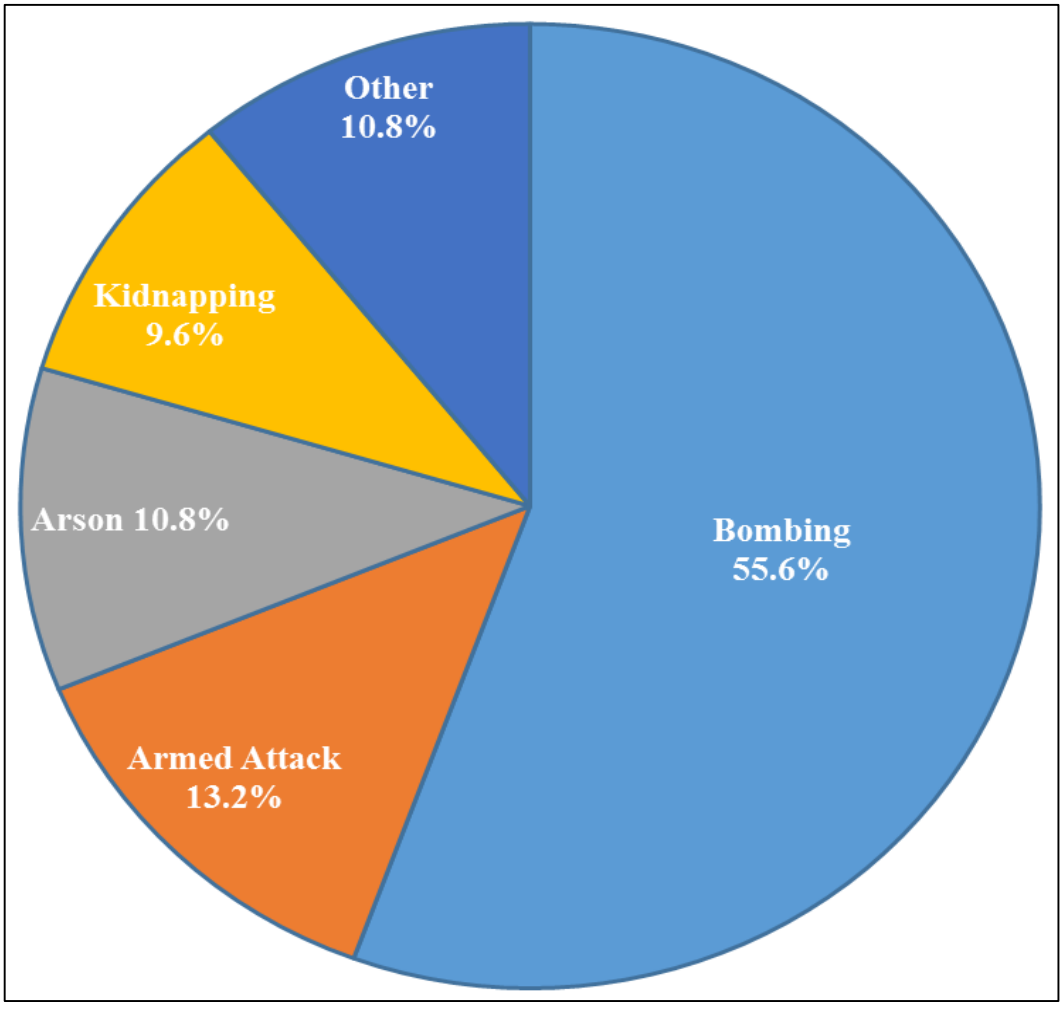


Fig. 1-3: Terror Tactics against the U.S. Worldwide: 2001 - 2009 (data from RAND Database of Worldwide Terrorism Incidents, at http://www.rand.orgnsrd/projects/terrorism-incidents.html)

The U.S.'s infrastructure has been a prime terrorist target for years (Muhlhausen and McNeill, 2011). As shown in Fig. 1-4, terrorists have studied and advertised techniques to destroy critical transportation infrastructure. In 1993, a fundamentalist Islamic cleric from Egypt and nine other men were stopped from executing their plans to blow up the United Nations Building, the George Washington Bridge, and the Lincoln and Holland Tunnels (Eversley, 2014). Shortly after the September 11, 2001 attacks, U.S. officials gathered intelligence indicating that high-profile bridges in San Francisco were identified as follow-on targets (San Jose Mercury News, 2003). Just two years later, a U.S. citizen with ties to Al-Qa'ida was arrested for conspiring to use blowtorches to collapse the Brooklyn Bridge, one of the oldest suspension bridges in the U.S. (Muhlhausen and McNeill, 2011). In 2006, a resident of Lebanon who spent seven years at a university in Canada was arrested for planning a massive bombing attack using vehicle borne improvised explosive devices (VBIEDs), suicide bombers, and backpacks filled with explosives. Targets included both the Brooklyn Bridge and the Golden Gate Bridge (Hagmann and McCleod, 2006).

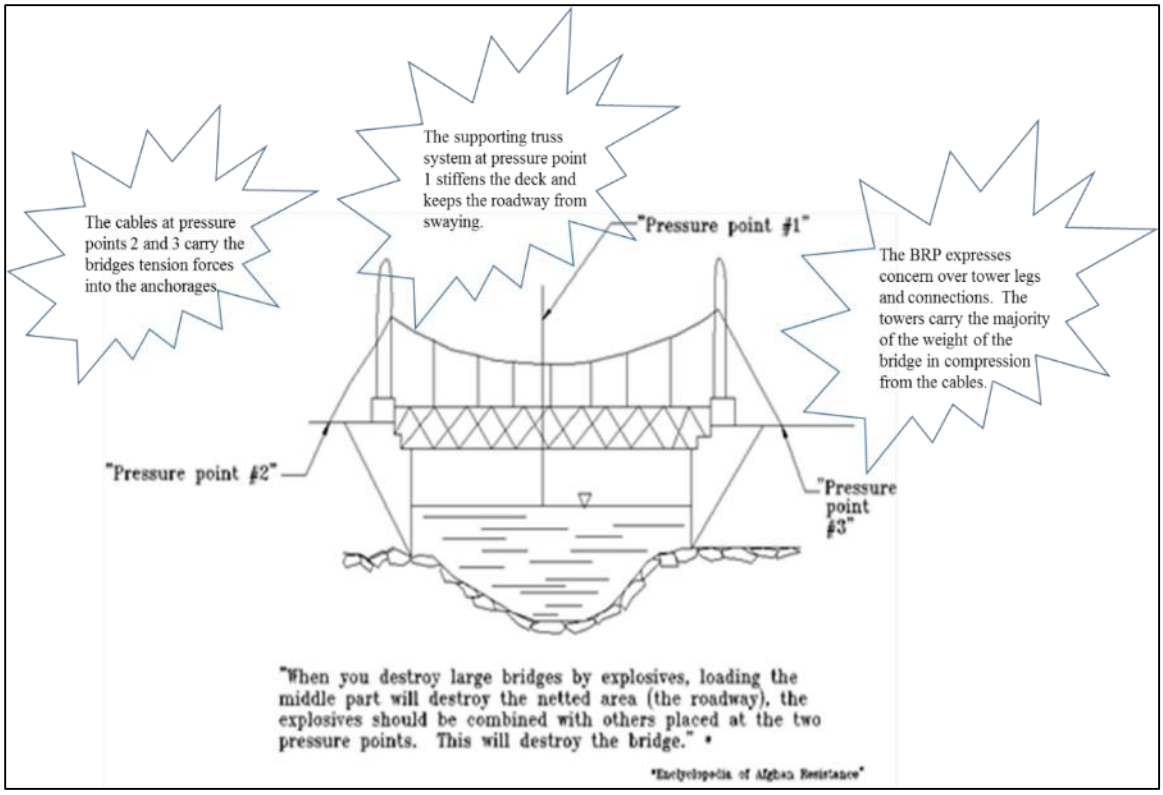


Fig. 1-4: Terrorist Attack Diagram from the Encyclopedia of Afghan Resistance (from Public Intelligence, 2009)

More recently, in 2013, transportation targets ranked 9th out of 20 different categories, accounting for 253 targets worldwide in 2013 (U.S. Department of State, 2013). In 2014, transportation targets once again ranked 9th among targets of terrorist attacks, accounting for 355 of the 13,911 targets (U.S. Department of State, 2014). As shown in Fig. 1-5, U.S. transportation infrastructure is considered a valuable target to terrorists. To make matters worse, roadways and bridges are not privy to the layered security checks afforded our nation's airplanes and skies. There are no passenger screenings or watch lists

keeping people from crossing the Golden Gate Bridge, ranked one of the Seven Wonders of the Modern World by the American Society of Civil Engineers.

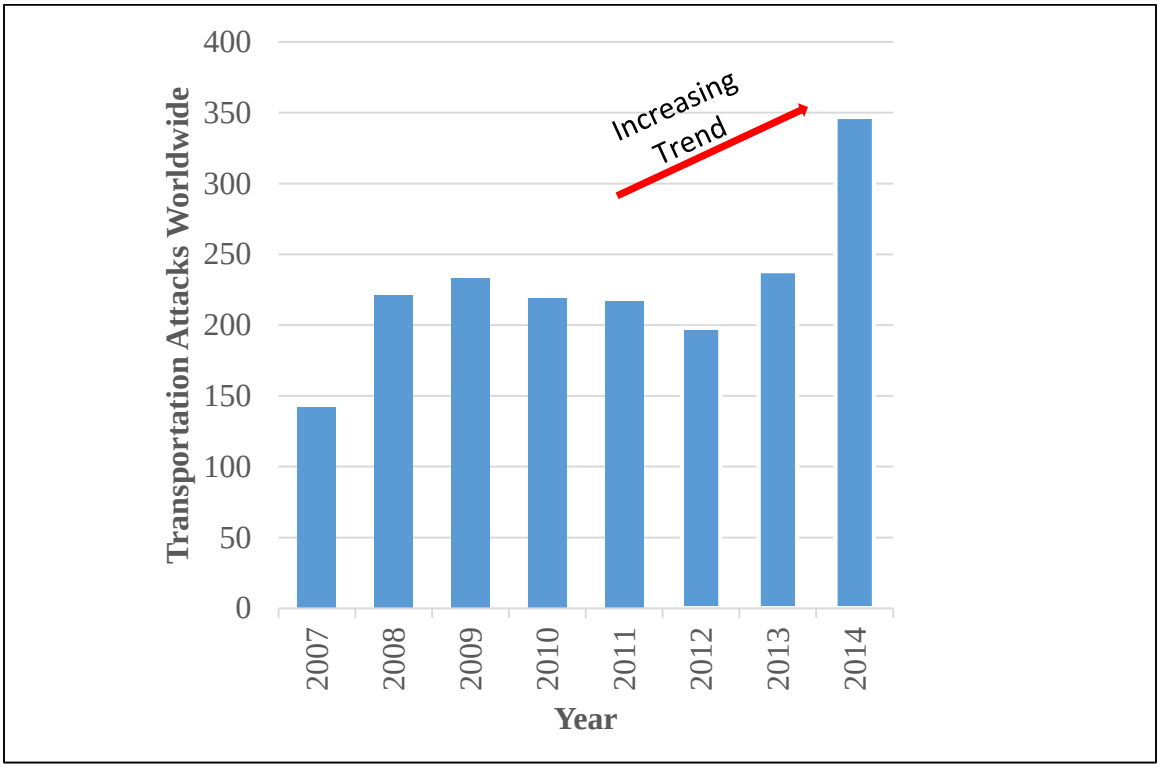


Fig. 1-5: Histogram of Transportation Terror Attacks Worldwide (data from Global Terrorism Database, at http://www.start.umd.edu/gtd/)

Despite the best efforts to eliminate terrorist attacks, it is simply not possible to secure every target in the world. Following the September 11, 2001, attacks, the American Association of State Highway and Transportation Officials (AASHTO) and the Federal Highway Administration (FHWA) teamed with bridge and tunnel experts from professional practice, academia, federal and state agencies, and toll authorities to form a Blue Ribbon Panel. Citing a 5% increase in Federal Bureau of Investigation (FBI) terrorism

investigations between FY 1997 and 2000 and anti-terrorism funding growing by 25% between FY 2000 and 2002 over concerns in domestic and international terrorism, these experts developed new strategies to deter, disrupt and mitigate terrorist attacks against U.S. bridges and tunnels (FHWA, 2003).

One of the first things most people think about when it comes to protecting a target from blast is to fortify it structurally. However, the most important tenet for blast and survivability to engineers in the field of protective construction and design is stand-off. Increasing stand-off, defined here as the desired distance between a target and an explosive device, diminishes the blast load intensity on the intended target. For transportation targets such as subways, trains, highways, and bridges, designing for stand-off is not a realistic option because of the inevitable proximity of people with bags, briefcases, and/or their vehicles. Furthermore, funding limitations make it practically impossible to protect every component of every bridge in the world which has led some to develop a risk-based methodology to prioritize mitigation strategies for bridges (Ray, 2007). Thus, it is imperative that engineers understand the response of critical infrastructure components subject to blast and continue to develop innovative ways to protect them. An undoubtedly key bridge component easily accessible to terrorists is suspension bridge towers, illustrated in Fig. 1-6. While the nation's older bridges have withstood the test of time, there is concern that extreme loads such as blast could cause severe damage beyond which these components can safely withstand. In addition to the significant loss of life, the Blue Ribbon Panel estimates that the loss of a critical bridge or tunnel could exceed $10 billion (FHWA, 2003). With little to no research previously done on these riveted steel panels and

connections, there is a serious need to understand the behavior of rivets subjected to this real threat. As stated by the Army's Chief of Staff in July 2015, the fight against ISIS will last at least 10 to 20 years (Mehta, 2015). In short, the terror threat is not a problem that is going away any time soon.

Fig. 1-6: Riveted Golden Gate Bridge South Tower (photo from SFGate, at http://www.sfgate.com)

## 1.3 RESEARCH APPROACH

With a clear motivation for understanding the response of suspension bridge towers to terrorist attacks, the primary objective of this research is to advance the body of knowledge on riveted connectors subjected to blast loads. Significant structural damage to a suspension bridge tower or connection could initiate collapse of an entire bridge. Significant effort is ongoing to mitigate the effects of blast loads on bridges and bridge components. To date, however, nothing has been written with respect to the response of a riveted panel or connection, which are critical structural elements in some of our nation's iconic bridges. Understanding this behavior will provide a contribution to the bridge engineering community and to those developing countermeasures to mitigate blast effects. The aim of this research is to provide a major contribution to the protective design of steel structures with riveted connections by achieving three main objectives:

- Provide guidance on modeling rivets using a nonlinear transient dynamic finite element analysis software package and reveal modeling issues that could lead to inaccuracies and shortcomings of the numerical modeling tools;

- Provide recommendations with respect to modeling strain rate effects for steel rivets;

- Apply the recommended material model to a practical problem in determining the response of long riveted connections to dynamic loads.

This dissertation is divided into five major sections. A review of relevant literature is provided in Chapter 2. This chapter focuses on experimental tests conducted on rivets and provides a review of the blast phenomena and structural loads resulting from blasts. Details of the LS-DYNA (2013) modeling of a rivet and riveted panel, in conjunction with a review of the work done by ERDC (Rabalais, 2015), which served to provide the test data needed to validate the finite element models developed for the research presented in this dissertation, are presented in Chapter 3. Chapter 4 addresses strain rate modeling recommendations and provides an application of the recommended model to long riveted connection behavior under high loading rates. Chapter 5 contains a discussion and summary of the main objectives, their significance to the structural engineering community, and recommendations for future research.

# Chapter 2: Literature Review

*"You can get help from your teachers, but you are going to have to learn a lot by yourself, sitting alone in a room."*

-Dr. Seuss, 1986

## 2.1 A Brief History of Rivets

As evident in some of our nation's most well-known suspension bridge towers, rivets were once the principal fastener of choice for steel construction. However, its rare use as a structural fastener today makes it unfamiliar to many young engineers. For the most part, current knowledge is focused around retrofit of older riveted structures. The actual first uses of rivets date back to 3000 BC as an Egyptian joining element to create tools, and they were also used during the 7th and 8th century by the Vikings to install the planking of their boats (Collette et al., 2011). With the development of a hot riveting process and the need to connect sheets of iron due to its limited production size capability, the use of rivets as a connector became widely accepted in the 1800s. Despite its popularity, engineers focused their attention on developing machines rather than on the intricate details of the rivets holding everything together. As a result, there were a number of disastrous explosions that revealed some important limitations of riveted connections (de Jonge, 1945). After seeing clear fractures along lines of rivets and permanent elongation between

rivet holes, double-riveted and triple-riveted lap joints developed. While attempting to consolidate and provide a comprehensive reference guide for riveted connections, A.E. Richard de Jonge uncovered the first known written document regarding riveted joints (de Jonge, 1945). The document was entitled "Report on Explosions of Steam Boilers" by the Committee of Franklin Institute of the State of Pennsylvania, for the Promotion of the Mechanical Arts in 1837.

Between the 1840s and 1940s, the popularity and use of hot rivets expanded beyond boilers into the shipbuilding industry and into bridge and other structural work, becoming the primary fastener used to fabricate metal structures. In what is described by one historian as "the first great bridge to span a navigable stream in the United States", the infamous John Augustus Roebling led the construction of 1857 Sixth-Street Bridge across the Allegheny River between Allegheny City and Pittsburgh. This suspension bridge was the first to have iron towers and wrought iron trusses in lieu of wood (West, 2015). This project expanded engineers' research and understanding of the behavior of riveted connections across a number of applications. Throughout the second half of the 1800s, as steel gradually replaced wrought iron in construction applications, engineers continued to study the strength of riveted joints. This increased use of riveted connections, in combination with years of suspension structure design experience, led to the construction in 1884 of the Brooklyn Bridge, spanning the East River between Manhattan and Brooklyn. In what was at the time the longest spanning bridge in the world (main span of approximately 1600 feet), the metal components of the bridge were fastened together with rivets. By the 1930s, confidence in the performance of rivets was at an all-time high, leading to the three year

and five month construction of the Golden Gate Bridge. Connecting San Francisco with the County of Marin, the six-lane iconic suspension bridge with a central span of 4,200 feet was constructed with over 600,000 rivets in each of the bridge's two cellular towers (Starr, 2010).

In spite of the rivet's popularity, installation costs were so high that it led engineers to investigate alternatives. This high cost of installation was an issue engineers had been looking into since the turn of the century, leading engineers to compare high-strength bolted and riveted connections to determine relative capacities. Even though early experiments found a somewhat superior strength of steel rivets to steel bolts, engineers suggested that bolts could be used in lieu of rivets. By the late 1930s, engineers started shifting their test procedures and comparison in performance from static loading to a variation of load or repeated load (fatigue). Despite the efforts of engineers and the use of rivets in iconic structures for decades, there was no AISC standard to address joints and their fasteners until the formation of the Research Council on Riveted and Bolted Structural Connections (currently known as the Research Council on Structural Connections or RCSC) in 1947. The formation of the RCSC led to a joint effort with the American Society for Testing and Materials (ASTM) to develop a high-strength bolt specification and a subsequent specification for structural joints in 1951. This specification authorized rivets to be replaced by bolts on a one-to-one basis (Fisher and Struik, 1974). The development and approval of high-strength bolts that required little skill to install subsequently reduced labor costs and caused the popularity of structural riveting to fade away. Of the last more renowned riveted bridges constructed in the U.S. were the Delaware Memorial Bridge

crossing the Delaware River between Delaware and New Jersey and the I-35W Bridge over the Mississippi River. Both of these bridges were completed before 1970 (Vermes, 2007). For decades, millions of people have relied upon and enjoyed these bridges on a daily basis, and the millions of rivets required to construct these bridges and keep them intact remain pivotal. Of particular note is the fact that there was no in-depth design standard for dynamic loads until the AISC Seismic provision was released in 1990. While this provision is relevant to earthquake loads, there are no references available regarding a monotonic dynamic load (i.e., blast) causing shear/bearing failure in a rivet connector.

## 2.2 Rivet Material and the Riveting Process

While the rivet seemed to be a simple structural element, installing a rivet required an experienced crew of four or five workers. First a hole had to be either punched or drilled in the materials that were going to be connected. The hole had to be slightly larger (about 0.0625-in.) than the nominal diameter of the rivet. A rivet was developed from a circular steel or iron rod and was manufactured with a head on one end. While there was both a cold-riveting and hot-riveting technique, hot-riveting was more widely used due to its positive effect on the strength of a joint (Collette et al., 2011). Thus, rivets were heated to almost 2000 degrees Fahrenheit (often described as reaching a light cherry-red color) in a portable forge and then thrown to the riveter by a *rivet boy*. Once placed in the hole, pressure was maintained on the preformed head. The plain end of the rivet was squeezed

to form a rounded head, and the shank of the rivet completely or nearly filled its inserted hole. If completed in the shop, this head was created by a single hit from a hydraulic press. If out in the field, this head was created from multiple vigorous blows using hand-held pneumatic hammers. A depiction of the riveting process is shown in Fig. 2-1.

Fig. 2-1: The Riveting Process: the rivet heating (left); the rivet head forging with pneumatic hammer (right) (from www.efd-induction.com)

As the hot-driven rivet cooled, it contracted both longitudinally and laterally. The longitudinal contraction creates a residual tensile stress in the rivet that clamps the gripped material. This clamping force varied significantly from rivet to rivet and was not counted on for design calculations. The riveting process, with a great deal of uncertainty and

variability, undoubtedly required a high skill level. In fact, to account for this variability, it was considered standard practice in the field to install between 20 and 25 percent additional rivets than called for in design (Vermes, 2007). Fig. 2-2 shows the components of an installed rivet.

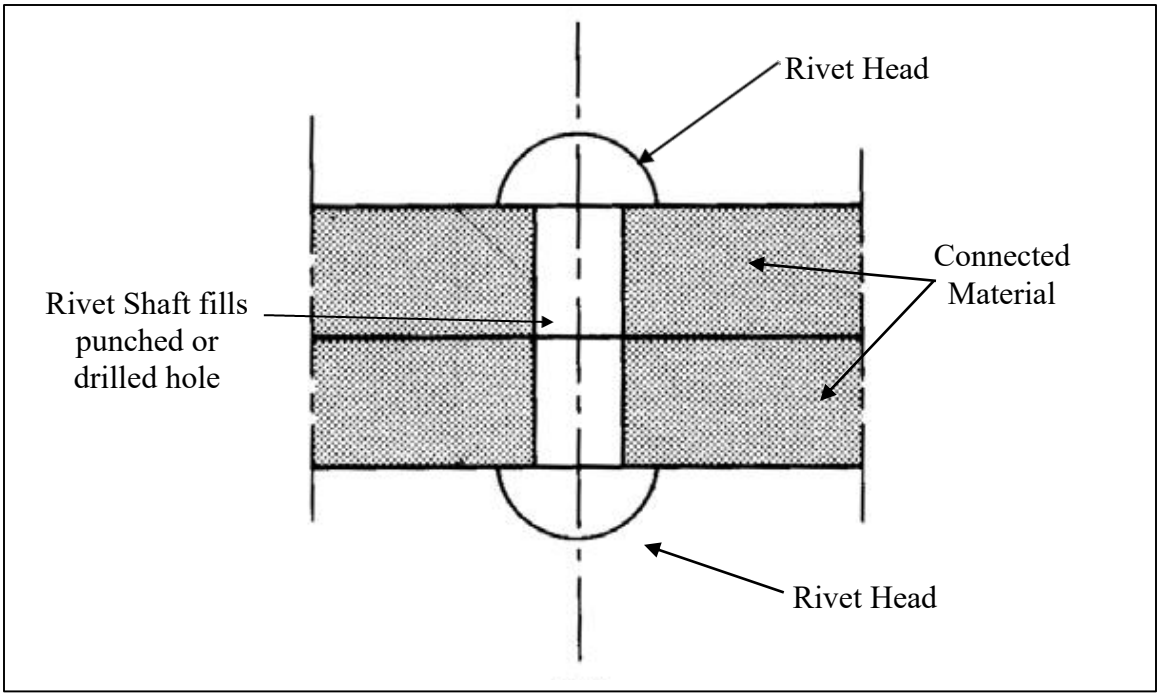


Fig. 2-2: Installed Structural Rivet (from *Guide to Design Criteria for Bolted and Riveted Connections*, 1987)

While properly installing a rivet was a difficult task under normal conditions, this task became even more of a challenge for some of the more extravagant projects. On the infamous Golden Gate Bridge, riveters experienced additional stresses: working in confined spaces, working in darkness, riveting at tremendous heights with difficult access,

and dealing with occupational deafness and lead poisoning. On this particular iconic project, coal forges were typically placed on tower scaffolding where rivets were "warmed white" by a construction worker (Van Der Zee, 1986). This worker sent rivets into poorly ventilated and poorly lit 3.5 $ft^2$ cell to the rivet team using pneumatic tubes. After catching the rivet with a cone, the rivet team used tongs to place the hot rivet into a prepared hole and used an iron bar to hold it in place until the riveter used their gun to forge the head.

Rivet inspectors tested the adequacy of the riveting by hitting individual rivets with a hammer to see if they were loose. Loose rivets were cut out and replaced, costing the rivet team about 50 rivets of time. On the Golden Gate Bridge, shown in Fig. 2-3, experienced riveters would typically have to replace four to five rivets per day, while less experienced riveters had to replace between ten to twenty (Van Der Zee, 1986).

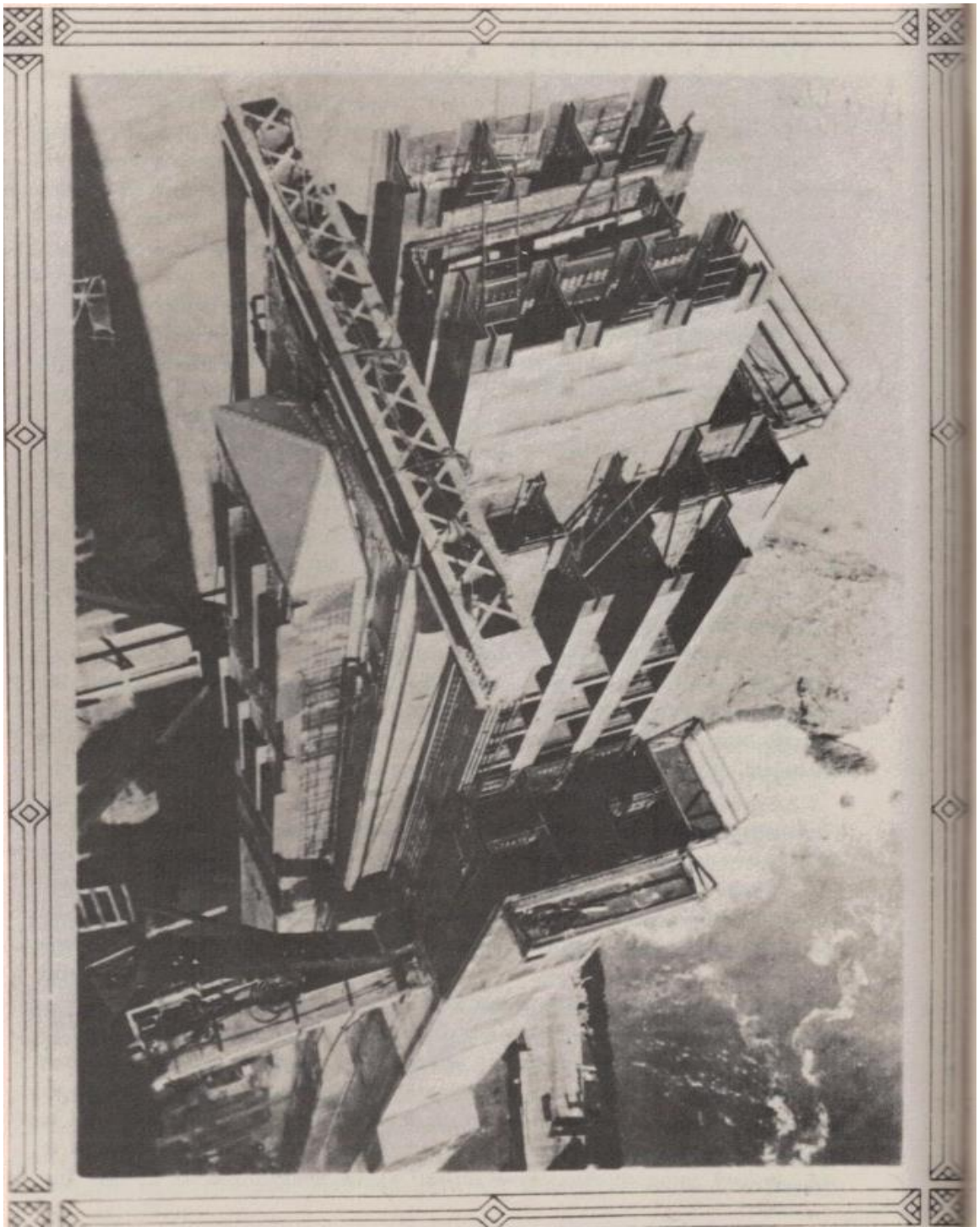

Fig. 2-3: View of Golden Gate Bridge Tower Cellular Nature (from Van Der Zee, 1986)

Other iconic projects involving the use of rivets experienced similar challenges. A lack of professional installation and the use of substandard material is largely attributed to the sinking of the once considered unsinkable Titanic cruise ship. With its strength provided from its steel shell plating and more than 3,000,000 hydraulically driven rivets, clues from the hull of the sunken ship and information gathered from archives reveal that the Northern Ireland builders' substandard practices led to the tragic sinking and over 1,500 deaths. During this time, the shipbuilding industry was shifting from using No. 4 iron bar to using steel rivets. However, as shown in Fig. 2-4, the builders only used steel rivets in the Titanic's central hull, where the stresses were expected to be the greatest.

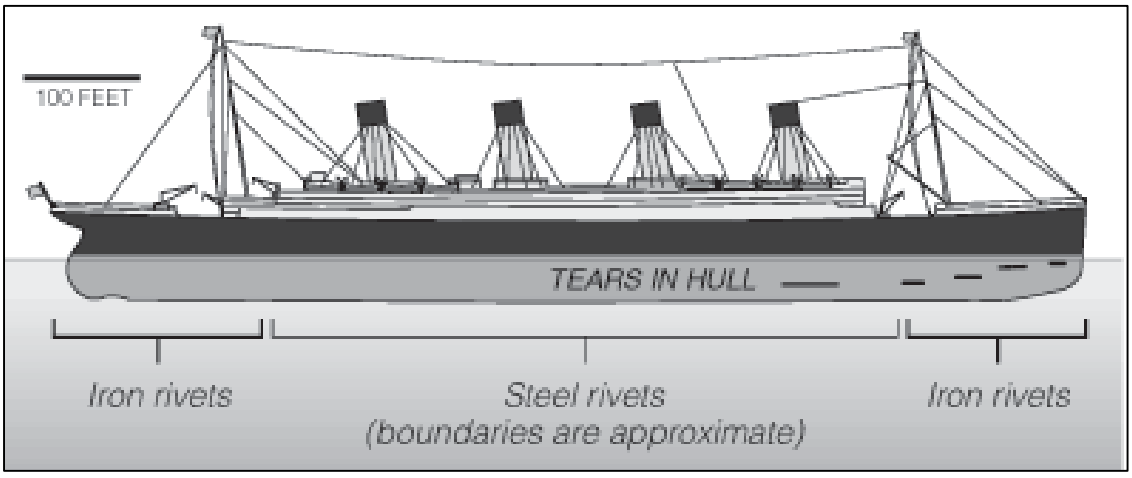


Fig. 2-4: Titanic Rivet Material Flaws (from Jennifer Hooper McCarty and Tim Foecke at http://www.nytimes.com)

The impact between the iceberg and the bow opened up six seams in the bow plates close to where the rivets transitioned from iron to steel. Faced with the pressure of

completing the ship in time for a set sail date, archives revealed the company expressed concern over the lack of skilled riveters. Mediocre work in getting the iron precisely heated to a cherry red color and beaten by the proper hammer blows likely resulted in an improper fit. To make matters worse, instead of using No. 4 iron bar in the stern and bow, the company used an even cheaper and weaker No. 3 bar. Dr. Tim Foecke, a specialist in metal fracture at the National Institute of Standards and Technology, conducted a microstructural analysis and found great variability in the results. In his analysis, he was astonished to find about three times more slag, which is a glassy residue of smelted metals, than occurs in modern wrought iron (Broad, 2008). The decohesion of an iron and slag interface served as a point of cracking and failure, especially when oriented perpendicularly to the load. Fig. 2-5 shows image analysis of micrographs along two recovered rivet cross-sections and reveals the high concentration of slag particles in the rivet heads oriented 90 degrees to the loading axis (McCarty, Weihs and Foecke, 2007).

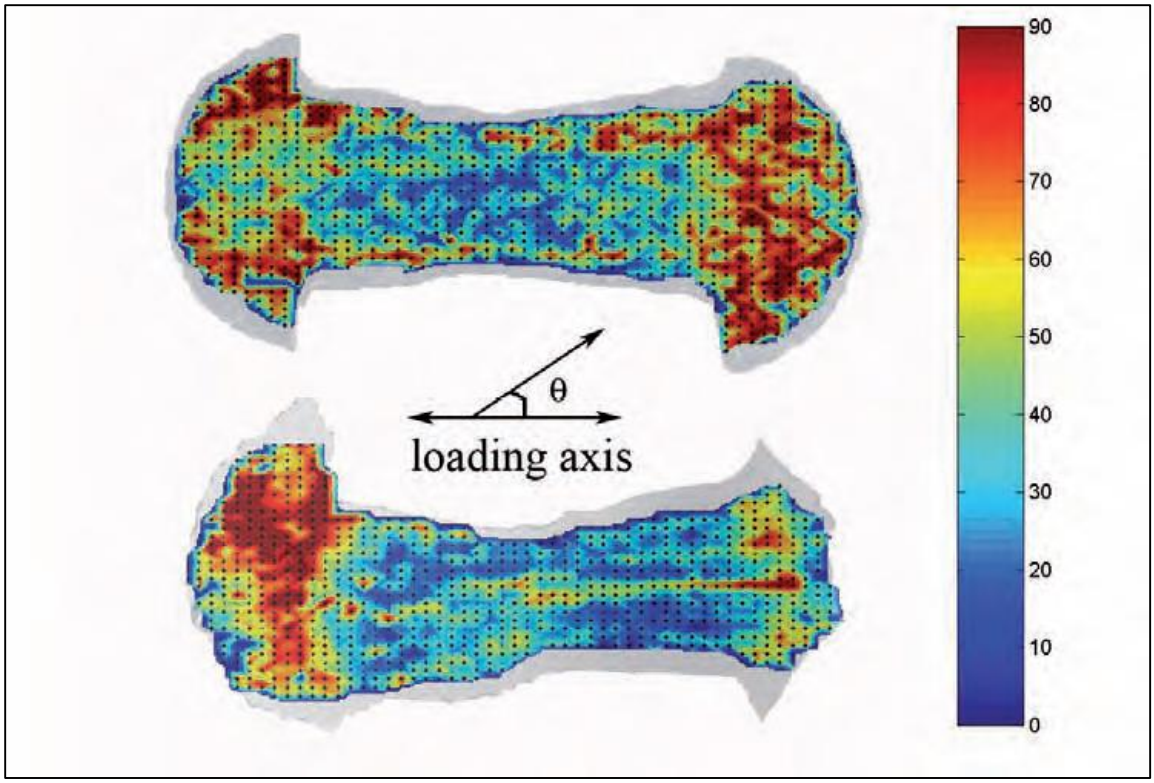


Fig. 2-5: Loading Axis (from McCarty et al., 2007)

The unskilled workers clearly worked the wrought iron inadequately and at too low of a temperature, causing brittle rivets prone to fracture along the rivet head and shaft seam. Investigation of the rivet holes also found small cracks that were ignored by shipbuilders at the time because they were so small. With the thought that a well-driven rivet exerts a clamping stress that would negate any risk from these cracks caused from the cold-punched holes, residual stresses from the punching process and impact of the plate at low temperatures could have caused these cracks to grow in a brittle manner (Foecke, 1998). The Titanic case study demonstrated the difficulty of finding experienced and technically proficient *rivet boys*, exposed a general lack of understanding at the time of the connector's

importance in design, and revealed the importance of the development of stronger rivet material properties in the design of subsequent structures.

While steel replaced iron in most structural components in the late 1800s, the transition from iron to steel rivets took some time. In the early 1900s, rivet steel was specified as ASTM A9 for buildings and ASTM A7 for bridges. After 1933, rivet steel was ordinarily specified as ASTM A141. This ASTM specification was withdrawn in 1967 and replaced with ASTM A502. Today, rivets in the construction industry are made from bar stock by either hot or cold forming the manufactured head in one of three ASTM A502 grades recognized in the 1986 specifications. The ASTM A502 structural rivet, however, was withdrawn in 1999 with no replacement. Table 2-1 summarizes the material specifications used for rivets.

Table 2-1: Structural Rivet Types (from *Guide to Design Criteria for Bolted and Riveted Joints*, 1987 and Historical Building Construction, 2010)

| **Rivet Type** | **Composition** | **Details** |
|---|---|---|
| ASTM A7 and A9 | A7 for bridges;<br>A9 for buildings | Tensile strength 45 ksi – 60 ksi; no specified level or high level of carbon led to poor weldability; popular from 1900 – 1933 |
| ASTM A141 | Mild Steel<br>(< 0.1% carbon) | Tensile strength 52 ksi – 62 ksi; popular from 1933 – 1967 |
| ASTM 502 Grade 1 | Carbon Steel Rivet | Used for general purposes; tensile strength 52 ksi – 62 ksi |
| ASTM 502 Grade 2 | Carbon-Manganese Rivet Steel | Used with high-strength carbon and high-strength low alloy structural steels; tensile strength 68 – 82 ksi |
| ASTM 502 Grade 3 | Carbon-Manganese Rivet Steel | Used with high-strength carbon and high-strength low alloy structural steels with enhanced corrosion resistance |

## 2.3 Riveted Connections and Member Limit States

Engineers use a myriad of design procedures for structural members and connections that include determining and following a load path to each component and subsequently designing or analyzing that component for applicable limit states. Limit states are the conditions of a structural element or connection that cause it to cease to perform its intended function. The typical limit states to consider as it pertains to riveted connections include: block shear rupture, member yielding, member rupture at the connection, bearing/tear out, and failure of the rivet. An in-depth discussion of each of these limit states is provided in the Steel Construction Manual (Muir et al., 2011); thus, only a brief

discussion of each is presented in the following subsections. Because the focus of this research is on the behavior of the rivets themselves as it pertains to riveted plate connections subject to blast loads, the focus of Sections 2.4, 2.5, and 2.6 is on the rivet connector subjected to three significant loading conditions:  pure shear, pure tension, and a combination of shear and tension.

### 2.3.1 Block Shear Rupture

The tearing limit state of block shear rupture typically occurs when the connecting elements are thin or the holes for the rivets are close together, causing plates to tear along the riveted holes. This two-part limit state consists of tension rupture on a plane perpendicular to loading and a shear yield or rupture on a plane parallel to loading. As demonstrated in Fig. 2-6, this failure can occur in either of the connecting elements.

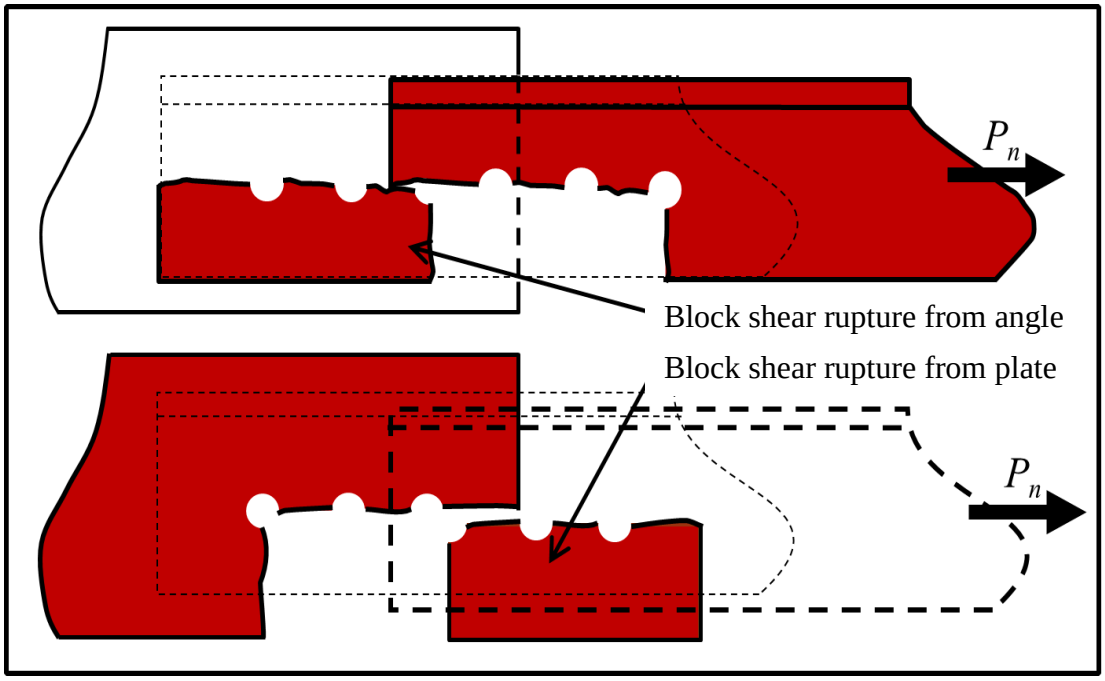


Fig. 2-6: Block Shear Rupture (modified from AISC Tools Core Teaching Aids, aisc.org)

### 2.3.2 Member Yielding and Member Fracture

Member yielding is unrelated to connection behavior, and this limit state is checked over the gross cross-sectional area of the connected member. For this limit state to occur, the entire cross section must reach its yield stress, resulting in a stretching or excessive deformation failure of the member that occurs away from the connection. It is rare that this limit state would control a design unless the designer did so intentionally in order to design for ductility. This limit state would be calculated the same way for both a bolted and a riveted connection. On the contrary, the fracture limit state occurs at the connection and involves tearing at the holes and through the member. This limit state

differs from the block shear limit state because it involves a tension failure only that occurs perpendicular to the direction of the load. Unlike the yielding limit state which fails in the member and away from the connection, this fracture (rupture) failure occurs along the holes at the connection. This is demonstrated in Fig. 2-7.

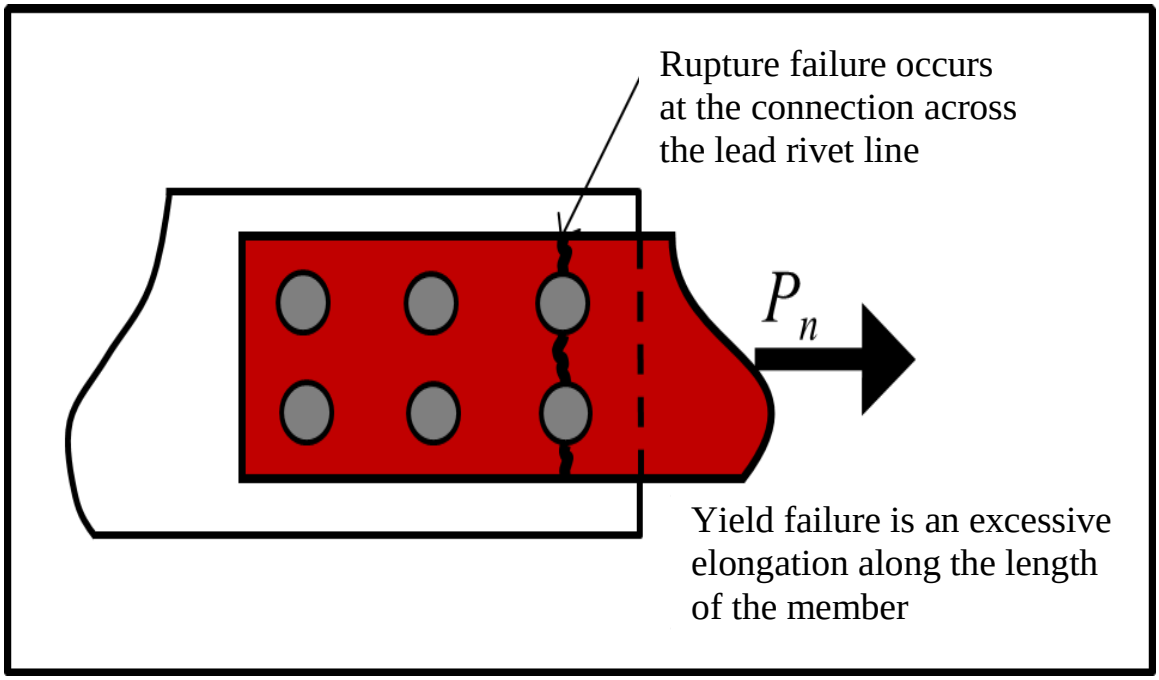


Fig. 2-7: Member Yielding and Member Fracture (modified from AISC Tools Core Teaching Aids, aisc.org)

### 2.3.3 Rivet Bearing / Tear Out

The material strength of a rivet is typically greater than the material it is bearing on; thus, it is common to check for bearing issues on the material of the connected parts.

Bearing failures, as shown in Fig. 2-8, cause material crushing and subsequent excessive deformation around the rivet hole.

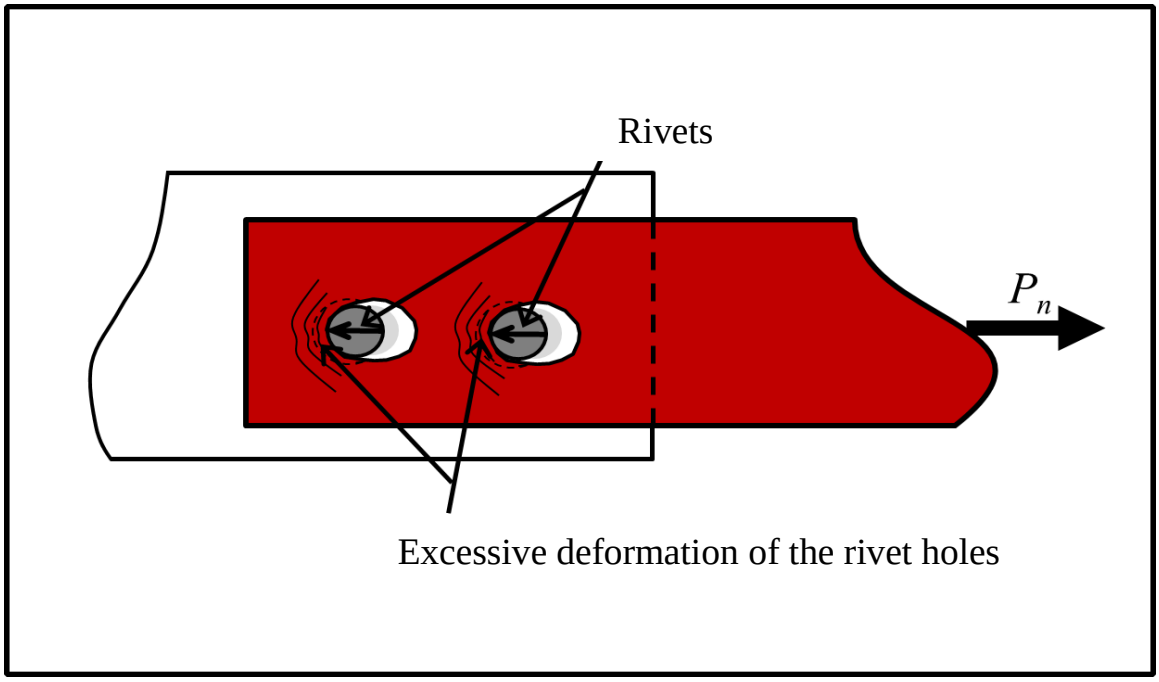


Fig. 2-8: Bearing Limit State (modified from AISC Tools Core Teaching Aids, aisc.org)

When the clear space to an adjacent hole or an edge is insufficient, the limit state of shear in the connecting material, also known as tear out, can control. As shown in Fig. 2-9, the result is either a piece of the connecting material tearing between holes in the direction of force or a tearing out at the end of a connection.

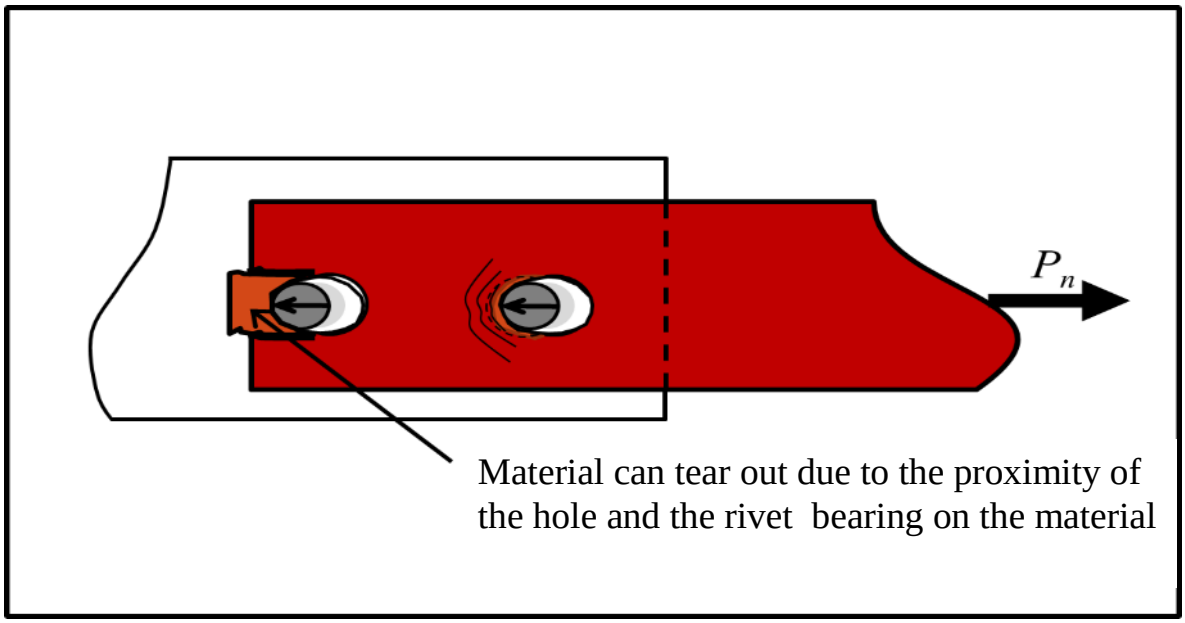


Fig. 2-9: Tear Out Limit State (modified from AISC Tools Core Teaching Aids, aisc.org)

## 2.4 Rivets in Pure Tension

Variability associated with the riveting process leads to a great deal of uncertainty with respect to the amount of clamping force within a rivet shank. Differences in rivet dimensions, the driving and finishing temperatures, and driving time and pressure all contribute to that variability. The residual clamping force and pre-stressing in a rivet develops as the hot rivet cools and shrinks, pulling plates together. With so many variables however, a simplistic design assumption is made that no load is transferred between adjoining members through friction.

For the most part, design specifications have been in agreement with the shear capacity of a rivet. However, until testing was conducted by the Research Council on Riveted and Bolted Structural Joints and others between the 1930s and 1950s, design specifications were against the use of rivets to carry tensile forces, as demonstrated in Fig. 2-10. Those that did allow the use of tension, such as in the American Association of State Highway Officials' (AASHTO) specification, did so under the restriction that they could only be used in direct tension under one half the value allowed in shear. In 1946, the American Institute of Steel Construction (AISC) specification increased the allowable tension to 1.33 times the value allowed in shear (Higgins and Munse, 1952).

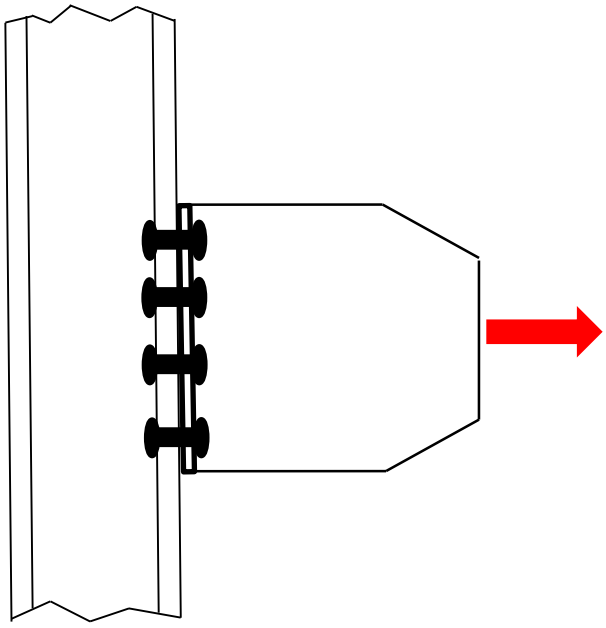

Fig. 2-10: Example of Rivet Connector in Pure Tension

As indicated previously, most engineers today are familiar with the behavior and ultimate strength of A325 and A490 bolts, but they have little if any knowledge of rivets. Typical stress-strain curves for an undriven A502 rivet steel compared to today's bolts are shown in Fig. 2-11. According to the *Guide to Design Criteria for Bolted and Riveted Joints*, the tensile strength for the more common A502 grade rivets range from 60 ksi for Grade 1 to 80 ksi for Grade 2 and Grade 3 (Kulak et al., 1987).

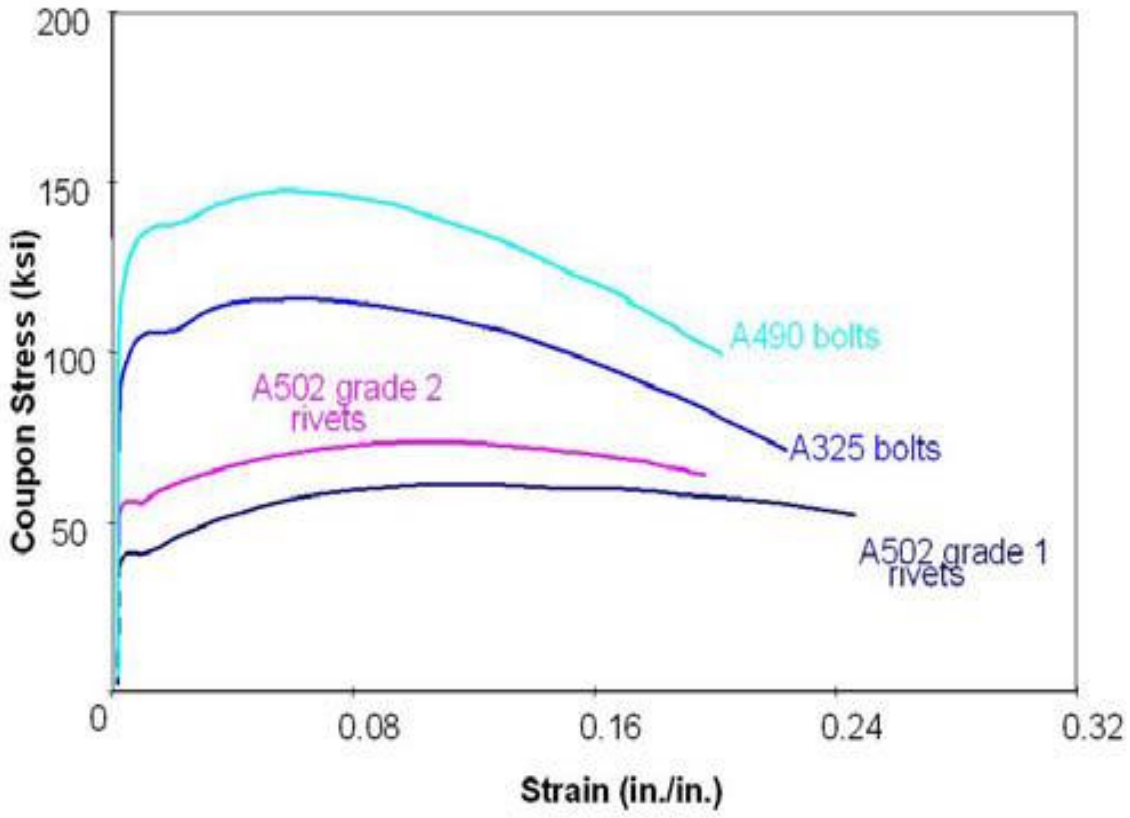


Fig. 2-11: Coupon Stress versus Strain Relationship for Rivet and Bolt Materials (from *Guide to Design Criteria for Bolted and Riveted Joints* by Kulak et al., 1987)

Before the testing conducted by the Research Council on Riveted and Bolted Structural Joints, engineers were concerned with the existing tension in rivets approaching the elastic limit of the steel as a result of the stresses induced during the cooling process. The thought was that the rivet would be unable to resist additional tension and the rivet head would pop off. Pure tension studies conducted at the University of Illinois and the University of Toronto involved multiple tests of rivets in pure tension (Young and Dunbar, 1928 and Wilson and Oliver, 1930). In the testing, variables such as type of head, length of grip (thickness of material being riveted), heating temperature when driven, and driving conditions were considered. It was determined that rivets with flattened heads failed in the head, even though they still developed 90% of the strength of the rod from which they were made. For all other rivets, the strength of the rivets was greater than the tensile strength of the rods from which they were made. It was also determined that rivets with a longer grip were not as strong as rivets with a shorter grip because the longer rivets did not fill the holes over the entire length as completely as the shorter ones. Rivets with a longer grip also had a greater initial stress than those with shorter grips. Variations in furnace temperature, soaking times, and driving times each had only a small effect on the ultimate strength of the rivets.

Subsequent testing at the University of Illinois discovered that the biggest impact on rivet strength was the driving process (Wilson and Thomas, 1938). Hot-driven rivets had tensile strengths of 10% to 20% higher than undriven rivets, with the difference based on whether the rivet was driven using a pneumatic hand riveting hammer or a hydraulic riveting machine. A summary of these tests is shown in Table 2-2. It is clear that the early

fear engineers had for using rivets in tension was unwarranted. Pulling on the rivet head already in stress due to shrinkage does not increase the stress on the rivet. Instead, it relieves the pressure on the plates, unless the added tension exceeds the tension already in the rivet.

Table 2-2: Comparison of Tensile Strength of Driven and Undriven Rivets (data from Fatigue Tests of Riveted Joints by Wilson and Thomas, 1938)

| Rivet Steel Material | Grip (in) | Driving Temp (deg F) | Driving Method | Driven Ultimate Strength (ksi) | Undriven Rivet Strength (ksi) | Percent Increase |
|---|---|---|---|---|---|---|
| Carbon | 3 | 2030 | Hammer | 75.35 | 57.62 | 21.5% |
| Carbon | 5 | 2030 | Hammer | 68.38 | 57.62 | 15.7% |
| Manganese | 3 | 1850 | Hammer | 105.15 | 79.75 | 24.1% |
| Manganese | 5 | 1850 | Hammer | 93 | 79.75 | 14.2% |
| Carbon | 3 | 1780 | Hydraulic | 78.25 | 57.62 | 26.4% |
| Carbon | 5 | 1780 | Hydraulic | 73.23 | 57.62 | 21.3% |
| Manganese | 3 | 1740 | Hydraulic | 110 | 79.75 | 27.5% |
| Manganese | 5 | 1740 | Hydraulic | 100.77 | 79.75 | 20.9% |

## 2.5 Rivets in Pure Shear

When the lines of action between members are parallel, rivet connectors resist the pure shear between their connected parts through the friction generated between the two parts. As indicated earlier, this friction is due to the tension in the rivet that builds during the cooling process and has inherent variability due to the installation process. A contact pressure develops due to interaction between the riveted and connected parts. As shown in Fig. 2-12, this bearing stress is determined by multiplying the axial load in the plates causing the bearing by the characteristic area perpendicular to it.

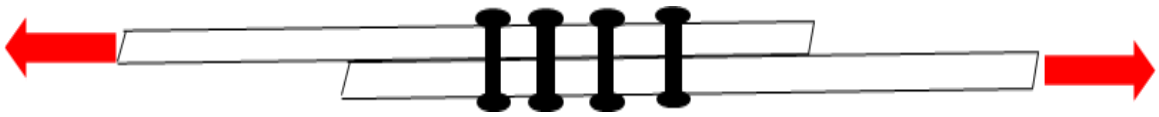

Fig. 2-12: Example of Rivet Connector in Pure Shear

As summarized in Table 2-3, tests conducted at the University of Illinois Urbana showed a direct correlation between the tensile strength and shear strength (Munse and Cox, 1956). Because the riveting installation process increases the tensile strength of a rivet, it also increases the shear strength.

Table 2-3: Comparison of Shearing Strength of Driven and Undriven Rivets (from Historical Building Construction by Friedman, 2010)

| Rivet Material | Driven Rivet Strength based on Nominal Rivet Diameter (ksi) | Undriven Rivet Strength (ksi) | Percent Increase |
|---|---|---|---|
| Carbon Steel | 58.96 | 46.28 | 21.5% |
| Manganese Steel | 80.52 | 66.26 | 17.7% |

In fact, common practice is to express the shear strength in terms of its tensile strength. The *Guide to Design Criteria for Bolted and Riveted Connections* reports an average shear-to-tensile strength ratio varying from 0.67 to 0.83, with an average of 0.75 (Kulak et al., 1987). Testing variables such as rivet size, grip length, method of driving, and the method of rivet manufacturing all contribute to the range, although all have little effect on the average value. A summary of some of 403 tests that included tests on 0.75-in., 0.875-in., and 1-in. rivets that were cold-formed or hot-formed, and were either hand-pneumatic driven or machine driven at a steel fabrication shop, is provided in Table 2-4.

Table 2-4: Comparison of Shearing Strength of Driven and Undriven Rivets (from Historical Building Construction by Friedman, 2010)

| Series Number (insignificant for purposes of this summary) | Strength in Shear (ksi) | % Shear Strength to Tensile Strength |
|---|---|---|
| 1 | 47.7 | 75.7 |
| 2 | 46.0 | 70.5 |
| 3 | 44.2 | 78.7 |
| 4 | 44.7 | 77.9 |
| 5 | 46.2 | 75.4 |
| 6 | 45.5 | 74.6 |
| 7 | 42.5 | 76.5 |
| 8 | 42.6 | 76.5 |

For current ASTM A502 Grade 1 and Grade 2 rivets with tensile strengths of 60 and 80 ksi respectively, expected shear strengths are between 45 ksi and 60 ksi for Grade 1 rivets and between 60 ksi and 80 ksi for Grade 2 rivets. Typical load versus deformation curves for ASTM A502 Grade 1 rivets are in Fig. 2-13.

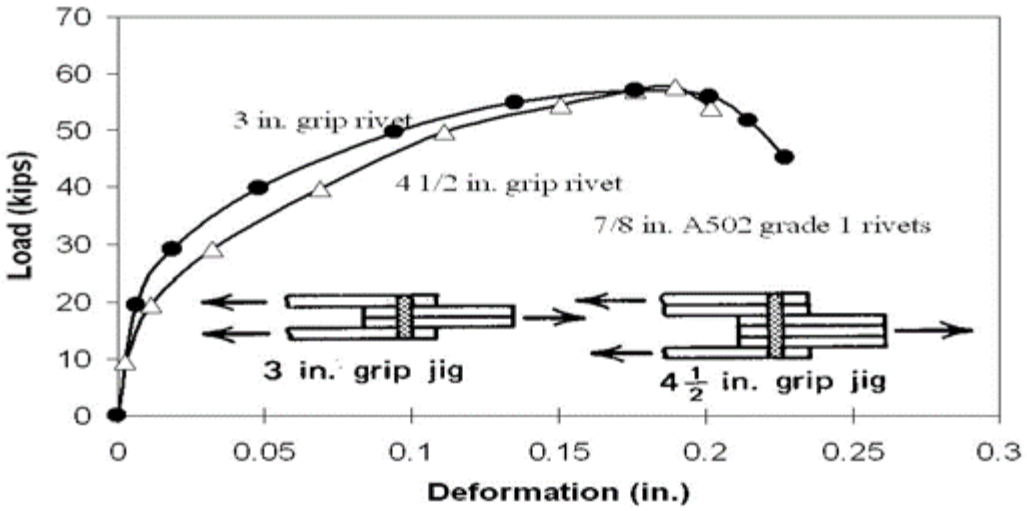


Fig. 2-13: Shear vs. Deformation Curves for A502 Grade 1 Rivets (from *Guide to Design Criteria for Bolted and Riveted Connections*, 1987)

The *Guide to Design Criteria for Bolted and Riveted Connections* (1987) provides the shear resistance, $S_u$, of a rivet as:

$$S_u = 0.75\, m\, A_b\, \sigma_u \qquad (2\text{-}1)$$

where: $m$ is the number of shear planes,

$A_b$ is the cross-sectional area of the rivet before driving ($in^2$),

$\sigma_u$ is the tensile strength of the rivet, and

0.75 accounts for the ratio of shear strength to tensile strength.

As shown in Eq. (2-1), the shear resistance is directly proportional to the number of shear planes and the cross-sectional area of the rivet. Reviewing more recent literature, the AASHTO Manual for Bridge Evaluation (MBE) (2011) indicates in Eq. (2-2) that the factored resistance of rivets in shear, $\phi R_n$, is determined by:

$$\phi R_n = \phi F_r \cdot m \cdot A_r \tag{2-2}$$

where: $\phi F_r$ is the factored shear strength of one rivet in single shear (ksi) from Table 2-5,

$m$ is the number of shear planes, and

$A_r$ is the nominal cross-sectional area of the rivet before driving ($in^2$).

The values shown in Table 2-5 are based on the von Mises shear yielding theory, which gives a ratio of 0.58 for shear-to-tensile yield strength, and a $\phi$-factor of 0.67 (Ocel, 2013). Computed shear strength values using this approach are lower relative to those recommended in the *Guide to Design Criteria for Bolted and Riveted Connections* (1987).

Table 2-5: Rivet Factored Shear Strength, AASHTO 2nd Edition MBE (2011)

| **Rivet Type or Year of Construction** | **$\phi F_r$, ksi** |
|---|---|
| Constructed prior to 1936 or of unknown origin | 18 |
| Constructed after 1936 but of unknown origin | 21 |
| ASTM 502 Grade 1 | 25 |
| ASTM 502 Grade 2 | 30 |

Based on more current research conducted by D'Aniello, Portioli, and Landolfo (2011), both the AASHTO and the Eurocode factored shear design strength equations underestimate actual measured capacities. The authors tested 64 riveted connections made from the 1950s with different rivet diameters. The connections varied in eccentricity (symmetric or unsymmetric), geometry, configuration (single shear and double shear), and length. The authors compared their results to those predicted by the Eurocode EN 1993: 1-8 (2002), which states that the shear strength of rivets, $F_v$, can be computed using Eq. (2-3):

$$F_V = 0.6 \cdot f_{ur} \cdot A_0 \tag{2-3}$$

where: $f_{ur}$ is the ultimate tensile strength of a rivet, and

$A_o$ is the area of the hole.

In their testing, the authors calculated the rivets to have a mean tensile strength of 59.8 ksi, while noting a noticeable variability in the data attributed to a lack of quality control in the construction industry during that era. While not all of the connections failed by the limit state of rivet shear, the authors specified results of tests in which rivet shear was the controlling limit state. A comparison of measured data from the authors and results calculated using various codes is shown in Table 2-6. Based on these results, it is clear that current design guides and specifications provide rivet shear strengths lower than tested capacities (D'Aniello et. al, 2011).

Table 2-6: Rivet Ultimate Shear Stress Comparisons (portions from D'Aniello et. al, 2011)

| Test Specimen | Rivet Dia. (in.) | Shear Type | Rivet Rows | Tested Shear Failure (k) | Eurocode Shear Failure (k) | AASHTO Shear Failure (k) | Design Guide Shear Failure (k) |
|---|---|---|---|---|---|---|---|
| U-16-10-1 | 0.630 | Single | 1 | 18.034 | 11.18 | 9.77 | 13.97 |
| U-19-10-1 | 0.748 | Single | 1 | 22.814 | 15.76 | 13.77 | 19.69 |
| U-19-12-1 | 0.748 | Single | 1 | 26.433 | 15.76 | 13.77 | 19.69 |
| U-22-10-1 | 0.866 | Single | 1 | 32.548 | 21.12 | 18.46 | 26.40 |
| U-22-12-1 | 0.866 | Single | 1 | 32.548 | 21.12 | 18.46 | 26.40 |
| U-16-10-2 | 0.630 | Single | 2 | 34.881 | 22.35 | 19.54 | 27.94 |
| U-19-10-2 | 0.630 | Single | 2 | 47.219 | 31.48 | 27.55 | 27.94 |
| U-22-12-2 | 0.866 | Double | 2 | 61.078 | 42.24 | 36.92 | 52.80 |

Research conducted by Olson (2010) and Wang (2013) has also demonstrated AASHTO's equation (2010) underestimates actual measured capacities. They tested salvaged individual rivets from a Washington State Department of Transportation bridge, noting that testing by D'aniello et al., (2011), was done on old unused rivets stored in a warehouse. As shown in Fig. 2-14, Olson and Wang were interested in the shear capacity

of rivets with different levels of corrosion and that had been in service experiencing years of cyclic loading. The authors found that corrosion effects on the shear capacity of the rivets was negligible and determined the shear strengths were twice that predicted by AASHTO (2010).

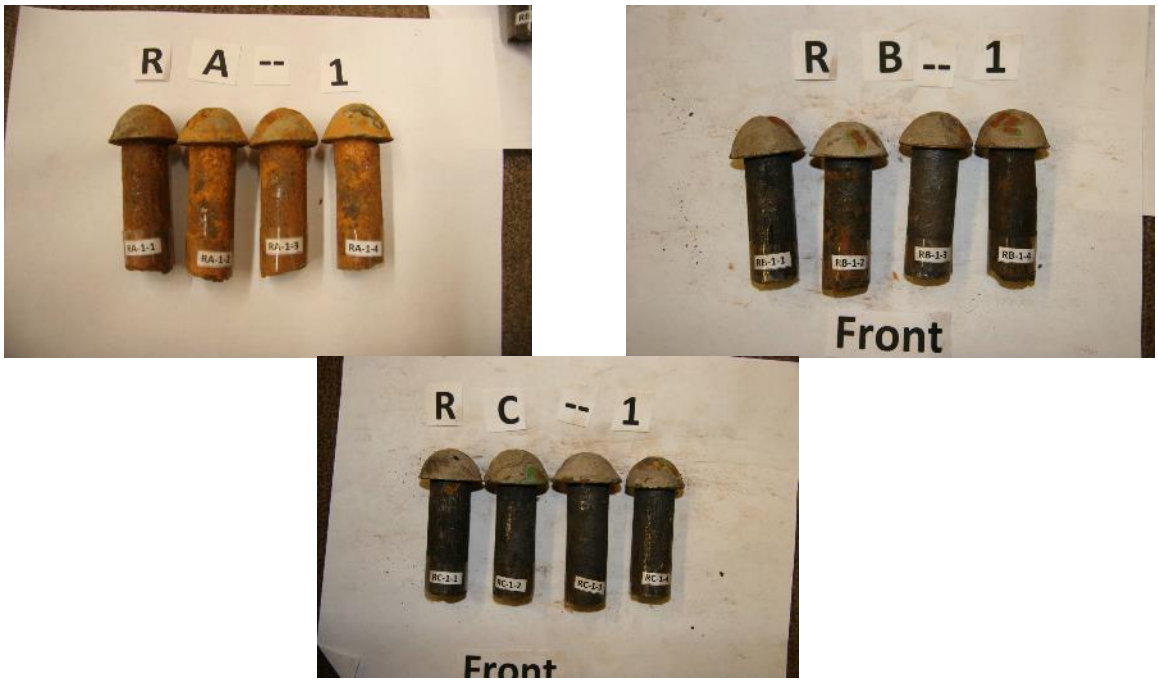


Fig. 2-14: Three Different Corrosion Levels for Tested Rivets (from Wang, 2013)

For riveted connections with a length greater than 50-in., as measured between extreme fasteners on one side of the connection, the factored shear strength of rivets is 80 percent the value of its typical factored shear strength (Kulak et al., 1987). As a structural joint is loaded, the end fasteners take on a greater percentage of the stress. When these end

fasteners deform, load is redistributed to the other fasteners. The redistribution depends on the fasteners' ductility. Once a fastener no longer has the ability to deform without fracture, it fails prematurely in shear. As a result, the end fastener fails before the other fasteners and starts an *unbuttoning* process in which each subsequent row of fasteners also fails. Hence, there is guidance to reduce the factored shear strength for long connections.

Batho used the Principle of Least Work to confirm experimental research concluding rivets at the ends of connections would have a higher load than rivets in the middle of connections in the elastic state (Batho, 1916). Subsequent experimental work from the University of California in support of the construction of the San Francisco-Oakland Bay Bridge systematically tested a myriad of connections with varying lengths, steel types, and rivet patterns (Davis et al., 1940). With long connection joints, the authors noted rivet shear failure premature to the sum of each rivet shear capacity in which the first row of rivets failed first, followed by each subsequent row in an *unbuttoning* or *unzipping* fashion. Bendigo, Hansen, and Rumpf (1963) and Fisher, Kulak, and Beedle (1965) tested several long structural splices connected by high-strength bolts of varying lengths and bolt patterns. All observed a decrease in the average connector ultimate strength with an increase in connection length. At shorter connection lengths, loads were distributed approximately equally among fasteners; however, for longer connection lengths, fasteners near the center of a joint carried only about half of the load carried by the fasteners on the end. In comparing riveted and bolted joints, Dlugosz (1962) concluded that while both failed in an unbuttoning mode, riveted connections demonstrated a more level stress distribution. Dlugosz (1962) also noted that rivet deformation changed significantly from

ultimate load to rupture load. In comparing A141 rivet deformation to A325 bolt deformation, the rivet deformed 20% more than the bolt after ultimate load, demonstrating the rivet's ability to effectively redistribute load.

The *Guide to Design Criteria for Bolted and Riveted Connections* (1987) demonstrates the influence of joint length on the ultimate strength of connectors, as shown in Fig. 2-15. Shorter connections tested to capacity in shear demonstrate a simultaneous shearing. For joints longer than approximately 10-in., however, fasteners start to exhibit an unzipping shear failure. More recent work by Olson (2010) and Wang (2013) demonstrates that the 20% blanket reduction for all long connections is too conservative. The authors conclude that the fastener capacity only needs the 20% reduction when connecting weak plates, or plates with a yield capacity less than the sum of the rivet shear strength. They found that long riveted connections connecting strong plates do not exhibit an unbuttoning failure mode; as a result, they recommend a smaller 10% reduction as a factor of safety.

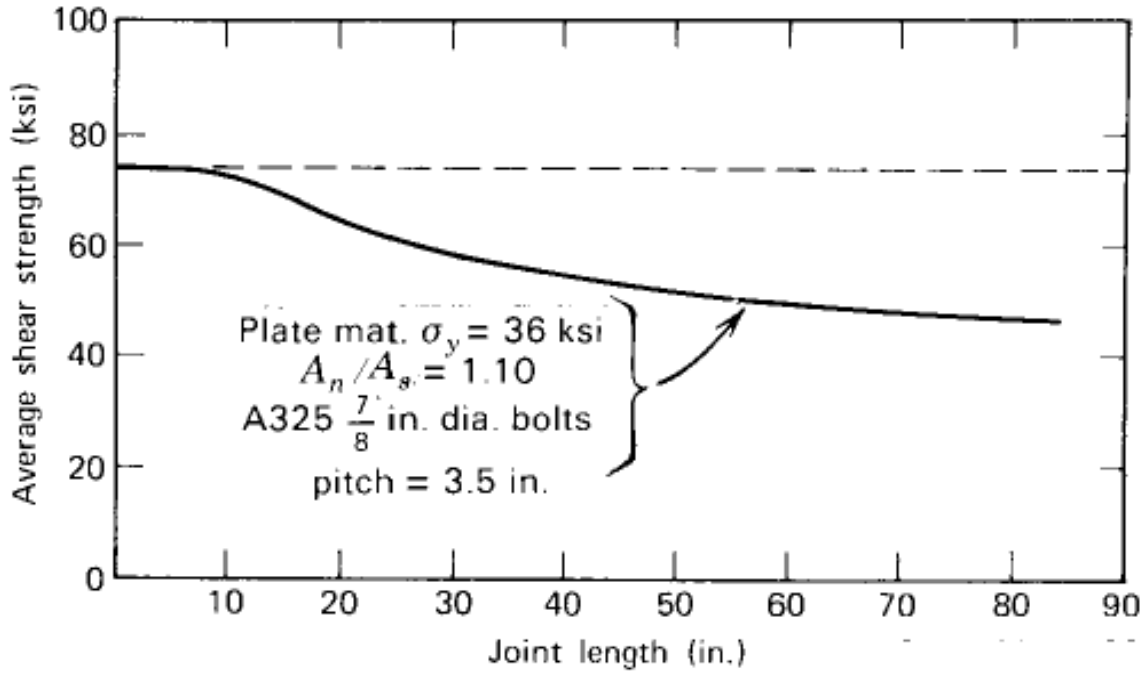


Fig. 2-15: Effect of Joint Length on Ultimate Strength (from *Guide to Design Criteria for Bolted and Riveted Connections*, 1987)

## 2.6 RIVETS IN COMBINED SHEAR AND TENSION

Rivets are often subjected to some combination of shear and tension loads, as shown in Fig. 2-16. Past research has led to an elliptical interaction curve to describe the strength of rivets under combined shear and tension. In experimental work at the University of Toronto, while varying the amount of shear and tension on rivet connectors, it was concluded that adding shear to the rivet weakened the connector (Young and Dunbar, 1928). In this testing, rivets with a tensile force equal to twice the shearing force had ultimate strengths about four percent lower than the ultimate strength of rivets in direct

tension. Meanwhile, rivets tested with a tensile force equal to the shearing force had ultimate strengths about 35 percent less than the ultimate strength of rivets in direct tension.

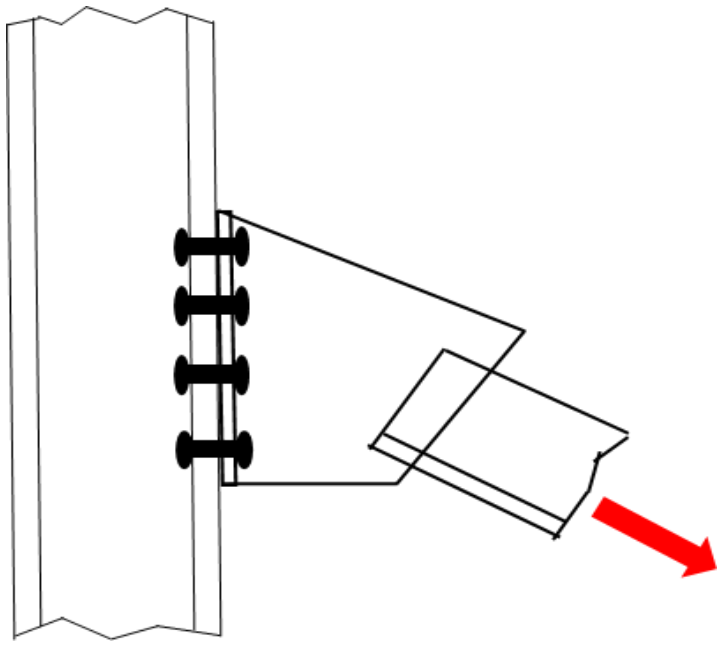

Fig. 2-16: Example of Rivet Connectors in Combined Tension and Shear

Tests done at the University of Illinois, Urbana, using ASTM A141 rivets were used to observe trends for different combinations of tension and shear (Munse and Cox, 1956). Consistent with prior tests conducted by these researchers, variables included rivet diameter, driving procedure, and manufacturing process. The biggest difference in the capacity for each test lied in the amount of tension or shear implemented for that test. Typical fractures of different shear-tension ratios for the 403 tests are shown in Fig. 2-17. By inspection, it is clear there is a substantial difference in deformation capacity between

the different tests. The rivet deformation capacity increased as the loading changed from pure shear to increasing amounts of tension.

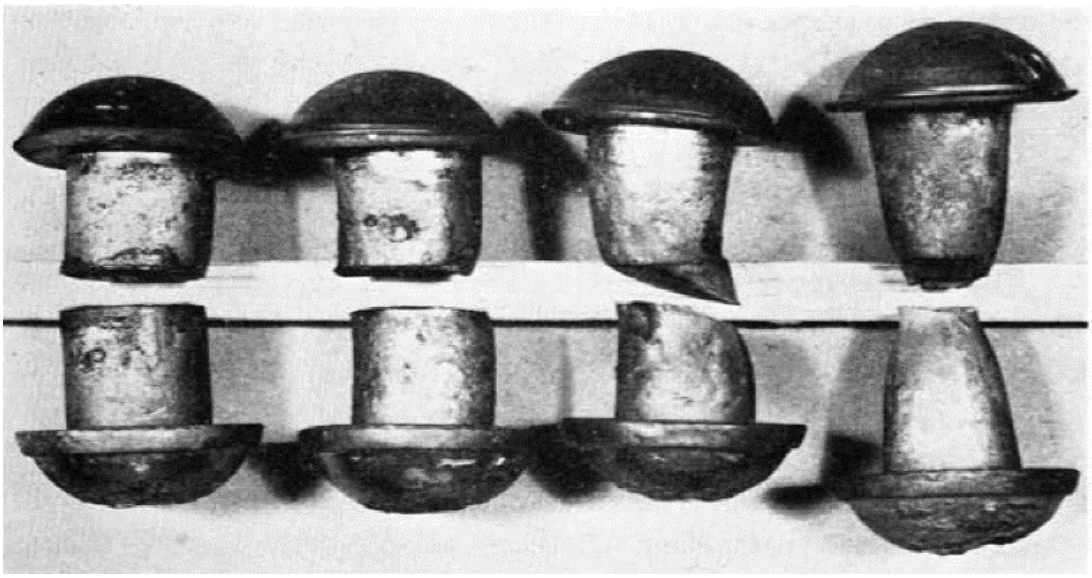


Fig. 2-17: Typical Fractures at Four Shear-Tension Ratios (from Munse and Cox, 1956)

The findings from this testing led to the development of Eq. (2-4) which determines the rivet strength, *S*, at any tension-to-shear ratio:

$$S = r \times S_S \tag{2-4}$$

where: $r$ is calculated directly from Eq. (2-5) and ranges from a value of 1.0 when the rivet is in direct shear and 1.333 when the rivet is in direct tension,

$m$ = ratio of tensile force component to shear force component, and

$S_s$ = shear strength of the rivet.

$$r = 1.333\sqrt{\frac{1+m^2}{(1.333)^2+m^2}} \tag{2-5}$$

Munse and Cox (1956) also presented the strength of rivets at any shear-tension ratio graphically in the shape of an ellipse using Eq. (2-6):

$$\frac{y^2}{1.33^2}+\frac{x^2}{1.00^2}=1.0 \tag{2-6}$$

where: $y$ = ratio of tensile component of force on rivet at ultimate strength to the ultimate shear strength of rivet, and

$x$ = ratio of shear component of force on rivet at ultimate strength to the ultimate shear strength of rivet.

The latest version of this equation differs from Eq. (2-6) in that it is modified in terms of the ultimate tensile strength of the rivet. It appears in the *Guide to Design Criteria for Bolted and Riveted Connections* (Kulak et al., 1987) as:

$$\frac{x^2}{0.75^2} + y^2 = 1.0 \qquad (2\text{-}7)$$

where: $x$ = ratio of shear stress to the rivet ultimate tensile strength, and

$y$ = ratio of tensile stress to the rivet ultimate tensile strength, with stresses determined from the applied loads and the strengths determined from pure tensile and pure shear capacity (Kulak et al., 1987).

As was the case with (2-6), using (2-7) provides an elliptical interaction curve as shown in Fig. 2-18. The equations and elliptical curve reiterate the fact that rivets demonstrate a higher shear-to-tensile capacity than typically recommended for steel in the research literature (typically 0.6). As indicated in the *Guide to Design Criteria for Bolted and Riveted Connections*, the tested average shear-to-tensile strength ratio varies from 0.67 to 0.83, with an average of 0.75 (by Kulak et al., 1987). As a result, the elliptical curve in Fig. 2-18, portraying rivet shear or tensile strength normalized by the rivet tensile strength, normalized by the rivet tensile strength, provides a value of 1 under pure tensile load, and a value of 0.75 under pure shear load. Of particular note is the fact that adding shear to a rivet weakens the connector. For example, when the tensile force is twice the shear force, the capacity of the rivet in comparison to the tensile strength only drops by 4%. When the amount of shear force on the rivet is equal to the tensile force on the rivet, however, the capacity of the rivet relative to the tensile strength drops by 35%.

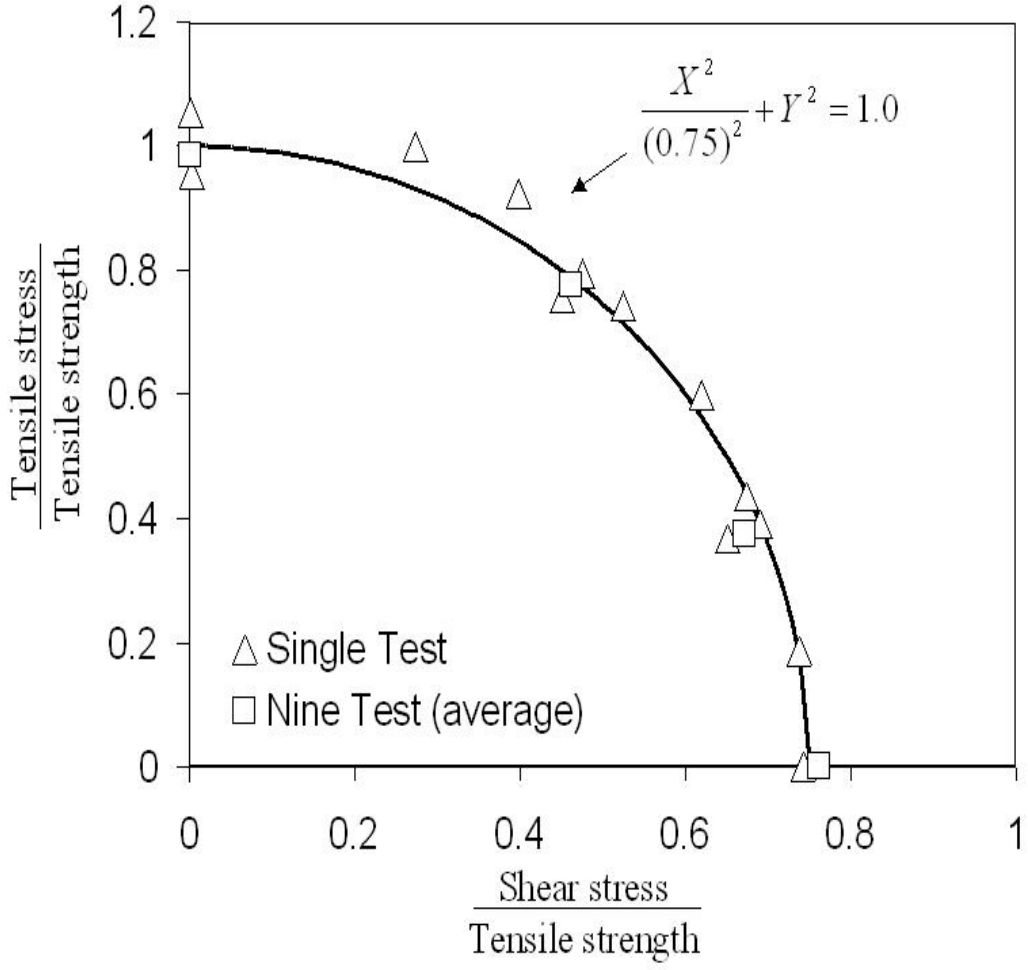


Fig. 2-18: Combined Tension and Shear Interaction Curve (from *Guide to Design Criteria for Bolted and Riveted Connections*, 1987)

## 2.7 BLAST LOADS AND SHOCK PHENOMENA

A review of the relevant literature shows that rivets were studied in detail up until the 1950s. At that time, high-strength bolts gained preference as a connector for structural steel. Although several in-depth studies provide a good understanding of rivet behavior

under a range of loading conditions, little to no work focused specifically on rivet behavior under high rates of loading such as those associated with blast. Testing of rivets considered only conventional loads such as dead, live, and wind. These loads are applied slowly and can remain constant for a relatively long period of time. Unless earthquake loads are considered, structures subjected to conventional loads are normally designed to stay in their elastic range. With the on-going and arguably never-ending threat that terrorists present to our infrastructure, it is important to understand how steel components joined by rivets behave under blast and other extreme loads they were not initially designed to resist. Unlike conventional loads, blast loads are impulsive, with peak pressures that can be extremely large relative to the material yield strength, though these pressures typically act over a very short duration (milliseconds). The detonation of an explosive generates a sudden release of energy that dissipates through blast waves, propulsion of fragments from the explosive casing or propelled debris, and thermal radiation. A simple example of energy dissipating through blast waves due to a detonation is illustrated in Fig. 2-19. The blast loading and impulse for many design scenarios typically remain localized and do not have to necessarily engage the entire structure as other dynamic loads do, such as wind and earthquake.

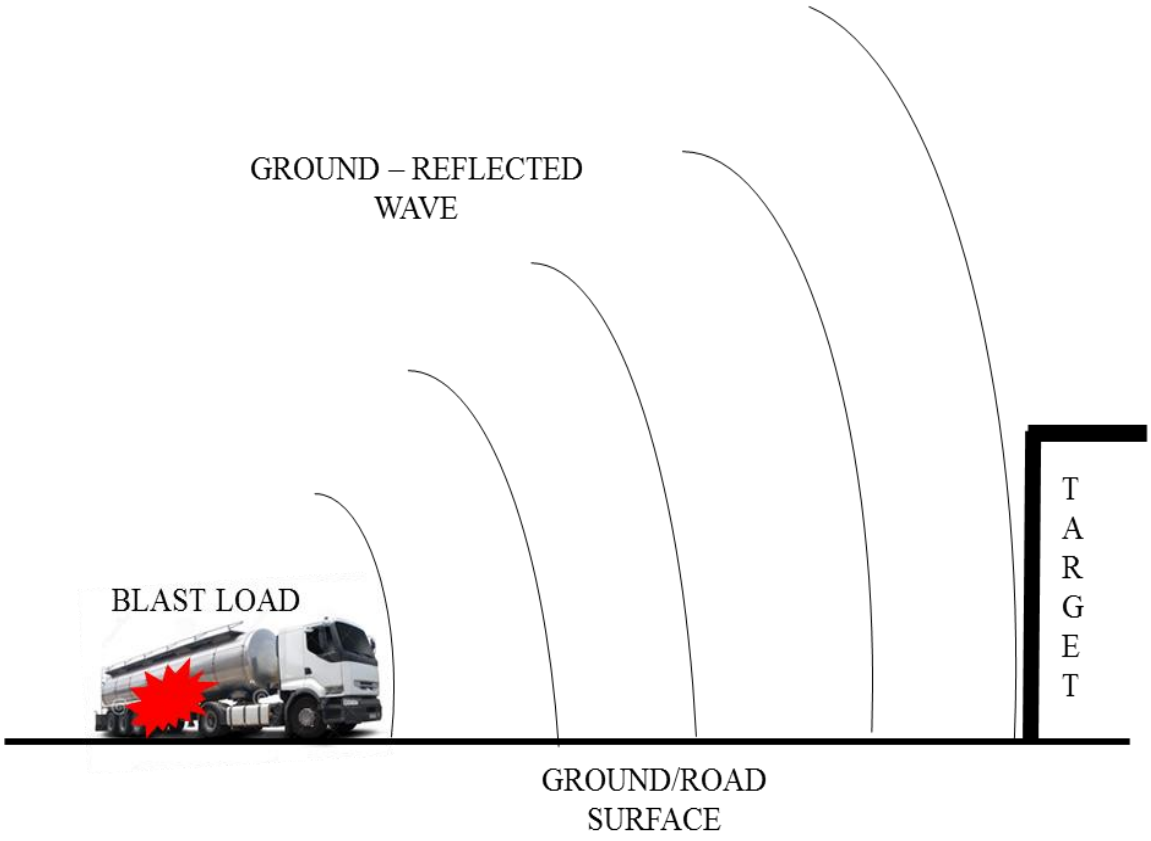


Fig. 2-19: Blast Wave Propagation Demonstration

The high pressures associated with an explosion can be categorized into either a deflagration or a detonation. A deflagration is a thermally initiated oxidation reaction that propagates below the speed of sound (typically at speeds ranging between 3 - 330 ft/sec) in the unreacted material (e.g., natural gas and air; gasoline vapor and air). The resulting pressure wave that radiates from the explosion source has a finite rise time.

Unlike deflagrations, a detonation is an extremely rapid chemical reaction that proceeds through the explosive material at a supersonic velocity that typically ranges from 22,000

to 28,000 ft/sec for high explosives (e.g., Composition C-4 expands at 26,400 ft/sec) (UFC 3-340-02, 2008). Fig. 2-20 shows a detonation within the first few microseconds of detonation and again at approximately one millisecond.

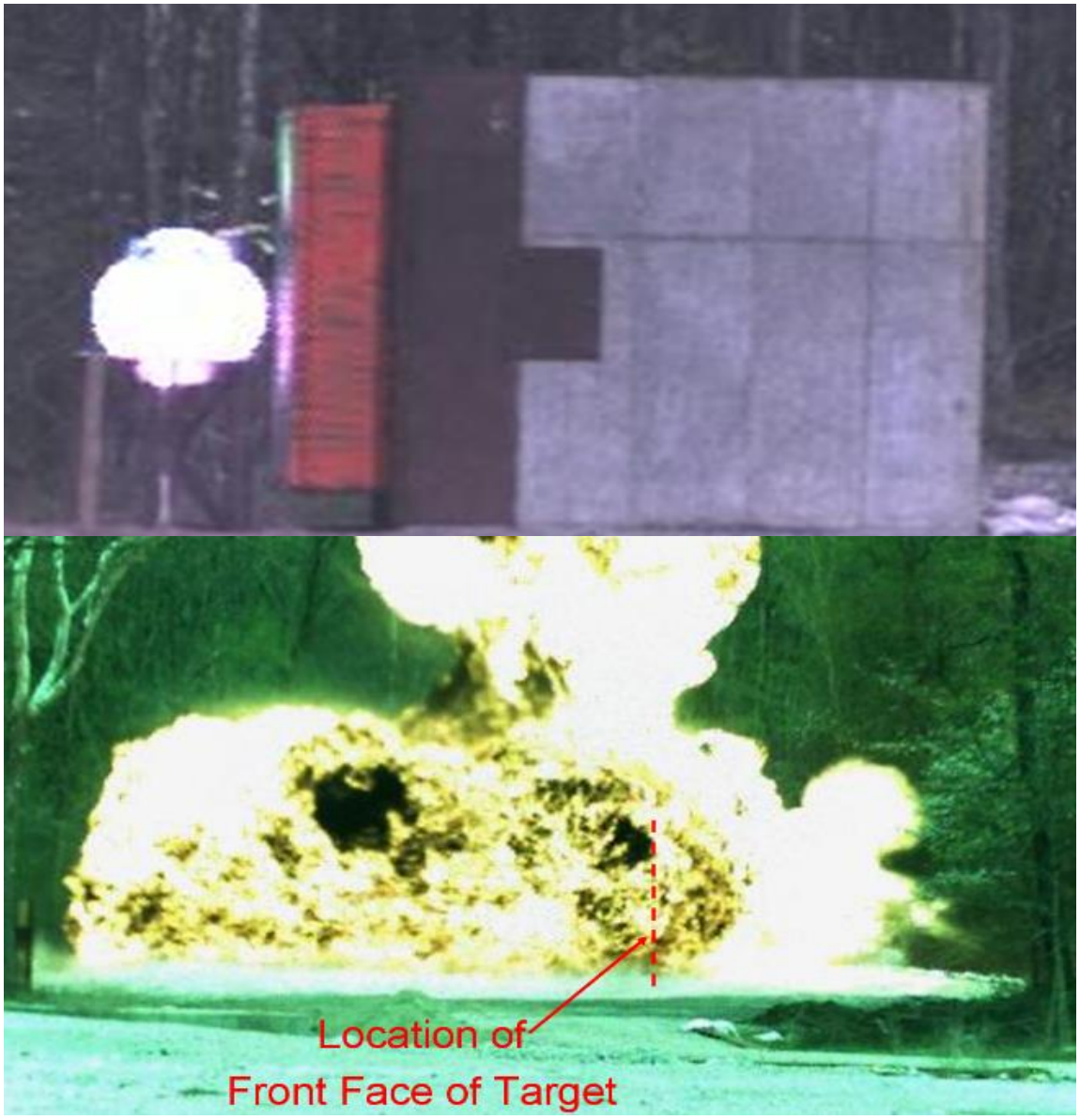


Fig. 2-20: Detonation at First Few Microseconds (top) and Detonation at Approximately 1 msec (bottom) (from Ray et. al, 2012)

The extremely fast detonation reaction rate results in an essentially instantaneous rise in pressure that is much higher than that from a deflagration. This incident wave, also defined as a "shock wave", is generated as the explosive is converted from its solid, liquid, or gas physical state into a hot, dense, and high-pressure gas equal to its speed of detonation that expands and decreases speed as it propagates outward from the source of the explosive into the surrounding air. Fig. 2-21 illustrates the differences between a deflagration pressure wave and a detonation shock wave.

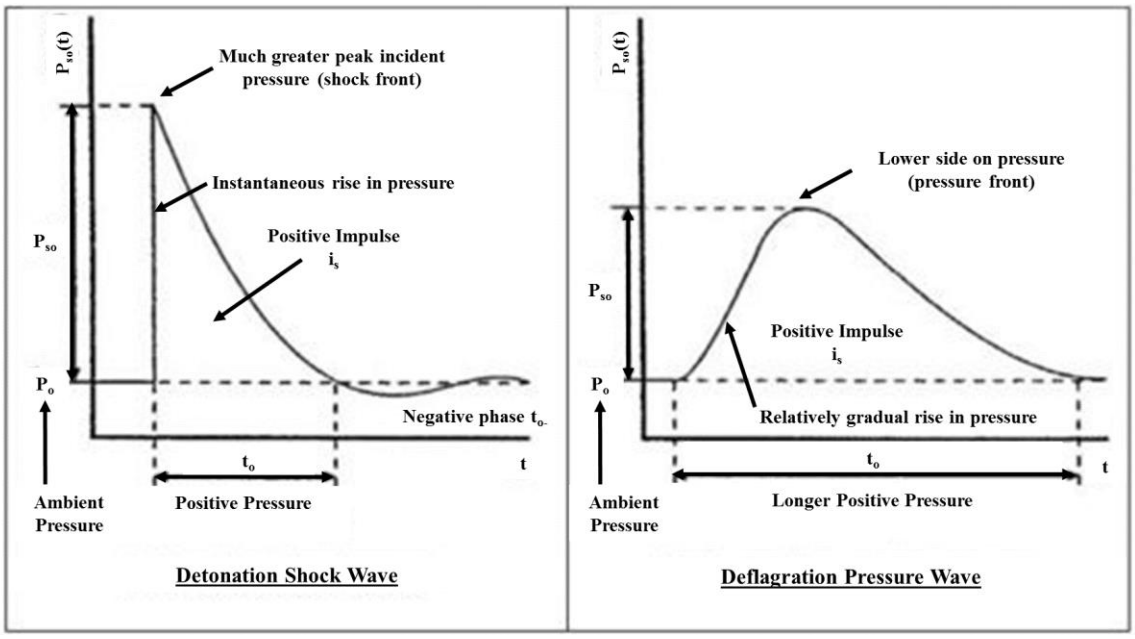


Fig. 2-21: Blast Wave (Detonation) vs. Pressure Wave (Deflagration) (modified from http://www.hysafe.net/wiki/BRHS/ChemicalExplosions)

When reflected off a surface, the incident wave becomes a reflected wave. Because the incident wave heats and compresses the air in the immediate vicinity of the reflected wave, the reflected wave travels through the heated and compressed air at a greater velocity than the incident wave. As shown in Fig. 2-22, the supersonic velocity of the shock wave at impact can cause a pressure enhancement up to 13 times the incident pressure.

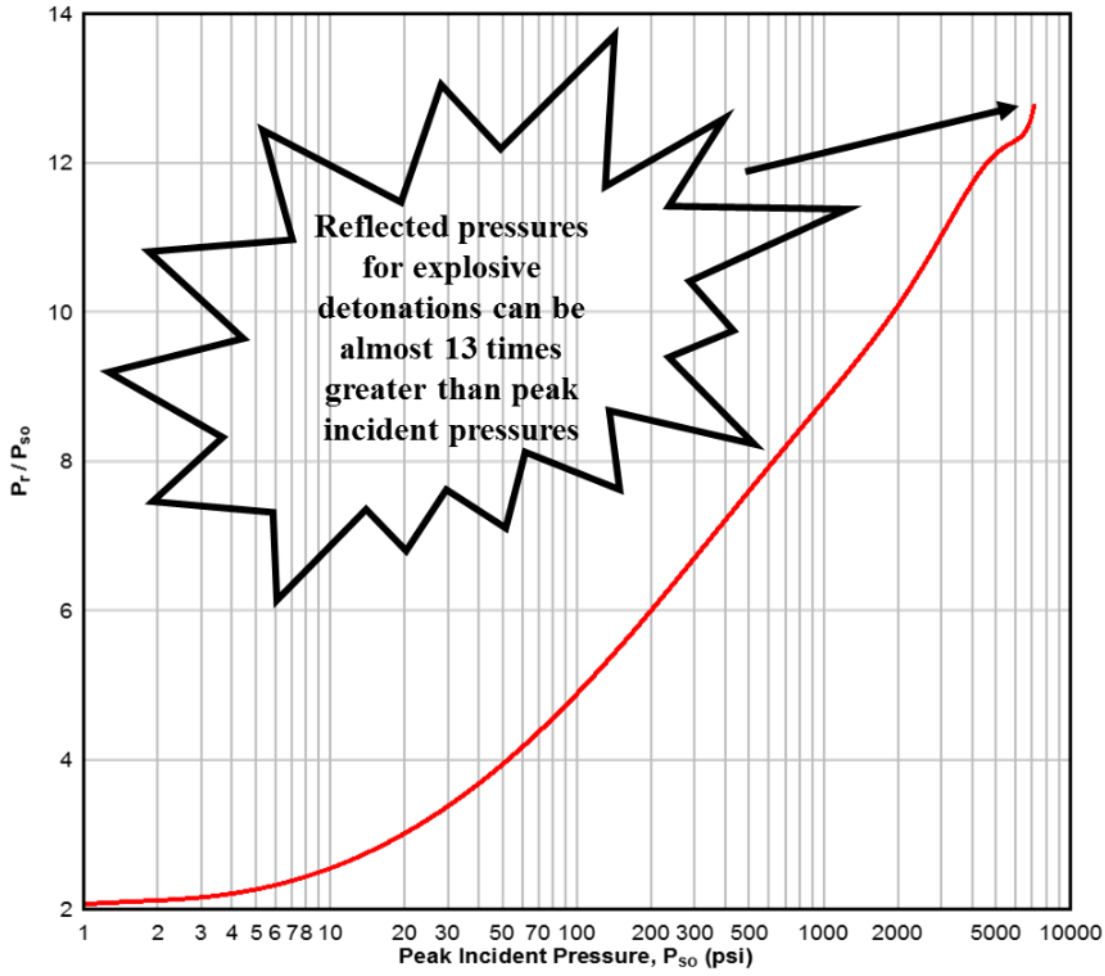


Fig. 2-22: Peak Incident Pressure vs. Ratio of Normally Reflected Pressure/Incident Pressure for a Free Air Burst (modified from UFC 3-340-02, 2008)

When a blast wave reflects off of a rigid surface such as the ground, as shown in Fig. 2-23, the reflected shock merges with the incident shock to produce the resultant shock, also known as the Mach front. The point at which the initial wave, the reflected wave, and the Mach front meet is called the triple point. This new wave is assumed to have a uniform pressure distribution. If the triple point is above the height of the target, the target experiences this uniform pressure distribution. In the event of an explosion close to the target, as would be likely for a riveted suspension bridge panel or riveted bridge connection, the triple point could hit below its full height. In this case, the Mach front uniform pressure impacts up to the triple point, resulting in two distinct pressure pulses above and below the triple point.

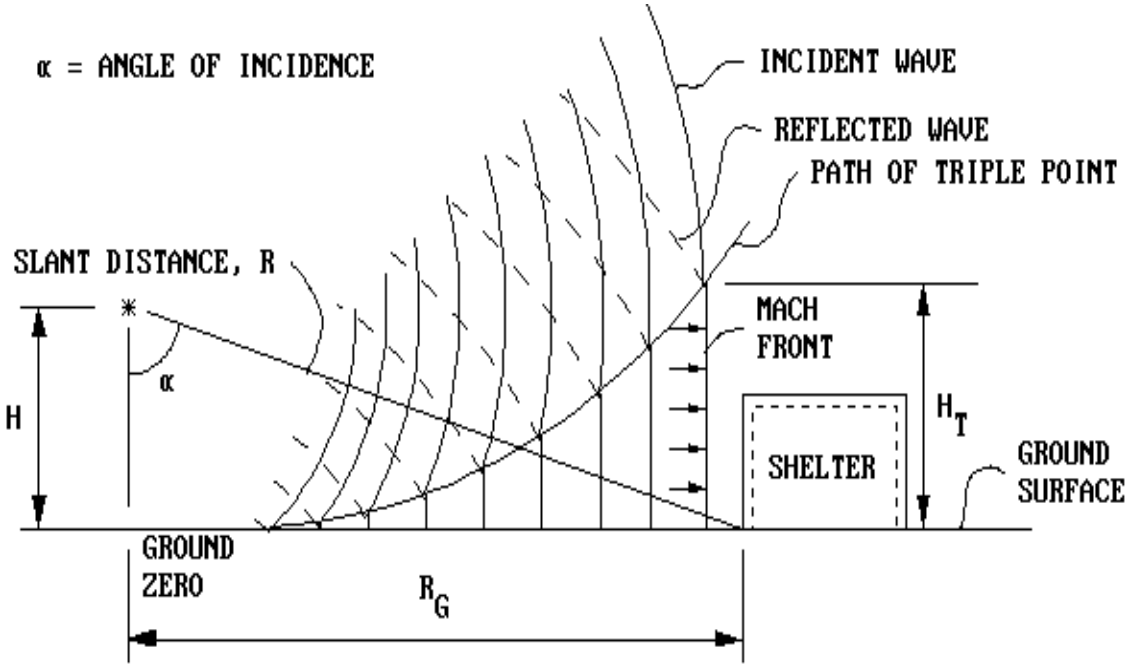


Fig. 2-23: Formation of the Triple Point (from UFC 3-340-02, 2008)

The most important blast load parameters needed to determine structural response are the peak overpressure, the net impulse, and fragments. Pressure-time histories, such as the airblast shockwave pressure-time history shown in Fig. 2-24, provide information regarding the peak overpressure and net impulse. Once explosives are detonated at time $t = 0$, there is a finite time, $t_a$ (arrival time) before the nearly instantaneous shock front impinges its target. This instantaneous rise in pressure above the ambient atmospheric pressure is referred to as the peak positive incident overpressure, the free-field overpressure, or side-on overpressure ($P_{so}$). Over a total positive phase duration of $t_o$, this front decays exponentially, typically within milliseconds, as the shock wave expands outward from the detonation source. This positive phase duration is the most destructive time for a structure as it experiences both the peak overpressure and the positive specific impulse, $i_s$. This impulse is determined by taking the area under the positive pressure curve. Shortly thereafter, the pressure immediately behind the front drops below the ambient pressure, $P_o$. This negative phase, over a time, $t_{o-}$, is analogous to a suction, which can reverse load on a structure, albeit at a significantly smaller magnitude than the positive phase. This suction often has the ability to pick up and move debris back toward the explosion source. While all of the airblast shockwave pressure-time histories will have this same idealized form, the values for each parameter change with explosive charge and standoff distance.

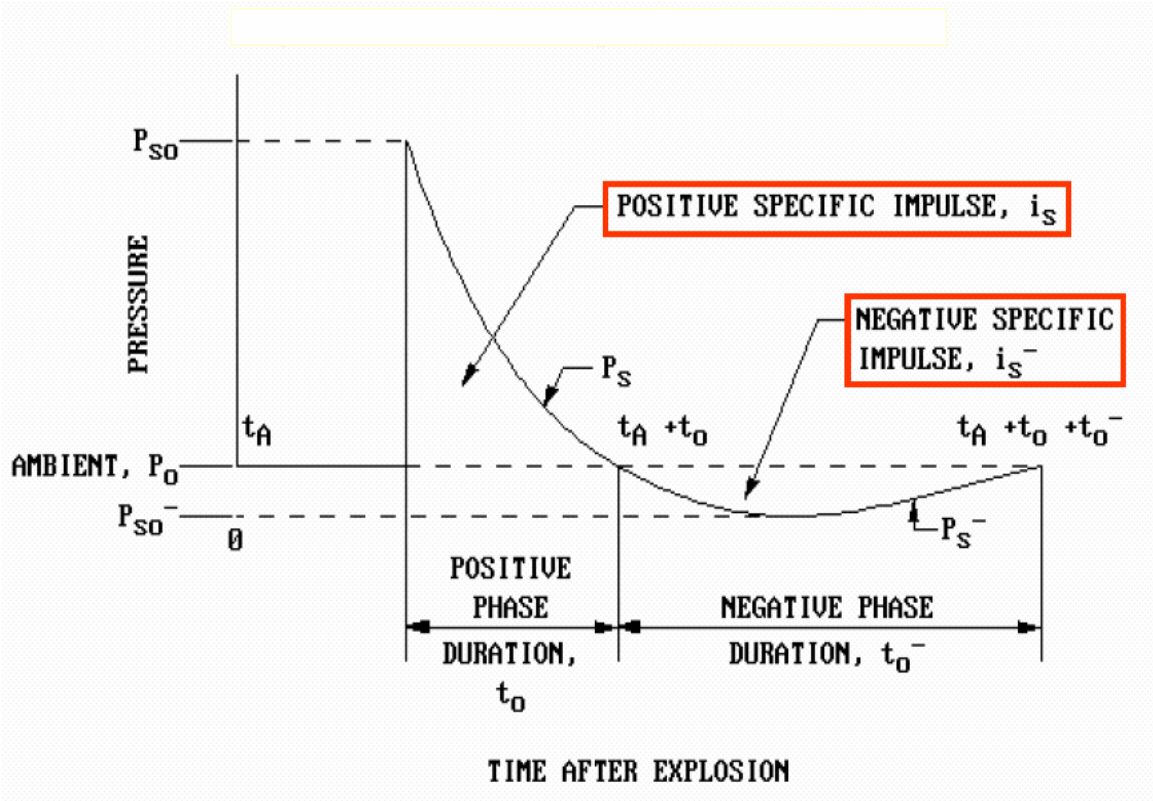


Fig. 2-24: Free-Field Pressure-Time History (from TM 5-855-1, 1986)

As discussed previously, reflected pressures are generated when an incident pressure wave reflects off of a surface that is not parallel with the direction of travel of the incident wave. With the reflected wave propagating through the heated and higher pressure air, the peak pressure is greater than the incident wave. Even so, the reflected pressure-time history has the same general shape as the free-field pressure-time history, with exact magnitudes governed by the magnitude of the incident wave and the angle of the inclined surface (location of the structure relative to the explosion source). A comparison of a typical reflected pressure-time history and free-field pressure-time history is shown in Fig. 2-25.

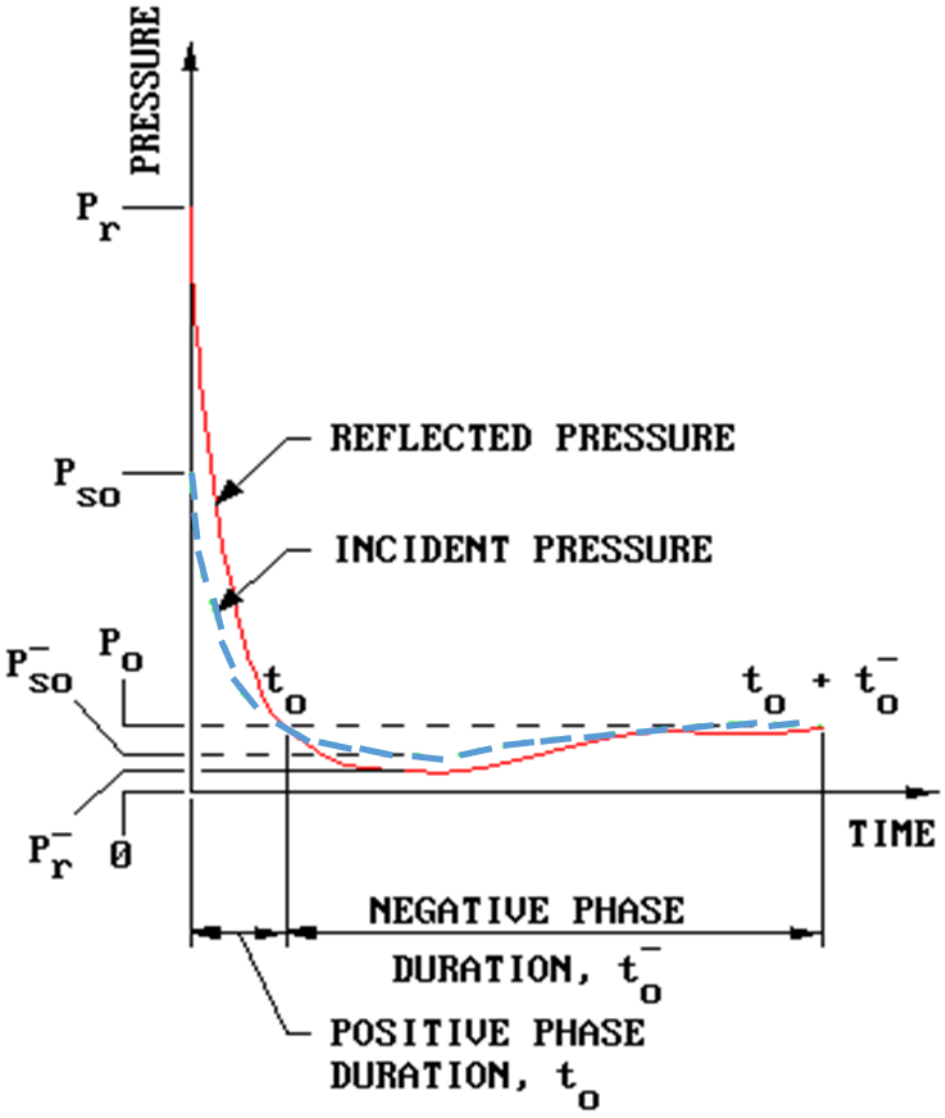


Fig. 2-25: Reflected Pressure-Time History compared to Free-Field Pressure-Time History (from UFC 3-340-02, 2008)

While there are any number of bulk explosive threat scenarios that could adversely affect riveted steel bridge panels and connections, there is a large amount of TNT experimental data available to characterize blast waves. Hence, it is common practice to

use empirically derived blast parameters in terms of an equivalent amount of spherical TNT. The TNT-equivalent charge weight dictates the amount of TNT required to produce a selected shock wave parameter magnitude (blast pressure, blast impulse, or explosion energy) equal to that produced by a unit weight of the explosive in question.

Blast load effects vary significantly based on the parameters of spherical TNT equivalent charge weight ($W$) and stand-off from the center of the explosive source ($R$). Once the equivalent spherical TNT charge weight ($W$) is determined (available readily on a number of publicized charts), scaling equations relate the parameters needed to define pressure-time history curves. The most common practice to scale high explosive blast parameters was originally formulated by B. Hopkinson in 1915 and independently by C. Cranz in 1926 in a law known as Hopkinson-Cranz or "cube-root" scaling. This law states that "self-similar blast waves are produced at identical scaled distances when two explosive charges of similar geometry and of the same explosive, but of different sizes, are detonated in the same atmosphere" (Conrath, 1999). Verified experimentally, this equation is not applicable for scaled distances less than 0.4 ft/lb$^{1/3}$. The scaled standoff ($Z$, in ft/lb$^{1/3}$) in Eq. (2-8) reveals the intensity of the blast load, which is in turn used to determine the parameters that define a blast wave.

$$Z = \frac{R}{W^{1/3}} \tag{2-8}$$

In lieu of using the Hopkinson-Cranz scaling, average pressure and impulse TNT equivalencies for a number of explosives are provided in various publications. While these are suitable for design, it is important to again be aware that actual equivalency varies as a function of geometry, target orientation, and atmospheric conditions. In the event an explosive is detonated on or near a perfect reflecting surface, a simple approach for hemispherical burst airblast parameters can be approximated by doubling the effective charge weight. When significant ground cratering is present, 1.8 is more realistic to use as a reflection factor (Conrath, 1999).

When a target is far away from the source, "cube-root" scaling is satisfactory. However, the concept behind this "cube-root" scaling is that the energy released from the center of the explosive source propagates with an expanding sphere of the shock wave. When the charge is close to the target, as would be the case when a riveted suspension bridge tower or riveted connection to a bridge is targeted, the shape of the charge defines the shock front. So while "cube-root" scaling would still be applicable for a spherical charge, a square root scaling might be used for an explosive cylindrical charge where the energy disseminates with an expanding cylindrical shock wave.

Once a scaled distance, *Z*, is determined, "spaghetti" charts from the UFC 3-340-02 are often used to determine the magnitude for the key shock wave parameters (combinations of peak side-on overpressures, positive phase durations and corresponding impulses and dynamic wind pressures) both positive and suction/negative, that define the loading on the target. These "spaghetti" charts earned their name because of the many highly nonlinear curves that appear on a single log-log graph, which resembles a plate of cooked spaghetti.

These charts were developed from a combination of experimental data and theoretical predictions. Charts are available for both spherical (Fig. 2-26) and hemispherical (Fig. 2-27) explosions. Other shaped charges fail to give pressure distributions with rotational symmetry; thus, information in design manual for other shapes should be used with caution for close-in explosions (Conrath, 1999).

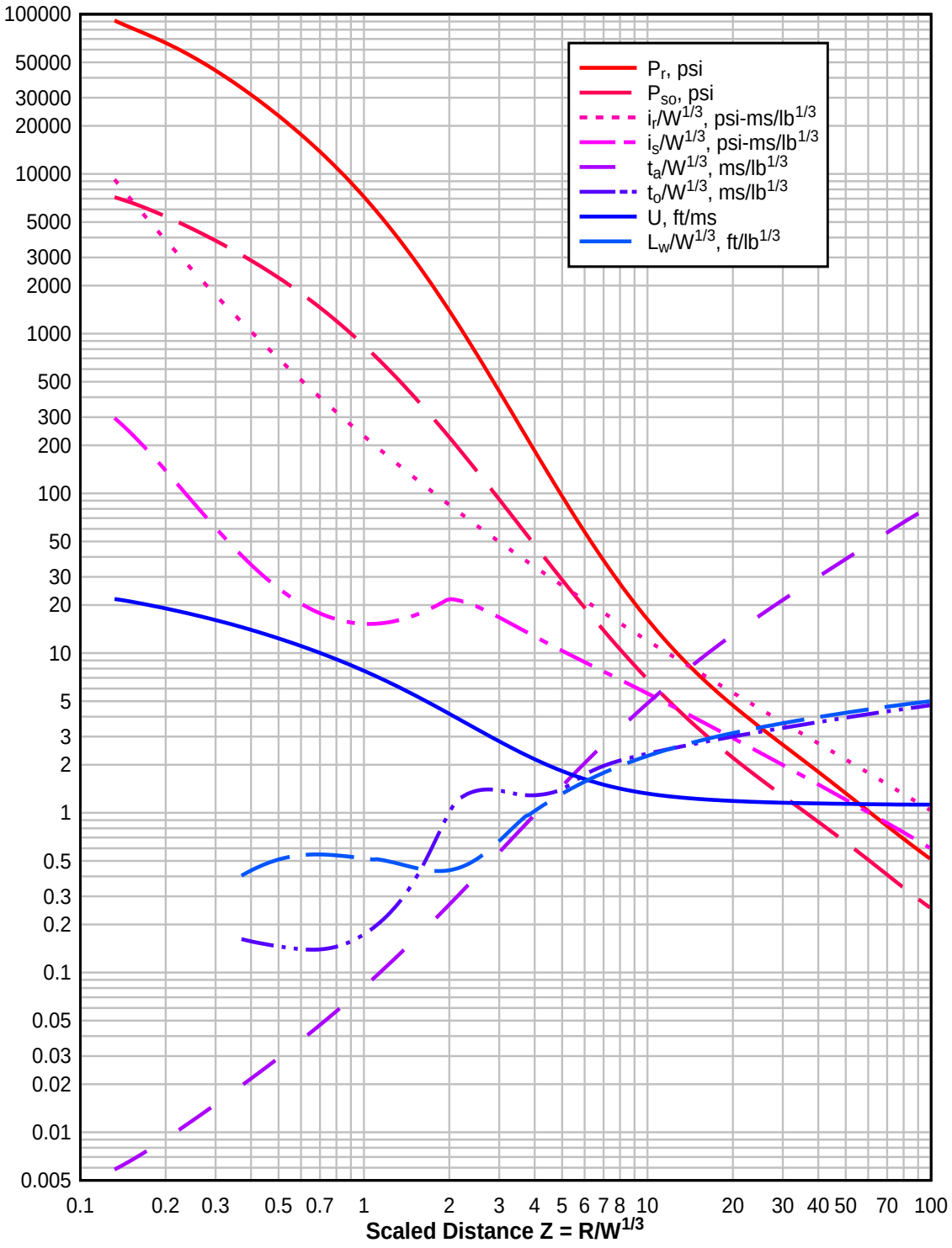


Fig. 2-26: Positive Phase Shock Wave Parameters for Spherical TNT Explosion in Free Air at Sea Level (from UFC 3-340-02, 2008)

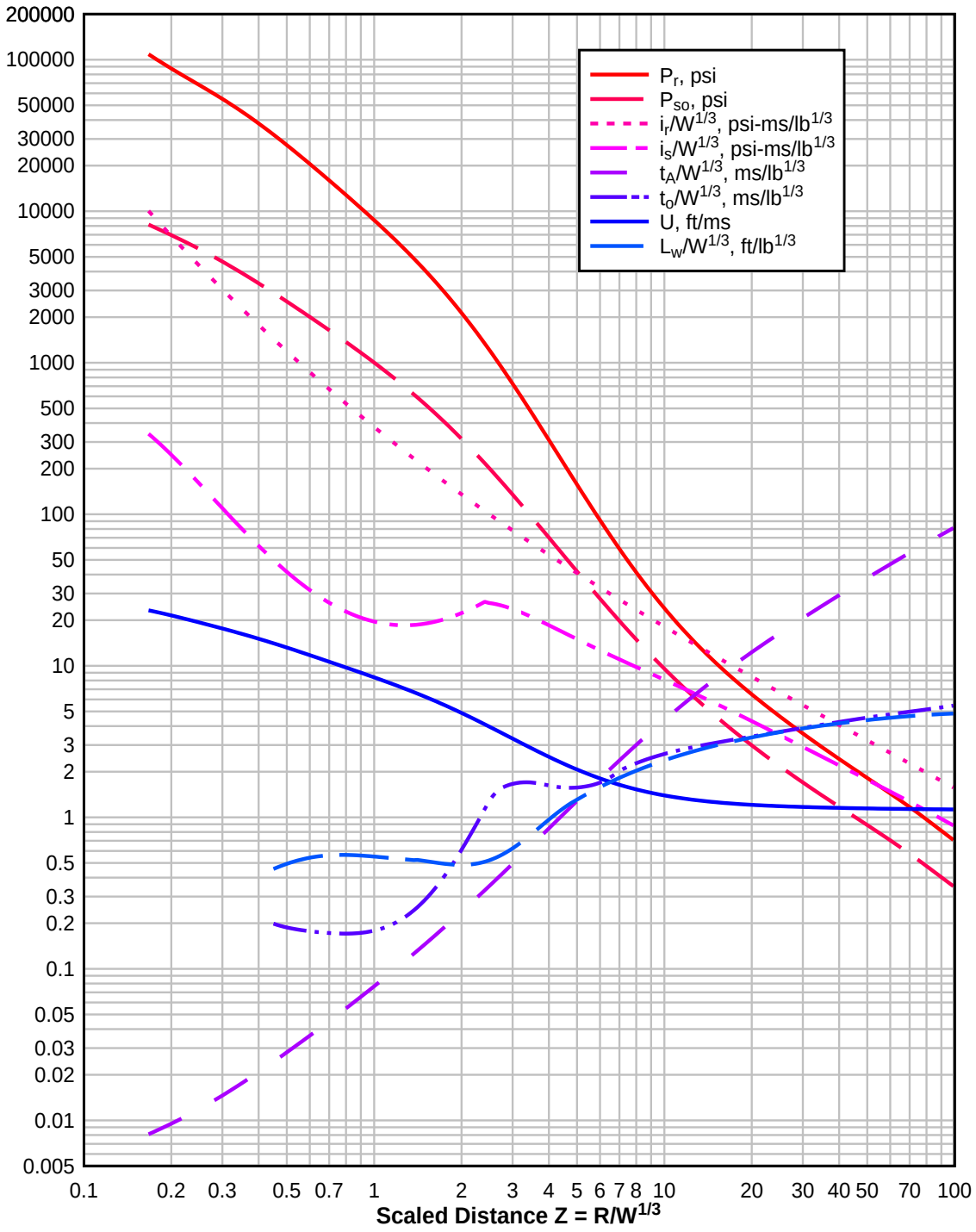


Fig. 2-27: Positive Phase Shock Wave Parameters for a Hemispherical TNT Explosion in Free Air at Sea Level (from UFC 3-340-02, 2008)

As indicated previously, a third major consideration as it pertains to blast effects is the loading that can result from fragments. Some fragments originate from the casing of the explosive charge, while others are generated from debris or from damaged structural components. When near a target, blast waves travel at a greater velocity than fragments. Coupling the two could potentially expose the target to an amplified impulse relative to the blast acting alone. Conversely, when further away from the target, fragments may arrive before the blast wave. Many times, designers choose to ignore fragment loads because overpressure and impulse often dominate the response, and most threat scenarios involving terrorist attacks with large explosives rely on VBIEDs. VBIEDs are likely to come from thinly sheeted trucks, and fragments from such a scenario are expected to be inconsequential for structural response. Exceptions include large masses thrown from the VBIED (e.g. axle, engine block, or transmission). Cased military weapons can also produce a significant fragment load on structures, but such weapons are typically not considered in terrorist threat scenarios because they require access to such weapons and highly sophisticated personnel to properly execute them. Even when fragment loads occur, they can be very difficult to model and quantify because of their irregular shape and mass distribution. The research presented in this dissertation will specifically focus on the response of riveted connections under high loading rates. Fragment loading is not an element of this research.

## 2.8 Structural Response to Blast Loads

As described in Section 2.7, a blast load is unique when compared to conventional loads. It is time dependent, acts over a very short duration, and could have pressures that are extremely high. Thus, not only are special criteria required to determine the load on a structure, determining structural response also requires analysis methods that are not typically employed for conventional loads. Analysis must consider dynamic structural response, inertial effects, and ineleastic material response under high strain rates. An increase in material strength under high loading rates improves a material's structural resistance. A look at previous incidents involving terrorist attacks against buildings and the response of bridges to cased military weapons provided some of the initial understanding regarding how bridges might respond to a variety of terrorist threats (Williamson, 2010). Depending on the location of a blast relative to a bridge, uplift forces beneath a bridge deck could cause structural components to be loaded in a direction for which they are not otherwise designed. Tensile stresses can occur under compressive loadings and vice versa. Thus, it is both a material's plastic (permanent) deformation ability to absorb explosion energy and its position relative to the blast that are critical to determine the component/system/material strength and response.

Part of the complexity in analyzing response to blast is due to non-linear inelastic material behavior. A material's behavior is usually predicted through determination of its mechanical properties, such as its stress versus strain relationship. The stress versus strain relationships for common grades of steel are shown in Fig. 2-28. Strain energy, *U*, which

is also often referred to as internal work, is the energy per unit volume stored in a deformed material. Graphically recognized as the area under the true stress-strain curve, with units of in-lbf/in$^3$, it is the strain energy of a member that dissipates the kinetic energy of the blast. Physically, as a structural member is stressed into its inelastic region, plastic hinges develop within the member and absorb the blast energy. As a result, a material's ability to achieve large deformations is a valuable characteristic of blast resistance.

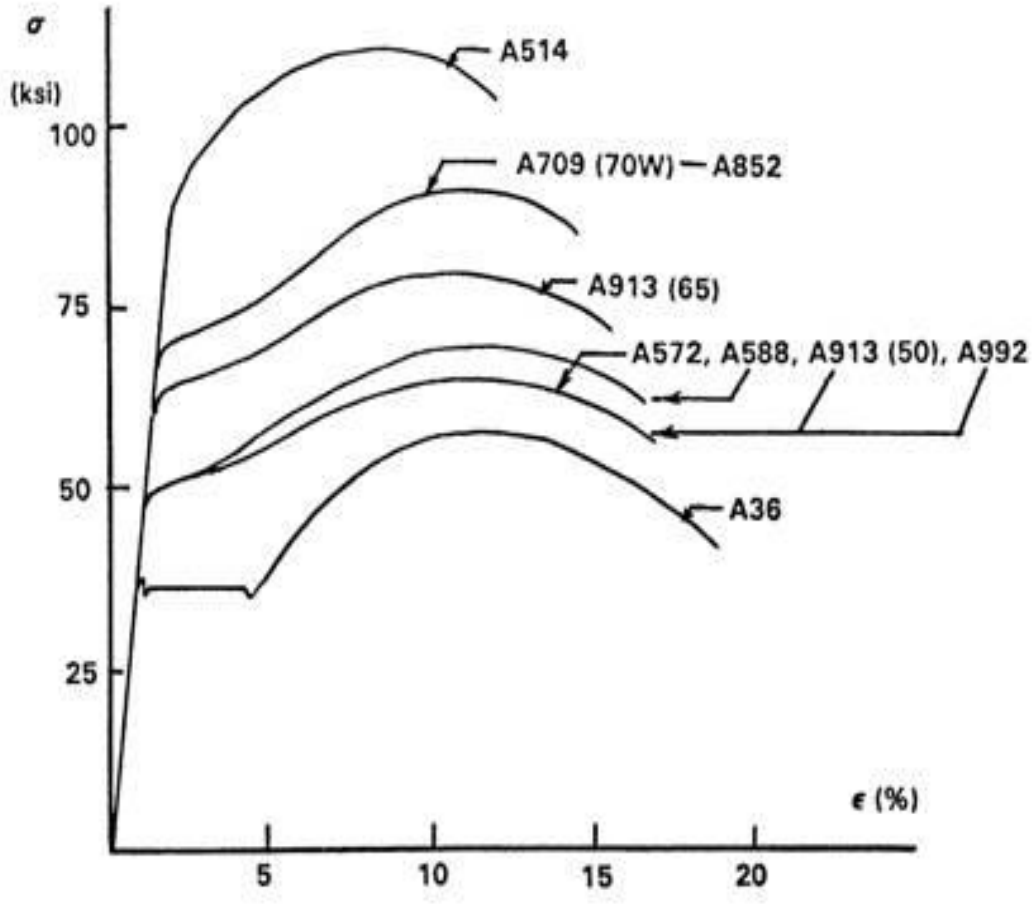


Fig. 2-28: Engineering Stress-Strain Curves for Different Steel Grades (from www.metalpass.com)

The ductility of low-carbon and medium-carbon steels such as A36, A572, and A992, allows them to achieve large strains prior to rupture. Higher-strength steels generally have less ductility than steels with lower strengths and may have less resistance to blast loads. While the higher-strength steels will have greater elastic resistance, defined as the area under the stress versus strain curve up to yield, internal resistance continues to increase as plastic regions are formed in a structural member. As a high-strength material begins to yield, the yield region becomes highly nonlinear. After achieving greater stress under additional load, a high-strength material typically has brittle fracture problems. Lower carbon steels, however, have long, flat yield plateaus after the defined yield point is reached. While the fracture strain shown for A36 and A992 steel are shown at approximately 20% in Fig. 2-28, testing reveals that the percent elongation reaches up to 40%, providing a significantly larger amount of strain energy capacity than some of the higher-strength steels. The inelastic deformation of structural members dissipates energy from a blast. This suggests that lower carbon steels are often better suited for blast-resistant design because they deform well beyond the elastic limit without rupturing.

When predicting the material properties for steel response, it is critical to know the true static properties of the material. Specifications provide various minimum and maximum requirements on a number of chemical and mechanical properties. For example, A36 steel has a required minimum yield strength of 36,000 psi and ultimate strength in the range of 58,000 – 80,000 psi (ASTM A36, 2014). Manufacturers in practice usually go well above the minimum requirements dictated by ASTM. In fact, the average yield strength is

typically 25% higher than the minimum required yield strength, and the typical actual tensile strength is 10% higher than minimum required tensile strengths (Engelhardt, 2015). The 2010 AISC Seismic provisions refers to this higher yield strength and tensile strength as expected material strengths. As shown in Table 2-7, the expected yield strength of an A36 plate is 1.3 times higher than the specified minimum yield and 1.2 times higher than the specified ultimate tensile strength. In Table 2-7, the $R_y$ term is the ratio of the expected yield stress to the minimum yield stress, while $R_t$ is the ratio of expected tensile strength to the specified minimum tensile strength. The UFC 3-340-02 (2008) makes a much broader recommendation for strength increase factor, and simply recommends using a 1.1 strength increase factor for structural steels with a specified static yield strength of 50 ksi or less. For higher-strength steels, the UFC recommends ignoring any increase in ultimate strength because the average increase is likely below 5 percent (UFC 3-340-02, 2008).

Table 2-7: Expected Material Strengths for Different Steels (from AISC Seismic Provisions, 2010)

| **Application** | **Ry** | **Rt** |
|---|---|---|
| Hot-rolled structural shapes and bars: | | |
| *ASTM A36/A36M | 1.5 | 1.2 |
| *ASTM A1043/1043M Gr. 36 (250) | 1.3 | 1.1 |
| *ASTM A572/572M Gr. 50 (345) or 55 (380), ASTM 913/913M Gr. 50 (345), 60 (415), or 65 (450), ASTM A588/A588M, ASTM A992/A992M | 1.1 | 1.1 |
| *ASTM A1043/A1043M Gr. 50 (345) | 1.2 | 1.1 |
| *ASTM A529 Gr. 50 (345) | 1.2 | 1.2 |
| *ASTM A529 Gr. 55 (380) | 1.1 | 1.2 |
| Hollow structural sections (HSS): | | |
| *ASTM A500/A500M (Gr. B or C), ASTM A501 | 1.4 | 1.3 |
| Pipe: | | |
| *ASTM A53/A53M | 1.6 | 1.2 |
| Plates, Strips and Sheets: | | |
| *ASTM A36/A36M | 1.3 | 1.2 |
| *ASTM A1043/1043M Gr. 36 (250) | 1.3 | 1.1 |
| *A1011/A1011M HSLAS Gr. 55 (380) | 1.1 | 1.1 |
| *ASTM A572/A572M Gr. 42 (290) | 1.3 | 1.0 |
| *ASTM A572/A572M Gr. 50 (345), Gr. 55 (380), ASTM A588/A588M | 1.1 | 1.2 |
| *ASTM 1043/1043M Gr. 50 (345) | 1.2 | 1.1 |

Not only do steel members typically require an adjustment in their strength values due to steel suppliers surpassing minimum standards, but steel members also are found to be sensitive to rapidly applied loads. Under impulsive loadings associated with blast events, the strain rate, defined as the rate of deformation as a function of time, can drastically change the dynamic mechanical properties of steel and its corresponding structural behavior. Blast loads especially produce very high strain rates (greater than $10^2$/s) in comparison to conventional static strain rates (less than $10^{-1}$/s). Ranges for dynamic modes of loading are shown in Table 2-8.

Table 2-8: Dynamic Modes of Loading vs. Strain Rate (portions from Impact Engineering by Hayashi and Tanaka, 1988)

| **Strain Rate (1/s)** | **$10^{-5} – 10^{-1}$** | **$10^{-1} – 10^{1.5}$** | **$10^{1.5} – 10^{4}$** | **$> 10^{4}$** |
|---|---|---|---|---|
| **Loading Mode** | Static or quasi-static | Dynamic | Impact | Hyper velocity impact |
| **Examples** | Dead or live load on structure | Impulse pressure effects on high-speed craft | Explosion, ship collision | Bombing |

Under high rates of dynamic loading, steel materials achieve an enhanced strength that boosts their ability to resist loads. As the material is loaded rapidly, it cannot deform at the same rate at which the load is applied. A greater load is required to produce the same

deformation than at a lower strain rate. For most steels, the modulus of elasticity and ultimate strain of steel are largely unaffected; however, a high strain rate creates an increase in the stress level at which both the yield stress occurs (up to 35%) and the ultimate stress occurs (up to 10%). These large increases are too significant to be ignored when predicting response. The increase in strength associated with the rapidly applied load is known as the dynamic increase factor (DIF) and is expressed numerically as the ratio of dynamic-to-static stress. A typical change in the stress versus strain relationship for steel due to a change in strain rate is demonstrated in Fig. 2-29.

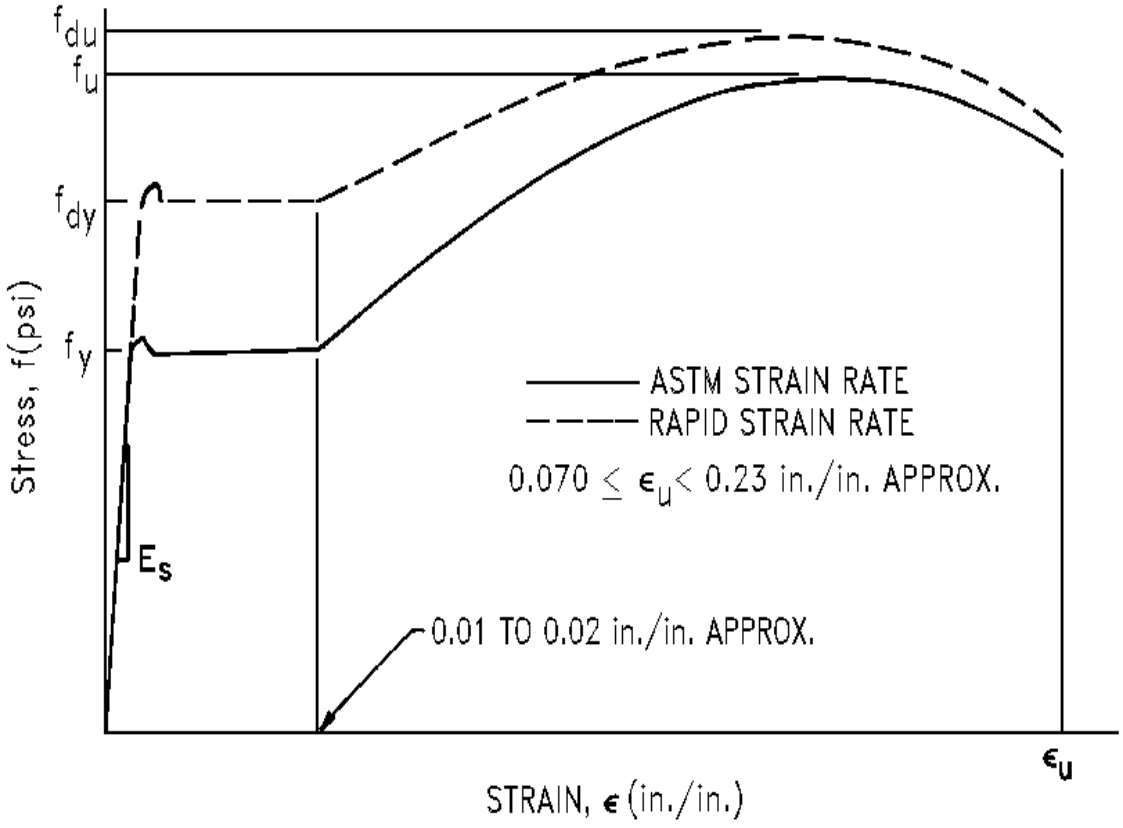


Fig. 2-29: Typical Strain Rate Impacts on Steel (from UFC 3-340-02, 2008)

The degree of enhanced strength depends on the strain rate, the type of stress, and the strength of the material. As Fig. 2-30 demonstrates, the greater the strain rate, the greater the effect on yield strength DIF.

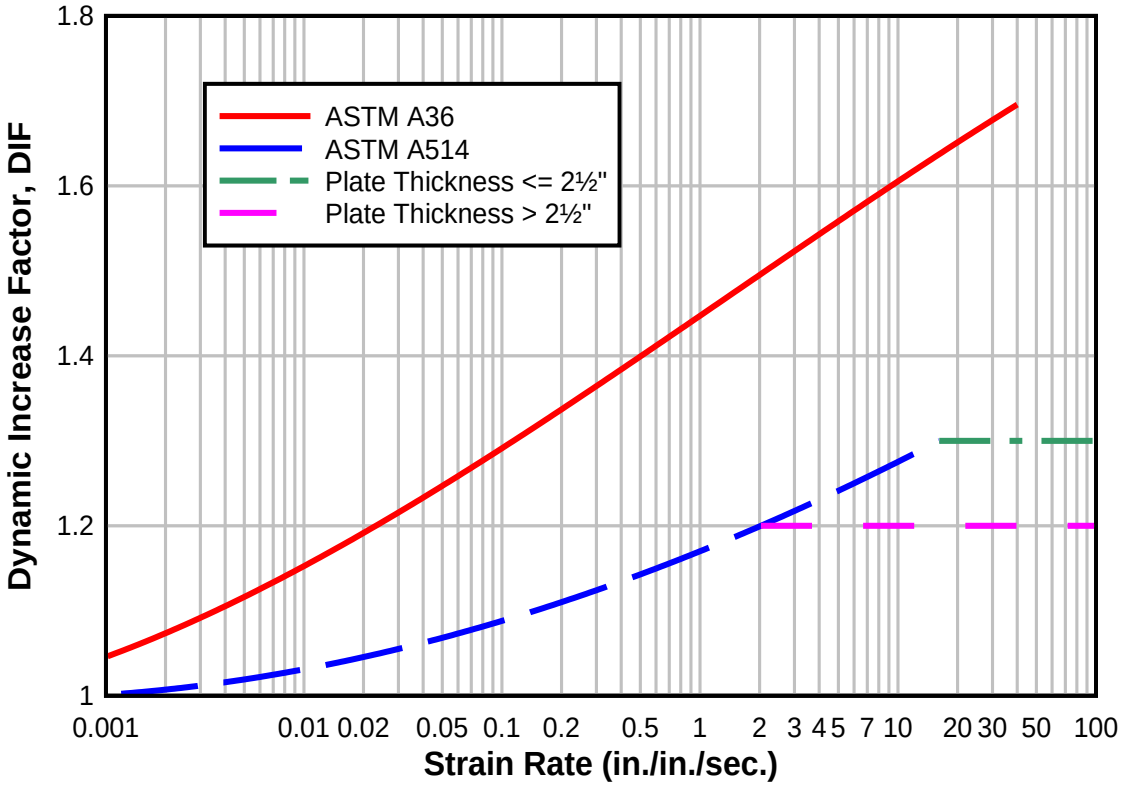


Fig. 2-30: Yield Stress DIF as a Function of Strain Rate (from UFC 3-340-02, 2008)

For ultimate strength DIF values, the values are independent of the low pressure or high pressure categories of Table 2-10. According to UFC 3-340-02, and as Table 2-9 shows, there is simply one DIF provided for ultimate strength based on material type only.

Regarding stress type, the DIF differs because the peak value for one failure mode (e.g., flexural stress) is different than the peak value for another (e.g., shear). Flexural failures are considered a more ductile failure, allowing greater enhancement, while a more brittle shear failure requires conservativism. As Table 2-10 shows, for specific strain rates, the UFC provides DIF values for specific structural steels and different failure modes. Furthermore, lower-strength materials see a larger strength enhancement from dynamic effects.

Table 2-9: Ultimate Strength DIF for Different Steels (from UFC 3-340-02, 2008)

| **Material** | ***C*** |
|---|---|
| **A36** | 1.10 |
| **A588** | 1.05 (Estimated) |
| **A514** | 1.00 |

Table 2-10: Yield Strength DIF at Specific Strain Rates for Different Failure Modes (from UFC 3-340-02, 2008)

| **Material** | **Bending** | | **Tension or Compression** | |
|---|---|---|---|---|
| | **Low Pressure** ($\dot{\varepsilon}$ = 0.10 in./in./sec) | **High Pressure** ($\dot{\varepsilon}$ = 0.30) | **Low Pressure** ($\dot{\varepsilon}$ = 0.02) | **High Pressure** ($\dot{\varepsilon}$ = 0.05) |
| **A36** | 1.29 | 1.36 | 1.19 | 1.24 |
| **A588** | 1.19 (est.) | 1.24 (est.) | 1.12 (est.) | 1.15 (est.) |
| **A514** | 1.09 | 1.12 | 1.05 | 1.07 |

## 2.9 Material Testing and Constitutive Models for High Strain Rates

Often, high strain-rate material testing is performed using the Split Hopkinson Pressure Bar test. As demonstrated in Fig. 2-31, this test involves four long pressure bars (striker, incident, transmission, and throw off/stop). The bar material is specifically selected to remain elastic. With the tested material specimen loaded between the transmission and incident bars, the striker bar, which is propelled by a highly compressed gas gun, strikes the incident bar generating a wave propagation, known as the incident wave. A portion of the stress pulse transmits through the specimen (transmitted wave) and into the transmission bar. The material specimen deforms, and the stop bar absorbs the impact of the transmission bar. This test allows the specimen to be taken to large strains. Instantaneously, another portion of the stress pulse is reflected back (reflected wave) to the incident bar as a tensile stress pulse. Strain gages capture the stress waves in both bars and measure the strain duration and amplification in the bars at a given strain rate. The reflected and transmitted waves are proportional to the specimen's strain rate and stress, respectively, while the strain is determined by integrating the strain rate. The material specimen stress-strain properties are determined from a compilation of the data from the incident and transmission bars. Hopkinson Bar Tests are often conducted under varying temperatures by simply enclosing the tested material specimen within an oven or electric resistance furnace for several minutes prior to testing (Campbell and Ferguson, 1970). With modifications, this technique is effective for compression, tension, and torsion testing. The sole focus of the research presented in this dissertation was on the performance of a variety

of riveted connections subjected to high loading rates that put the rivets in shear. The laboratory testing done to date with respect to A502 Grade 2 rivets, described in depth in Chapter 3, did not include the Split Hopkinson Pressure Bar.

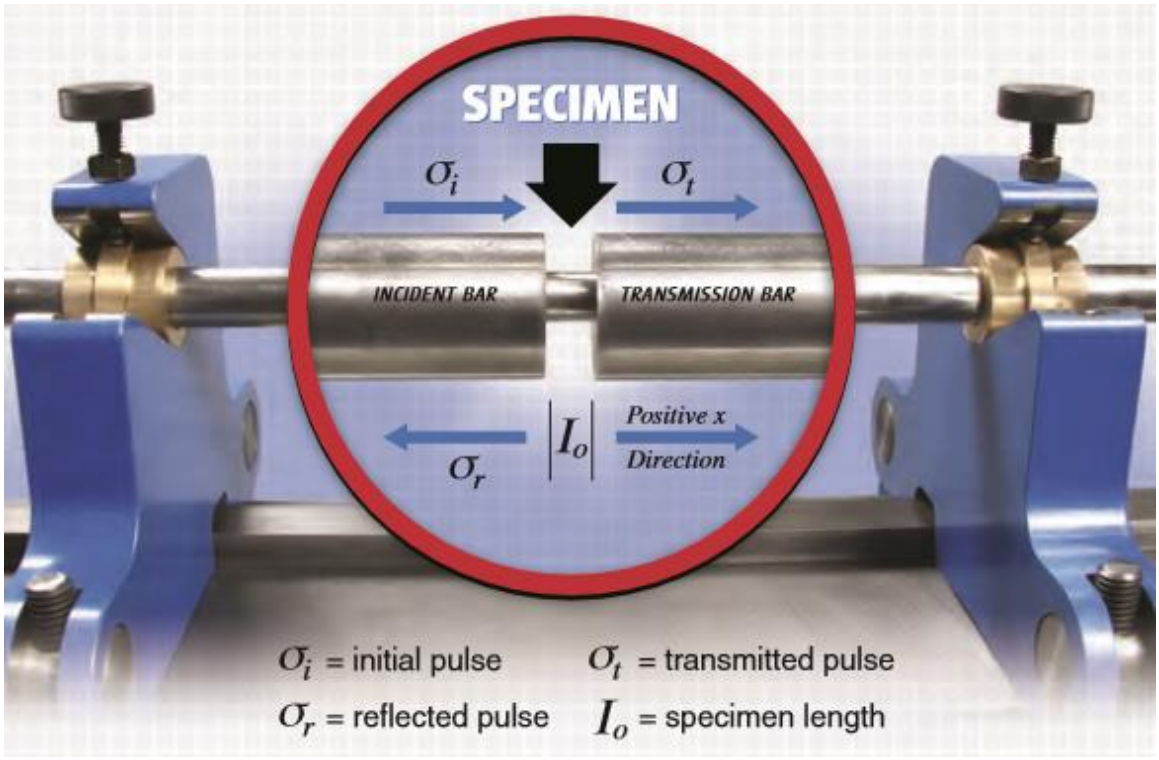


Fig. 2-31: Dynamic Hopkinson Bar Testing (from relinc.net)

In order for engineers and scientists to utilize tested material specimens in other applications, a constitutive model is often used to characterize the behavior of the material. Several empirical and semi-empirical models exist in the literature that capture the strain-rate behavior of metals. In fact, some models include both strain-rate and temperature effects. Modern computer programs have incorporated many of these constitutive models

in their analysis codes providing results that are often limited only by the accuracy of the material characteristics input by the user.

One of the most popular constitutive models used to describe the response of steel and other ductile metals at high strain rates is the Johnson-Cook model. The Johnson-Cook model is purely empirical and is incorporated and widely used within most commercial finite elements packages. The model (Johnson and Cook, 1983) states that the equivalent von Mises flow stress, $\sigma_Y$, is given by Eq. (2-9):

$$\sigma_Y = (A + B(\varepsilon_{eff}^p)^N)(1 + C\ln\dot{\varepsilon})(1 - (T_H)^M) \tag{2-9}$$

where: $A$ = yield stress of the material obtained from experiment,

$B$ = hardening constant obtained from experiment,

$\varepsilon_{eff}^p$ = effective plastic strain,

$N$ = hardening exponent obtained from experiment,

$\dot{\varepsilon}$ = normalized strain rate,

$C$ = strain rate constant obtained from experiment,

$M$ = thermal softening exponent, and

$$T_H = \frac{T - T_{ref}}{T_{melt} - T_{ref}} \tag{2-10}$$

where: $T$ = temperature of material,

$T_{ref}$ = room temperature, and

$T_{melt}$ = melting temperature.

As demonstrated in both Eqns. (2-9) and (2-10), the model consists of both material specific characteristics and different experimentally obtained parameters. This makes the model extremely useful in that it can be calibrated experimentally to specific materials. It captures strain hardening through $B$ and $N$, strain rate effects logarithmically through $\dot{\varepsilon}$, and thermal softening through $M$. It is phenomenological in that it is not based on traditional plasticity theory. Tested parameters for A36 hot rolled steel are shown in Table 2-11 (Schwer, 2007):

Table 2-11: Johnson-Cook Parameters for A36 Steel

| ***A* (ksi)** | ***B* (ksi)** | ***n*** | ***C*** | $\dot{\varepsilon}_p^*$ | ***M*** |
|---|---|---|---|---|---|
| 41.5 | 72.54 | 0.228 | 0.017 | 1.0 | 0.917 |

Most software packages have also included the Johnson and Cook (1985) expansion of their basic model. This expanded model includes a cumulative-damage fracture model that accounts for stress triaxiality ( $P / \sigma_{eff}$ ), strain rate, and local heating (Schwer, 2007). This model, as shown in Eq. (2-11), requires five additional material model parameters.

$$\varepsilon^F = (D_1 + D_2 \exp(D_3 \frac{P}{\sigma_{eff}}))(1 + D_4 \ln \dot{\varepsilon})(1 + D_5 T_H) \quad (2\text{-}11)$$

where: $\varepsilon^F$ = fracture strain,

$D_{1\text{-}5}$ = various material model parameters obtained from experiment,

$\sigma_{eff}$ = effective stress, and

$P$ = mean stress (pressure).

Eq. (2-11) allows the computation of damage through the damage parameter $D$, in Eq. (2-12). Once the damage parameter reaches unity, failure occurs, and the failed element is deleted.

$$D = \sum \frac{\Delta \varepsilon_{eff}^p}{\varepsilon^F} \text{ (failure occurs when } D = 1) \quad (2\text{-}12)$$

Another methodology to capture the differences in dynamic and static load effects is the Cowper Symonds model. In 1957, Cowper and Symonds proposed the following constitutive equation (Eq. (2-13)) to calculate the dynamic yield strength of a material based on the strain rate ($\dot{\varepsilon}$) and two empirical coefficients ($C$, $q$) that have been determined through testing:

$$\sigma_{Yd} = \sigma_Y + \sigma_Y \left(\frac{\dot{\varepsilon}}{C}\right)^{1/q} \quad (2\text{-}13)$$

Unlike the logarithmic dependence of the Johnson-Cook model, the Cowper Symonds equation has an exponential strain rate dependence. Table 2-12 shows various coefficients for the Cowper Symonds equation.

Table 2-12: Cowper-Symonds Coefficients

| **Test** | ***C* (1/s)** | ***q*** | **Reference** |
|---|---|---|---|
| Mild steel under uniaxial tension with mild strains | 40.4 | 5 | Cowper & Symonds (1957) |
| High tensile steels under compression | 3200 | 5 | Paik & Chung (1999) |
| Mild Steel under compression Split Hopkinson Pressure Bar tests | 844 | 2.207 | Marais et al. (2004) |
| Mild steel under uniaxial tension with large strains | 802 | 3.585 | University of Liverpool ref. by Abramowicz and Jones (1986) |
| Mild steel square tubes axially crushed | 6884 | 3.91 | Abramowicz and Jones (1986) |
| Square tubular steel beams subjected to transverse blast loads | 844 | 2.207 | Jama, Bamback, Nurick, Grzebieta, and Zhao (2012) |

The original Cowper Symonds (1957) parameters ($C$ = 40.4 $s^{-1}$ and $q$ = 5) were obtained from dynamic uniaxial tests having small strains that approached the yield strain. Similar dynamic uniaxial testing done at the University of Liverpool for large strains determined drastically different coefficients with $C$ = 802 $s^{-1}$ and $q$ = 3.585 (Abramowicz

and Jones, 1986). Comparing large strain testing coefficients reveal a large difference in recommended $C$ coefficient values while the $q$ coefficient values are comparatively close. Differences in coefficient values are likely due to differences in material composition and testing techniques. While unable to find any literature regarding the behavior of steel rivets under high loading rates outside of the testing described in Chapter 3 of this dissertation, careful study of the constitutive models used for the behavior of other ductile steel provides valuable insight into likely coefficients to examine with regard to rivets under high loading rates.

## 2.10 Literature Review Summary

The literature review presented for this dissertation provides a summary of the history of the use of rivets from approximately 3000 B.C. to today. In addition, there is discussion of the challenging riveting process, resulting in the construction industry transitioning to high-strength bolts in the 1950s. Following an in-depth look at the structural behavior of rivets and previously completed rivet experimental testing, this chapter provides an overview of blast loads and the structural response of steel to this physical phenomenon. The intent of this chapter was to provide a technical foundation upon which to build with the research from this dissertation. The next two chapters repeatedly depend on the knowledge gained from this literature review in order to develop a rivet model using a nonlinear transient dynamic finite element analysis software package, provide

recommendations with respect to constitutive modeling within the software package, and apply the developed model towards an untested practical problem.

# Chapter 3: Modeling Simple Riveted Connections

*"A good plan violently executed now is better than a perfect plan executed next week."*

*"A good solution applied with vigor now is better*

*than a perfect solution applied ten minutes later."*

*-George S. Patton, 1944*

## 3.1 An Introduction

From 1860 until the late 1950s, rivets dominated as the construction industry's primary fastener of choice for bridge construction. Furthermore, as highlighted throughout the Chapter 2 Literature Review, rivets were also the most studied structural connection. However, the focus of this past research was on behavior in tension, shear, a combination of shear and tension, and fatigue. No attention was given to the behavior of riveted connections under blast loads, as the need to conduct such testing was previously nonexistent. The steady increase in terrorist attacks and fatalities since 1970 has changed the testing landscape. The Mineta Transportation Institute's most recent report discussing long-term trends in attacks on public surface transportation reveals that 65% of attacks worldwide were bombings (Jenkins, 2016). With bridges such as the five mile Mackinac Bridge in Michigan shown in Fig. 3-1 and others mentioned throughout this dissertation

being held together with millions of rivets (4,851,700 steel rivets for the Mackinac Bridge) (Steinman and Nevill, 1957), an understanding of their behavior under high loading rates is critical. This Mineta Transportation Institute report in combination with the data compiled and summarized in the rest of Chapter 1 have led to a rise in interest within the engineering community to gain an understanding of connection behavior subjected to blast loads.

Fig. 3-1: Construction of the Five Mile Mackinac Riveted Bridge (from Mulcahy, 2007)

This chapter opens with a summary of the limited field testing completed on riveted and bolted panels. This recent testing explains the importance of understanding the behavior of rivets specifically as it pertains to shear strength when experiencing high rates of loading. A summary of the laboratory testing involving simple riveted connections follows and serves as the comparative basis for the LS-DYNA (2013) modeling of simple connections conducted by this author. The primary focus of this chapter is to provide and validate the details for modeling simple riveted connections. As a necessary first step in the process towards validation, a finite element model was developed and simulated using quasi-static loading. This initial step was taken prior to the more complex validation of simulation using dynamic loading because of the large amount of quasi-static data available in literature. Thus, validation is achieved by comparing the computational results of ten different simple rivet connections under quasi-static loading with both recent experimental testing results (Rabalais, 2015) and the historical data discussed throughout Chapter 2. After this validation discussion, the chapter ends with a concluding summary. Further validation referencing high rate loading will be discussed in Chapter 4.

## 3.2 The Results of Field Testing of Riveted Panels Under Blast Loads

Despite a clear need to investigate the blast loading response of riveted connections, no research had been started in this regard until laboratory and field tests were completed

by the Engineer Research Development Center (ERDC), U.S. Army Corps of Engineers. In research performed for the U.S. Department of Homeland Security and the Federal Highway Administration, ERDC conducted comparative explosion tests on a number of bridge tower components. Initial tests included an investigation of scaled models of steel bridge tower components using A36 steel (Walker et al., 2011a, 2011b, 2011c, 2011d, 2011e). Subsequent work expanded on this research by comparing the A36 panel response with the response of vintage, pre-1940 A7 steel (Crane et al., 2015). Additional testing built upon these extensive tests by varying the types of fasteners used in the panels (Crane et al., 2015).

From these previous studies, the most relevant research for this dissertation is the testing of front plate suspension steel panels subjected to blast loadings, comparing the response of riveted panels with bolted panels. Specifically, this testing evaluated the ductility and fracture behavior of the different panels. Because the previous testing involving vintage A7 steel and modern A36 steel revealed a similar response to blast loads (Crane et al., 2015), it was determined suitable to conduct all testing using the same modern A36 steel. As a result, both the panels and their connecting angles for the models were constructed using A36 steel.

The fasteners used to replicate pre-1950 construction were ASTM A502 standard strength rivets (ASTM, 2003). The fasteners used to replicate post-1950 construction were fully tensioned ASTM A307 standard strength bolts (ASTM, 2014). Targets were bolted or riveted in the exact same configuration with explosive charges suspended above each specimen.

When evaluating the response of the bridge panel connected with the fully tensioned ASTM A307 standard strength bolts, the authors noted that the front face was severely damaged in a brittle fashion. There was very little reduction in the cross-sectional area of the plates along failure sites, defined as the portion of the plate supported by the stiffeners where the fracture propagated along the edge. This observation indicates that the blast load acting on the bolted panels resulted in a brittle, shear failure of the plates. In addition, as shown in Fig. 3-2, the bolts failed exclusively in shear as there was no noticeable tensile strain in the bolts. The diameter of the bolts following the tests was virtually identical to the diameter of the bolts prior to the test.

Fig. 3-2: View of Bolts Shear Failure Following Testing (from Crane et al., 2015)

While the bolted plates failed in a brittle shear fashion, the steel plates connected with ASTM A502 standard strength rivets had a more ductile tension failure. This failure was evident by the significant reduction in steel plate cross-sectional area at the failure site, as shown in Fig. 3-3. In fact, the reduction in plate thickness at the tears was measured at nearly 35% (Crane et al., 2015). Despite the fact that the riveted plate failed differently in comparison to the bolted plate, the rivets failed identically to the bolts as no large tensile strain was observed in the rivets. As demonstrated earlier in Fig. 2-17 (Munse and Cox, 1956), rivets have a varying amount of necking at failure depending upon the state of stress; there is no necking under a pure shear failure and significant necking under a pure tensile failure.


Fig. 3-3: Significant Necking of Riveted Plate Material (from Crane et al., 2015)

Because the brittle failure of specimens with modern steel plates and fasteners provided a conservative estimate of the response of vintage plates fastened with rivets, the authors concluded that subsequent testing could be conducted effectively using modern materials and construction methods rather than go through the cost and expense to reclaim vintage steel that would be later fastened with rivets (Crane et al., 2015).

These findings also validate the need to further understand the behavior of vintage rivets. With challenges in constructing and funding field tests, coupled with the difficulty in obtaining riveted samples to test and in finding the expertise to build riveted models, a numerical approach to study the behavior of riveted connections using sophisticated software is a valuable contribution to the engineering community. Furthermore, as mentioned in the quote to open the chapter, good numerical solutions available to engineers through relatively quickly obtained numerical models are better than perfect solutions obtained through exhaustive field or laboratory tests that will undoubtedly take a lot longer.

## 3.3 Experimental Testing of Simple Riveted Connections

The field testing conducted by Crane et al. (2015) and described in Section 3.2 in this dissertation demonstrated that connectors of cellular suspension panel plates failed in shear regardless of connector type (bolt versus rivet). Simultaneous laboratory research narrowed the focus of the research to the behavior of the fastener under quasi-static and

dynamic loads. Specifically, riveted, non-pretensioned bolted, and pretensioned bolted lap-spliced specimens were tested in both quasi-static and dynamic loads to investigate how the different simple connections behaved under quasi-static and dynamic loads (Rabalais, 2015). Testing included an investigation of four distinct variables: fastener type, single shear or double shear, joint configuration type and loading type.

To conduct the laboratory testing, the authors used the 200-kip dynamic loader shown in Fig. 3-4 to apply loads to lap-spliced specimens. The 0.5-in. and 1-in. A36 structural steel plates and spacing of the fasteners for each configuration were selected and designed to ensure the connectors would fail before the occurrence of any of the other connection failure methods (block shear rupture, member yielding, member fracture, bearing, and tear out) detailed in Section 2.3 of this dissertation.

Fig. 3-4: 200-kip Dynamic Loader (from Rabalais, 2015)

To evaluate the behavior of different fasteners, A502 Grade 2 standard strength rivets were compared with A307 Grade B standard strength bolts because they have similar mechanical properties. A picture of the typical fasteners used for single-shear configurations is shown in Fig. 3-5. The bolted fasteners had a nominal diameter of 0.5-in., while the riveted fasteners had a nominal diameter of approximately 0.5625-in. As

expected, the rivets ended up with a greater nominal diameter because rivets tend to fill the hole to varying degrees during the hot-driving process. As described as typical practice in Section 2.2 of this dissertation, rivets for this laboratory testing program were driven by a hydraulic riveter after being heated to between 1500 and 1950 degrees Fahrenheit. A picture of the hot riveting process used for this experimentation is shown in Fig. 3-6.

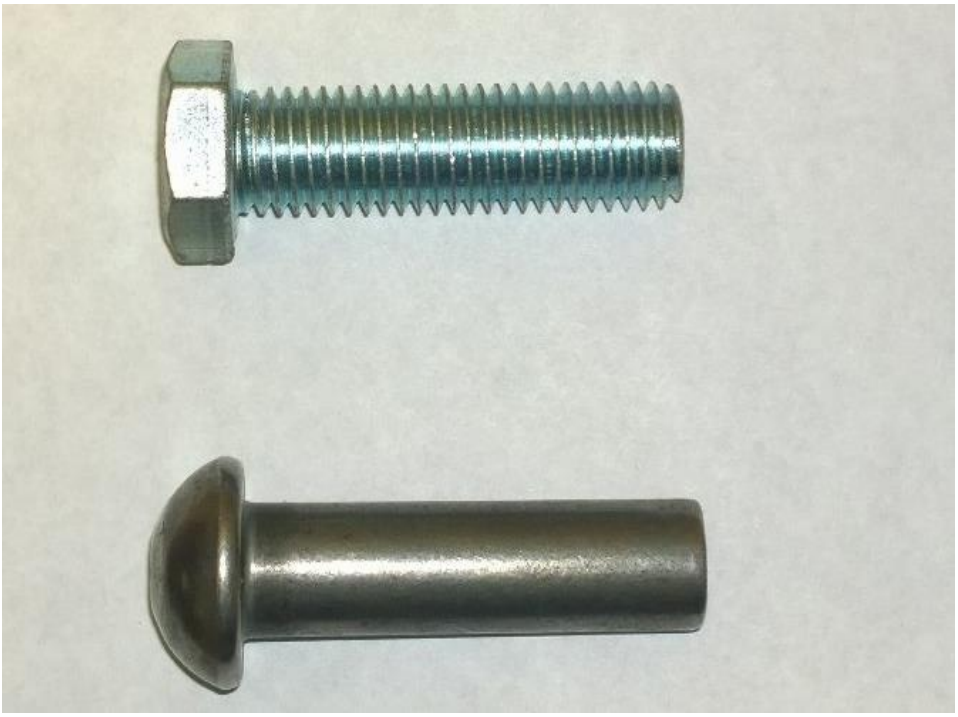

Fig. 3-5: A307 Grade B Bolt vs. A502 Grade 2 Rivet (modified from Rabalais, 2015)

Fig. 3-6: Riveting Process for Laboratory Testing (from Rabalais, 2015)

As shown in Fig. 3-7, the second variable tested was the number of shear planes. Specifically, the testing involved fasteners in single shear or double shear. Single-shear tests consisted of two 0.5-in. steel plates connected by fasteners, while double-shear tests consisted of two 0.5-in. steel plates and one 1-in. plate connected by fasteners. While the bolt diameter remained unchanged, it was anticipated and revealed that the rivet diameter was smaller for the double shear tests. As explained in Section 2.5, longer rivets tend to

have a slightly lower strength than shorter rivets because longer rivets do not fill the hole throughout their entire length as well as rivets with shorter lengths (Munse and Cox, 1956). This laboratory testing demonstrated an average rivet diameter for single-shear rivets of 0.560-in. (stress area 0.246 $in.^2$) and an average rivet diameter for double shear rivets of 0.545-in. (stress area 0.233 $in.^2$) (Rabalais, 2015).

Fig. 3-7: Single Shear with Two 0.5-in. Plates (left) vs. Double Shear with Two 0.5-in. Plates and One 1-in. Plate (modified from Rabalais, 2015)

Rarely is a single rivet used as a connector in practical applications. Thus, in addition to the simple Configuration 1: Single Rivet (as shown in Fig. 3-7), the authors also investigated multiple fastener configurations. The other four configurations tested

included: Configuration 2: Two Rivets Horizontal; Configuration 3: Two Rivets Vertical; Configuration 4: Four Rivets Square; and Configuration 5: Four Rivets Staggered. Each of the configurations was tested in single-shear and double-shear. These four multiple fastener configurations are shown in Fig. 3-8.

As indicated previously, the 200-kip dynamic loader applied the quasi-static and dynamic loads to the lap-spliced specimens. To apply a quasi-static load, the loader was operated at the slowest loading rate. Under these conditions, failure of the rivets occurred between approximately 500 and 4000 milliseconds. When applying a dynamic load, the loader was operated at the fasted loading rate possible. For this case, failure of the rivets occurred between approximately 1 and 6 milliseconds. Specific loading rates were not measured. However, the 200-kip dynamic loader advertises an approximate range of 10 to 100,000 lbf/msec (Rabalais, 2015).

This section summarized the details of the 224 tests setup and executed by Chris Rabalais (2015) to determine the behavior of fasteners under quasi-static and dynamic loads. The remainder of this chapter focuses on model validation for quasi-static loaded specimens.

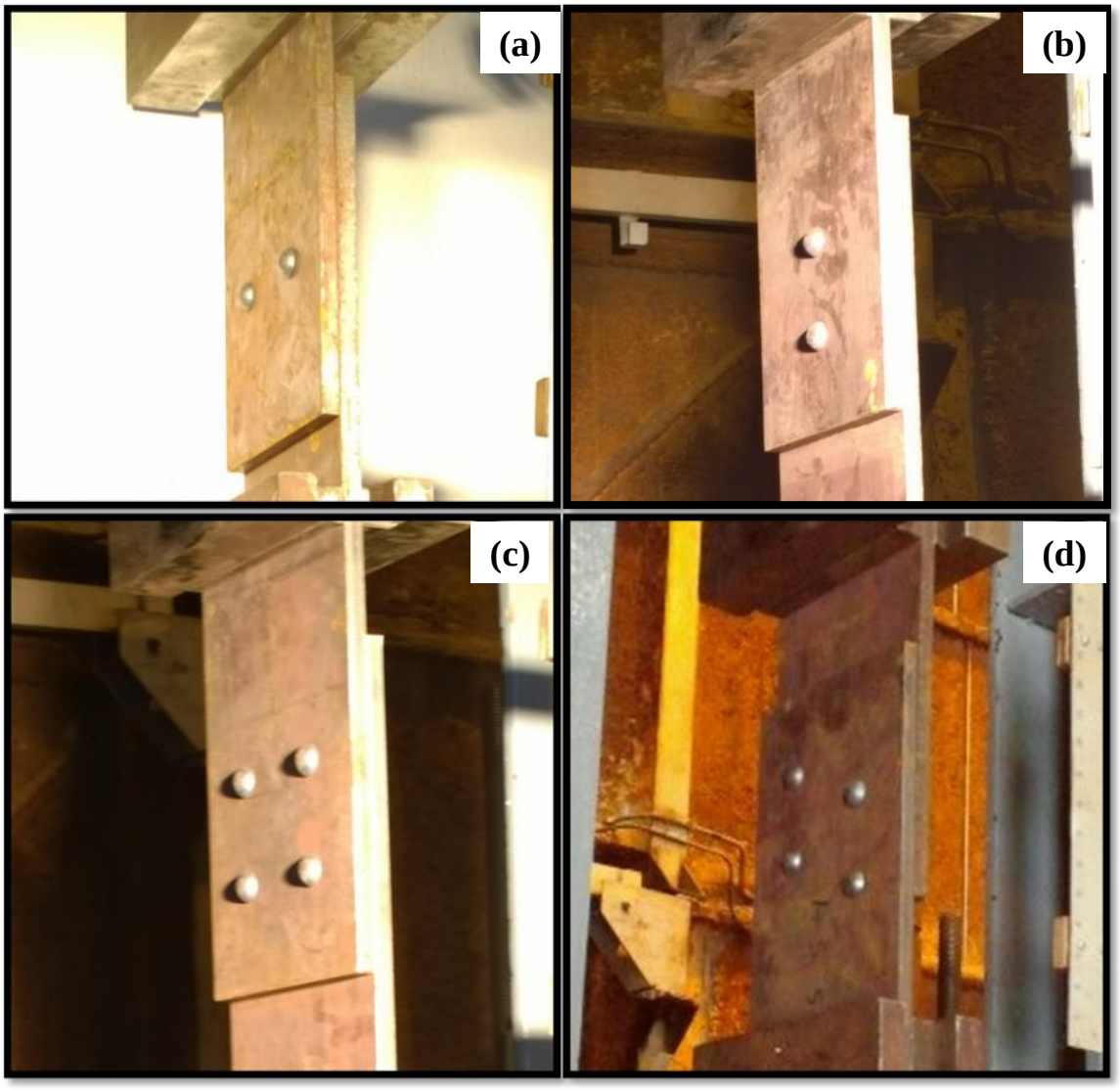


Fig. 3-8: Multiple Rivet Configurations: (a) Configuration 2, (b) Configuration 3, (c) Configuration 4, and (d) Configuration 5 (modified from Rabalais, 2015)

## 3.4 THE FINITE ELEMENT METHOD AND LS-DYNA (2013)

Selection of finite element software was required to develop and analyze the response of riveted connections. A large variety of finite element analysis software capable of modeling riveted connections under high loading rates includes ANSYS, ABAQUS, and LS-DYNA (2013). However, with LS-DYNA (2013) largely considered the industry leader as it pertains to the response of structures under blast loads, LS-DYNA (2013) was selected as the solver to conduct the analysis. Developed by Livermore Software Technology Corporation, LS-DYNA (2013) is a multi-purpose finite element software package that offers both implicit and explicit numerical integration of the governing equations of motion.

Finite element analysis is one of several numerical methods available to estimate solutions to physical problems. Other examples include the finite difference method, the finite volume method, and the boundary element method. Numerical methods require the replacement of a physical domain by a set of geometric points, lines, triangles, quadrilaterals, or some other geometric entity. Elements, connected at points referred to as nodes, are assembled into a finite element structure creating a mesh. This mesh is programmed by the user to exhibit specific material and structural properties. Numerical models vary in intricacy, from simple one-dimensional models, to more complex two-dimensional and three-dimensional models. Through discretization, the physical system with an infinite number of degrees of freedom is approximated into a finite number of degrees of freedom. Once discretized, the user defines all boundary conditions and loads.

Numerically, the discretized mesh leads to a system of algebraic equations. The numerical solver assembles these mathematical approximations and solves for unknown parameters at the nodes. Solutions are approximated element by element over the entire structure. In theory, a highly discretized system that is modeled correctly can nearly match the behavior of a complex physical system.

Highly complicated three-dimensional models often involve significant time to both create and to analyze. However, this time requirement is small in comparison to the time required to conduct experimental testing, especially when it pertains to blast loads. On the contrary, experimental testing can often be very useful to users of numerical software packages because the collected data can serve as a validation tool for the numerical results. This validation helps engineers conducting numerical simulations gain confidence in their results and avoid consequences ranging from embarrassing to catastrophic.

The rest of this chapter focuses on the use of LS-DYNA (2013) to conduct finite element analyses of rivets under the simple and often tested quasi-static condition. Specific topics of discussion include the discretization, approximation of boundary conditions and loading, and determination of a material model to dictate behavior. LS-DYNA (2013) simulates the response of the defined model by conducting a highly nonlinear, transient dynamic finite element analysis using explicit time integration. The analysis is nonlinear in that the rivet experiences severe deformations prior to rupture, the rivet material properties exhibit nonlinear response, and the contact between parts (the rivet(s) and the plates) changes over time. The analyses conducted in Chapter 4 of this

dissertation are of transient dynamic models in which the plates are pulled in tension and rivet(s) fracture in shear over a matter of milliseconds. Thus, inertial forces become extremely important for this type of analysis.

## 3.5 3-D Finite Elements

One of the useful characteristics of finite elements is that there are no geometric restrictions on the systems or structures that can be modeled. The models created within LS-DYNA (2013) are limited only by the expertise of the user. Each finite element analysis program has its own element library with a variety of user-defined elements that can be selected. LS-DYNA's (2013) library includes beams, discrete elements, lumped inertias and masses, accelerometers, sensors, seatbelts, shells, solids, and thick shells. The two predominant element types for blast and impact simulations are shells and solids. Shells are typically used to model parts that have in-plane dimensions that are much greater than the through-thickness direction, whereas solids are more general and can be used to represent a variety of parts. With such a powerful tool available for this research—and with the intent of this research to serve as a building block for future blast modeling—solid elements were used to model the rivets and plates. The advantages to solid elements are that they are three-dimensional finite elements that can model solid bodies and structures without geometric simplifications. The solid elements can have any arbitrary shape; thus, the assembled finite element mesh visually approximates the

physical system. With a three-dimensional solid element, the user can input force vectors in any arbitrary direction, providing results that include six potential stress components (three normal and three shear) and corresponding deformations and displacements in all three dimensions.

The 4-node and 10-node tetrahedral and 8-node hexahedra are typical solid elements used in three-dimensional analyses. Each of these solid elements is shown in Fig. 3-9, and each has their own characteristics with respect to nodes, surfaces, and degrees-of-freedom. For example, the 4-node tetrahedron element has four nodes and four surfaces per element. Because each element has three degrees of freedom (*u*, *v*, and *w*), there are a total of 12 degrees-of-freedom for the 4-node tetrahedron element. Meanwhile, the 8-node hexahedral element predominately used in this research has eight nodes, six faces, and 12 sides per element. Literature revealed that the 8-node hexahedra elements were easier to visualize than the tetrahedron elements, are computationally more efficient than tetrahedron elements, and have proven to provide more accurate results than the other element types (Erhart, 2011). More specifically, tetrahedron elements behave poorly in cases where elements are loaded in shear, while hexahedron elements with adequate discretization refinement approximate analytical solutions (Erhart, 2011).

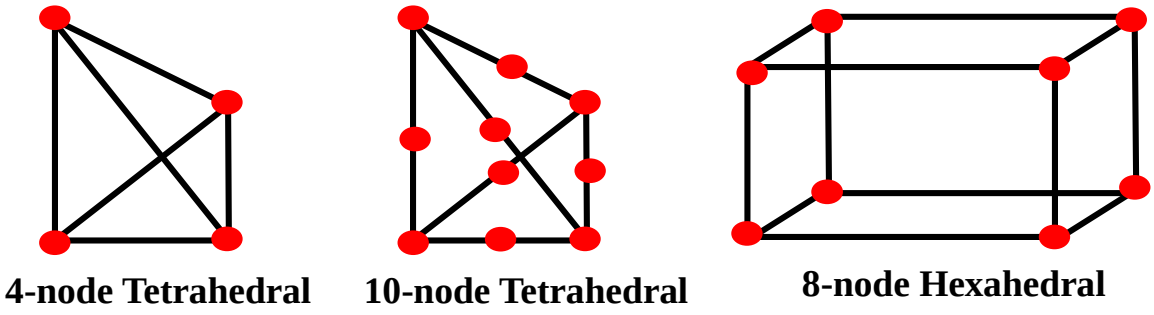


Fig. 3-9: Examples of Solid Elements

After choosing the 8-node hexahedra elements, decisions regarding element formulation were required. This decision is critical to the user as it impacts the accuracy of the results and the cost required to analyze the model under consideration. Stresses and strains are calculated at each integration point, and displacements are calculated at each node. Options considered for this research within LS-DYNA (2013) included ELFORM 3 (fully integrated solid elements), ELFORM 2 (partially integrated solid elements), and ELFORM 1 (under-integrated constant stress elements). Under-integrated elements describe an element formulation in which stresses and strains are only calculated at the mid-point of each element, as shown in Fig. 3-10. The full integration and reduced integration options are typically two to four times more costly than the under-integrated element formulation, because they have to calculate the stiffness and mass at several more sampling (or integration) points within an element. When attempting to analyze relatively slower quasi-static models, using the fully- or partially-integrated elements for a simple model took several weeks to run. Comparatively, the quasi-static analysis with the under-integrated element formulation ranged between an hour and two days to run,

depending on the complexity of the rivet configuration. Not only is the under-integrated element formulation considerably more efficient than the other considered element formulations, but it has been shown to be more accurate in situations with significant deformations (LS-DYNA Theory Manual, 2006). Thus, while the accuracy of integration is increased with additional integration points, the finite elements results are not necessarily improved.

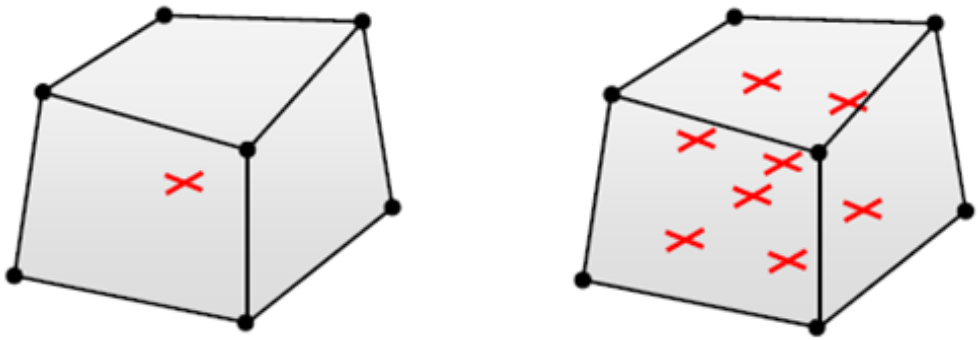

**ELFORM 1** **ELFORM 2**

Fig. 3-10: Under-Integrated vs. Partially-Integrated Element Formulations (from Erhart, 2011)

Despite the potential for improved performance, one of the issues with the under-integrated element formulation is the possibility of spurious deformation modes of the finite element mesh. An example of this phenomenon is shown in Fig. 3-11. In a situation where this element is subjected to pure bending, neither of the element characteristic lengths (*a* to *b* and *c* to *d*) change in length. The under-integrated stiffness matrix for this element only contains information at the center of the element (in this example, where the

two dashed lines meet). The result is a zero-energy mode. No strain energy is generated, and all the components of stress at the single integration point are zero. The element has no stiffness in this mode and is unable to resist this type of deformation. An accumulation of this energy mode throughout a mesh may provide inaccurate results to the user.

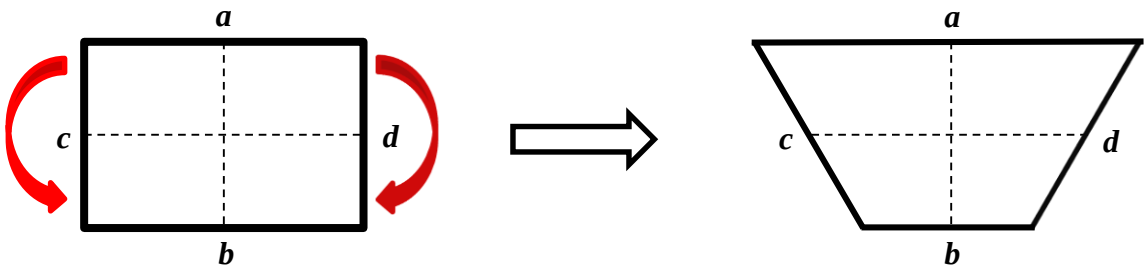


Fig. 3-11: Spurious Deformation for Under-Integrated Element

LS-DYNA (2013) provides the user with a warning of spurious deformations by providing the histories of the *hourglass* energy, defined as the energy generated by unrealistic element behavior in which no stresses or strains are generated in those elements. As a general rule, the hourglass energy should be less than 5% - 10% of the internal energy. Physically, hourglass issues are evident by the zig-zag appearance of element shapes, as shown in Fig. 3-12.

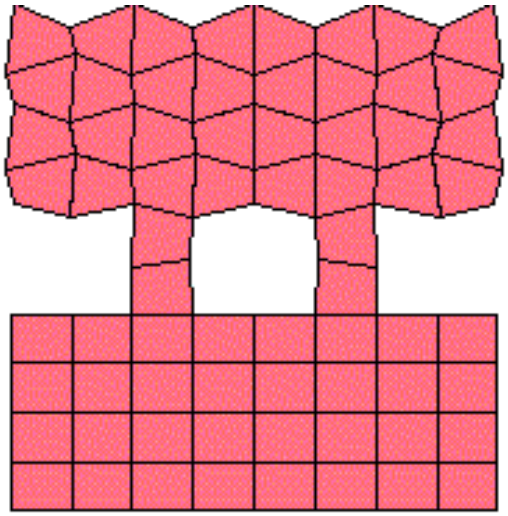

Fig. 3-12: Example of Hourglassing (from http://www.dynaexamples.com/process_simulation/hourglass)

LS-DYNA (2013) offers 12 different hourglass modes to help control spurious deformations for solid elements. These algorithms provide forces, or hourglass energy, to resist hourglass modes and take away from the physical energy of the system. A simple example of this is shown in Fig. 3-13 where internal nodal forces are introduced to counteract the hourglass mode issue demonstrated in Fig. 3-15. LS-DYNA (2013) offers several hourglass algorithms. The viscous forms of hourglass control (HG1, HG2, and HG3) are designed for analyses involving high strain rates as the algorithm generates hourglass forces proportional to the components of nodal velocity contributing to the hourglass modes (Forsberg, 2013). The stiffness forms of hourglass control (HG4 and HG5) are typically preferred for slower strain rate problems; they generate hourglass forces proportional the components of nodal displacement contributing to the hourglass modes (Forsberg, 2013).

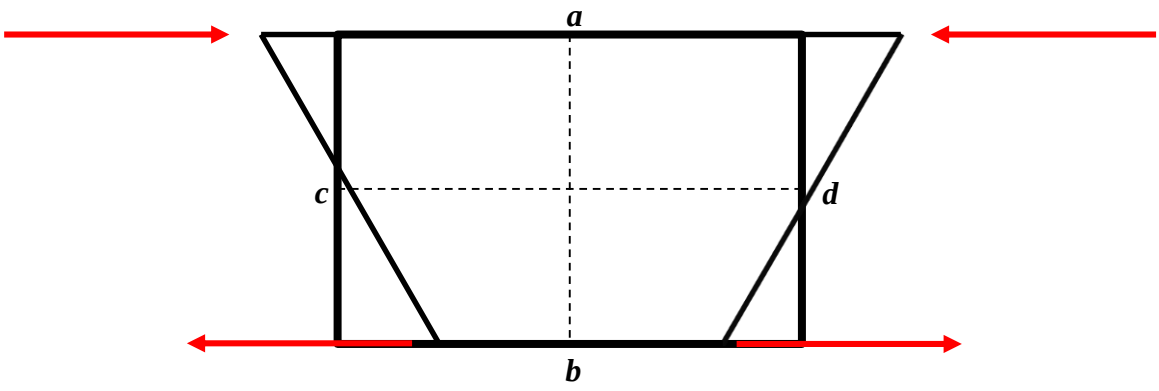


Fig. 3-13: Illustration of Internal Nodal Forces Counteracting Hourglassing

The other type of hourglass control considered for this research was the Belytschko-Bindeman (1993) formulation, known as HG6 within LS-DYNA (2013). This formulation dictates that the material properties of each element are used to calculate an assumed stress field from an assumed strain field. This calculated stress field is integrated over the element domain using a closed form to develop the hourglass forces required for fully-integrated element behavior (LSTC, 2012). After noticing little difference in the computed results among the different considered hourglass algorithms, a decision was finally made to use the Belytschko-Bindeman (1993) formulation for this research for two reasons. First, within LS-DYNA (2013), this hourglass type is required for implicit analyses. When replicating static uniaxial tension tests within LS-DYNA (2013) to develop a material model for the rivets, an implicit analysis was conducted because the number of steps required to conduct this test explicitly would be excessive and have a significant computational cost. The Belytschko-Bindeman (1993) is also permitted for explicit analyses, which were required for the dynamic testing of the rivets to capture the

rate-dependent aspects of the solution. With a desire to maintain as much consistency as possible among LS-DYNA (2013) analyses, it was deemed suitable for this research effort to select a single hourglass formulation. Secondly, LS-DYNA literature (LSTC, 2012) advertises that the Belytschko-Bindeman (1993) algorithm is typically more effective than both the viscous hourglass controls and the stiffness hourglass controls when dealing with elements that become significantly skewed. With elements in the shaft of the rivet experiencing significant deformation under high shear stress, choosing the Belytschko-Bindeman (1993) proved appropriate for this research.

LS-DYNA (2013) warns the user that the Belytschko-Bindeman (1993) formulation may artificially stiffen the results and that a reduced hourglass coefficient may be required to minimize this stiffening effect. This research described in this dissertation used an hourglass coefficient of 0.01, which is a reduction from the default value of 0.1 but is within the LS-DYNA (2013) recommended reduced range of 0.001 to 0.01 for solid elements. Throughout this research, checks were made to ensure meaningful hourglass issues were not apparent visually (i.e., no zig zag distorted deformations) and numerically (hourglass energy was less than 10% of the internal energy for both the whole system via the *glstat* file (*DATABASE_GLSTAT) and each part via the *matsum* file (*DATABASE_MATSUM)) within LS-DYNA (2013).

Another technique used to avoid element distortion was the use of invariant node numbering. Rivets under high shear to the point of fracture might lead to numerical issues where the distortion of elements change the element coordinate system and subsequently adversely impact element connectivity. By turning on invariant node numbering within

LS-DYNA (2013) using *CONTROL_ACCURACY (INN=3 for solid elements), element rotation calculations were independent of the order of the nodes, and the results were insensitive to the element connectivity. While early iterations that were run prior to turning on invariant node numbering admittedly provided similar results, turning on the invariant node numbering was highly recommended by LS-DYNA (2013) in modeling problems with large shear forces (Forsberg, 2013).

### 3.6 Boundary Conditions and Loading

Another powerful aspect of finite element modeling is that a wide range of loadings and boundary conditions can be specified. Any concentrated or distributed force can be applied to one area of a body while another part of a body can be supported. With the decision to choose solid elements (as discussed in Chapter 3.5 above), loadings and boundary conditions are treated more realistically because they are applied on a three-dimensional model in the same manner without dimensional simplifications.

Several different boundary condition configurations and loadings were used within LS-DYNA (2013) to try to replicate the shear testing conducted by Chris Rabalais (2015) using the 200-kip dynamic loader. Care is required in dictating these support conditions within LS-DYNA (2013). Even the smallest changes that appear to be trivial have the potential to have a major impact on the computed results. Thus the details and intent of the laboratory setup were critical in determining modeled boundary conditions.

In the laboratory testing, one end of a riveted connection was attached to a reaction structure (the top of the loader) and was held in such a way that it was unable to move. The other end of the riveted connection was attached to a piston. The pressure needed to hold one end of the riveted connection in place and to move the other end of the riveted connection was provided from a compressible fluid. This piston moved downward at a rate of speed that depended upon how pressure was released through different sized orifices, ranging from 4.5-in. diameter (high loading rate) to 0.0625-in. diameter (quasi-static loading rate).

The gripping mechanism used to attach each end of the loader is shown in Fig. 3-14. The grips were designed to minimize slip and ensure failure occurred in the riveted connection. Each end of the grips consisted of six A490 bolts to tighten SAE 4140 steel plates to the riveted lap splice connection and six A490 bolts to attach the SAE 4140 steel plates to a main “T” grip that was shimmed and gripped into the loader.

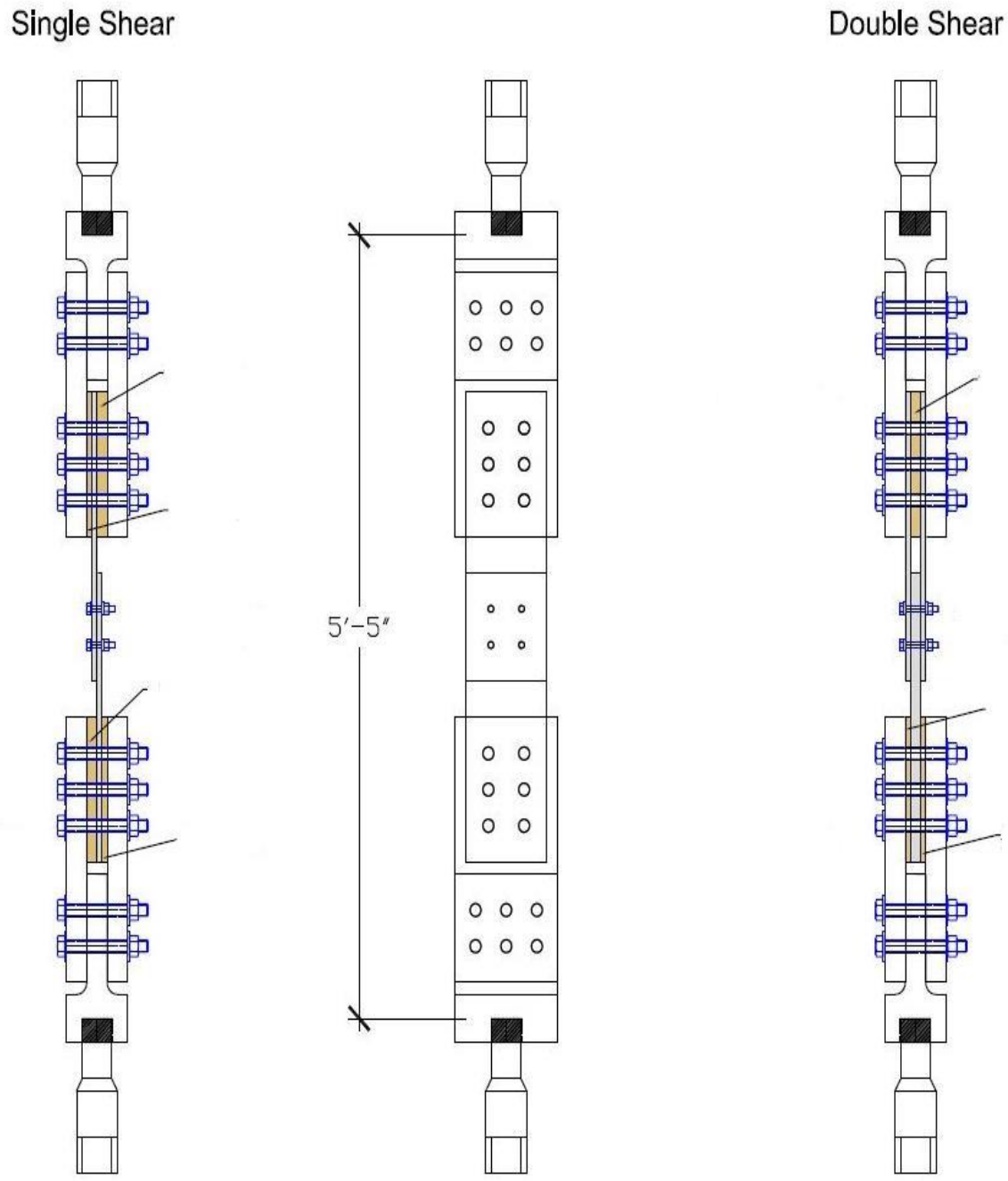


Fig. 3-14: Gripping Mechanism Assembly (from Rabalais, 2015)

While not impossible, modeling the exact gripping mechanism assembly with the dynamic loader system was unnecessary to meet the objectives of this research. As a result, simplified models were used to replicate the testing in such a way as to obtain timely yet useful results. The model created in LS-DYNA (2013) simplified the gripping mechanism system at the plate end that was stationary in the dynamic loader by applying a fixed boundary condition at every node on that end of the plate. Thus, all displacements in three-dimensional space were prohibited from moving (DOFX, DOFY, DOFZ within LS-DYNA (2013) under *BOUNDARY_SPC_SET). Similarly, the gripping mechanism system and piston that pulled down on the other end of the riveted plate was simplified in LS-DYNA (2013) by applying a displacement-controlled prescribed motion of that moving end for each analysis. A comparison of the model to the test setup is illustrated in Fig. 3-15.

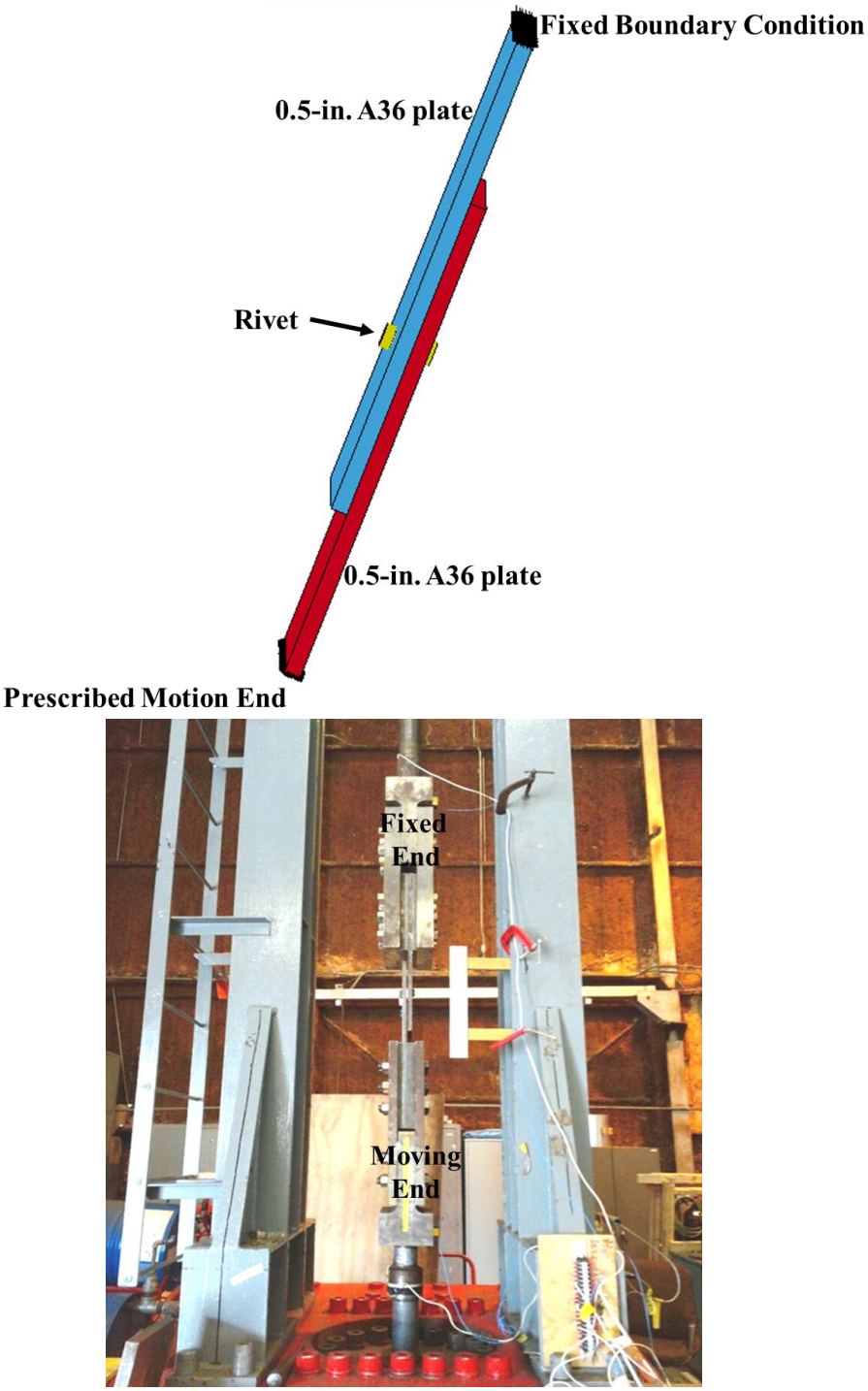


Fig. 3-15: Model Setup (top) and Laboratory Setup (bottom) (photo from Rabalais, 2015)

One challenge with finite element modeling is that boundary conditions are not always perfectly clear. Concern existed that this boundary condition may be insufficient to limit movement of the plates in such a way that bending occurs instead of axial tension. With this uncertainty, an attempt was made to obtain a bounded solution by conducting a second analysis with modified boundary conditions (as shown on right of Fig. 3-16). This subsequent analysis included out-of-plane boundary conditions on the outside of each plate to restrict plate bending (DOFZ within LS-DYNA (2013)). An illustration of each of these analyses on plates in single shear under Configuration 1 is shown in Fig. 3-16. After observing negligible differences in the results, subsequent analyses were conducted with boundary conditions only on a plate end (DOFX, DOFY, DOFZ on end of one plate as shown on left of Fig. 3-16).

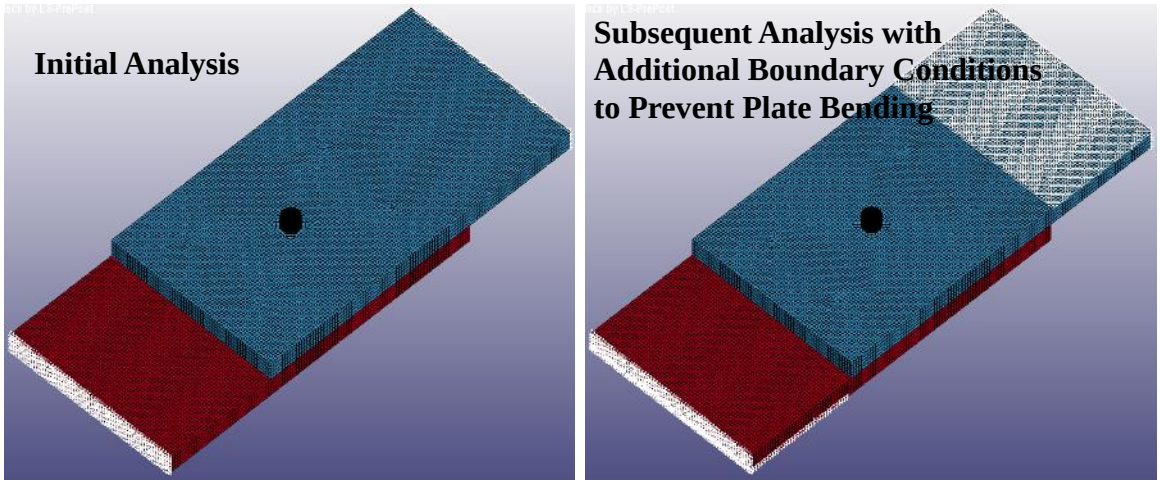


Fig. 3-16: Boundary Condition Considerations for Axial Tension in Plates

Similar evaluations were conducted when modeling double-shear configurations. It was initially unclear whether results would differ within LS-DYNA (2013) if different ends were fixed and pulled. Recall that in the double-shear tests, one end would have two 0.5-in. plates supported or displaced while the other end would have one 1-in. plate supported or displaced. An illustration of these tests is shown in Fig 3-17. Again, negligible differences in the results eliminated the need for further consideration of this concern.

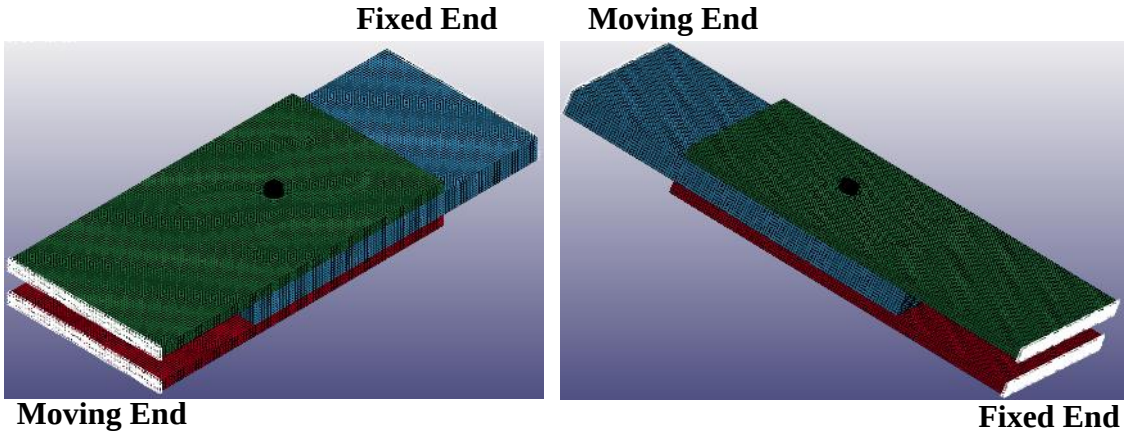


Fig. 3-17: Boundary Condition Considerations in Double Shear

For initial model validation under quasi-static loading, several analyses were conducted to get the rivet to fail in a manner that accurately represented the experimental tests (Rabalais, 2015). This was a challenge because the experimental loading rates were not recorded and differed for each configuration. Experimentally, failure for each rivet under quasi-static loading occurred between 500 to 4000 milliseconds (Rabalais, 2015).

Table 3-1 shows the displacement-controlled prescribed motion applied to each quasi-static test conducted for each configuration in single- and double-shear. This displacement was applied at one end of one plate along one axis (*x*-translational DOF in LS-DYNA (2013) for each model). In some of the more complex cases involving double shear and/or multiple rivets, a slower prescribed motion was used after the initial run indicted a response that reached peak strength faster than what was observed in testing. As shown in Appendix A, the displacement-controlled prescribed motion applied within LS-DYNA (2013) produced a shear failure within the tested time frame observed in experimental testing.

Table 3-1: Prescribed Motion Curve Input for Quasi-Static Analyses by Configuration

| **Configuration # and Description** | **Point 1** **(Time in seconds, Displacement in inches)** | **Point 2** **(Time in seconds, Displacement in inches)** |
|---|---|---|
| 1: One rivet, single shear | (0, 0) | (2, 0.1) |
| 1: One rivet, double shear | (0, 0) | (2, 0.1) |
| 2: Two rivets horizontal, single shear | (0, 0) | (2, 0.1) |
| 2: Two rivets horizontal, double shear | (0, 0) | (4, 0.1) |
| 3: Two rivets vertical, single shear | (0, 0) | (3, 0.1) |
| 3: Two rivets vertical, single shear | (0, 0) | (3, 0.15) |
| 4: Four rivets square, single shear | (0, 0) | (6, 0.2) |
| 4. Four rivets square, double shear | (0,0) | (7, 0.2) |
| 5. Four rivets staggered, single shear | (0,0) | (5, 0.15) |
| 5. Four rivets staggered, doubled shear | (0,0) | (5, 0.15) |

Contact within a finite element program allows unmerged elements to interact with each other via impact, sliding, and bearing. In analyses dealing with high strain rates and blast, deformations can be significant. How and where this contact takes place can be extremely difficult to determine. As a result, analyses dealing with high strain rates and blast typically use an automatic contact option. The automatic contact options within LS-DYNA (2013) are non-oriented and detect penetration from all directions. Described as the most efficient and reliable contact option within LS-DYNA (2013), *CONTACT_AUTOMATIC_SINGLE_SURFACE was used for all analyses (LS-DYNA Support, 2014). Though LS-DYNA (2013) allows the user to define any number of contacts in an analyses, just one was suitable for this research. Contact was defined by identifying part sets that included the plates and the rivets. During each time step, a search was made to check for potential penetration. A soft constraint-based approach was used (SOFT=1) with the automatic single surface contact option. This was not only recommended for most explicit impact analyses, but it was also recommended in situations when dissimilar materials (in this case the A502 Grade 2 rivets with A36 steel) come into contact (LS-DYNA Support, 2014).

In constructing each model, care was taken to place each rivet symmetrically within each plate hole. However, this manual procedure was not without the possibility of human error. LS-DYNA (2013) offers an option within their automatic contacts to offset initial penetration issues by selecting IGNORE=1 via *CONTACT. Another option within LS-DYNA (2013) is for the user to input values for static (FS) and dynamic (FD) friction parameters. These parameters impact sliding behavior. Omitting these values tells

the software to assume friction-less behavior. Defining both values tells LS-DYNA (2013) to consider the relative velocity with which the parts are sliding. There are a wide range of values recommended within different reference manuals, papers, and engineering forums for steel, often dependent on the surface conditions. The *Civil Engineering Reference Manual* (Lindeburg, 2003) recommends values between 0.08 and 0.42 for steel-on-steel contact for FD and between 0.10 and 0.78 for FS. Several combinations of coefficients were used in preliminary analyses and done so with FD less than FS because it takes more force to accelerate a mass from rest than to keep it moving. However, after no noticeable differences in the Load versus Time output and in an attempt to avoid the creation of additional noise (unwanted, random response excitations), FS and FD were set to equal at 0.4 for all analyses (dynasupport.com, 2016). Another noise related decision within contact was made with the viscous contact damping (VDC) parameter. Because contact oscillations between the plates and the rivet(s) can lead to unwanted noise in the response, the VDC parameter within *CONTACT improves model stability and reduces noise. Based on the LS-DYNA (2013) guidelines for metals in contact, a value of 20 percent (input as 20, not 0.2 within LS-DYNA) was used throughout all analyses in order to smooth out response (LS-DYNA Support, 2014).

## 3.7 MATERIAL MODEL DEVELOPMENT

As finite element modeling software has directed significant effort at computations for high-velocity loading problems, the limitations to achieving similar results to experimental testing and replication of real-world incidents often lies in the ability of the user to adequately define material characteristics (Johnson and Cook, 1983). LS-DYNA (2013) has over 130 material models available to simulate a wide range of engineering materials. With a large variety of models to choose from, the decision was made to start off with MAT24, a piecewise-linear plasticity model, because it is widely considered the most popular material model for modelling rate-dependent phenomena (Lobo, 2016). MAT24 consists of an elastic-plastic curve that is defined by the user. Failure occurs when the material reaches a maximum strain from the elastic-plastic curve.

A great deal of effort was used to accurately capture the material model. First, a thorough search was made to see if any literature existed that captured modeling A502 Grade 2 rivets within finite element software. This search did not identify any available information. However, Dr. Paul Allison, professor from the University of Alabama, conducted three ASTM E8 (2015) milled rivet tension tests on behalf of Chris Rabalais (2015). These tests presented a challenge due to the extremely small size of the specimens. The diameter of the coupons were 0.113385-in.; thus, the testing was conducted in accordance with Specimen 5 from the “For Test Specimens with Gauge Length Four Times the Diameter”, as shown in Table 3-2 (ASTM E8, 2015). All three rivets tested by Dr. Allison produced virtually identical stress-versus-strain curves.

Furthermore, as shown in Fig. 3-18, the average undriven ultimate rivet tensile strength was 77 ksi. This value was consistent with the *Guide to Design Criteria for Bolted and Riveted Joints*, which estimated the ultimate tensile strength of an undriven A502 Grade 2 rivet to be approximately 80 ksi (Kulak et al., 1987). As mentioned in Chapter 2, the riveting process has shown to increase the ultimate tensile strength and subsequently the shear strength of the rivets by 10 to 20 percent. Thus, the probable tensile strength of the rivets used in Chris Rabalais' research (2015) ranged from 85 to 92 ksi.

Table 3-2: ASTM E8 Dimension Requirements (from ASTM E8, 2015)

| | |
|---|---|
| **Gage Length (in.)** | 0.450 +/- 0.005 |
| **Diameter (in.)** | 0.113 +/- 0.002 |
| **Radius of fillet, min (in.)** | 0.094 |
| **Length of reduced section min (in.)** | 0.625 |

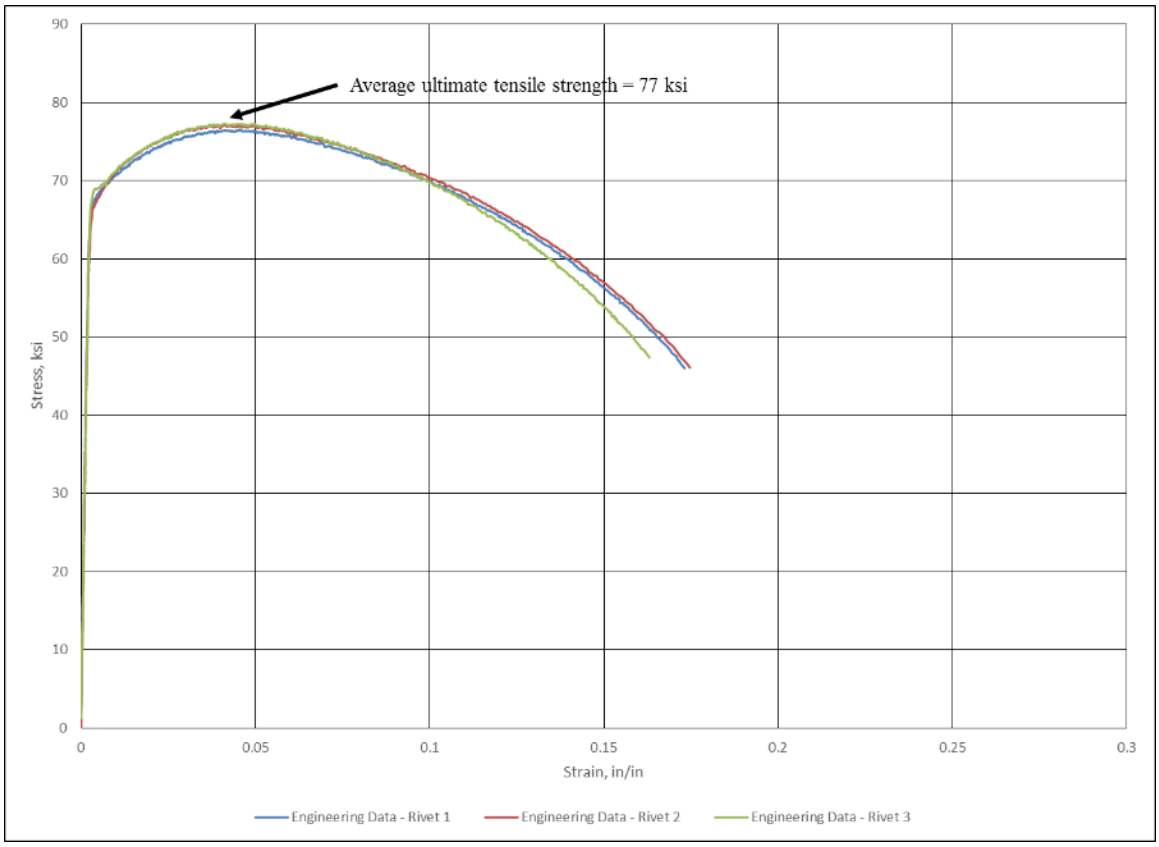


Fig. 3-18: Stress vs. Strain Data for Undriven A502 Grade 2 Rivet Material (data provided by Allison, 2015)

Attempts were made to mimic this tension test as closely as possible under the anticipation that matching the stress-strain results from laboratory testing would provide the details required for the rivet material model. The rivet coupon was created using AutoCAD Civil 3D (2013), saved as an *igs* file, and imported into LS-PrePost 4.1 (2014). A comparison of the meshed rivet tested in LS-DYNA (2013) with the experimentally tested rivet is shown in Fig. 3-19.

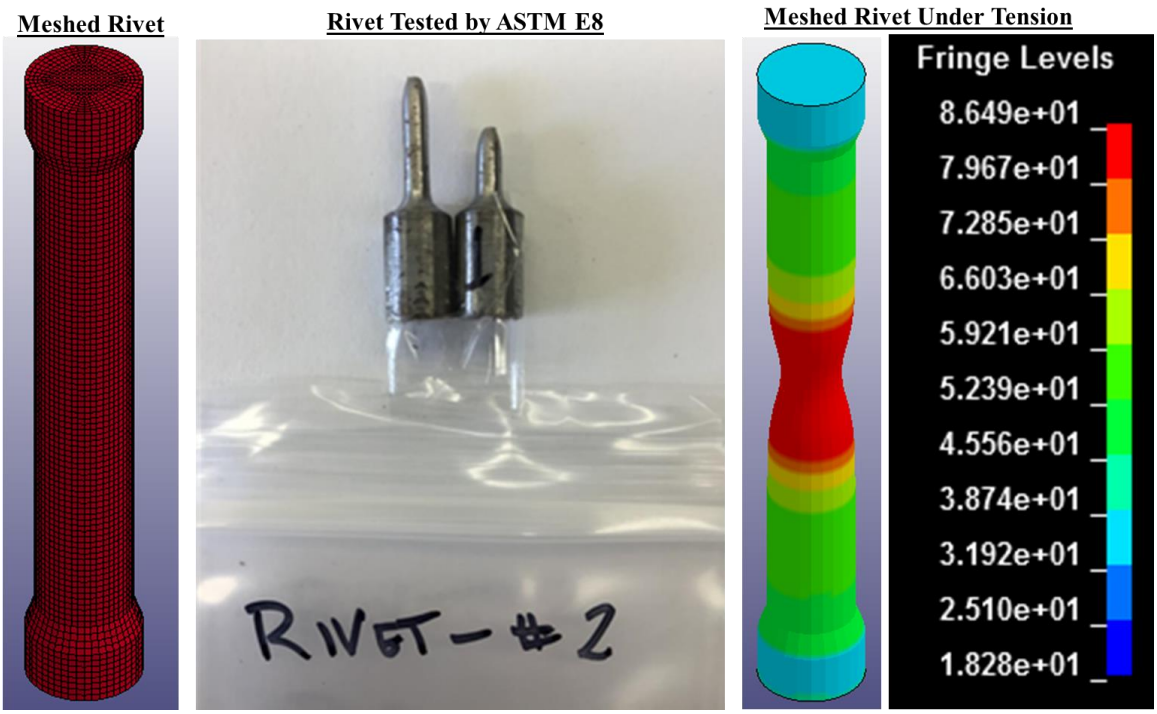


Fig. 3-19: Tested Rivet Comparison with LS-DYNA (2013) Analysis (rivet photo provided by Allison, 2015)

The MAT24 model within LS-DYNA (2013) offers the user a total of 8 stress and strain values to define the behavior of the material being modeled. When entering data into LS-DYNA (2013), the stress and strain values must represent true stress and true strain values. The data provided from the ASTM E8 (2015) test presented back in Fig. 3-22, however, was in terms of engineering stress and engineering strain. Engineering stress and engineering strain are determined from the measured load and deflection, typically from load cells and an extensometer. The values are calculated using the original coupon's cross-sectional area, $A_0$, and length, $L_0$, as shown in Eq. (3-1).

$$\sigma_E = \frac{P}{A_o} \qquad (3\text{-}1)\ (a)$$

where: $\sigma_E$ = engineering stress,

$P$ = measured load in tension,

$A_o$ = original coupon cross-sectional area, and

$$\varepsilon_E = \frac{\delta}{L_o} \qquad (3\text{-}1)\ (b)$$

$\varepsilon_E$ = engineering strain,

$\delta$ = measured change in length, and

$L_o$ = original coupon (extensometer) length.

True stress versus true strain curves do not use original area and length values. Instead, true stress and true strain curves give a more direct measure of the specimen's response by taking an increment of strain to be the incremental increase of displacement divided by the length prior to the incremental change. As this length increases, the cross-sectional area of the coupon decreases. This incremental change in area is used in lieu of the original area. Equations to derive the true stress and true strain values from the engineering stress and strain values are shown in Eq. (3-2).

$$\sigma_T = \sigma_E(1+\varepsilon_E) \qquad \text{(3-2) (a)}$$

where: $\sigma_T$ = true stress, and

$$\varepsilon_T = \int_{L_o}^{L} \frac{dL}{L} = \ln(1+\varepsilon_E) \qquad \text{(3-2) (b)}$$

where: $\varepsilon_T$ = true strain.

As is the case with steel, the early portion of the engineering stress strain curve for A502 Grade 2 rivets exhibits linear behavior. This behavior, known as Hooke's Law, is measured by taking the engineering stress divided by the engineering strain up to the proportional limit to compute Young's Modulus, which is typically estimated to be 29,000 ksi for steel. This value was used extensively throughout this research for both the A502 Grade 2 rivets and the A36 plates. The relationship between true and engineering stress and strain works well within this region. In fact, this relationship is valid up to the point where a specimen begins to neck. However, once necking begins, strain is no longer linear and uniform along the length of the specimen as essentially all deformation takes place within the necked region. For the eight stress and strain points within LS-DYNA's (2013) MAT24, the first strain value must be defined as zero to use the input for Young's Modulus (29,000 ksi).

At the onset of necking, a trial-and-error process was used to create the post-necking portion of the true stress versus true strain curve. After making educated guesses on the true stress and true strain values after necking, an LS-DYNA (2013) analysis simulation was executed. Following the completion of an analysis, the *d3plot* file was opened within LS-DYNA (2013), and engineering stress versus engineering strain data were plotted. This simulated engineering stress versus engineering strain curve was compared with the experimental engineering stress versus engineering strain curves provided from Dr. Allison (2015). The input post-necking stress versus strain values that provided an engineering stress versus engineering strain curve closest to the experimental values was considered the best approximation of the material's actual stress versus strain relationship. The input values for effective plastic strain, EPS, in units of in./in. and corresponding yield stress, ES, in units of ksi that most closely matched the experimental behavior is shown in Table 3-3. A comparison of the true stress versus true strain and the engineering stress versus engineering strain curves is shown in Fig. 3-20. As opposed to the engineering stress versus engineering strain curve, the stress magnitude for the true stress versus true strain curve continues to rise until failure, when the necking region becomes unstable, reaches an ultimate strain, and fractures.

Table 3-3: A502 Grade 2 Stress versus Strain Input for MAT24 in LS-DYNA (2013)

| **EPS1** | **EPS2** | **EPS3** | **EPS4** | **EPS5** | **EPS6** | **EPS7** | **EPS8** |
|---|---|---|---|---|---|---|---|
| 0.0 | 0.01 | 0.02 | 0.04 | 0.06 | 0.3 | 0.55 | 0.85 |
| **ES1** | **ES2** | **ES3** | **ES4** | **ES5** | **ES6** | **ES7** | **ES8** |
| 68.0 | 72.0 | 76.0 | 79.5 | 81.0 | 86.0 | 86.25 | 86.5 |

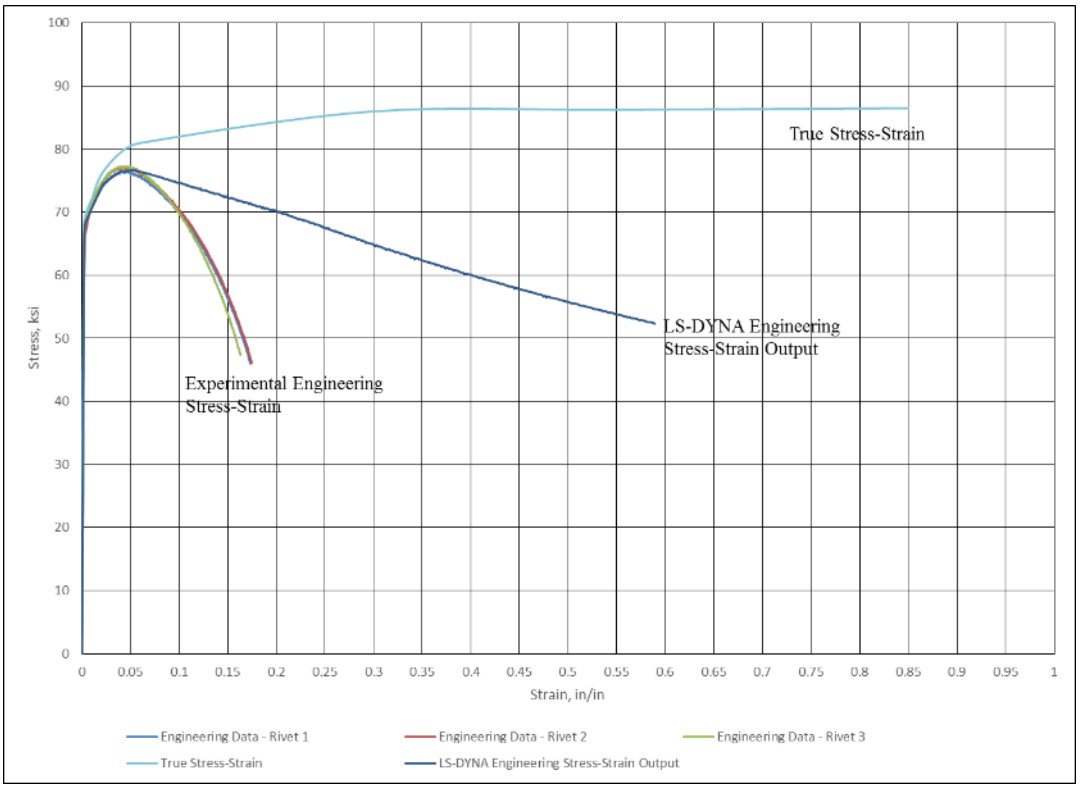


Fig. 3-20: True Stress-Strain versus Engineering Stress-Strain

At this point in the simulation, and as shown in Fig. 3-20, the simulated engineering stress versus engineering strain curve was not acceptably accurate. Thus, an attempt was made to refine the mesh to a smaller size in order to increase accuracy. Mesh convergence was conducted by plotting simulated engineering stress versus engineering strain plots using the input from Table 3-3 for each mesh size and comparing it against the experimental engineering stress versus engineering strain plots. Several simulations were run to achieve convergence. Local mesh refinement in the middle third of the rivet coupon was considered; however, with the desire to use the same mesh density range for

the rivet models, the decision was made to maintain a consistent mesh density throughout the entire coupon. This decision also prevented potential issues with misrepresented geometry and unsuitable mesh transitions which could adversely affect accuracy. Fig. 3-21 shows the engineering stress versus engineering strain results for four of the mesh sizes analyzed. As a point of reference, the coarsest mesh, with 0.096-in. between nodes, was the same mesh size used to develop Fig. 3-24 (LS-DYNA Engineering Stress Strain Output). As shown in Fig. 3-21, as the mesh size decreased, the accuracy of the simulated engineering stress versus engineering strain curve improved. At a mesh size of 0.0037-in. between nodes, the simulated engineering stress versus engineering strain curve approximated the experimental tension test results.

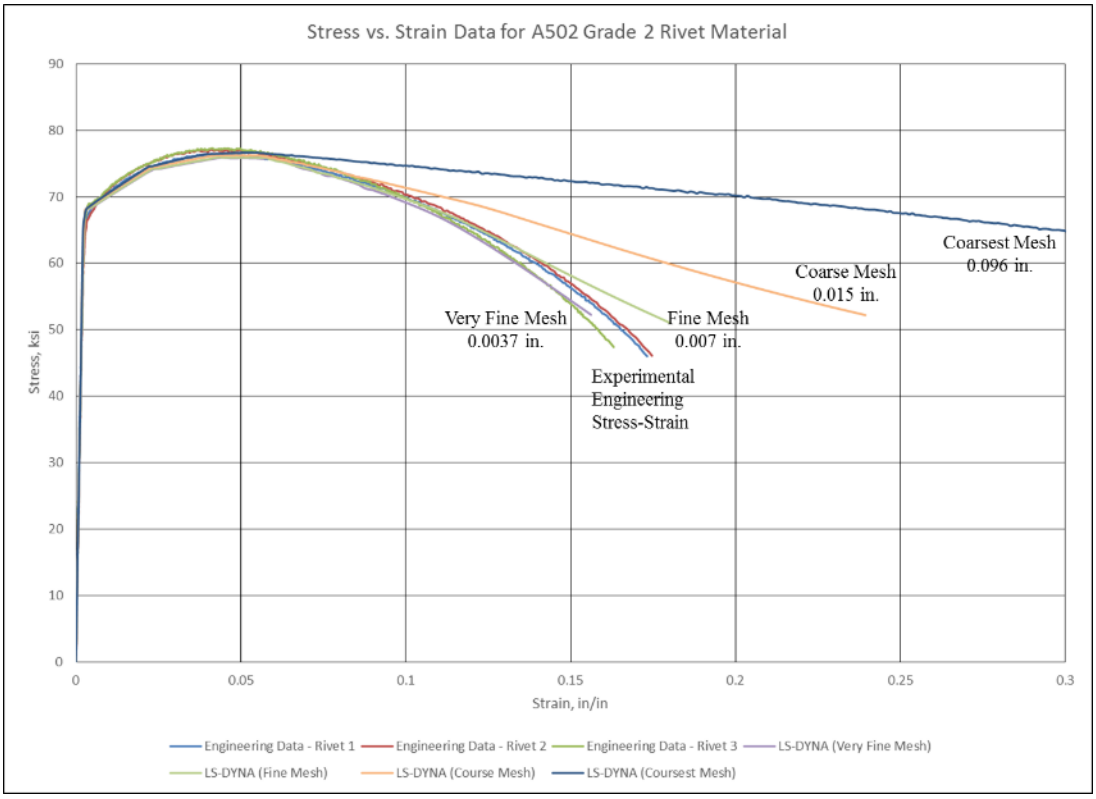


Fig. 3-21: Results of Mesh Sensitivity Analysis for Tension Testing

With confidence in an accurate material model for tension, research efforts shifted into creating the quasi-static rivet shear test. To replicate the A36 steel plates with 0.5625-in. holes for the various configurations, the plate was created within AutoCAD Civil 3D (2013). To get the imported *igs* file to mesh within LS-PrePost (2014), the plate was first quartered within AutoCAD Civil 3D (2013). The decision was made to automesh the quartered plate. A mesh sensitivity study was not done on the A36 plate because the plate was experimentally designed to allow the rivets to fail and was not a focal point of this research. Once the quartered plate was automeshed, the quartered plate was duplicated three times and moved into place until nodes with shared surfaces were

close enough to merge. An illustration of this process is shown in Fig. 3-22. The created plate was assigned ELFORM 1 (under-integrated constant stress) and HOURGLASS 6 formulation (Belytschko-Bindeman, 1993) as described in Section 3.5. The material model used for the plates was the MAT24 piecewise-linear plasticity model. Instead of assigning eight true stress versus true strain points as was done for the rivet, a simple input using expected material strengths (modulus of elasticity, yield stress, tangent modulus, and failure strain) was used as shown in Table 3-4. Again, with the rivets and not the plates serving as the focus of the research, extensive effort for precise plate material properties was unessential.

Table 3-4: A36 Plate Material Properties for LS-DYNA (2013) Analysis

| **E (ksi)** | **SIGY (ksi)** | **ETAN (ksi)** | **FAIL** |
|---|---|---|---|
| 29000 | 47.2 | 75.0 | 0.3 |

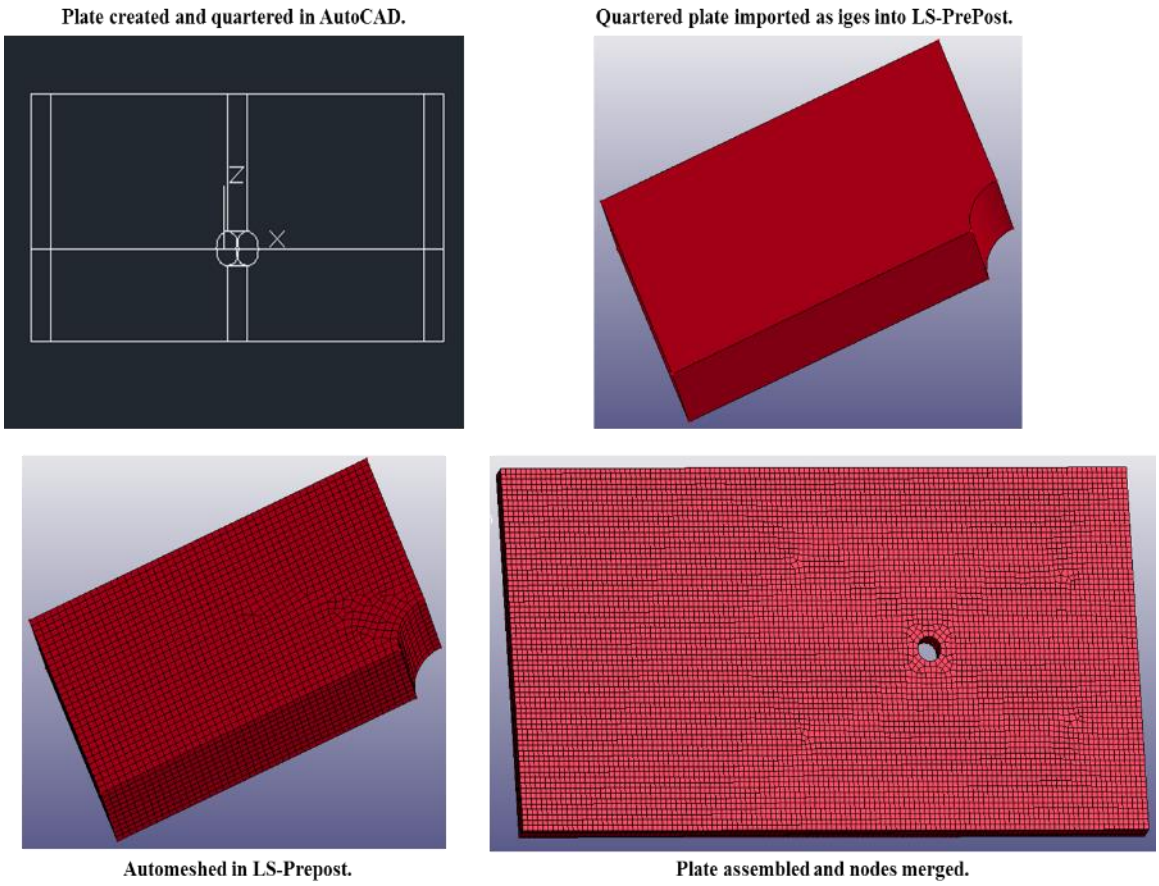


Fig. 3-22: Illustration of Plate Creation for LS-DYNA (2013) Analysis

Because the tension coupon model of the rivet material was already subjected to the convergence study, it was considered logical that the corresponding shear rivet model would have a nearly identical level of accuracy given that the models were not significantly different. As a result, the initial models for shear consisted of an analysis of Configuration 1 (one single rivet) in single shear using a rivet model with a mesh size of 0.0037-in. This mesh size corresponded with the mesh size that best approximated the

engineering stress versus engineering strain curve obtained from experimental testing. This initial analysis did not work, however, as the mesh size in combination with the size of the rivet required too much computer memory. As a result, coarser meshes that were considered relatively accurate in the tension coupon analyses were considered, leading to a subsequent mesh sensitivity study for rivets in shear. A sample of this study is shown in Fig. 3-23. In each case, a successive level of mesh refinement involved splitting the elements of the previous model in all directions. In comparing the meshes from Fig. 3-23 with the mesh size samples from the coupon tension tests from Fig. 3-21, Mesh A corresponds with the Coarsest Mesh results, Mesh B corresponds with an analysis between the Coarsest Mesh and the Coarse Mesh, Mesh C corresponds with the Coarse Mesh results, and Mesh D corresponds with the Fine Mesh results.

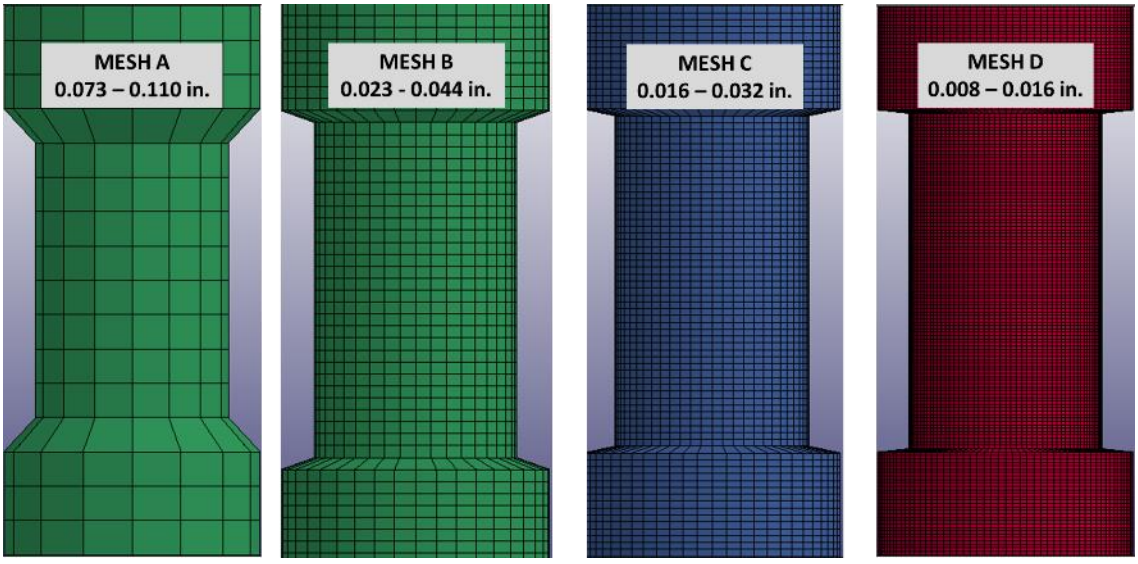


Fig. 3-23: Sample of Mesh Sensitivity of Rivets in Shear

Unlike the plates and the coupon of rivet material created in AutoCAD Civil 3D (2013) and imported into LS-Prepost (2014), the rivets were created using the block mesher provided within LS-Prepost (2014). The rivets were generated by way of *butterfly blocks*, a three-dimensional automatic solid block mesh in LS-Prepost (2014) illustrated in Fig. 3-24. For rivets in single shear, a radius of 0.28125-in. was input to represent the rivet completely filling the hole. For subsequent testing involving double shear, a reduced radius of 0.2725-in. was used to replicate the rivet material not completely filling the hole. The radius used for these analyses were consistent with the findings of Chris Rabalais (2015). Single-shear rivets had a length of 1.6-in., and the double-shear rivets had a length of 2.6-in. The center 1-in. or 2-in. of the rivet shaft corresponded to the two 0.5-in. thick plates used in single-shear testing and the two 0.5-in. thick and one 1-in. thick plate used in double-shear testing, respectively. The remaining 0.6-in. was used to simulate a head on each end of the rivet. The additional input used to create the rivets in single shear using the block mesher butterfly block method is shown in Table 3-5. The terms *Num Elem R* and *Num Elem L* within the table represent the number of elements in the *R* and *L* directions of the cylinder as shown in Fig. 3-24.

Table 3-5: Butterfly Block Input for Rivet Creation within LS-DYNA (2013)

| **Mesh** | **A** **(0.073–0.110 in.)** | **B** **(0.023–0.044 in.)** | **C** **(0.016 – 0.032 in.)** | **D** **(0.016 – 0.008 in.)** |
|---|---|---|---|---|
| Density | 4 | 10 | 14 | 28 |
| Num Elem R: | 3 | 10 | 14 | 28 |
| Num Elem L: | 16 | 48 | 80 | 160 |

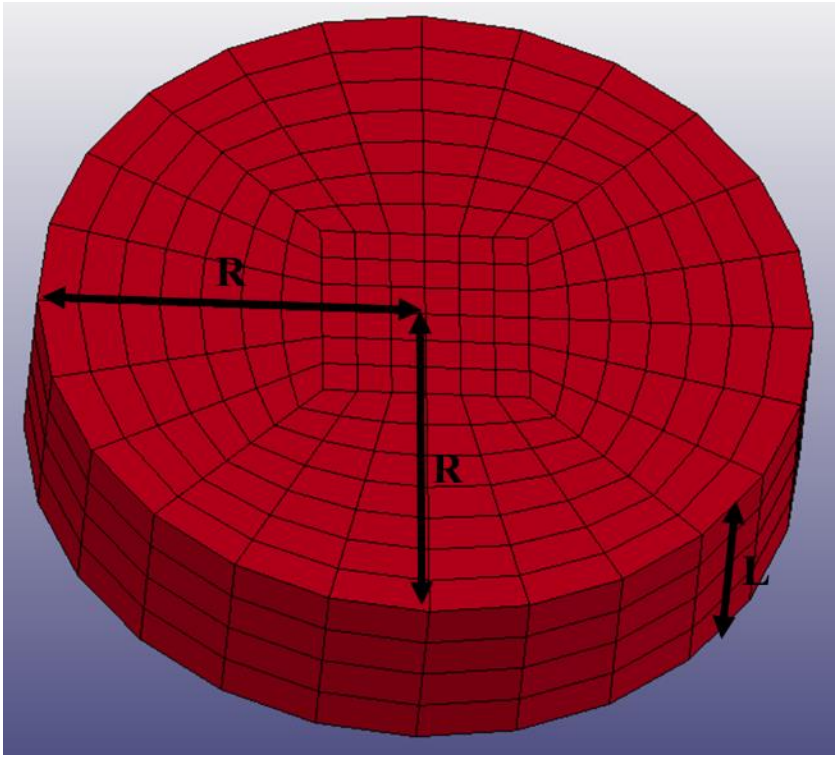


Fig. 3-24: Butterfly Block Creation Template (from LSTC, 2011)

Results from this mesh sensitivity study, as summarized in Table 3-6, provided valuable information with respect to research going forward. First, the peak load results for each test were reasonable. For an average experimental tensile strength of 77 ksi, the expected shear strength is 0.75 times the tensile strength times the rivet area of 0.2485 $in^2$, or 14.35 kips. As shown in Fig. 3-25 and Table 3-6, the peak load for each mesh simulation was within 1 kip of the anticipated value and was well within the range of the experimental data, represented by curves RS1S1, RS1S2, RS1S3, and RS1S4. In fact, regardless of the mesh size, there was very little scatter in the simulated results with respect to shear strength, as the data varied by only 1.4 kips. As a point of comparison,

this difference in peak load between mesh sizes is a mere one-third of the range of the experimental data (16.7 kips maximum value and 12.6 kips minimum value).

The significant difference in response based on mesh size was in the computed ductility. Recall in Fig. 3-21 during the rivet material coupon testing that mesh size played an insignificant role with respect to accuracy in ultimate tensile strength. Capturing the ultimate tensile strength was solely a function of accurate material model input. However, as the rivet material coupon's mesh size decreased, the accuracy with respect to ductility improved significantly. This same pattern is demonstrated in Fig 3-25. With the coarser mesh sizes from Mesh A (0.073 in. – 0.110 in.) and Mesh B (0.023 in. – 0.044 in.), the rivets demonstrated unrealistic ductility. In fact, for the duration of the quasi-static testing, the rivets never failed. With the finer mesh sizes of Mesh C (0.016 in. – 0.032 in.) and Mesh D (0.008 in. – 0.016 in.), however, the rivets demonstrated reasonable ductility consistent with the experimental results.

Table 3-6: Mesh Sensitivity Results for Single Rivet in Single Shear

| **Mesh** | **A** **(0.073–0.110 in.)** | **B** **(0.023–0.044 in.)** | **C** **(0.016 – 0.032 in.)** | **D** **(0.016 – 0.008 in.)** |
|---|---|---|---|---|
| Peak Load (kips) | 15.3 | 14.3 | 14.1 | 13.9 |
| Fail Time (msec) | No Fail | No Fail | 1700 | 1400 |
| Cost (min) | 143 | 151 | 200 | 653 |

The mesh sensitivity study not only showed important revelations with respect to ultimate shear strength and ductility, it also revealed critical information with respect to computational cost. As expected, the amount of time it took LS-DYNA (2013) to process each model was dependent on the mesh size of the rivet. The finest mesh size tested, Mesh D, took more than three times as long as the other mesh sizes; whereas, there was a relatively insignificant difference in cost for the other mesh sizes. With Mesh C and Mesh D providing similar results with respect to maximum shear stress and ductility, subsequent analyses were conducted with the finest mesh, Mesh D, for simple cases and with Mesh C for more complex scenarios. Worthy of note is that despite the fact that the mesh size considered suitable for material model validation via tension testing (0.0037-in.) was smaller than the mesh size considered suitable for rivet shear simulations (0.016-in.), the mesh-size-to-specimen-diameter ratios were similar (0.0037-in. mesh size / 0.113-in. diameter, or 30.54 for the tension tests, and 0.016-in. mesh size / 0.5625-in diameter, or 35.2 for the shear tests). Thus, a minimum mesh-size-to-specimen-diameter ratio of 30 could be a potential valuable modeling recommendation or starting point for future researchers investigating rivets of different diameters.

As mentioned in Section 2.4, the riveting process involves heating and cooling of the rivets and results in the development of residual forces which clamp plates together. Previous research by Wallaert and Fisher (1962), Higgins and Ruble (1955), Munse et al. (1955), Kaplan (1959), and Bendigo et al. (1963) concluded that the amount of pre-tension in fasteners had no effect on their ultimate shear strength. The predominant conclusion of these researchers was that regardless of the number of fasteners, how they

were configured, the number of shear planes, or the strength of the fastener, the amount of tension developed during installation had an insignificant effect on the fastener's ultimate shear strength. Thus, with all analyses focused on the behavior of rivets under shear loading, the decision was made to ignore the effects of thermally induced residual forces in the rivet.

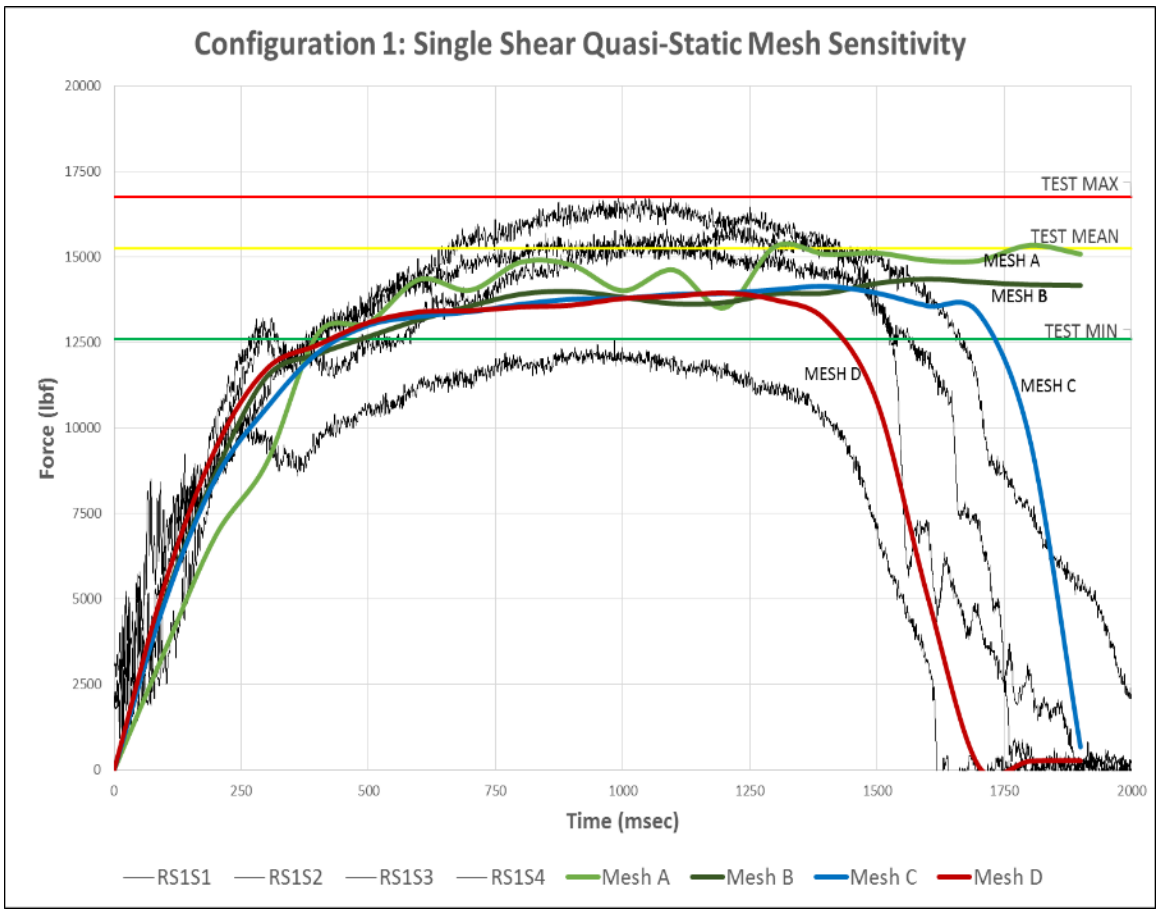


Fig. 3-25: Illustration of Mesh Sensitivity Study for One Rivet in Single Shear

## 3.8 QUASI-STATIC MODEL VALIDATION

Preliminary analyses to investigate model development strategies, including mesh size sensitivity, led to the creation of a model capable of capturing all essential features of a rivet loaded in shear through plate bearing. To ensure this modeling approach would work under a variety of scenarios, models were developed to represent all of the quasi-static testing results reported by Rabalais (2015). Thus, three-dimensional solid hexagonal elements were used to model rivets and plates for the five configurations described previously in this chapter (see Sections 3.4 – 3.7). Elements in the finite element mesh were assigned their respective piecewise-linear plasticity models and analyzed using an under-integrated constant stress formulation with the Belytschko-Bindeman (1993) hourglassing control algorithm. The primary focus of the validation effort was on replicating the peak load (max shear stress) for each configuration. The secondary focus was to qualitatively compare the Load versus Time data from LS-DYNA (2013) simulations with the results from Rabalais (2015). Because the ductility of rivets during experimental testing was not explicitly measured with data limited to Load versus Time, qualitative comparison of the shape of the simulated Load versus Time curve with the experimentally produced curves for each configuration was the chosen methodology.

The initial goal to replicate the results from LS-DYNA (2013) simulations with the results from the experimental testing was slightly modified. This modification was due to the observed scatter in the quasi-static test results. As shown in Table 3-7, the

range of observed maximum load relative to the measured capacity for each configuration varied from 10 percent to 28 percent.

Table 3-7: Range of Experimental Results for Quasi-Static Testing (data extracted from Rabalais, 2015)

| Experimental Test Configuration | Experimental Quasi-Static Load (kips) Minimum | Experimental Quasi-Static Load (kips) Maximum | % Difference |
|---|---|---|---|
| Configuration 1: One Rivet, Single Shear | 12.6 | 16.7 | 24.8 |
| Configuration 1: One Rivet, Double Shear | 20.5 | 24.0 | 14.7 |
| Configuration 2: Two Rivets, Horizontal, Single Shear | 29.2 | 34.0 | 14.3 |
| Configuration 2: Two Rivets, Horizontal, Double Shear | 41.7 | 47.8 | 12.8 |
| Configuration 3: Two Rivets, Vertical, Single Shear | 23.8 | 33.0 | 28.1 |
| Configuration 3: Two Rivets, Vertical, Double Shear | 42.0 | 56.4 | 25.5 |
| Configuration 4: Four Rivets Square, Single Shear | 44.8 | 54.6 | 17.9 |
| Configuration 4: Four Rivets Square, Double Shear | 85.4 | 98.2 | 13.0 |
| Configuration 5: Four Rivets Staggered, Single Shear | 45.4 | 53.6 | 15.3 |
| Configuration 5: Four Rivets Staggered, Double Shear | 86.5 | 96.5 | 10.3 |

Because of the scatter observed between the measured and predicted values, the goal of this research was slightly modified to provide a reasonable model for subsequent

analyses. Of particular importance was the fact that the material model used for analysis within LS-DYNA (2013) was based on a conservative estimate of the tensile strength of the rivet material. As indicated in in Section 3.7, this material model was developed based on the tension testing conducted by Dr. Paul Allison (2015) which consisted of A502 Grade 2 material before the riveting process occurred. Recall from Sections 2.4 and 2.5 that the tensile strength and subsequent shear strength of rivet material typically increased by 10 to 20 percent after going through the riveting process. This variance was likely the largest contributor to the scatter observed in the experimental quasi-static testing results. Simulations were run with 10 percent and 20 percent enhancements to the LS-DYNA (2013) input and provided shear strengths that were up to 20 percent higher than simulations run with the material model developed in Section 3.7. While each simulation run still fell within the range of experimental results, the decision was made to utilize the developed material model from Section 3.7 in lieu of an arbitrarily enhanced model. This decision will provide the engineering community with an adequate model that provides a reasonable depiction of rivet behavior without artificially changing the verified material model.

The results of each of the 10 quasi-static LS-DYNA (2013) simulations are shown in Appendix A and Table 3-8. In nine of the 10 quasi-static rivet model simulations, the LS-DYNA (2013) prediction for maximum shear strength fell within the range of the experimentally measured shear strength values. In the one simulation that fell outside the range of the experimentally measured shear strength values (two horizontal rivets in single shear), the model provided a reasonable representation of the rivet behavior by

underestimating capacity by only 12%. While already reasonable, a 10 to 20 percent increase in the material model input to account for the riveting process would have likely adjusted the simulation result to fall within the experimental range. In addition, as demonstrated in the load versus time curves from Appendix A, the results of each simulation revealed a reasonable comparison to the experimental results with respect to time to failure.

Table 3-8: Model Data versus Experimental Data for Quasi-Static Loading

| **Test Configuration** | **Rivet Mesh Size:** **C: (0.016 in. - 0.032 in.)** **D: (0.008 in. - 0.016 in.)** | **Experimental Quasi-Static Load (kips) Minimum** | **LS-DYNA Quasi-Static Load (kips)** | **Experimental Quasi-Static Load (kips) Maximum** | **% Difference Outside of Range** |
|---|---|---|---|---|---|
| 1: One Rivet, Single Shear | D | 12.6 | 12.8 | 16.7 | In range |
| 1: One Rivet, Double Shear | D | 20.5 | 23.6 | 24.0 | In range |
| 2: Two Rivets Horizontal, Single Shear | D | 29.2 | 25.7 | 34.0 | 12.0 |
| 2: Two Rivets Horizontal, Double Shear | D | 41.7 | 47.0 | 47.8 | In range |
| 3: Two Rivets Vertical, Single Shear | D | 23.8 | 27.9 | 33.0 | In range |
| 3: Two Rivets Vertical, Double Shear | D | 42.0 | 53.8 | 56.4 | In range |
| 4: Four Rivets Square, Single Shear | C | 44.8 | 50.5 | 54.6 | In range |
| 4: Four Rivets Square, Double Shear | C | 85.4 | 94.7 | 98.2 | In range |
| 5: Four Rivets Staggered, Single Shear | C | 45.4 | 50.3 | 53.6 | In range |
| 5: Four Rivets Staggered, Double Shear | C | 86.5 | 94.4 | 96.5 | In range |

A further look at the LS-DYNA (2013) analysis results revealed that both the ultimate shear strength and the ratio of ultimate-shear-strength-to-ultimate-tensile-strength for each configuration were reasonable. Based on historical data collected and reported in the *Guide to Design Criteria for Bolted and Riveted Connections* (Kulak et al., 1987) and the ultimate tensile strength of the rivet coupon for this research, expectations were that the ultimate shear strength of the rivets would range between 53 ksi to 66 ksi. The shear load per plane demonstrated by the rivet and material model created from this research ranged from 50.4 ksi to 57.7 ksi. Any increase to the material model input to account for the riveting process would have likely fit the expected data even better. Furthermore, as mentioned in Section 2.5, the *Guide to Design Criteria for Bolted and Riveted Connections* (Kulak et al., 1987) revealed the average shear-to-tensile strength ratio for rivets varied from 0.67 to 0.83, with an average of 0.75. Table 3-9 reveals that the ultimate-shear-strength-to-ultimate-tensile-strength ratio, ranging from 0.65 to 0.75 from this LS-DYNA (2013) research, provided a reasonable response that was consistent with historical data. This percentage was calculated by comparing the shear load per plane from the LS-DYNA (2013) analysis results to the ultimate tensile strength obtained from the LS-DYNA (2013) coupon tests described in Section 3.7 (77 ksi).

Table 3-9: Ultimate Shear Stress to Ultimate Tensile Stress LS-DYNA (2013) Results

| Test Configuration | Modeled Rivet Stress Area ($in^2$) | LS-DYNA Quasi-Static Load (lbf) | Shear Load per Plane (ksi) | Percentage of Ultimate Shear Stress to Ultimate Tensile Stress |
|---|---|---|---|---|
| 1: One Rivet, Single Shear | 0.2485 | 12806 | 51.5 | 67% |
| 1: One Rivet, Double Shear | 0.2333 | 23615 | 50.6 | 66% |
| 2: Two Rivets Horizontal, Single Shear | 0.2485 | 25720 | 51.7 | 67% |
| 2: Two Rivets Horizontal, Double Shear | 0.2333 | 46997 | 50.4 | 65% |
| 3: Two Rivets Vertical, Single Shear | 0.2485 | 27875 | 56.1 | 73% |
| 3: Two Rivets Vertical, Double Shear | 0.2333 | 53848 | 57.7 | 75% |
| 4: Four Rivets Square, Single Shear | 0.2485 | 50549 | 50.9 | 66% |
| 4: Four Rivets Square, Double Shear | 0.2333 | 94680 | 50.7 | 66% |
| 5: Four Rivets Staggered, Single Shear | 0.2485 | 50317 | 50.6 | 66% |
| 5: Four Rivets Staggered, Double Shear | 0.2333 | 94371 | 50.6 | 66% |

As a final but important aspect of validity, a close investigation of the three-dimensional rivet models following the quasi-static simulations was conducted. As mentioned in Section 2.6, the fracture type and deformation changes significantly based on the loading type (shear, tension, or combination of both). Under pure shear deformation, as was the intent of the models for this research, necking should not occur. As illustrated in Fig. 3-26 (and similarly for each of the 10 quasi-static LS-DYNA (2013) simulations) no necking was evident in the fracture of the rivets, providing further confidence in the computational models developed for this research.

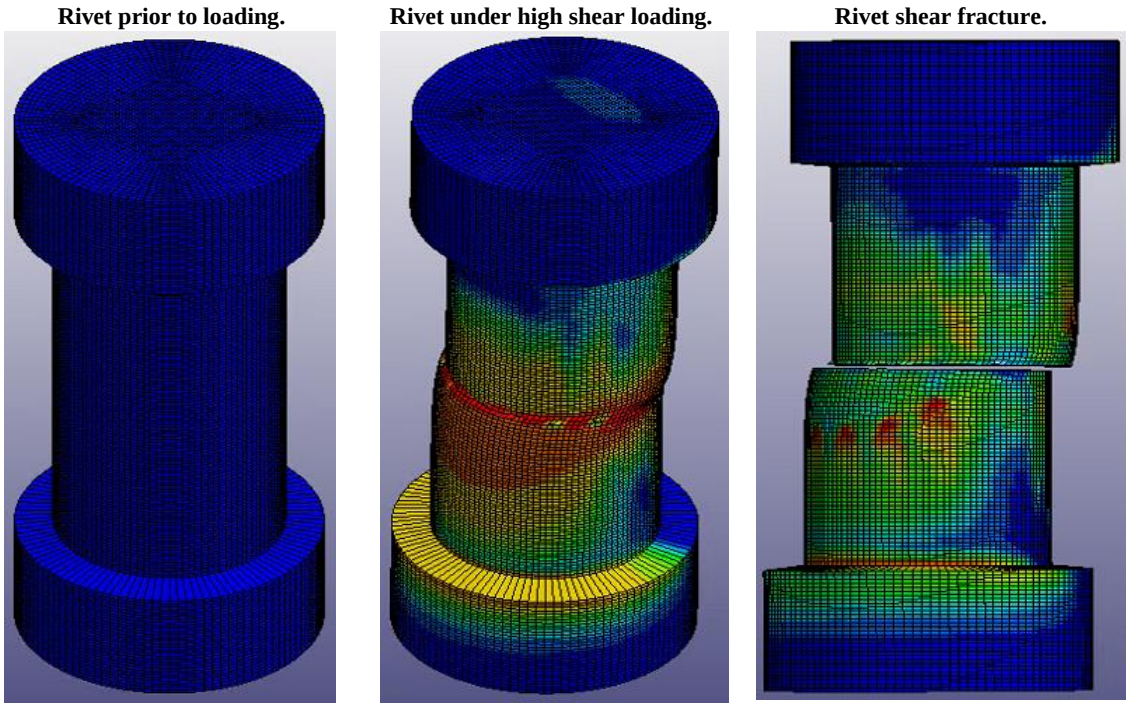


Fig. 3-26: Illustration of Shear Fracture of LS-DYNA (2013) Model

## 3.9 MODELING SUMMARY

This chapter opened with a thorough justification of the need to understand the behavior of rivets in shear under high strain rates and the results of recent experimental testing done as initial phases towards that goal. The remainder of the chapter provided a thorough description of the computational modeling performed to simulate the response of experimental quasi-static testing of rivets in shear. The goal of the computational studies of quasi-static testing was to gain confidence in modeling procedures so that they can be further expanded and used to predict the response of rivets under high loading rates. High-rate analyses are discussed in Chapter 4. Prior to conducting this computational modeling, the three-dimensional testing of A502 Grade 2 rivets using finite element modeling was not readily available in literature.

After conducting sensitivity studies of the rivet finite element model, the material model, mesh size, and other parameters noted throughout Chapter 3 were refined to provide a solution for future finite element model analyses. Appendix A includes the load versus time curves for all 5 configurations in single- and double-shear. The comparisons between the computational studies conducted for this dissertation with both the recent experimental testing by ERDC (Rabalais, 2015) and historical testing discussed throughout Chapter 2 is also included. Validation of the behavior of simple riveted connections under quasi-static shear loading was achieved, providing a contribution and baseline for additional studies considering other parameters.

# Chapter 4: Modeling Riveted Connections at High Strain Rates

*"Do not go where the path may lead, go instead where there is no path and leave a trail."*

-Ralph Waldo Emerson, (1803-1882)

## 4.1 An Introduction

As detailed in Chapter 3, numerous finite element analyses were performed to simulate the quasi-static response of simple riveted connections under shear loadings. Numerical models explicitly captured rivet response until failure, providing load versus time response data that was consistent with results from Rabalais (2015). With validation achieved in Chapter 3, the purpose of Chapter 4 is to detail the development and validation of a model to capture rivet behavior under high loading rates and the utilization of this model to investigate an untested problem.

Background research conducted for this dissertation and discussed in Section 2.9 narrowed focus for model selection to two constitutive models: Johnson-Cook (1985) and Cowper Symonds (1957). The Johnson-Cook (1985) model is available as a viable option within LS-DYNA (2013) as *MAT_TABULATED_JOHNSON_COOK (MAT 224) to capture rivet behavior under high loading rates. The model uses a table of curves that defines plastic failure strain as a function of triaxiality, strain rate, temperature, and element size. The development of plastic strain input curves required the execution of a

series of tension tests under various strain rates and temperatures. Despite a thorough search for this A502 Grade 2 steel information, the search did not identify any available information.

When compared to the Johnson-Cook (1985) model, the Cowper Symonds (1957) constitutive model is simple in that it only involves scaling the flow of stress as described in Section 2.9. Furthermore, the use of the Cowper Symonds (1957) constitutive model provided a great advantage to this research effort in that it was easily incorporated into the piecewise-linear plasticity material model (MAT24) described in detail in Section 3.7 and validated in Section 3.8 with rivet configurations under quasi-static loading. With these as clear advantages, the Cowper Symonds (1957) constitutive model was used throughout this research to capture the response of rivets under high loading rates.

Chapter 4 closes with the results of the investigation of an untested problem using validated material and constitutive models from this dissertation. While both quasi-static and dynamic experimental data existed with respect to simple riveted connections, there were no data with respect to the dynamic testing of long riveted connections. Thus, validated models developed as part of this dissertation were utilized to predict the behavior of long riveted connections, providing further valuable contributions to the engineering community.

## 4.2 COWPER SYMONDS AND LS-DYNA (2013)

The second objective of this dissertation was to recommend a constitutive model that accurately predicted the behavior of rivets under high strain rates while using the laboratory testing by Rabalais (2015) as validation. To achieve this objective, the Cowper Symonds (1957) constitutive model was used within LS-DYNA (2013) to capture rivet behavior. As explained in Section 2.9, this constitutive model captured the differences between dynamic and static load effects through the strain rate ($\dot{\varepsilon}$) and two empirical coefficients ($C$, $q$) that traditionally have been determined through experimental testing. The piecewise-linear plasticity material model (MAT24) within LS-DYNA (2013) allows a user to input a single quasi-static stress-strain curve as the basis for the empirical Cowper Symonds (1957) coefficients. With no need to input a separate true stress and true strain curve for each individual strain rate, the true stress and true strain values input into the piecewise-linear plasticity material model values for A502 Grade 2 rivet steel validated in Section 3.7 were suitable for use with this constitutive model. In the literature review performed for this research, there were no Cowper Symonds (1957) empirical coefficients for A502 Grade 2 rivets or any other steel rivet type reported.

The primary focus for validating rivet behavior in shear under high loading rates was to replicate the peak load (ultimate shear strength) for each configuration. The secondary focus was to ensure each simulated load versus time curve was comparable to that from experimental testing (Rabalais, 2015). Because the ductility of the rivets during experimental testing was not explicitly measured, qualitative comparison of the shape of

the simulated load versus time curves with the experimentally produced curves for each configuration was required. For the dynamic loading validation, all simulated tests resulted in rivets failing in shear in under 7 milliseconds, consistent with the experimental testing (Rabalais, 2015).

After conducting a detailed review of the measured test data, the initial goal to replicate the experimental results using LS-DYNA (2013) was slightly modified. This modification was due to the observed scatter in the experimental dynamic test results. As shown in Table 4-1, the range of observed maximum load for each of the five configurations in single- and double- shear varied from 10 percent to 54 percent. Given this scatter, the goal of this research was adjusted to provide a reasonable constitutive model for subsequent research.

Table 4-1: Range of Experimental Results for Dynamic Testing (data extracted from Rabalais, 2015)

| Experimental Test Configuration | Experimental Dynamic Load (kips) Minimum | Experimental Dynamic Load (kips) Maximum | % Difference |
|---|---|---|---|
| 1: One Rivet, Single Shear | 13.7 | 16.1 | 15.1 |
| 1: One Rivet, Double Shear | 31.0 | 44.7 | 30.7 |
| 2: Two Rivets Horizontal, Single Shear | 39.4 | 79.6 | 50.4 |
| 2: Two Rivets Horizontal, Double Shear | 55.9 | 85.5 | 34.7 |
| 3: Two Rivets Vertical, Single Shear | 54.2 | 60.3 | 10.1 |
| 3: Two Rivets Vertical, Double Shear | 79.8 | 132.6 | 39.9 |
| 4: Four Rivets Square, Single Shear | 54.4 | 117.4 | 53.7 |
| 4: Four Rivets Square, Double Shear | 102.9 | 147.8 | 30.4 |
| 5: Four Rivets Staggered, Single Shear | 66.4 | 94.5 | 29.7 |
| 5: Four Rivets Staggered, Double Shear | 147.6 | 213.2 | 30.8 |

The starting point to determine the appropriate Cowper Symonds (1957) coefficients for A502 Grade 2 rivets involved a literature review of testing that generated empirical values of $C$ and $q$ for mild steel. In analyzing these values, shown in Table 2-12, it was evident that the empirical value $q$ was relatively consistent for all mild steel dynamic testing, ranging from 2.2 to 5. Conversely, the empirical value $C$ demonstrated a large variability, with values ranging from 40.4 to 6884. The large difference in Cowper

Symonds (1957) parameter values and the considerable scatter in published experimental data suggested there were several factors contributing to the behavior of mild steel under high strain rates. These factors included the amount of dynamic strain (elastic behavior versus plastic behavior), loading differences (tension versus compression versus shear), testing techniques, and material composition. With such a large number of contributing variables, a decision was made to compare results using extreme values for $C$ and $q$ within LS-DYNA (2013) with the experimental test results (Rabalais, 2015). Thus, LS-DYNA (2013) simulations were conducted for every experimentally tested rivet configuration using the published bounding empirical values of the original Cowper Symonds (1957) parameters ($C$ = 40.4 $s^{-1}$ and $q$ = 5) and the Abramowicz and Jones (1986) parameters ($C$ = 6884 $s^{-1}$ and $q$ = 3.91). The original Cowper Symonds (1957) parameters were derived from experimental testing involving mild steel loaded axially in tension, while the Abramowicz and Jones (1986) parameters were obtained from experiments involving the dynamic axial crushing of mild steel tubes.

Of all the LS-DYNA (2013) parameters and settings validated and described in Chapter 3 of this dissertation, only the prescribed motion curve input required modification to impose dynamic loading. Similar to the quasi-static loading analysis, several simulations were required to get the rivet to fail in a dynamic nature similarly to the experimental work. This challenge was a function of undetermined experimental loading rates that were specimen dependent for the 200 kip loader and difficult to control (Rabalais, 2015). Experimentally, failure for each rivet under dynamic loading occurred in under 7 milliseconds. This time benchmark, in conjunction with the general shape of

the load versus time curves, served as the basis for qualitative acceptance. Table 4-2 shows the displacement-controlled prescribed motion applied within LS-DYNA (2013). A trial-and-error approach was used to impose displacement. There was a requirement to assume a displacement history because there were no experimental values to compare against. As demonstrated throughout Appendix B, the displacement-controlled prescribed motion applied within LS-DYNA (2013) for all 10 simulations produced rivet shear failure that was similar to the tested time frame observed in experimental testing (Rabalais, 2015).

Table 4-2: Prescribed Motion Curve Input for Dynamic Simulations

| **Configuration # and Description** | **Time (seconds)** | **Imposed Displacement (in.)** |
|---|---|---|
| Applicable to all configurations in single- and double-shear. | 0 | 0 |
| | 0.0025 | 0.025 |
| | 0.005 | 0.1 |
| | 0.0075 | 0.225 |
| | 0.01 | 0.4 |

### 4.3 LS-DYNA (2013) MODEL VALIDATION

Despite serving as bounding values for published recommended Cowper Symonds (1957) parameters, both the original Cowper Symonds (1957) parameters ($C$ =

40.4 $s^{-1}$ and $q$ = 5) and the Abramowicz and Jones (1986) parameters ($C$ = 6884 $s^{-1}$ and $q$ = 3.91) predicted reasonable rivet behavior under dynamic loads in LS-DYNA (2013). The results of the 10 dynamic LS-DYNA (2013) simulations for each set of Cowper Symonds (1957) parameters ($C$ = 40.4 $s^{-1}$ and $q$ = 5 versus $C$ = 6884 $s^{-1}$ and $q$ = 3.91) are shown in Appendix B and Table 4-3. Within Appendix B, dashed lines represent predicted rivet behavior from LS-DYNA (2013) using the original Cowper Symonds (1957) parameters ($C$ = 40.4 $s^{-1}$ and $q$ = 5). Bold solid lines represent predicted rivet behavior from LS-DYNA (2013) using Abramowicz and Jones (1986) parameters ($C$ = 6884 $s^{-1}$ and $q$ = 3.91). Light (unbold) lines represent experimental test data (Rabalais, 2015). Positive percentages from Table 4-3 indicate LS-DYNA (2013) models that provided an ultimate shear strength greater than the experimental test results (Rabalais, 2015). Likewise, any negative percentages from Table 4-3 indicate the LS-DYNA (2013) model provided an ultimate shear strength less than the experimental test results (Rabalais, 2015).

In comparing the LS-DYNA (2013) results with the experimental results, it is first important to point out two anomalies in the experimental output. While reporting a dynamic increase factor of approximately 1.72 for the rivets (Rabalais 2015), two of the configurations tested experimentally produced dynamic increase factors different than predicted. Likely contributors to these outlier experimental tests were internal flaws and the variable nature of dynamic loading (Rabalais e-mail, 2015). The redistribution of loads within materials can result in a premature failure when flaws exist because the loads will find the weakest point (Rabalais e-mail, 2015). For Configuration 1 (one rivet

in single shear), the anticipated ultimate shear strength based on a 1.72 dynamic increase factor ranged from 21.7 kips to 28.8 kips; however, the measured experimental values were much lower, ranging from 13.7 kips to 16.1 kips. When comparing the LS-DYNA (2013) results with the experimental and predicted results, as shown in Fig. 4-1, the originally published recommended parameters $C = 40.4\ s^{-1}$ and $q = 5$ demonstrated an ultimate shear strength that was within range of the predicted values. The parameters of $C = 6884\ s^{-1}$ and $q = 3.91$, however, provided an ultimate shear strength within LS-DYNA (2013) that was approximately 14 percent below the predicted ultimate shear strength.

Similarly, for Configuration 3 (two rivets vertical, single shear) the anticipated ultimate shear strength ranged from 40.8 kips to 56.8 kips. Meanwhile, the actual experimental test values were higher, ranging from 54.2 kips to 60.3 kips. The LS-DYNA (2013) results for this configuration exhibited a similar trend. As shown in Fig. 4-2, the original Cowper Symonds (1957) recommended parameters input within LS-DYNA (2013) produced an ultimate shear stress within the projected range, while the Abramowicz and Jones (1986) parameters input within LS-DYNA (2013) produced an ultimate shear stress approximately 20 percent below the projected range.

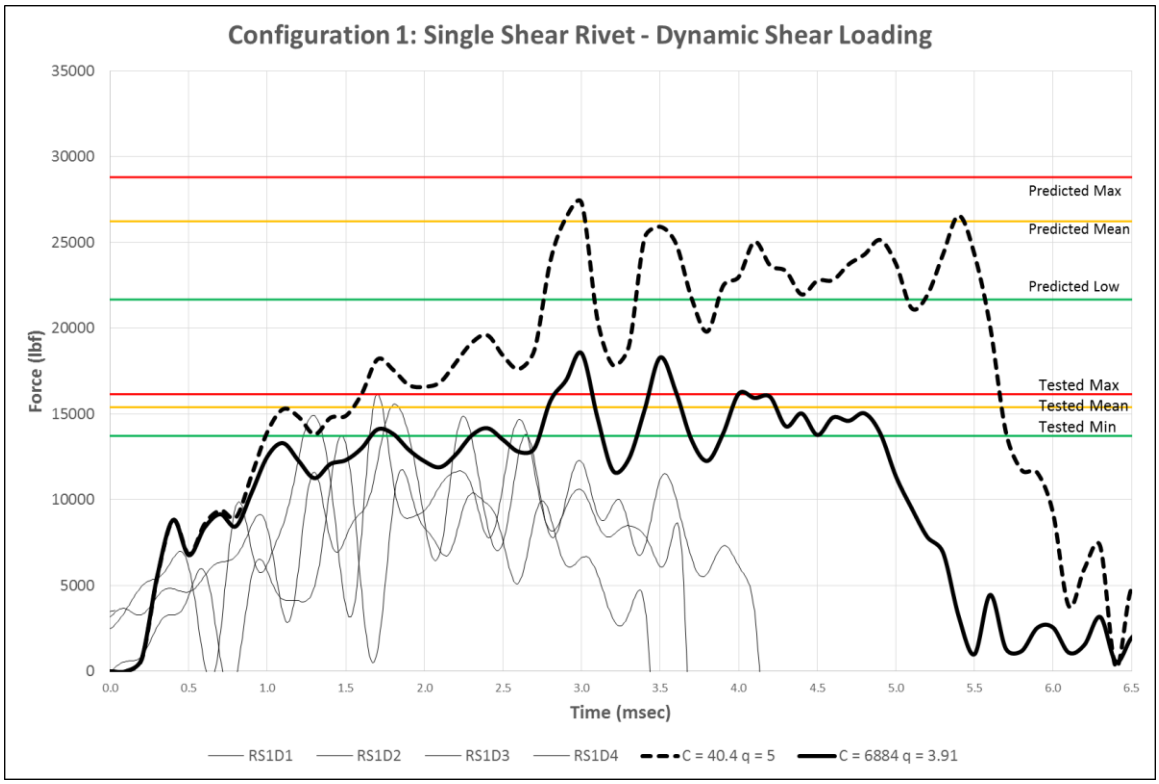


Fig. 4-1: Configuration 1 Anomaly

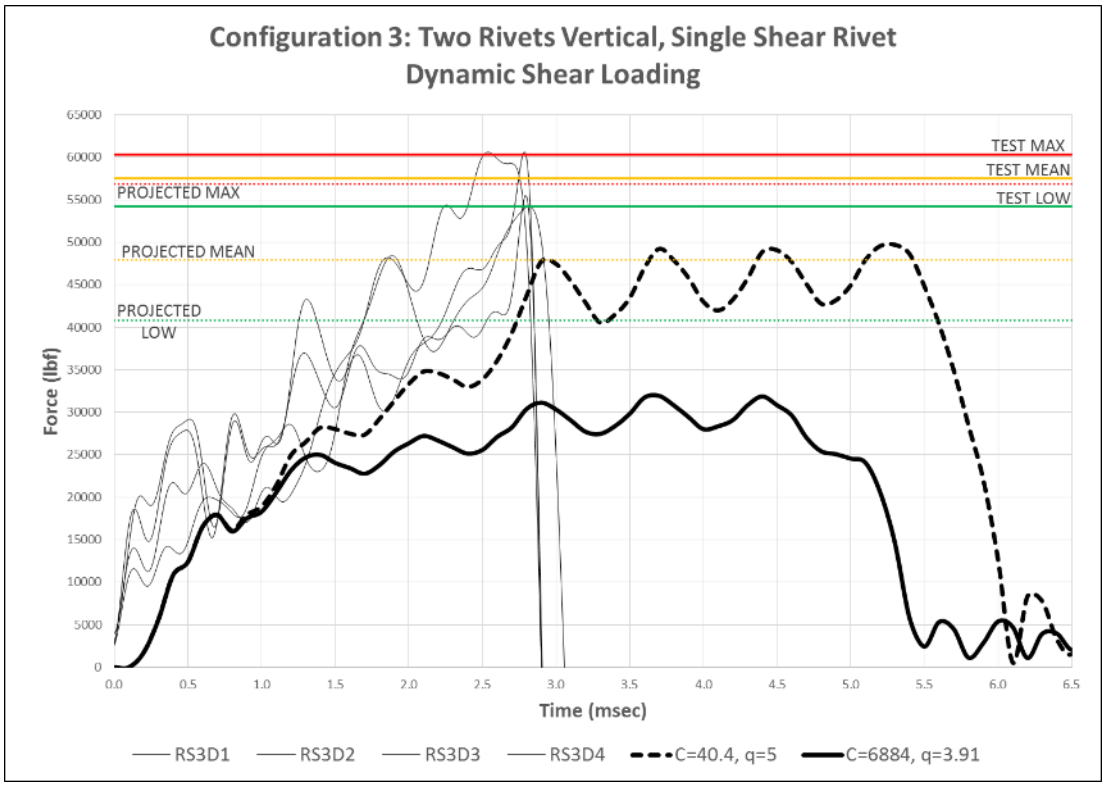


Fig. 4-2: Configuration 3 Anomaly

Regarding the remaining eight simulated dynamic rivet models, the original parameters ($C$ = 40.4 $s^{-1}$ and $q$ = 5) for Cowper Symonds (1957) input within LS-DYNA (2013) predicted an ultimate shear strength within the range of the experimental ultimate shear strength 50 percent of the time. For the other four configurations, the original parameters input within LS-DYNA (2013) predicted an ultimate shear strength that was greater than the experimental results by as much as 23.5 percent. When using the parameters ($C$ = 6884 $s^{-1}$ and $q$ = 3.91) recommended by Abramowicz and Jones (1986) within LS-DYNA (2013), the rivet configurations demonstrated an ultimate shear strength within the range of the experimental ultimate shear strength 37.5 percent of the

time. For the other five configurations, the Abramowicz and Jones (1986) parameters input within LS-DYNA (2013) predicted an ultimate shear strength that was less than the experimental results by as much as 16.3 percent. A summary of all the testing results are shown in Table 4-3 and Table 4-4, with the previously mentioned outlier experimental test results highlighted in yellow.

For both sets of parameters, the Cowper Symonds (1957) constitutive model provided reasonable representations of rivet behavior. However, the parameters recommended by Cowper Symonds ($C$ = 40.4 $s^{-1}$ and $q$ = 5) overestimated the strength of the rivets in several cases, which was unconservative given the already variable nature and behavior of rivets. Meanwhile, the Abramowicz and Jones (1986) parameters ($C$ = 6884 $s^{-1}$ and $q$ = 3.91) input within LS-DYNA (2013) provided a conservative estimate of the ultimate shear strength in cases where it was not within the range of the experimental values. Recall, also, that the material model for this research, described in Section 3.7, was based on the stress and strain relationship of the rivet steel prior to the riveting process. It is reasonable to expect a 10 to 20 percent increase in the material model input to account for the riveting process would adjust the Abramowicz and Jones (1986) simulation results to increase within the range of the experimental values. Nonetheless, an increase in the material model input would likely result in an even greater unconservative analyses in the case of the Cowper Symonds (1957) parameters. The load versus time curves from all of the LS-DYNA (2013) simulations demonstrated comparable shapes and end times to their experimental counterparts. The different Cowper Symonds (1957) parameters had little impact on the overall shape of the curves.

A subsequent analysis of the simulations examined the dynamic increase factor exhibited for each set of Cowper Symonds (1957) parameters. This analysis was done by comparing the LS-DYNA (2013) output from quasi-static simulations and comparing it to the LS-DYNA (2013) output from dynamic simulations. In doing so, it was determined that the original Cowper Symonds (1957) parameters ($C$ = 40.4 $s^{-1}$ and $q$ = 5) overestimated the dynamic increase factor of the rivets. As demonstrated in Table 4-5, the average dynamic increase factor within LS-DYNA (2013) was 2.0. Meanwhile, the average dynamic increase factor using the Abramowicz and Jones (1986) parameters ($C$ = 6884 $s^{-1}$ and $q$ = 3.91) within LS-DYNA (2013) was 1.3. As a point of comparison, the dynamic increase factor from the experimental testing, calculated by dividing the mean of the dynamic tests by the mean of the static tests, was 1.7 (Rabalais, 2015). Thus, the extreme Cowper Symonds (1957) parameters ($C$ = 40.4 $s^{-1}$ and $q$ = 5) and Abramowicz and Jones (1986) parameters ($C$ = 6884 $s^{-1}$ and $q$ = 3.91) provided reasonable upper and lower bounds, respectively, of rivet response under high loading rates.

Table 4-3: Dynamic Loading Simulation Results using Cowper Symonds (1956) Original Parameters (C = 40.4 $s^{-1}$ and q = 5) versus Experimental Results

| **Test Configuration** | **Rivet Mesh Size: C: (0.016 in. - 0.032 in.) D: (0.008 in. - 0.016 in.)** | **Experimental Dynamic Load (kips) Minimum** | **Experimental Dynamic Load (kips) Maximum** | **LS-DYNA Dynamic Load (kips) C = 40.4 $s^{-1}$, q = 5** | **% Difference Outside of Range** |
|---|---|---|---|---|---|
| 1: One Rivet, Single Shear | D | 13.7 | 16.1 | 27.3 | 40.8 |
| 1: One Rivet, Double Shear | D | 31.0 | 44.7 | 47.4 | 5.6 |
| 2: Two Rivets Horizontal, Single Shear | D | 39.4 | 79.6 | 50.2 | In range |
| 2: Two Rivets Horizontal, Double Shear | D | 55.9 | 85.5 | 105.2 | 18.7 |
| 3: Two Rivets Vertical, Single Shear | D | 54.2 | 60.3 | 49.7 | -8.3 |
| 3: Two Rivets Vertical, Double Shear | D | 79.8 | 132.6 | 103.0 | In range |
| 4: Four Rivets Square, Single Shear | C | 54.4 | 117.4 | 106.9 | In range |
| 4: Four Rivets Square, Double Shear | C | 102.9 | 147.8 | 193.1 | 23.4 |
| 5: Four Rivets Staggered, Single Shear | C | 66.4 | 94.5 | 101.0 | 6.5 |
| 5: Four Rivets Staggered, Double Shear | C | 147.6 | 213.2 | 176.6 | In range |

Table 4-4: Dynamic Loading Simulation Results using Abramowicz and Jones (1986) Parameters (C = 6884 $s^{-1}$ and q = 3.91) versus Experimental Results

| **Test Configuration** | **Rivet Mesh Size: C: (0.016 in. - 0.032 in.) D: (0.008 in. - 0.016 in.)** | **Experimental Dynamic Load (kips) Minimum** | **Experimental Dynamic Load (kips) Maximum** | **LS-DYNA Dynamic Load (kips) C = 6884 $s^{-1}$, q = 3.91** | **% Difference Outside of Range** |
|---|---|---|---|---|---|
| 1: One Rivet, Single Shear | D | 13.7 | 16.1 | 18.5 | 12.9 |
| 1: One Rivet, Double Shear | D | 31.0 | 44.7 | 30.9 | -0.2 |
| 2: Two Rivets Horizontal, Single Shear | D | 39.4 | 79.6 | 33.8 | -14.2 |
| 2: Two Rivets Horizontal, Double Shear | D | 55.9 | 85.5 | 64.0 | In range |
| 3: Two Rivets Vertical, Single Shear | D | 54.2 | 60.3 | 31.9 | -41.1 |
| 3: Two Rivets Vertical, Double Shear | D | 79.8 | 132.6 | 70.1 | -12.1 |
| 4: Four Rivets Square, Single Shear | C | 54.4 | 117.4 | 71.3 | In range |
| 4: Four Rivets Square, Double Shear | C | 102.9 | 147.8 | 116.3 | In range |
| 5: Four Rivets Staggered, Single Shear | C | 66.4 | 94.5 | 65.1 | -1.9 |
| 5: Four Rivets Staggered, Double Shear | C | 147.6 | 213.2 | 123.5 | -16.3 |

Table 4-5: Dynamic Increase Factor (DIF) of LS-DYNA (2013) Bounding Simulations

| **Test Configuration** | **LS-DYNA Quasi-Static Load (lbf)** | **LS-DYNA Dynamic Load (lbf) C = 40.4 $s^{-1}$, q = 5** | **Calculated DIF C = 40.4 $s^{-1}$, q = 5** | **LS-DYNA Dynamic Load (lbf) C = 6884 $s^{-1}$, q = 3.91** | **Calculated DIF C = 6884 $s^{-1}$, q = 3.91** |
|---|---|---|---|---|---|
| 1: One Rivet, Single Shear | 12806 | 27264 | 2.1 | 18535 | 1.4 |
| 1: One Rivet, Double Shear | 23615 | 47376 | 2.0 | 30934 | 1.3 |
| 2: Two Rivets Horizontal, Single Shear | 25720 | 50222 | 2.0 | 33847 | 1.3 |
| 2: Two Rivets Horizontal, Double Shear | 46997 | 105218 | 2.2 | 63999 | 1.4 |
| 3: Two Rivets Vertical, Single Shear | 27875 | 49730 | 1.8 | 31932 | 1.1 |
| 3: Two Rivets Vertical, Double Shear | 53848 | 102987 | 1.9 | 70131 | 1.3 |
| 4: Four Rivets Square, Single Shear | 50549 | 106880 | 2.1 | 71327 | 1.4 |
| 4: Four Rivets Square, Double Shear | 94680 | 193066 | 2.0 | 116330 | 1.2 |
| 5: Four Rivets Staggered, Single Shear | 50317 | 100979 | 2.0 | 65107 | 1.3 |
| 5: Four Rivets Staggered, Double Shear | 94371 | 176588 | 1.9 | 123524 | 1.3 |
| | | **Average DIF:** | **2.0** | **Average DIF:** | **1.3** |

Despite the fact that the investigated LS-DYNA (2013) parameters adequately bounded the ultimate shear strength, a goal of this research was to recommend one set of Cowper Symonds (1956) parameters for future research. In taking a closer look at previous testing published in literature, greater consideration was given to Cowper Symonds (1956) parameters derived from experimental studies most closely aligned with the research presented in this dissertation. Thus, because a correlative relationship exists between the behavior of rivets under tensile loading and rivets under shear loading, historical testing, such as original uniaxial dynamic tensile testing of mild steel from Cowper Symonds (1956), is a priority for consideration ($C$ = 40.4 $s^{-1}$ and $q$ = 5). Of note, however, is the fact that subsequent uniaxial dynamic tensile testing of mild steel by the University of Liverpool (Abramowicz and Jones, 1986) provided drastically different results ($C$ = 802 $s^{-1}$ and $q$ = 3.585). The marked difference between the two cases with respect to testing is that the Cowper Symonds (1956) experiments involved subjecting mild steel specimens to relatively small strains in the neighborhood of their yield value, while the University of Liverpool tests involved subjecting mild steel specimens to relatively large strains and plastic behavior. This observation, in conjunction with noticing the University of Liverpool parameters would likely provide ultimate shear strengths between the bounded values, led to running LS-DYNA (2013) simulations of the five configurations in single- and double-shear with the published University of Liverpool parameters ($C$ = 802 $s^{-1}$ and $q$ = 3.585).

After again setting aside the anomalies from the experimental testing, the Cowper Symonds (1956) constitutive model with the University of Liverpool parameters ($C$ =

802 $s^{-1}$ and $q$ = 3.585) clearly provided the best representation of rivet behavior in shear under high loading rates. In five of the eight analyses, the LS-DYNA (2013) output demonstrated ultimate shear strengths within the range of the experimental values. For the other three analyses, the LS-DYNA (2013) output predicted ultimate shear strengths within 4.5 percent of the low end of the experimental range. This was significantly more accurate than the simulation results when using the bounding Abramowicz and Jones (1986) parameters ($C$ = 6884 $s^{-1}$ and $q$ = 3.91) and Cowper Symonds (1956) parameters ($C$ = 40.4 $s^{-1}$ and $q$ = 5), which under-predicted response by as much as 16.3 percent and over-predicted response by as much as 23.4 percent, respectively. A summary of the testing results using the University of Liverpool parameters is shown in Table 4-6, with the previously mentioned outlier experimental test results highlighted in yellow. In addition, as demonstrated in Fig. 4-3, load versus time curves simulated within LS-DYNA (2013) demonstrated a qualitatively similar shape and time to failure when compared to the experimental data (Rabalais, 2015). Thus, the material and constitutive models exhibited comparable behavior and were considered adequate given the experimentally produced test results. All 10 curves using the University of Liverpool parameters ($C$ = 802 $s^{-1}$ and $q$ = 3.585) are shown in Appendix C.

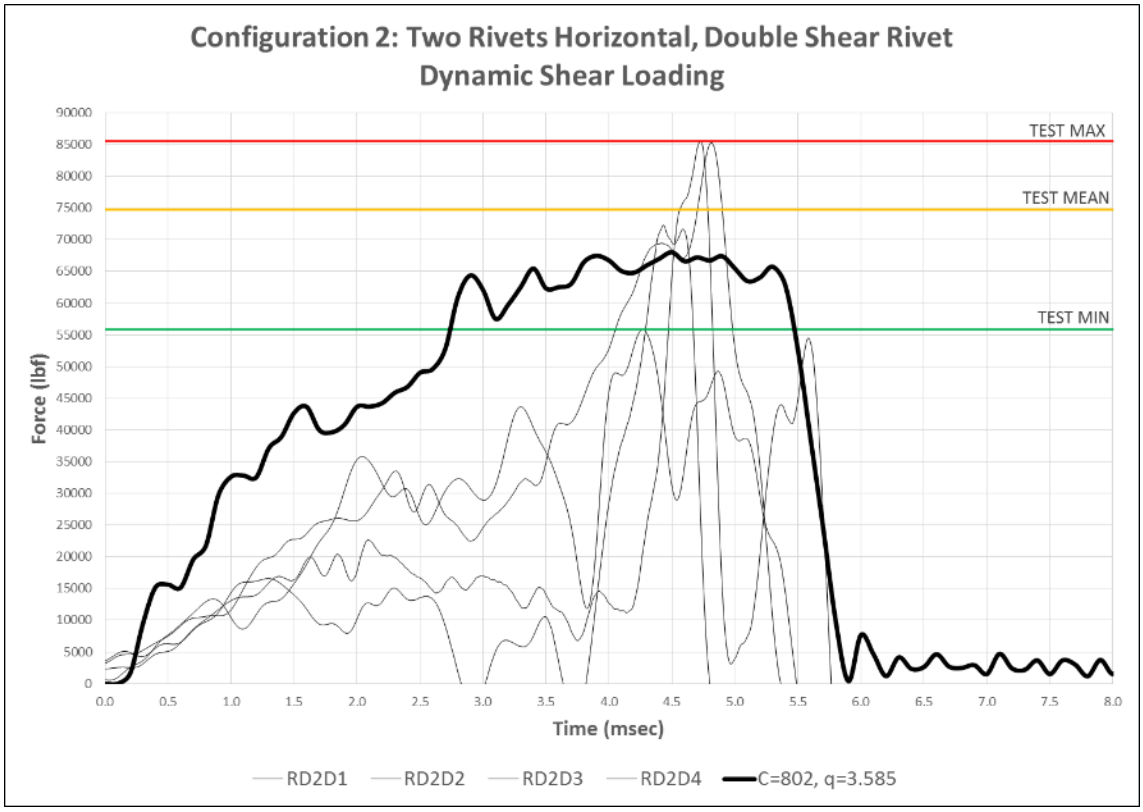


Fig. 4-3: Sample Load versus Time Plot using $C$=802, $q$=3.585

Table 4-6: Dynamic Loading Simulation Results using University of Liverpool Parameters (C = 802 $s^{-1}$ and q = 3.585) versus Experimental Results

| **Test Configuration** | **Rivet Mesh: C: (0.016 in. - 0.032 in.) D: (0.008 in. - 0.016 in.)** | **Experimental Dynamic Load (lbf) Min** | **Experimental Dynamic Load (lbf) Max** | **LS-DYNA Dynamic Load (lbf) C = 802 $s^{-1}$ , q = 3.585** | **% Difference Outside of Range** |
|---|---|---|---|---|---|
| 1: One Rivet, Single Shear | D | 13.7 | 16.1 | 20.5 | 21.3 |
| 1: One Rivet, Double Shear | D | 31.0 | 44.7 | 35.2 | In range |
| 2: Two Rivets Horizontal, Single Shear | D | 39.4 | 79.6 | 37.7 | -4.5 |
| 2: Two Rivets Horizontal, Double Shear | D | 55.9 | 85.5 | 68.0 | In range |
| 3: Two Rivets Vertical, Single Shear | D | 54.2 | 60.3 | 36.6 | -32.5 |
| 3: Two Rivets Vertical, Double Shear | D | 79.8 | 132.6 | 78.3 | -1.8 |
| 4: Four Rivets Square, Single Shear | C | 54.4 | 117.4 | 81.2 | In range |
| 4: Four Rivets Square, Double Shear | C | 102.9 | 147.8 | 142.7 | In range |
| 5: Four Rivets Staggered, Single Shear | C | 66.4 | 94.5 | 73.1 | In range |
| 5: Four Rivets Staggered, Double Shear | C | 147.6 | 213.2 | 147.0 | -0.3 |

A further look at the LS-DYNA (2013) analysis results from the University of Liverpool parameters revealed the calculated dynamic increase factor more closely matches the dynamic increase factor for A502 Grade 2 rivets calculated through the ERDC experimental testing (Rabalais, 2015). As demonstrated in Table 4-7, the average dynamic increase factor using the University of Liverpool parameters was 1.5, compared to 1.7 from experimental testing (Rabalais, 2015).

Table 4-7: Dynamic Increase Factor of LS-DYNA (2013) Simulations using University of Liverpool Parameters (C = 802 $s^{-1}$ and q = 3.585)

| **Test Configuration** | **LS-DYNA Quasi-Static Load (lbf)** | **LS-DYNA Dynamic Load (lbf) C = 802 $s^{-1}$, q = 3.585** | **Calculated DIF** |
|---|---|---|---|
| One Rivet, Single Shear | 12806 | 20528 | 1.6 |
| One Rivet, Double Shear | 23615 | 35270 | 1.5 |
| Two Rivets Horizontal, Single Shear | 25720 | 37667 | 1.5 |
| Two Rivets Horizontal, Double Shear | 46997 | 68026 | 1.4 |
| Two Rivets Vertical, Single Shear | 27875 | 36598 | 1.3 |
| Two Rivets Vertical, Double Shear | 53848 | 78299 | 1.5 |
| Four Rivets Square, Single Shear | 50549 | 81218 | 1.6 |
| Four Rivets Square, Double Shear | 94680 | 142735 | 1.5 |
| Four Rivets Staggered, Single Shear | 50317 | 73096 | 1.5 |
| Four Rivets Staggered, Double Shear | 94371 | 147066 | 1.6 |
| | | **Average DIF:** | **1.5** |

As a final, but important aspect of validity, a close investigation of the three-dimensional rivet models following the dynamic simulations was conducted. As mentioned in Section 2.6, the fracture type and deformation changes significantly based on the loading type (shear, tension, or combination of both). Under pure shear deformation, as was the intent of the models for this research, necking should not occur. An illustration of the dynamic loading and eventual failure of the rivets in pure shear is shown in Fig. 4-4 and Fig. 4-5. These illustrations demonstrate Configuration 4 (four rivets square) in double shear. As was consistent in each of the 10 dynamic LS-DYNA (2013) simulations, no necking was evident in the fracture of the rivets, providing further confidence in the models.

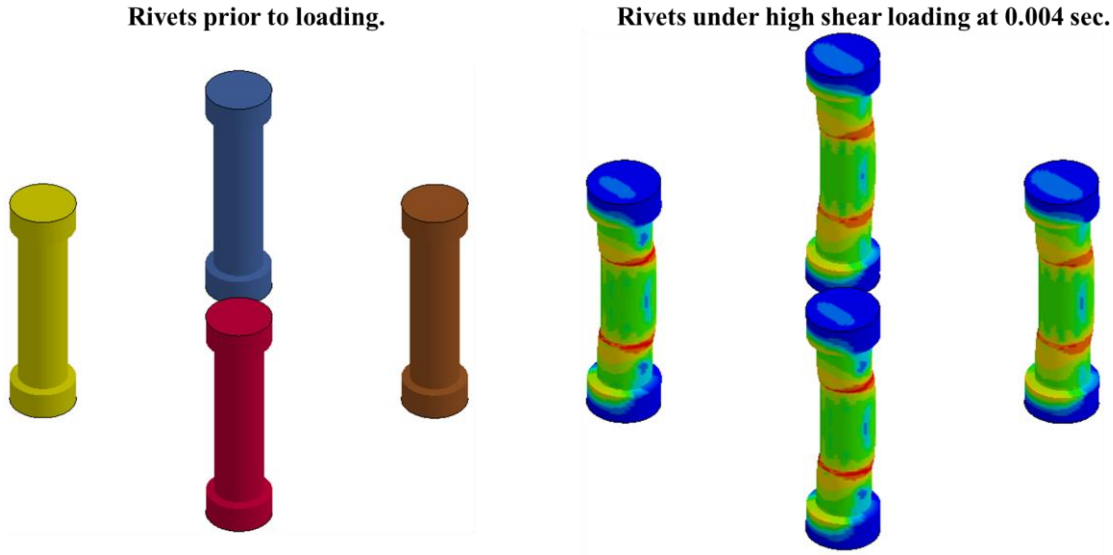


Fig. 4-4: Rivets Loaded under High Loading Rate

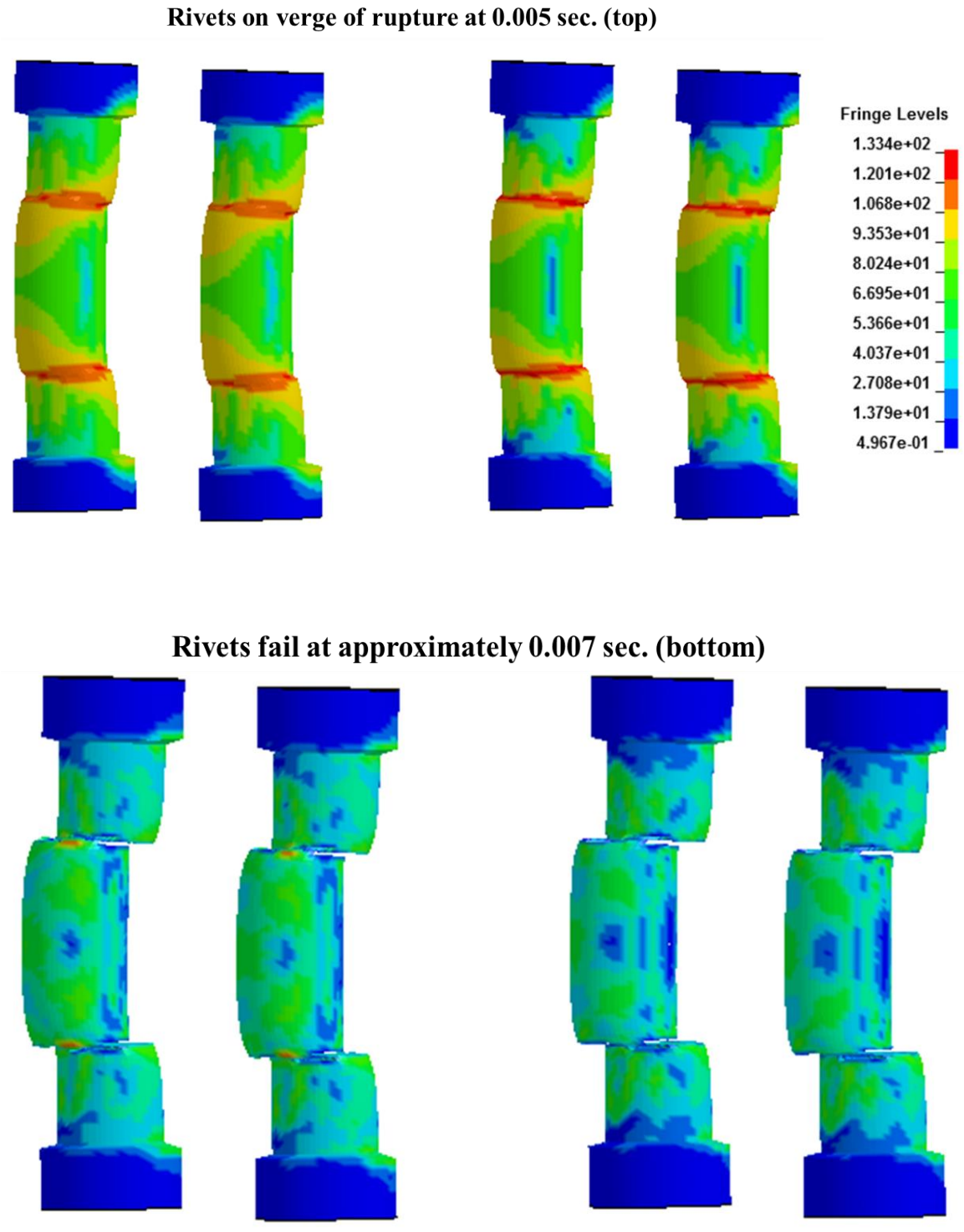


Fig. 4-5: Rivet Failure in Pure Shear under High Loading Rate

## 4.4 LONG RIVETED CONNECTIONS

Steel rivets were considered the critical connector for both the world's most well-known suspension bridges and other pre-1960 bridges and buildings. When used as a connector for bridges, the length of the connections was not limited to a few inches, as demonstrated thus far in this research presented in this dissertation. Several riveted connections were 10-in. and longer. Examples of such connections include connections for the Champlain Bridge over the Saint Lawrence River shown in Fig 4-6 and the Whirlpool Rapids Bridge shown in Fig. 4-7. As emphasized in Chapter 1, the human casualties, economic losses, environmental damage, and fear attributed to attacks against bridges make them attractive terrorist targets. In fact, the Royal Canadian Mounted Police, in conjunction with assistance from the FBI, stopped a planned attack against a passenger train in Toronto (Manzarpour, 2013). The Whirlpool Rapids Bridge, largely considered the target of this plot, is a riveted bridge between Canada and the United States that carries railway traffic on the upper deck and passenger vehicle traffic on the lower deck (Zennie, 2013).

Fig. 4-6: Champlain Bridge (photos provided by Dr. Charles Crane)

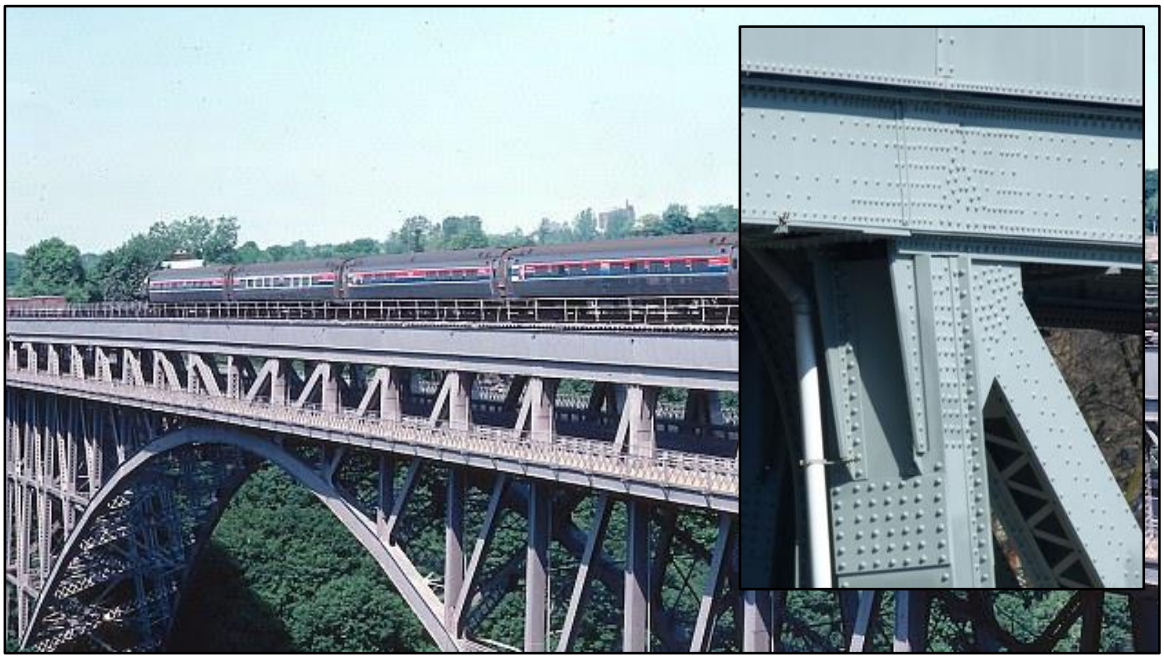

Fig. 4-7: Whirlpool Rapids Bridge with Top Chord Zoom (from Nathan Holth at http://historicbridges.org/)

As detailed in Section 2.5 of this dissertation, long riveted and bolted connections have been the focus of several research studies. As illustrated in Fig. 4-8, testing conducted by Sterling and Fisher (1966) consisted of determining and comparing the quasi-static shear strength of A490 bolts and A502 Grade 2 rivets in connections of various lengths. Once joint lengths surpassed approximately 10-in., the ultimate shear strength of fasteners decreased as the fasteners within the connection no longer shared an equal percentage of the load.

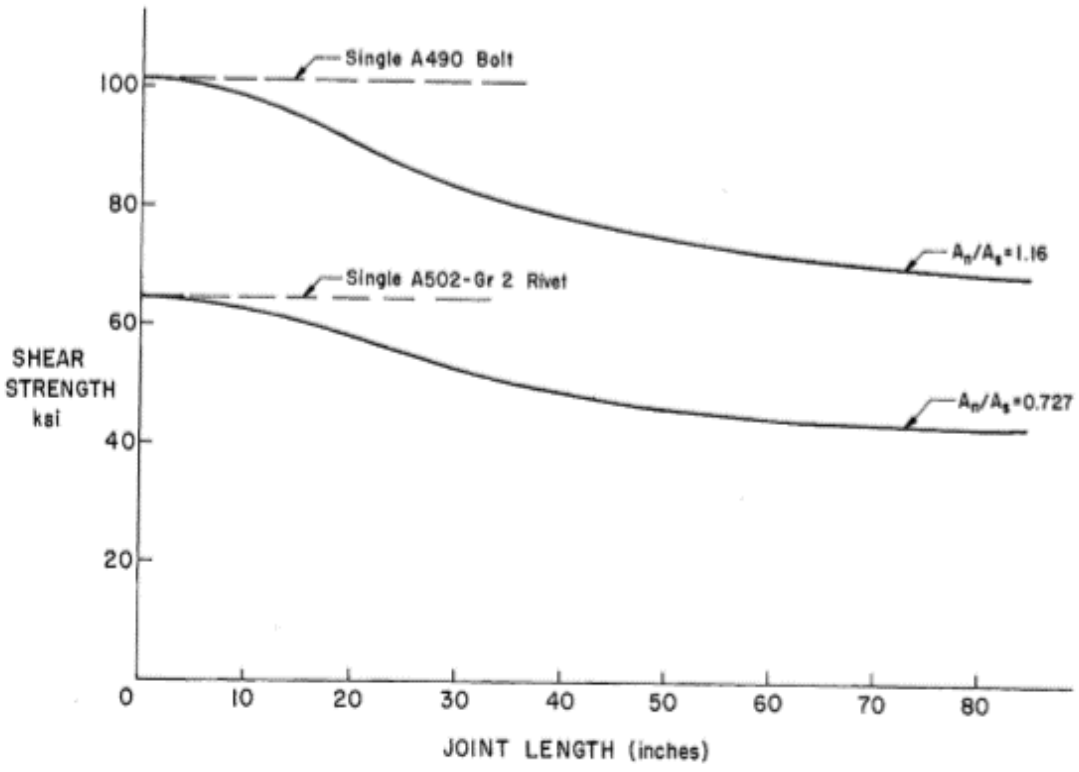


Fig. 4-8: Joint Length Historical Testing (by Sterling and Fisher, 1966)

To date, long riveted connections have only been tested quasi-statically. Recall the high loading rate testing by Rabalais (2015) was limited to short length connections (3-in. long) with no more than two rows. Thus, the final objective for this dissertation was to apply the newly developed material and constitutive models from the numerical modeling of riveted connections under high loading rates to predict the response of long riveted connections under rapidly applied loads applied parallel to the long axis of the connection.

The starting point of this investigation was to modify the existing LS-DYNA (2013) models from the quasi-static testing described and validated in Section 3.8. The models were modified to create longer riveted connections with lengths of 12-in., 21-in., and 30-in., as demonstrated in Fig. 4-9, Fig. 4-10, and Fig. 4-11, respectively. All simulations of long riveted connections involved single-shear configurations only.

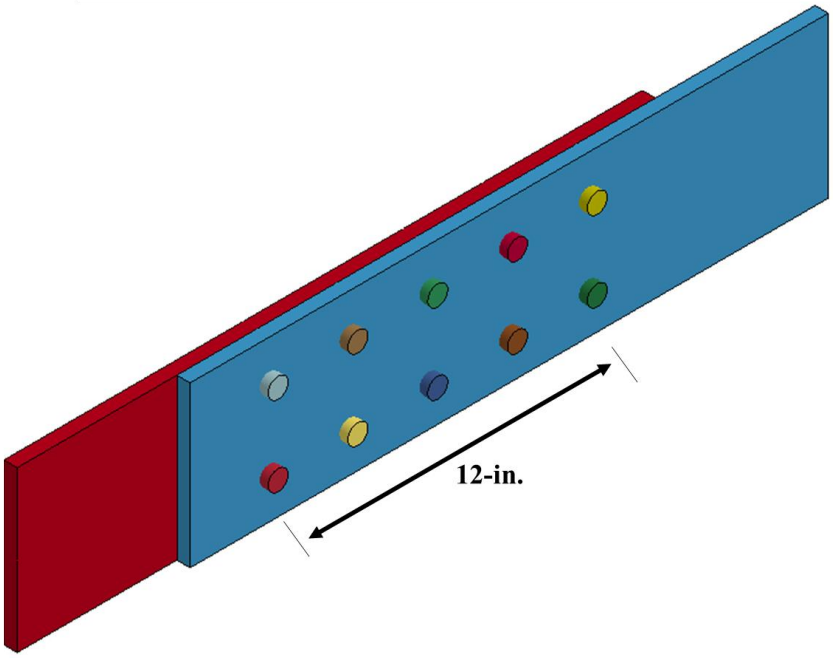


Fig. 4-9: Finite Element Model of 12-in. Long Connection

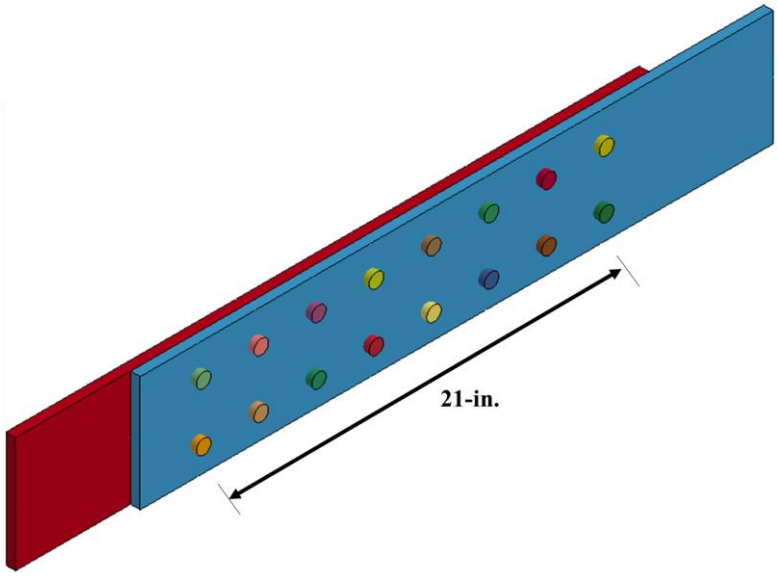


Fig. 4-10: Finite Element Model of 21-in. Long Connection

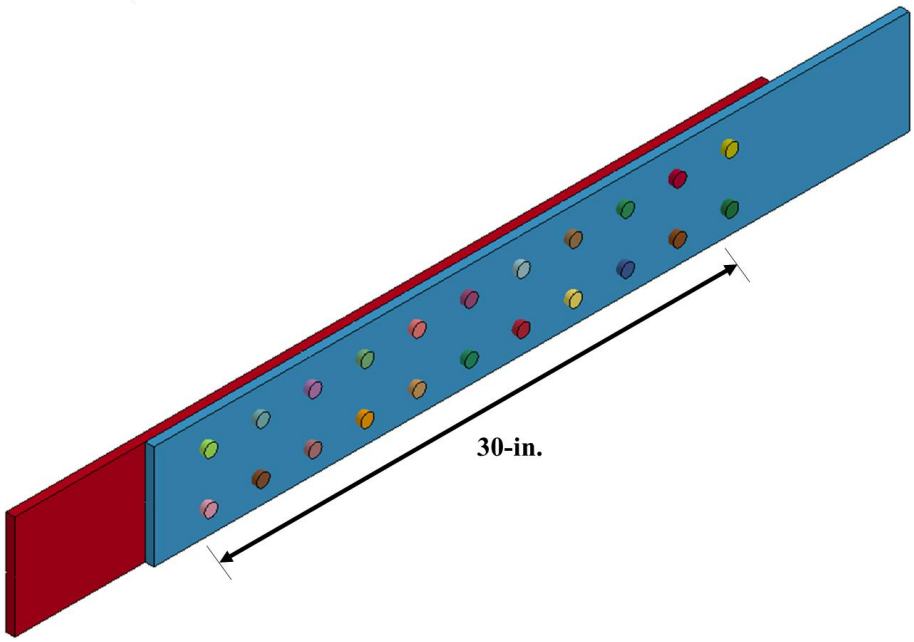


Fig. 4-11: Finite Element Model of 30-in. Long Connection

Outside of the change in lengths, two other modifications were required for the models. One change was to the material model of the plate. After attempting to run the models with the A36 plates used with the short connections in Chapter 3, it was clear that rivet shear failure was not going to control. In fact, the only plate configurations in which the rivets failed in shear were the 12-in. quasi-static and the 12-in. dynamic tests, as shown in Fig. 4-12 and Fig. 4-13.

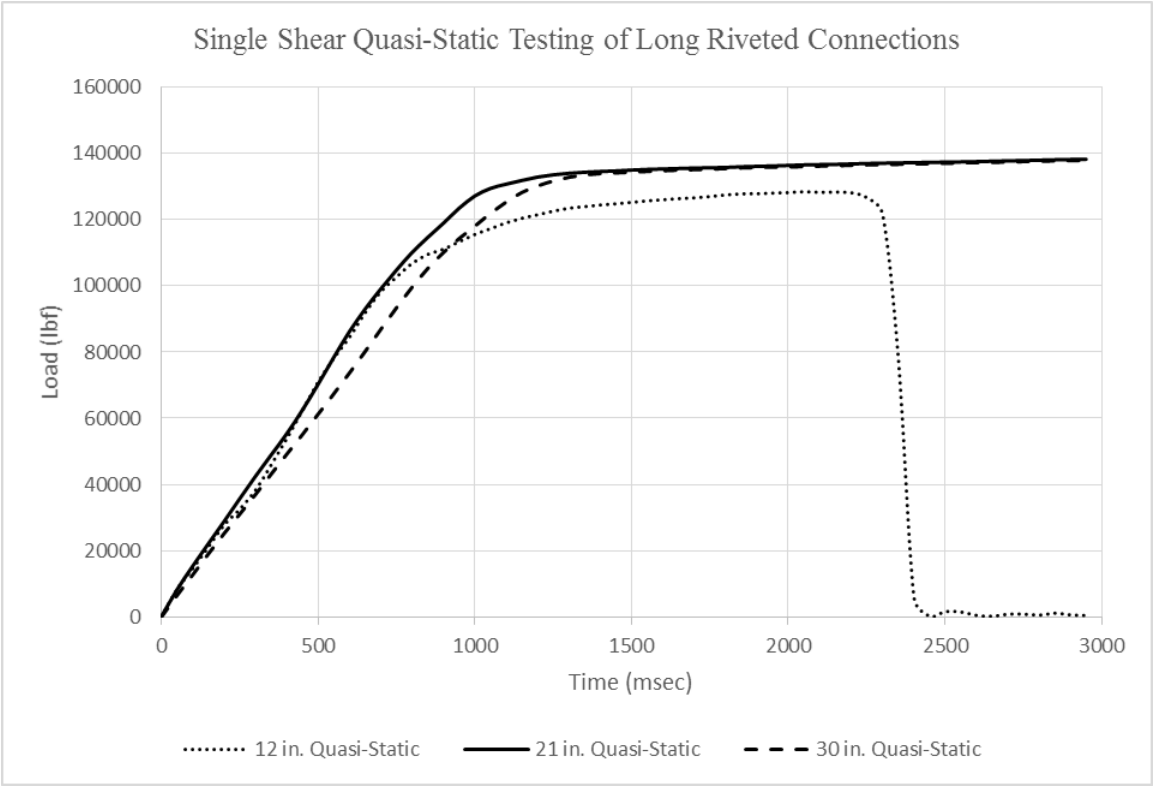


Fig. 4-12: Quasi-Static Load versus Time Plot of Long Connections with A36 Plates

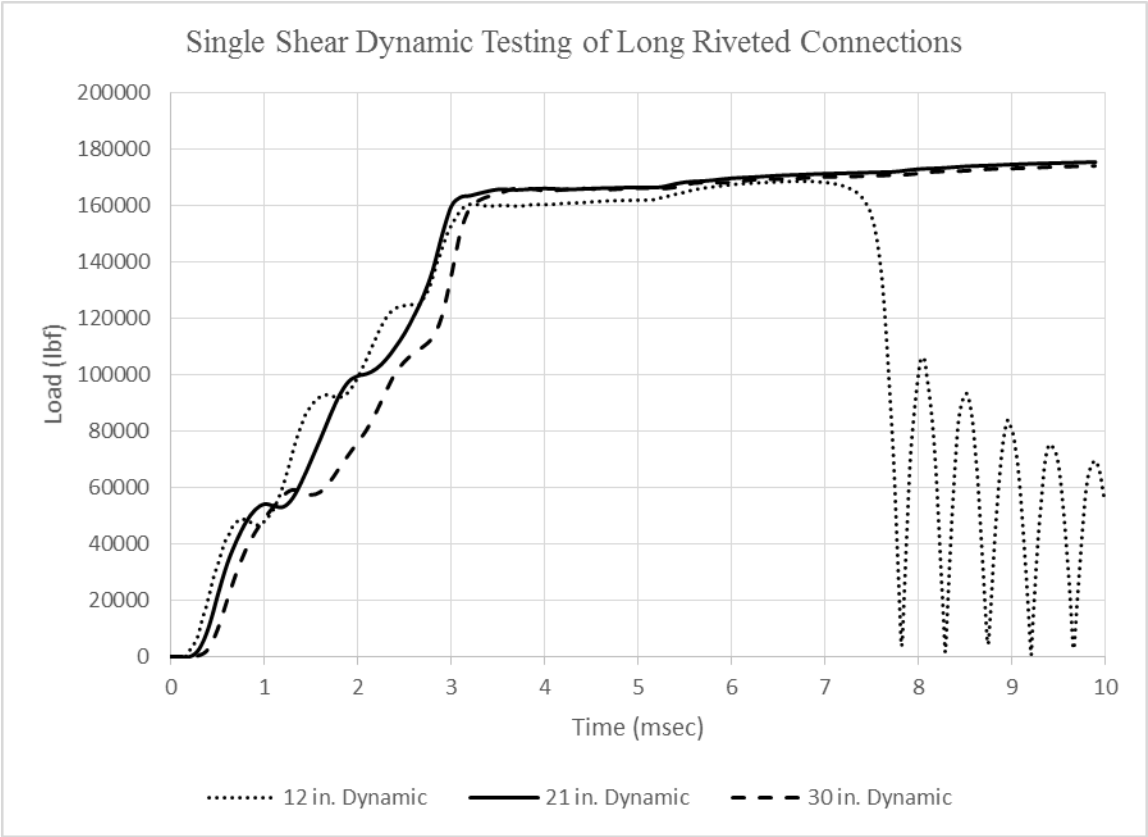


Fig. 4-13: Dynamic Load versus Time Plot of Long Riveted Connections with A36 Plates

For the longer length connections, the plates succumbed to the limit state of connecting member yielding. In addition, the yielding of the material around the exterior holes led to plastic behavior and excessive deformations in their respective rivets, as demonstrated in Fig 4-14, Fig. 4-15, and Fig. 4-16. This behavior set up the premature *unbuttoning* failure due to the *weak plate* condition (Wang, 2013), in which the sum of the rivet shear strength is greater than the yield capacity of the plate.

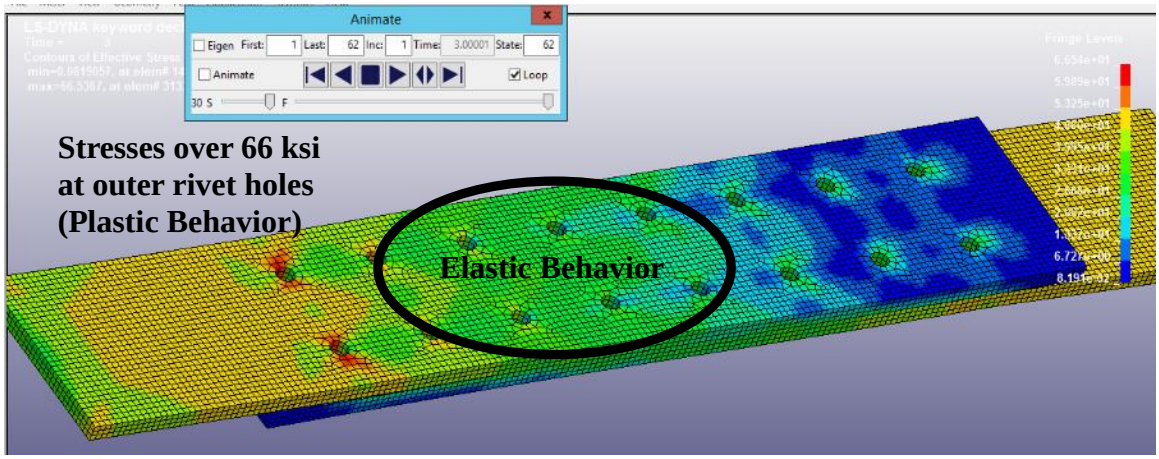


Fig. 4-14: A36 Plates Demonstrate Excessive Yielding in Outer Holes

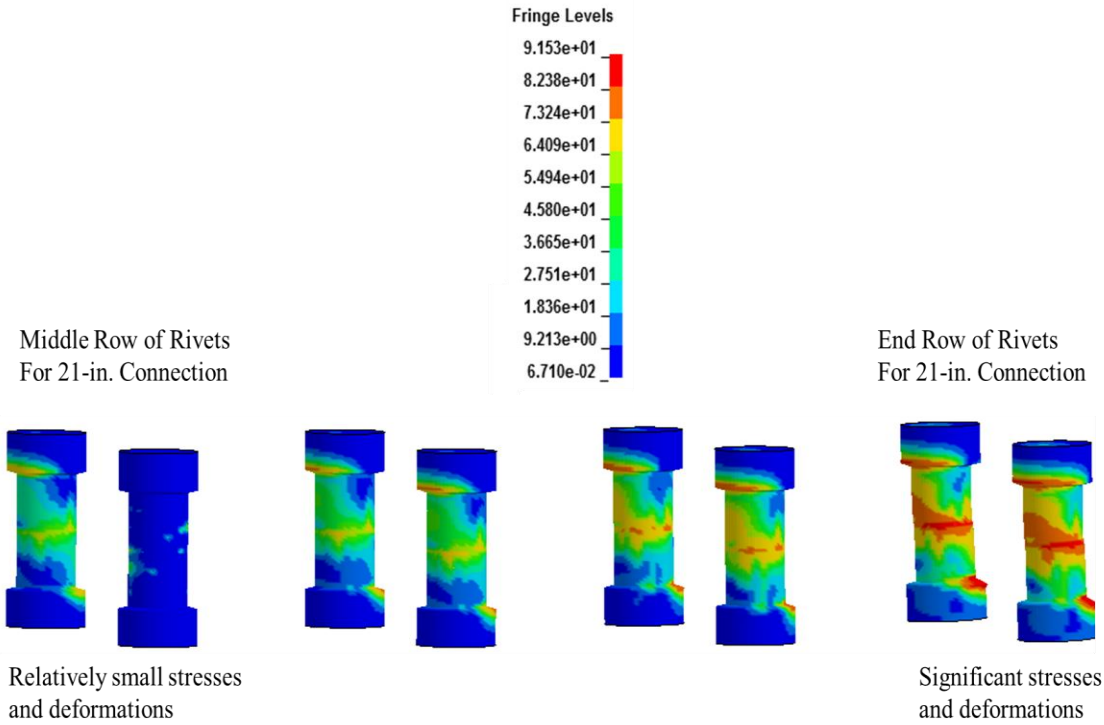


Fig. 4-15: Uneven Distribution of Load in Long Connection

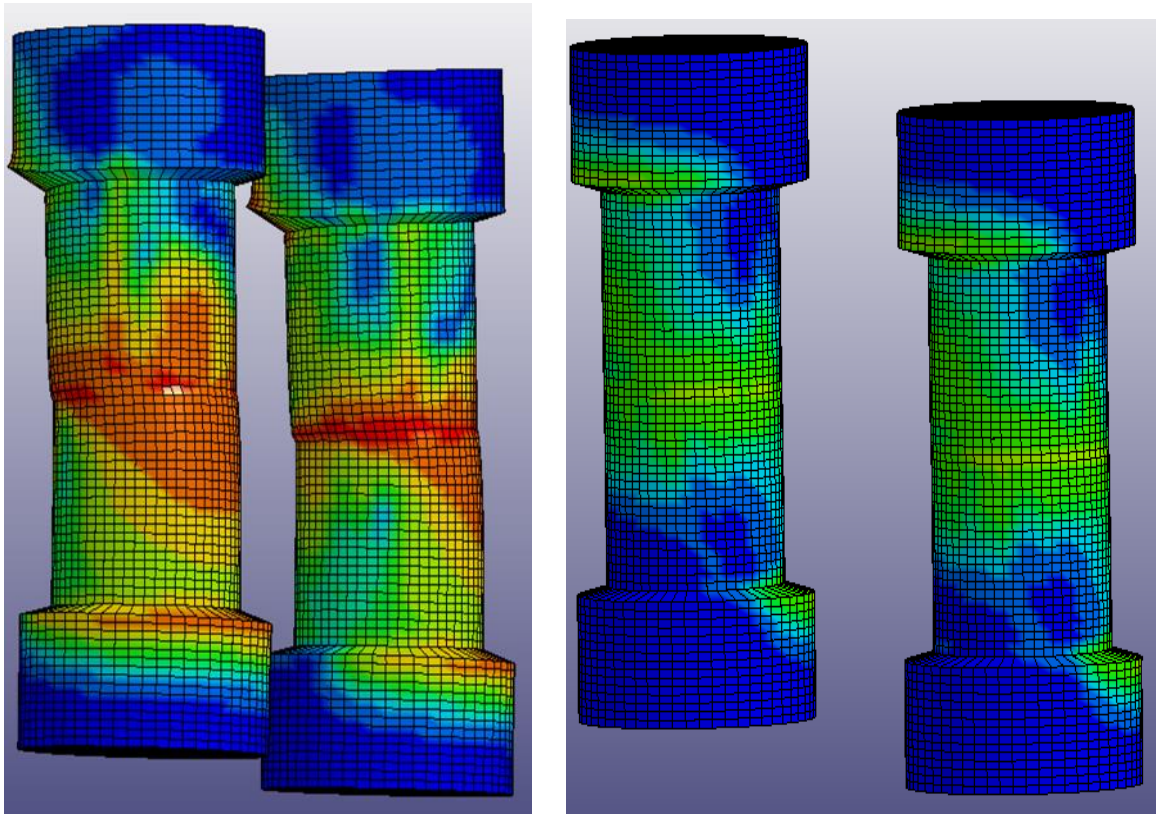

**Significant stress and deformation in end rivets.**

**Relatively small stress and deformation in middle rivets.**

Fig. 4-16: Close-up of Difference in Stress between End Rivets and Interior Rivets

In comparing the static results with the dynamic results, it is interesting to note that for the 12-in. connection, the rate of loading had no effect on the failure mode because unbuttoning occurred for both cases. The loading rate did, however, play a role in the maximum ultimate shear strength of the 12-in. connection. Under quasi-static loading, the max ultimate shear strength was 34.8 ksi. Under dynamic loading, the max

ultimate shear strength was 56.5 ksi, resulting in a dynamic increase factor of 1.31. For the longer 21-in. and 30-in. connections under the *weak plate* condition, the dynamic increase factor was 1.27 and 1.26, respectively. Thus, long riveted connections under the weak plate condition exhibit lower dynamic increase factors than short connections; furthermore, the dynamic increase factor decreases with increasing length.

With the focus of the research on rivet behavior, subsequent analyses were completed with a stronger A514 Carbon Steel Plate material to ensure rivet shear would control the mode of failure. With no experimental data to derive a true stress-strain curve for the A514 Steel Carbon Plate material model, values from Varmint Al's Engineering material properties database were used as input as shown in Table 4-8 (http://www.varmintal.com/aengr.htm).

Table 4-8: Material Model for A514 Steel Carbon Plate (from Varmint Al's Engineering)

| **Mass Density (kip-s$^2$/in)** | **E (ksi)** | **Poison's Ratio** | **Yield Stress (ksi)** | **Fail** |
|---|---|---|---|---|
| 7.332 e -7 | 30,000 | 0.29 | 112.5 | 1.365 |
| **EPS1** | **EPS2** | **EPS3** | **EPS4** | **EPS5** |
| 0.0 | 0.0098 | 0.0956 | 0.53 | 1.365 |
| **ES1** | **ES2** | **ES3** | **ES4** | **ES5** |
| 112.5 | 119 | 130 | 140 | 145.9 |

The second change for analysis was to the loading rates. In order to get the rivets to fail in a quasi-static and/or dynamic manner, several simulations were run using the previous iterations described in Section 3.6 as a guide. The points used to describe each curve for loading are shown in Table 4-9.

Table 4-9: Displacement Controlled Loading for Long Riveted Connections

| **Test** | **(Time (sec), Displacement (in.))** |
|---|---|
| 12-in. Quasi-Static | (0,0), (3,0.3) |
| 21-in. Quasi-Static | (0,0), (3,0.3) |
| 30-in. Quasi-Static | (0,0), (3,0.3) |
| 12-in. Dynamic | (0,0), (0.0025, 0.05), (0.005, 0.2), (0.075, 0.45), (0.01, 1) |
| 21-in. Dynamic | (0,0), (0.0025, 0.05), (0.005, 0.2), (0.075, 0.45), (0.01, 2) |
| 30-in. Dynamic | (0,0), (0.0025, 0.05), (0.005, 0.2), (0.075, 0.45), (0.01, 2) |

The load versus time responses for the quasi-static test and the high loading rate tests are shown in Fig. 4-17 and Fig 4-18, respectively. For each of the respective types of tests, the qualitative shapes of the 12-in., 21-in., and 30-in. curves are similar. Using the stronger A514 steel for the plates allowed the ultimate shear strengths of the rivets to dominate the failure mode. As a result, in both the quasi-static and dynamic loading cases, the longer connections carried a greater load than exhibited during the *weak plate* connection simulations.

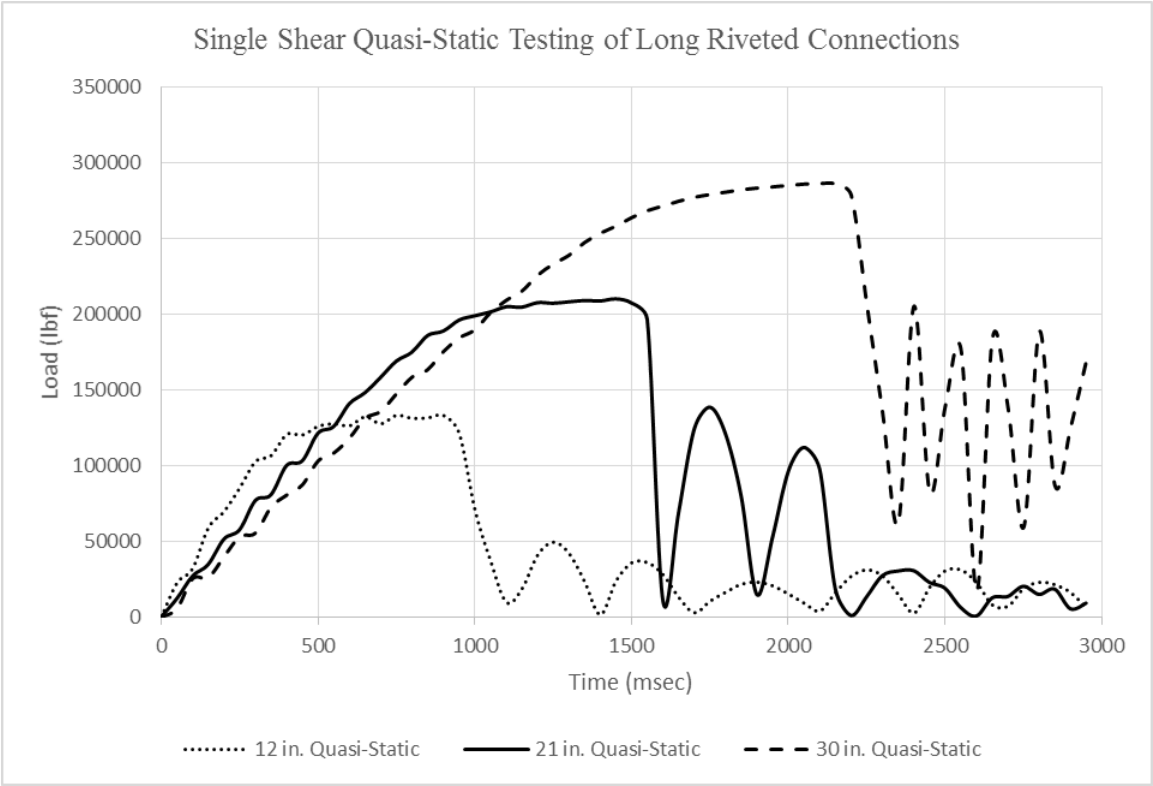


Fig. 4-17: Quasi-Static Load versus Time Results for Long Riveted Connections

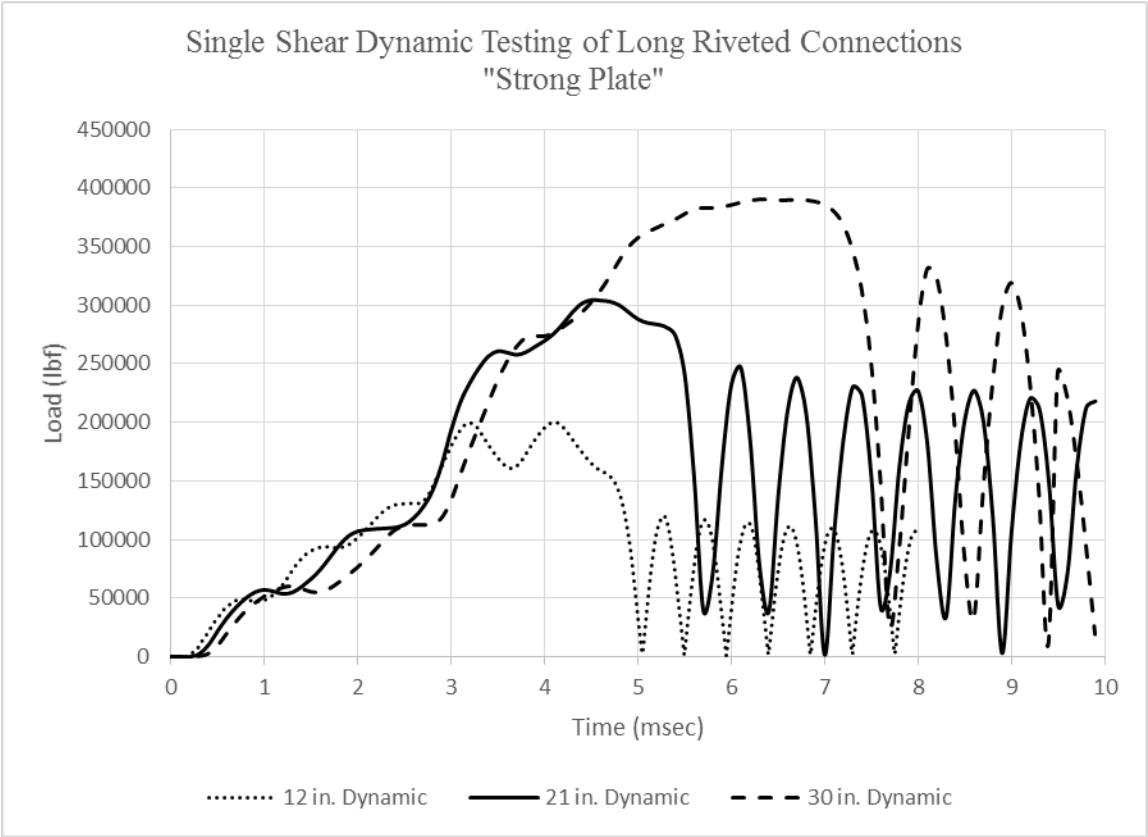


Fig. 4-18: Dynamic Load versus Time Results for Long Riveted Connections

When taking a qualitative look at the 12-in. long riveted connection, it appears that the rivets sheared approximately simultaneously, as shown in Fig. 4-19. As opposed to the longer 21-in. and 30-in. riveted connections, the rivets appeared to share the distribution of stresses nearly equally.

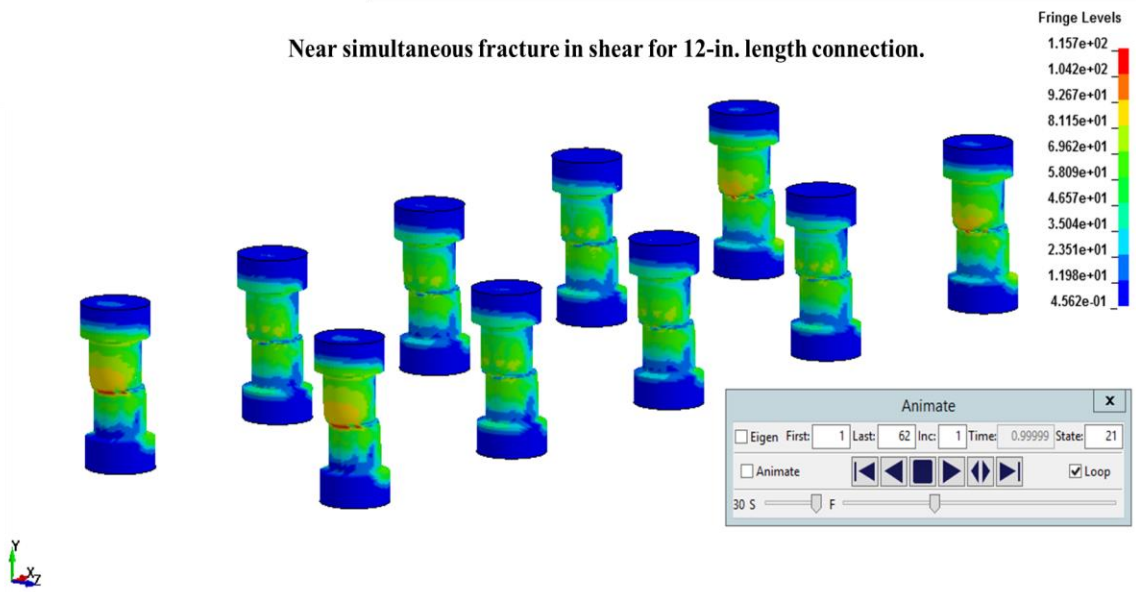


Fig. 4-19: Simultaneous Rivet Shear in 12-in. Length Riveted Connection

When investigating the behavior of the 21-in. and 30-in. connections, as shown in Fig. 4-20, it appears as though the unbuttoning phenomena started to influence the ultimate shear strength of the riveted connections. Larger deformations at the end (first row) of the connected plates generated unbalanced and significant deformations around the end rivets. This unequal distribution of stresses caused the end row to fail prematurely in comparison to the rivets in the middle of the joint.

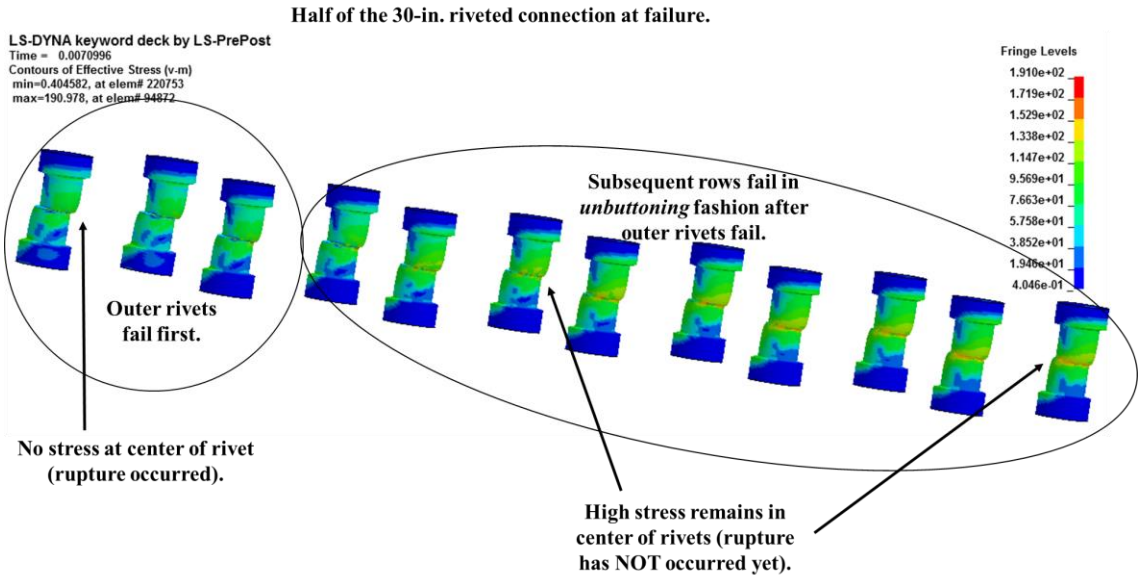


Fig. 4-20: Unbuttoning of Long Riveted Connections under High Loading Rates

When comparing the quasi-static ultimate shear strength to the dynamic ultimate shear strength for each of the long connections, the 12-in. long connection failed similarly to the short connections analyzed in Section 4.3. As was observed with the short one-row and two-row connections where the dynamic increase factor for the LS-DYNA (2013) simulated models was approximately 1.5, the dynamic increase factor for the 12-in. length riveted connection was also approximately 1.5. However, the calculated dynamic increase factor decreased as the length of the connection increased. In a *strong plate* condition, tests showed that fastener capacity under quasi-static loads changed very little in long connections (Wang, 2013). However, it is possible this correlation is more prevalent for long connections tested under quasi-static loading because the connection has more time to distribute the load equally along the length of the connection. Under a

high rate of loading, high stress concentrations at the end holes in a matter of milliseconds may result in a relatively premature failure of the end rivets before the load is equally distributed to the interior rivets. Results and dynamic increase factor calculations are shown in Table 4-10.

Table 4-10: Dynamic Increase Factor for Long Connections

| **Test** | **12-in. QS** | **21-in. QS** | **30-in. QS** |
|---|---|---|---|
| Load (kips) | 132.8 | 210.2 | 286.7 |
| **Test** | **12-in. DYN** | **21-in. DYN** | **30-in. DYN** |
| Load (kips) | 200.0 | 304.8 | 391.0 |
| **DIF** | 1.51 | 1.45 | 1.36 |

While the data captured from this investigation provide some insight into the behavior of long riveted connections under high loading rates, further investigation and at least some limited experimental validation is warranted. Nevertheless, given the validated models developed from simple riveted connections under both quasi-static and dynamic loads, it is reasonable to consider this information useful. From the data collected, initial recommended guides to predict the ultimate shear strength and dynamic increase factor for A502 Grade 2 rivets at different lengths are shown in Fig. 4-21 and Fig. 4-22. These simplified guides provide protective design engineers with useful information concerning

the anticipated ultimate shear strengths and dynamic increase factors for riveted connections of different lengths.

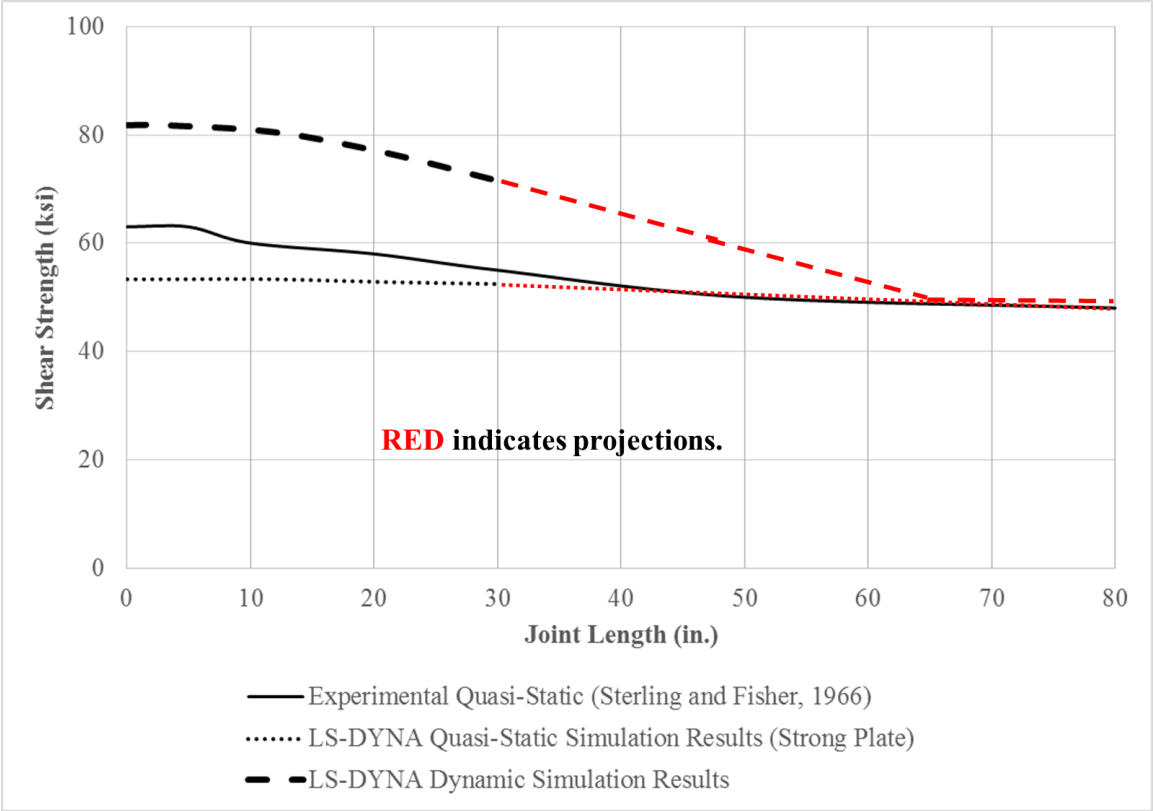


Fig 4-21: Ultimate Shear Strength Guide for Riveted Connections for Quasi-Static and Dynamic Loads (portions regenerated from Sterling and Fisher, 1966)

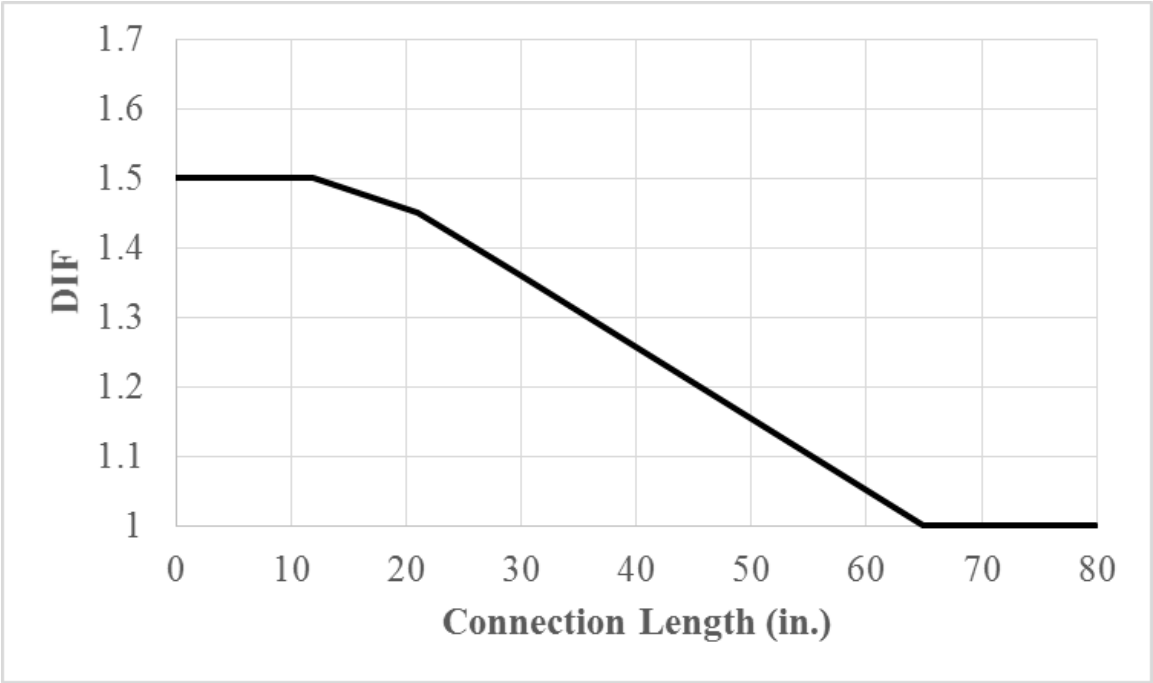


Fig. 4-22: Dynamic Increase Factor Guide for A502 Grade 2 Rivets

## 4.5 SUMMARY

With a validated model of rivet behavior under quasi-static loads developed in Chapter 3, the goals of Chapter 4 were to expand on the model to develop a validated constitutive model that captured simple riveted connections and then utilize it to investigate an untested problem. To capture the behavior of simple riveted connections under high loading rates, a validated constitutive model was developed using the Cowper Symonds (1956) model. Several sets of Cowper Symonds (1956) coefficients were utilized to determine appropriate parameters for material model input. After bounding a

solution, input values were selected that adequately captured the experimental rivet behavior and approached the experimentally calculated dynamic increase factor.

Based on the constitutive model developed for A502 Grade 2 rivets, this chapter closed with a look into the behavior of long riveted connections under high rates of loading. After a brief explanation of its relevance to the engineering community, a snapshot of previous research was provided to set the stage for the untested research. Three different lengths of long riveted connections in single shear were tested under quasi-static and dynamic loads to investigate the dynamic increase factors for long riveted connections. The results of these tests, in conjunction with the constitutive models developed in Chapters 3 and 4, serve as focal points for the conclusions and recommendations for future research discussed in Chapter 5.

# Chapter 5: Summary, Conclusions, and Future Work

*"This is not your grandfather's al-Qaida. There's a device, almost a devil on their shoulder all day long saying, 'Kill, kill, kill, kill.'"*

–James Comey, 2015

## 5.1 SUMMARY

With the U.S. and coalition forces in a seemingly never-ending operation to eliminate the Islamic State of Iraq and the Levant terrorists and the threat they pose around the world, prominent and high value infrastructure continues to be a target for terrorists. FBI Director James Comey shared the quote that opens this chapter at a Senate FBI oversight hearing in December 2015 by confirming there were more terrorist organizations with personnel, equipment, and safe havens than at anytime since the 9/11 attacks (Scott, 2015). With suspension bridges and other riveted bridges considered likely targets, the engineering community's need to understand the behavior of rivets and riveted connections under high loading rates is invaluable.

This dissertation presented an investigation into modeling riveted connections under both quasi-static and dynamic loadings. The study included the development of a material model, a detailed finite element analysis, and the application of the aforementioned to the behavior of long riveted connections. The detailed finite element

analyses provided validated predictions of simple riveted connection behavior under quasi-static and dynamic loadings, and practical predictions of long riveted connection behavior under high loading rates.

With a clear need to understand the behavior of rivets under high loading rates, justification to focus research on rivet behavior under shear loads specifically was due to the experimental field testing of riveted panels under blast loads discussed in Section 3.2. The relatively ductile failure of the panels when connected with rivets proved to be different than the brittle failure of the panels when connected with bolts. Challenges in setting up and executing tests of this nature, in addition to the exhaustive time associated with approval and execution, demand the need to develop and utilize sophisticated models to evaluate behavior. This research was designed to make valuable contributions to the engineering community in this regard.

## 5.2 CONCLUSIONS

This section of this dissertation is divided into three subsections corresponding to the three major objectives of this research. This information will be beneficial to those focused on the protective design of steel structures with riveted connections.

### 5.2.1 Validated Material Model for A502 Grade 2 Rivets

The first objective of this dissertation was to provide guidance on modeling rivets using a nonlinear transient dynamic finite element analysis software package. The purpose of this work was to reveal modeling issues that could lead to inaccuracies and shortcomings of the numerical modeling tools. Observations from the model development and simulations give rise to the following conclusions:

1. A502 Grade 2 rivets can be efficiently and accurately modeled in LS-DYNA (2013) and LS-Prepost (2014) using three-dimensional, 8-node hexahedra solid elements that utilize the under-integrated constant stress implementation (ELFORM 1) with the Belytschko-Bindeman (1993) formulation (HG6) for hourglass control.

2. The mesh density of a finite element model is critical for both accuracy and computational efficiency (i.e., computing time). In modeling A502 Grade 2 rivets, very fine mesh sizes yielded both accurate ultimate shear strengths and failure results; however, they resulted in significantly longer computational times. Coarser meshes provided accurate ultimate shear stress results with faster computational times, but failed to provide accurate failure results. Mesh sizes in the range of 0.073-in. to 0.110-in. provided the most accurate results with respect to rivet ultimate shear strengths and failure results. Given the large

computational demand of those simulations, however, this research recommends the use of mesh sizes in the range of 0.016-in. to 0.032-in. to model rivets for the best combination of accuracy and efficiency.

3. The piecewise-linear plasticity model (MAT24) within LS-DYNA (2013) provides users with the option of defining a true stress and true strain curve, consisting of up to eight linear segments, to approximate experimental non-linear engineering stress and engineering strain behavior. The input shown in Table 3-3 for effective plastic strain (in./in.) and corresponding yield stress (ksi) approximates the engineering stress and engineering strain behavior for A502 Grade 2 rivets.

### 5.2.2 Validated Constitutive Model for Strain Rate Effects

The second objective of this dissertation was to provide recommendations with respect to modeling strain rate effects for steel rivets. Observations from the model development and simulations lead to the following conclusions:

1. The Cowper and Symonds (1957) constitutive model within the piecewise-linear plasticity model (MAT24) of LS-DYNA (2013) provided a simple,

efficient, and accurate means of predicting the behavior of A502 Grade 2 rivet connections under high loading rates.

2. The Cowper and Symonds (1957) parameters ($C$ = 40.4 $s^{-1}$ and $q$ = 5) derived from subjecting mild steel specimens to relatively small strains in the neighborhood of their yield value provided an upper bound to the behavior of rivets under high loading rates. The Abramowicz and Jones (1986) parameters ($C$ = 6884 $s^{-1}$ and $q$ = 3.91) derived from the dynamic axial crushing of mild steel square tubes provided a lower bound to the behavior of rivets under high loading rates. Given the large scatter observed in experimental rivet response, both the upper-bound and the lower-bound parameters are recommended for examination when analyzing riveted suspension panels under blast loads as the difference in the two may affect the failure modes of the steel suspension panels.

3. With respect to the simulations conducted for this research, the University of Liverpool parameters ($C$ = 802 $s^{-1}$ and $q$ = 3.585) derived from subjecting mild steel specimens to large strains beyond their yield value provided the most accurate prediction of rivet connection behavior under high loading rates. These parameters are recommended as the sole parameters used in situations where time is limited or in the event where multiple simulations cannot be run.

### 5.2.3 A Prediction into the Behavior of Long Riveted Connections

The third objective of this dissertation was to apply the recommended material model to a practical, untested problem and predict the response of long riveted connections to high loading rates. Observations from the model development and simulations lead to the following conclusions:

1. In situations where the sum of the rivet strength is greater than the yield capacity of the plate, excessive yielding of the plate in and around the exterior holes results in premature failure by yielding of the connecting member and/or premature *unbuttoning* failure of the rivets. This behavior was also observed in quasi-static testing conducted by Wang (2013).

2. When the sum of the rivet strength is less than the yield capacity of the connecting plates, loading rate affects the ultimate strength of riveted connections. Using the recommended University of Liverpool parameters ($C$ = 802 $s^{-1}$ and $q$ = 3.585), simulations of riveted connections of varying lengths provided the following conclusions:

(a) For lengths up to 12-in., the ultimate shear strength of a rivet under dynamic loading rates similar to those considered by Rabalais (2015) is 1.5 times the quasi-static ultimate strength (i.e., DIF = 1.5).

(b) The dynamic increase factor associated with riveted connections decreases as the length increases beyond 12-in. (DIF = 1.45 at 21-in., DIF = 1.36 at 30-in., and DIF = 1.0 at 65 in. (projected)).

## 5.3 Recommendations for Future Work

Based on the results from this research, there are several different possibilities for future research, including both experimental testing and numerical simulations. While thorough and in-depth testing was conducted by Rabalais (2015), additional testing could potentially reduce some of the scatter in the results. Furthermore, investigation into different rivet types and rivet sizes may reveal insight into changes in dynamic increase factor recommendations for rivets. Riveted bridges, often susceptible to different levels of corrosion and degradation, may be of interest for investigation to determine if the dynamic increase factor is affected by its level of deterioration. Importantly, it is recommended that all future rivet testing include additional instrumentation and data gathering with respect to material ductility and strain rate. While the 224 tests by Rabalais (2015) were extremely

valuable, more comprehensive data acquisition would likely help improve the LS-DYNA (2013) modeling and analysis/comparison of results.

Immediate numerical testing opportunities exist by modeling and analyzing the simple suspension bridge panels. Valid model development would demonstrate rivets failing in shear and panels failing in a ductile, tensile manner. If interested in possibly improving the model of the rivet, simulations involving quasi-static combined loading (shear and tension) could serve as an additional verification of realistic rivet behavior. Comparison of these combined loading simulations with historical experimental tests and results from Munse and Cox (1956) could serve as a validation tool.

As terrorists appear to be on a never-ending desire to attack soft targets, this research provides valuable information with respect to modeling and understanding the behavior of riveted connections under quasi-static and dynamic loading rates. Results from these simulations and details from the developed numerical modeling approach can assist other engineers with future testing and in predicting the strength of a variety of different riveted connections under high loading rates. Understanding the capacity and behavior of these connections will assist in the development of mitigation strategies against terrorism.

# Appendix A: Quasi-Static Simulation versus Experimentation Results

Appendix A provides the load versus time output from five riveted connection configurations in single- and double-shear (10 total figures) under quasi-static loading. Each figure includes test data from Rabalais (2015) via light, black lines and LS-DYNA simulation output via a bold, black curve. In addition, there are red, yellow, and green lines on each plot that indicate the experimental maximum load, mean load, and minimum load, respectively. Above each load versus time plot is a LS-DYNA (2013) illustration of the applicable figure. Details regarding the development of these plots and an analysis of their significance are found throughout Chapter 3.

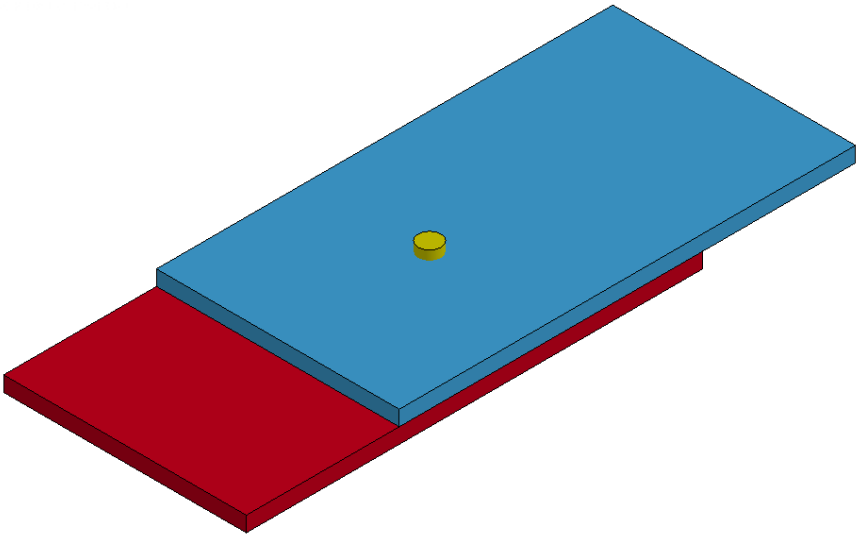

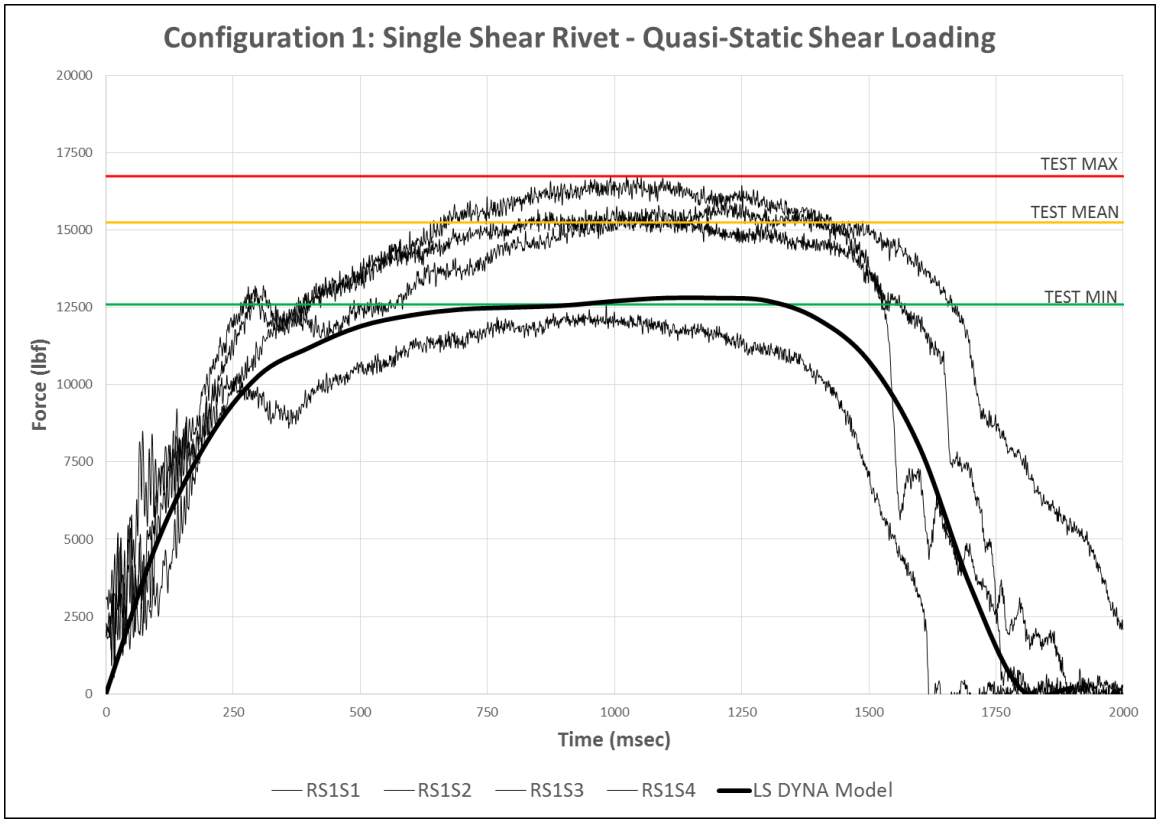


Fig. A-1: Configuration 1, Single Shear, Quasi-Static

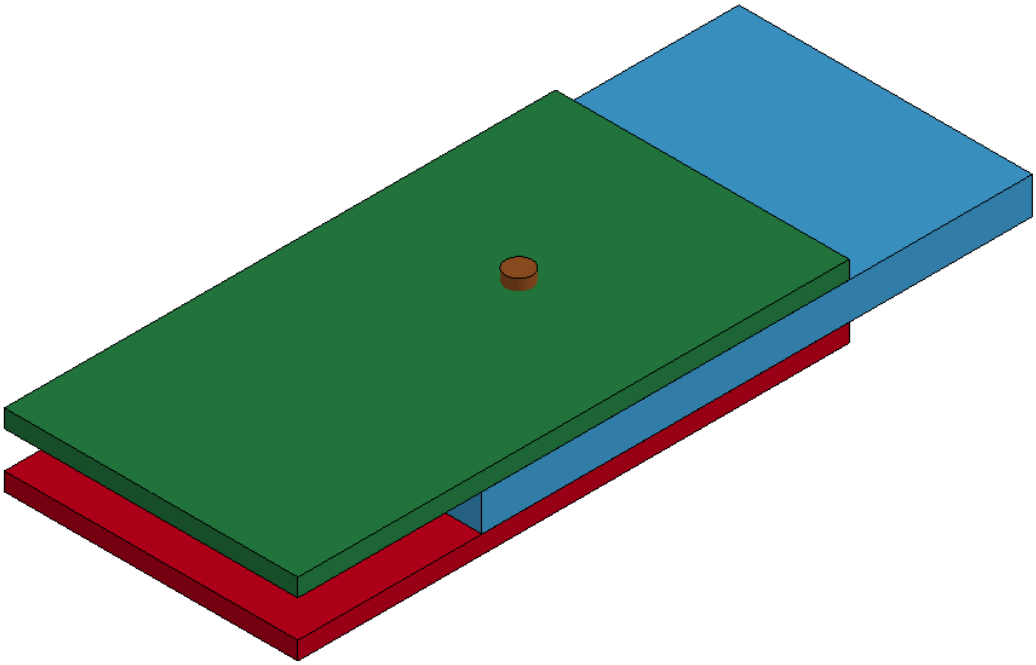

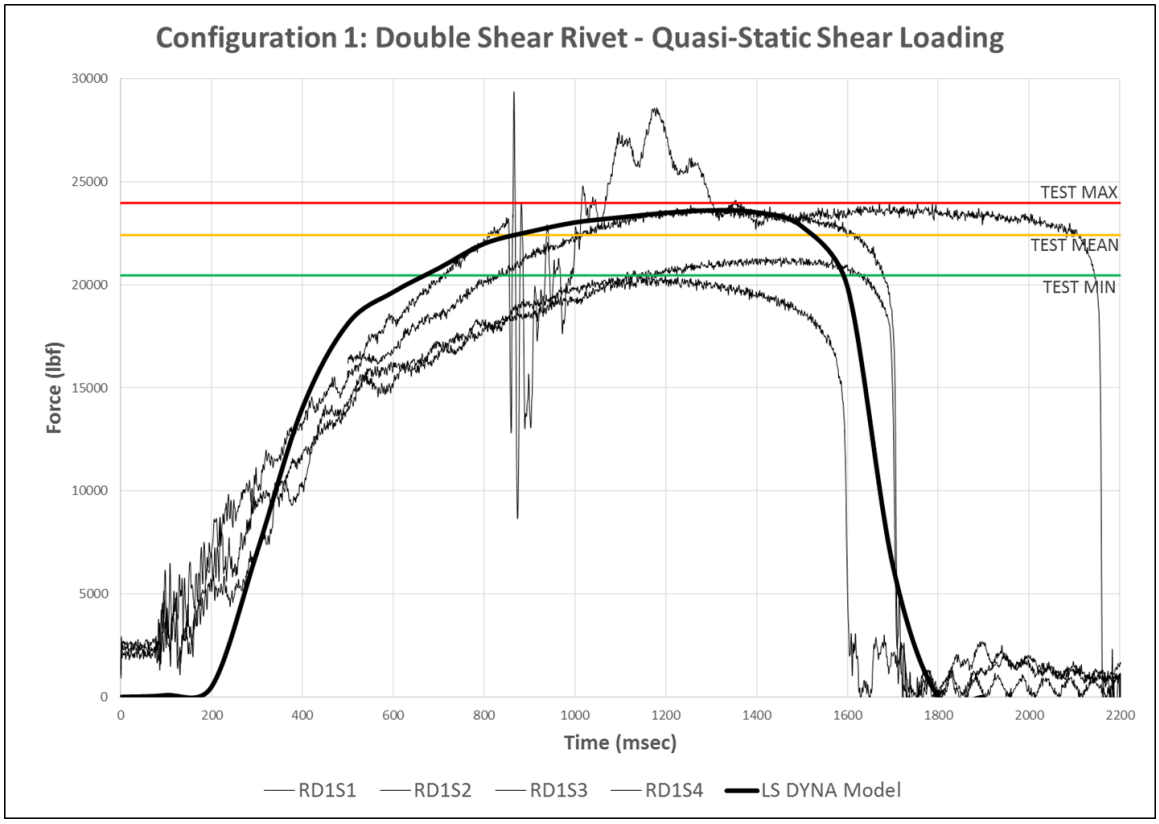


Fig. A-2: Configuration 1, Double Shear, Quasi-Static

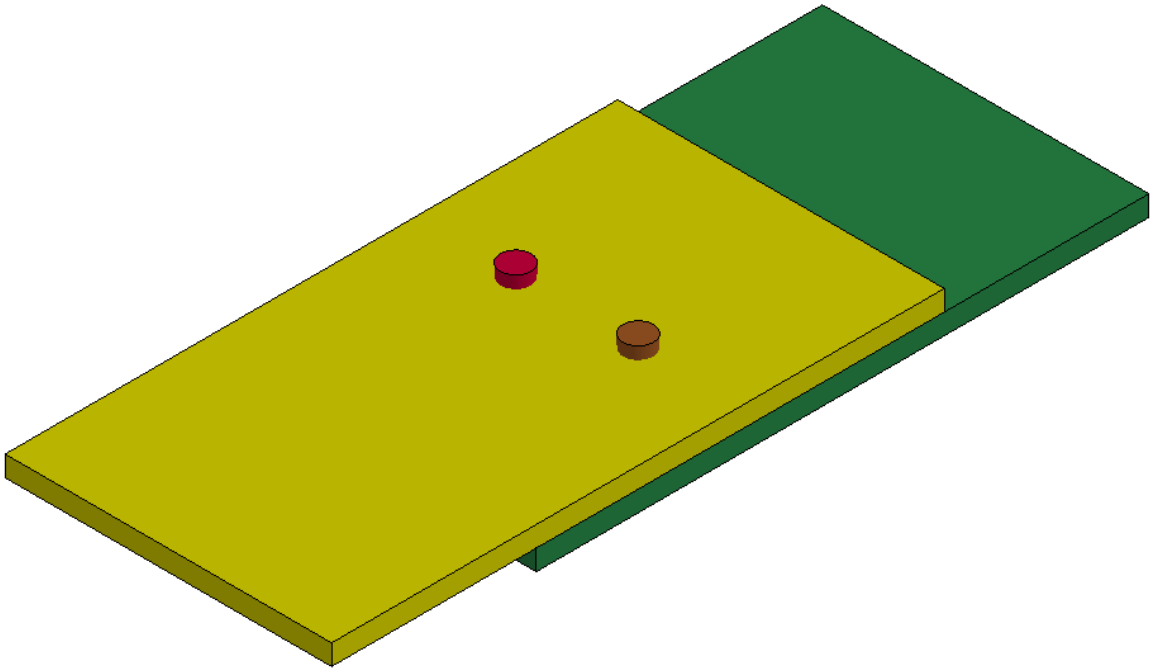

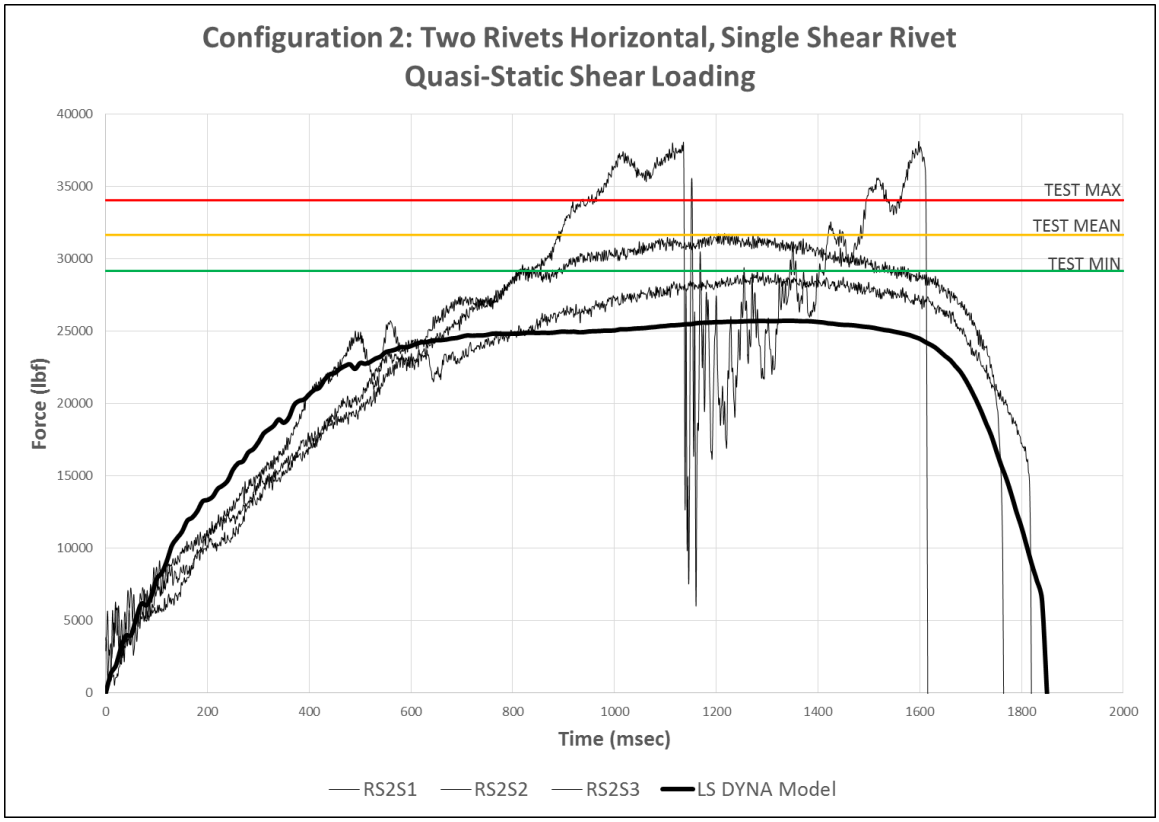


Fig. A-3: Configuration 2, Single Shear, Quasi-Static

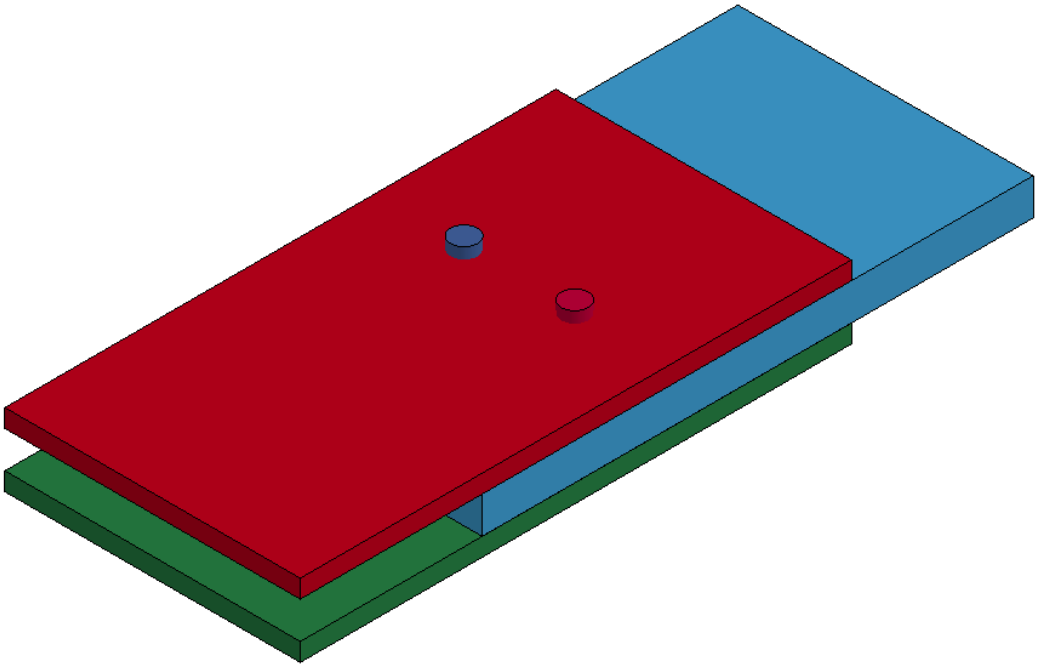

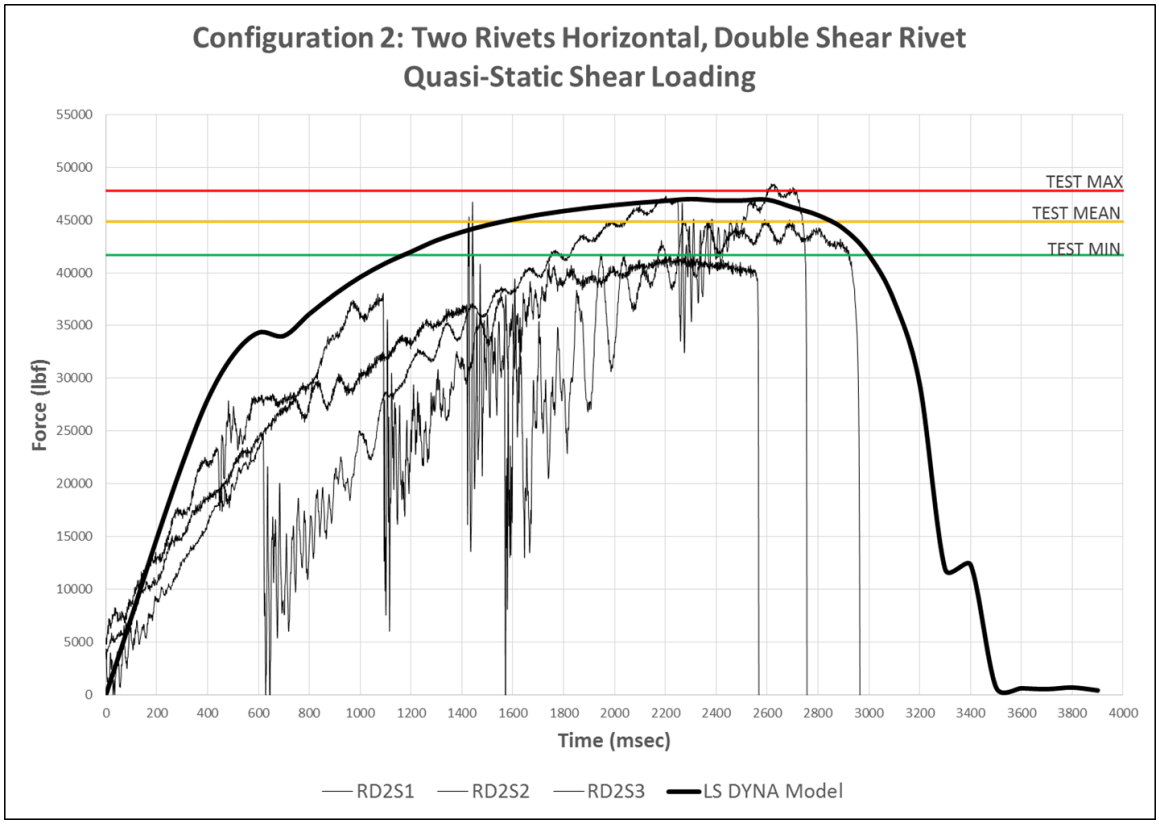


Fig. A-4: Configuration 2, Double Shear, Quasi-Static

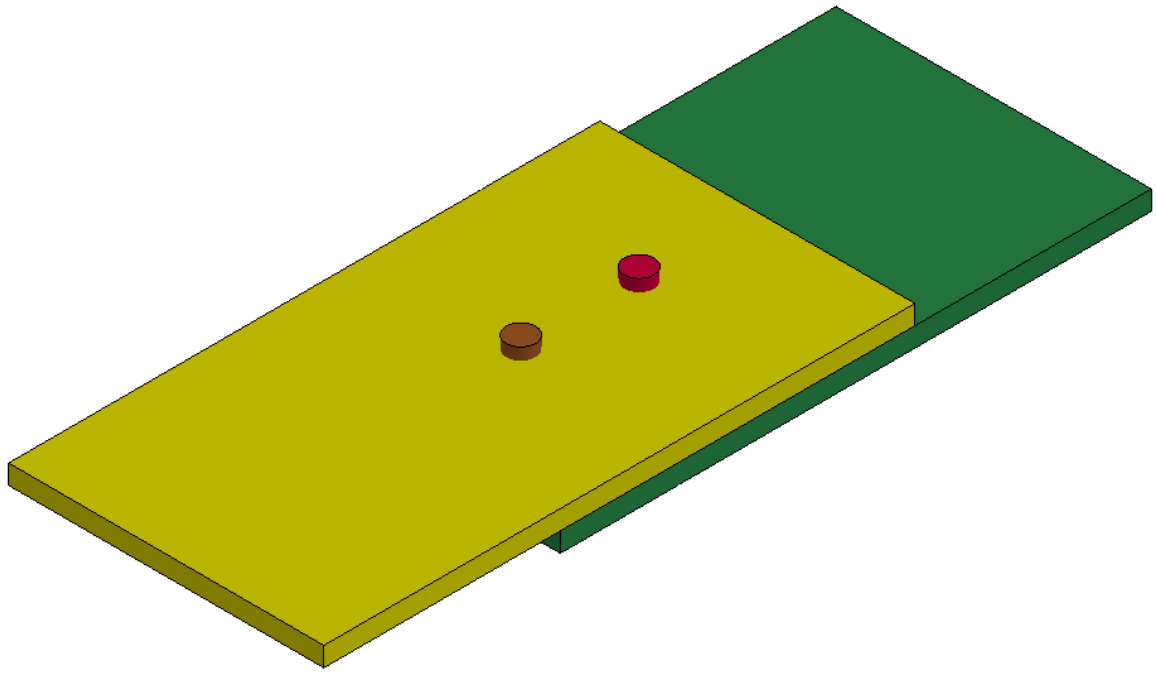

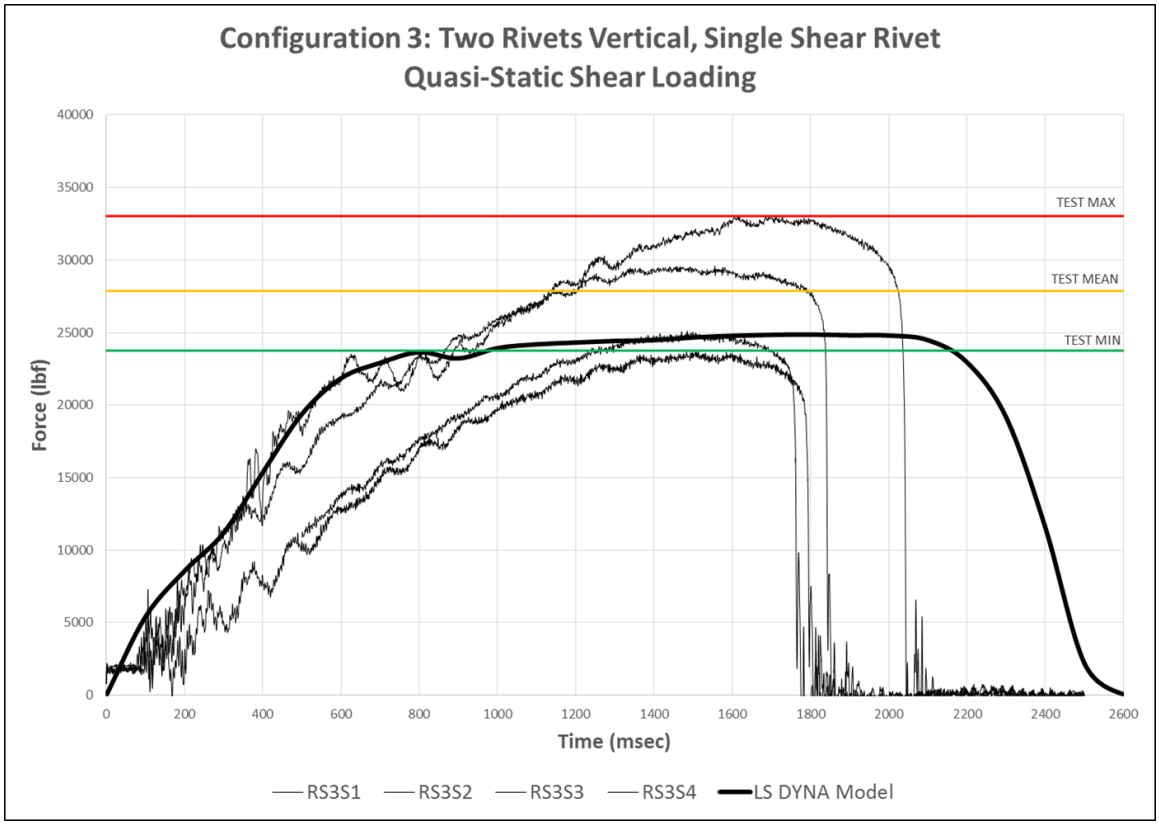


Fig. A-5: Configuration 3, Single Shear, Quasi-Static

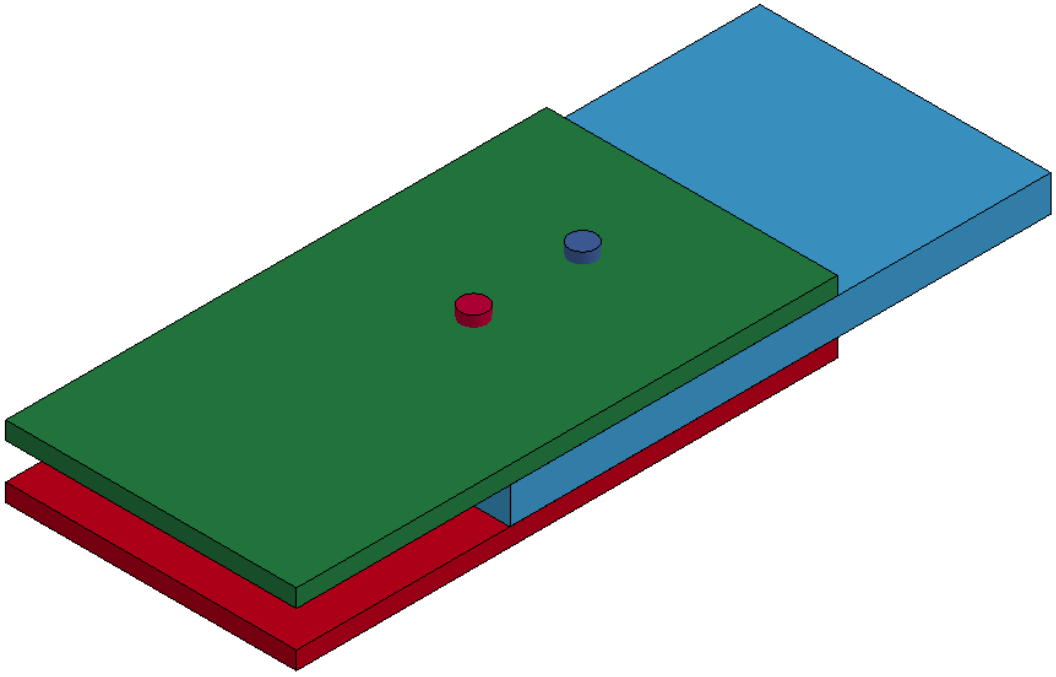

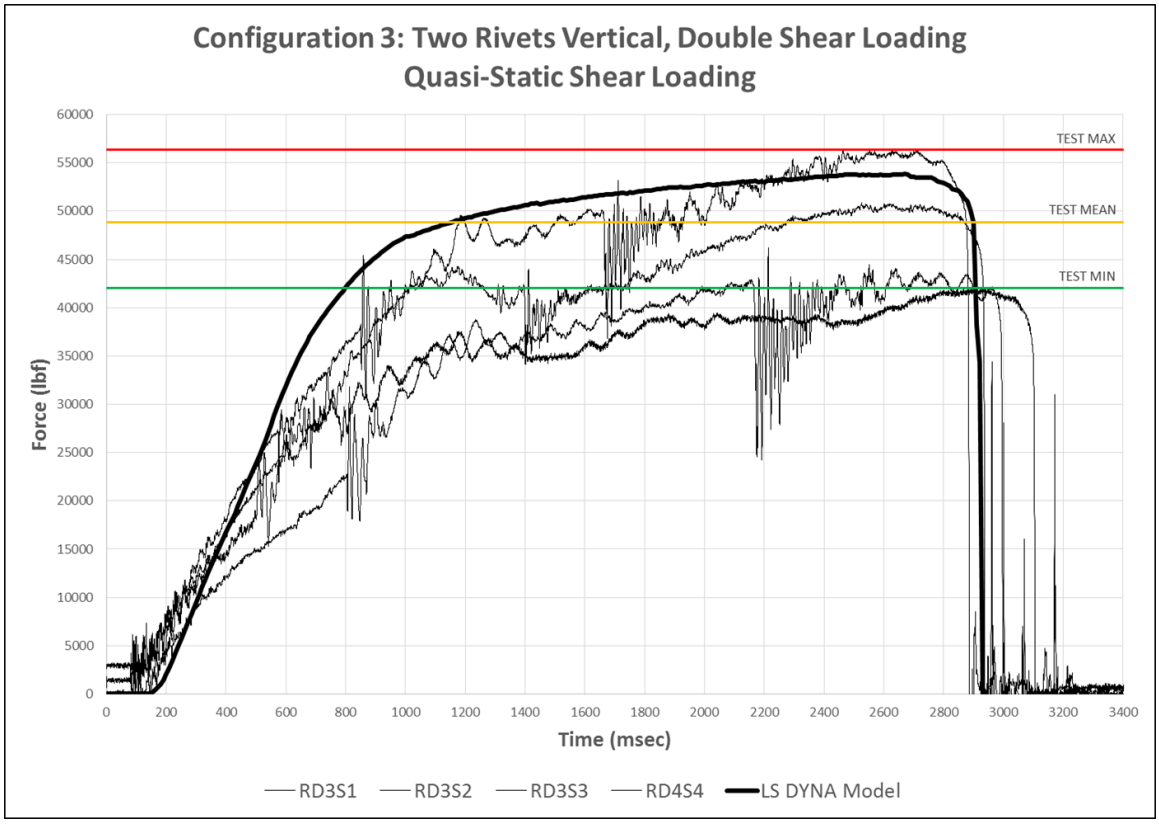


Fig. A-6: Configuration 3, Double Shear, Quasi-Static

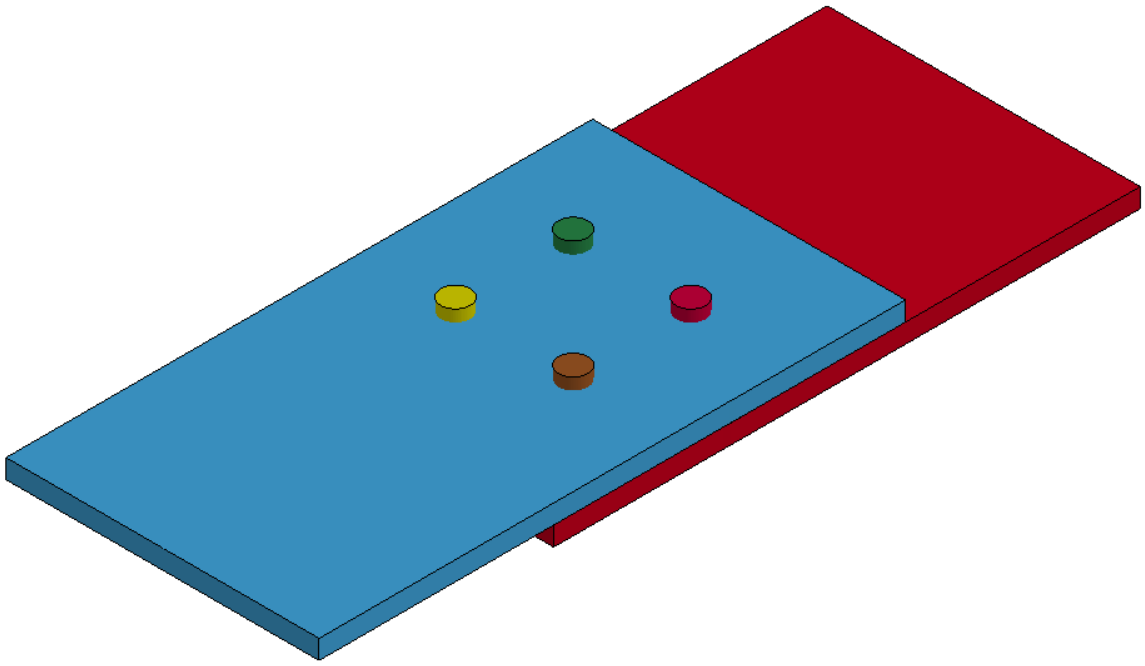

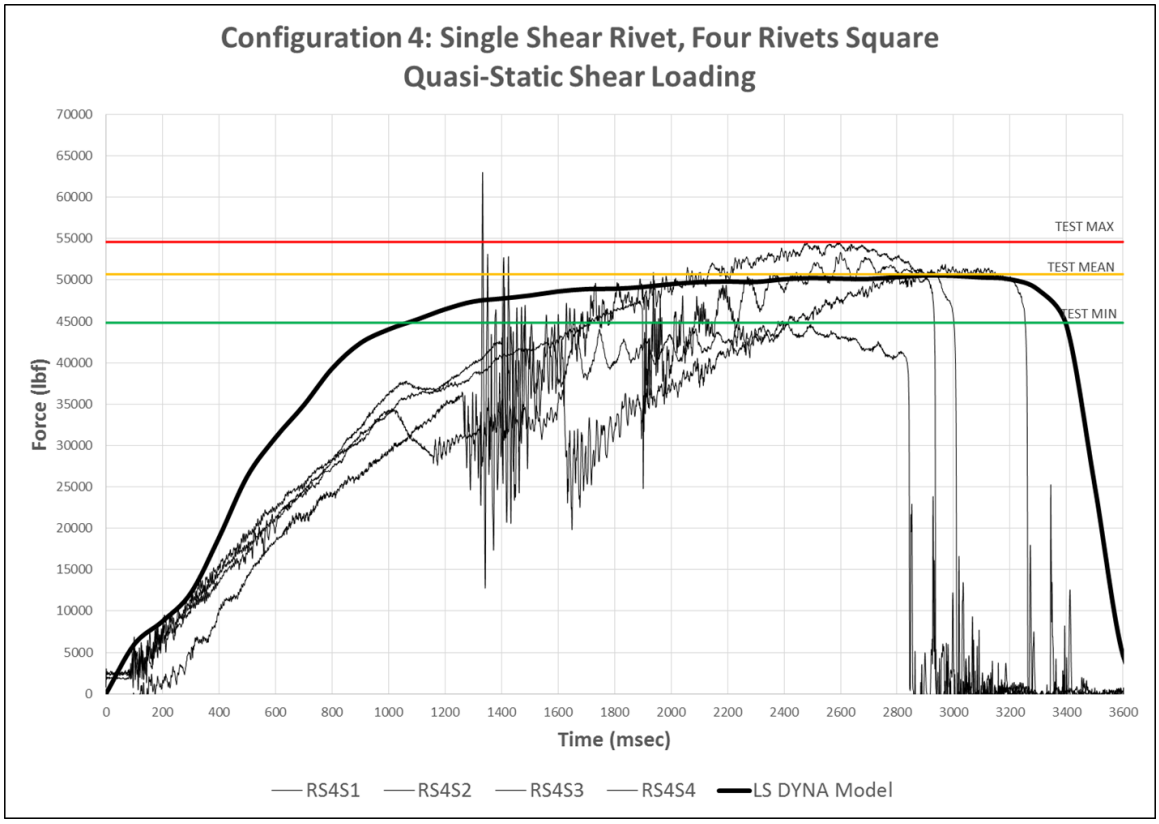


Fig. A-7: Configuration 4, Single Shear, Quasi-Static

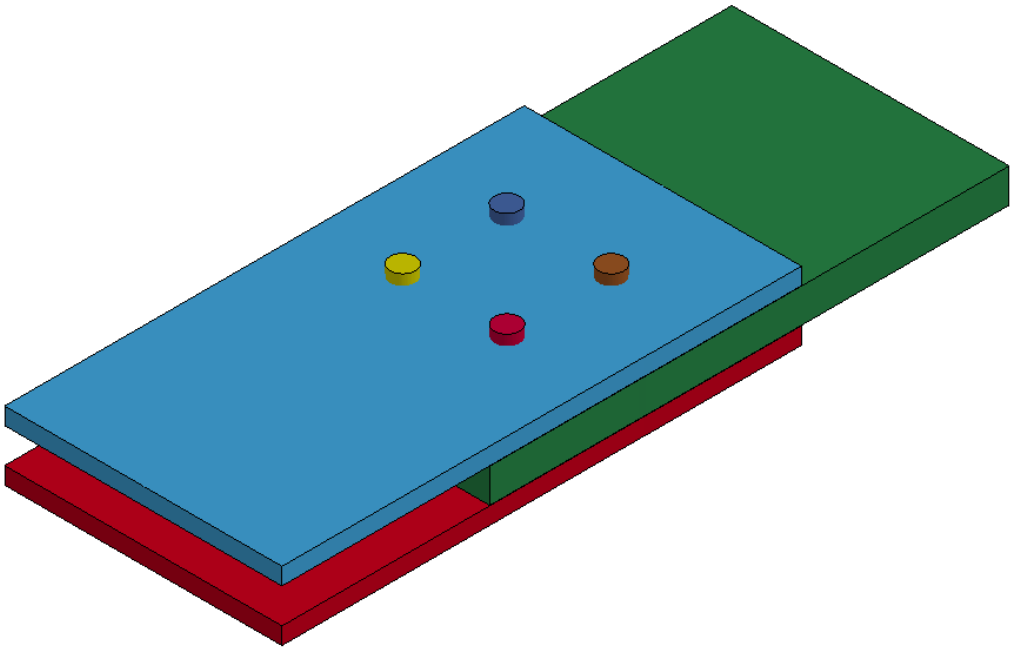

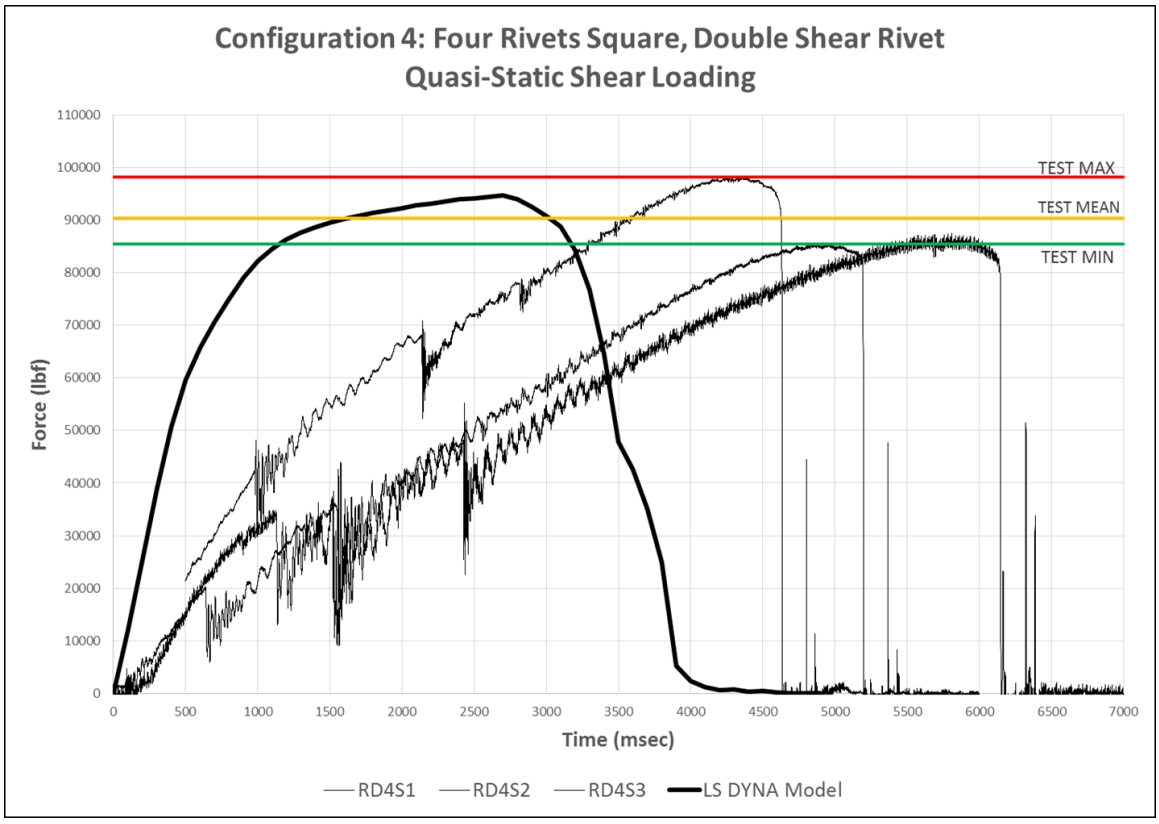


Fig. A-8: Configuration 4, Double Shear, Quasi-Static

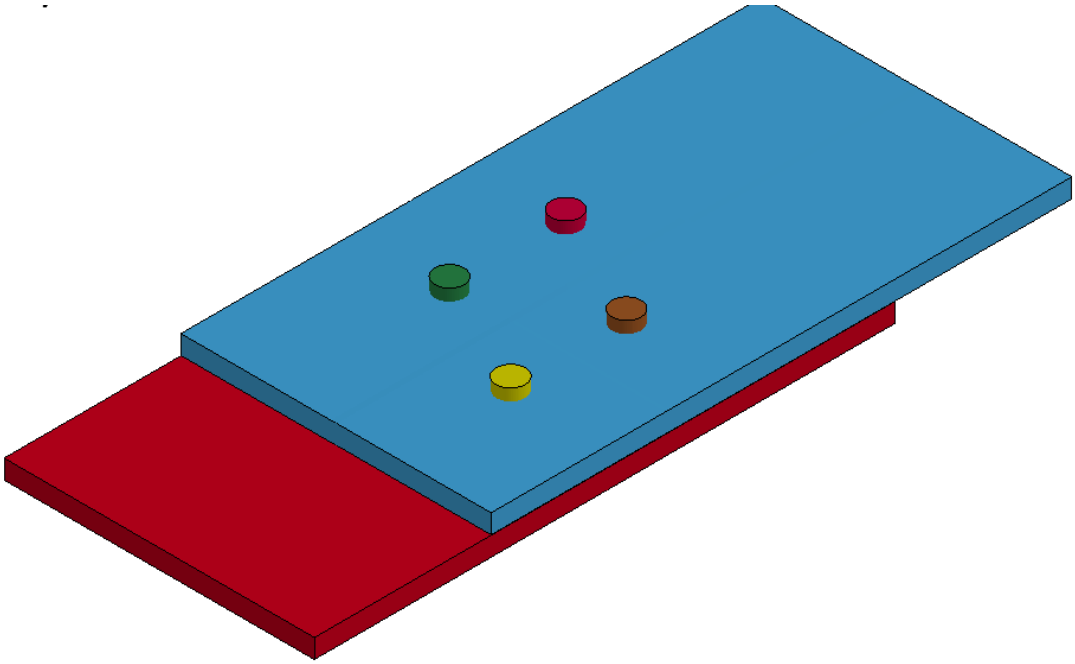

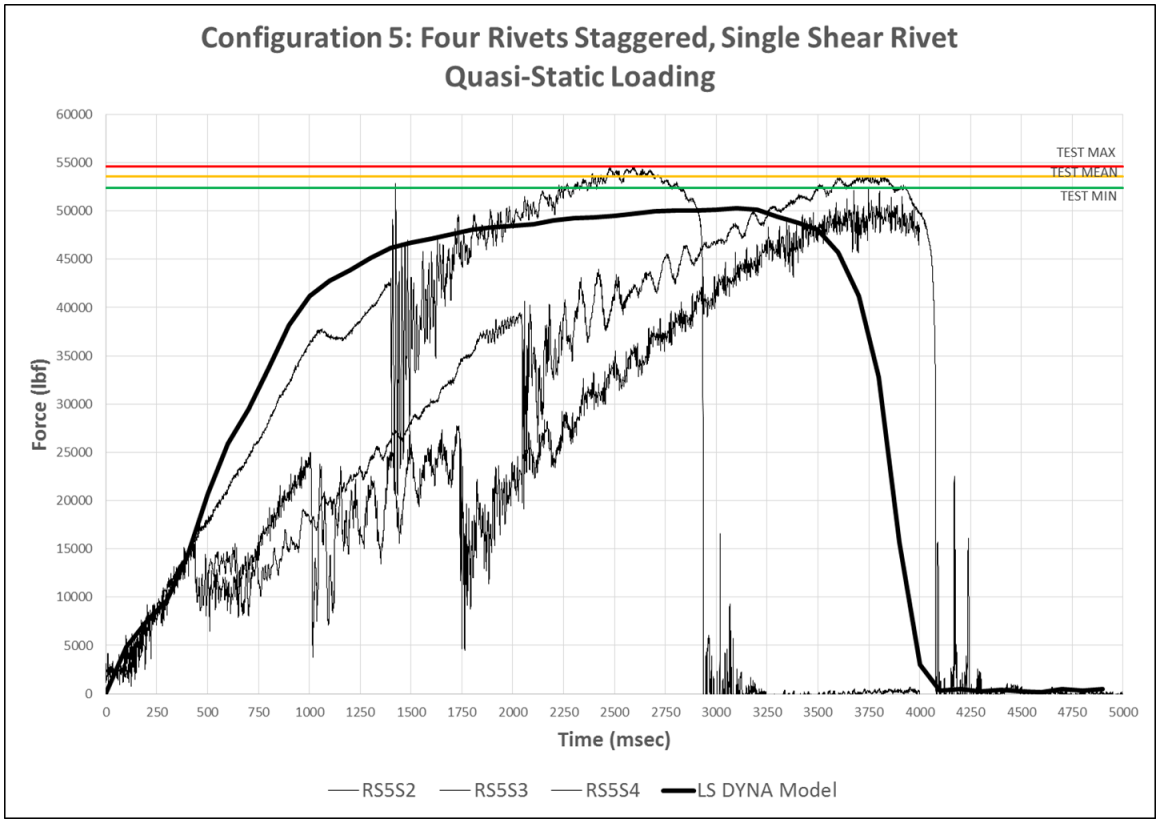


Fig. A-9: Configuration 5, Single Shear, Quasi-Static

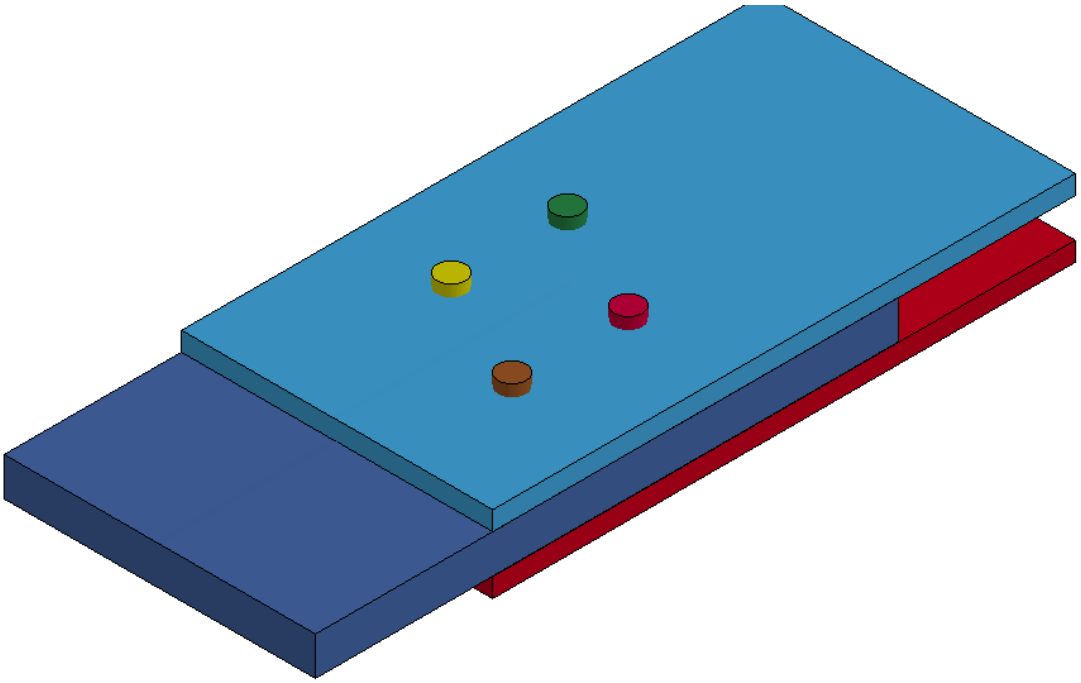

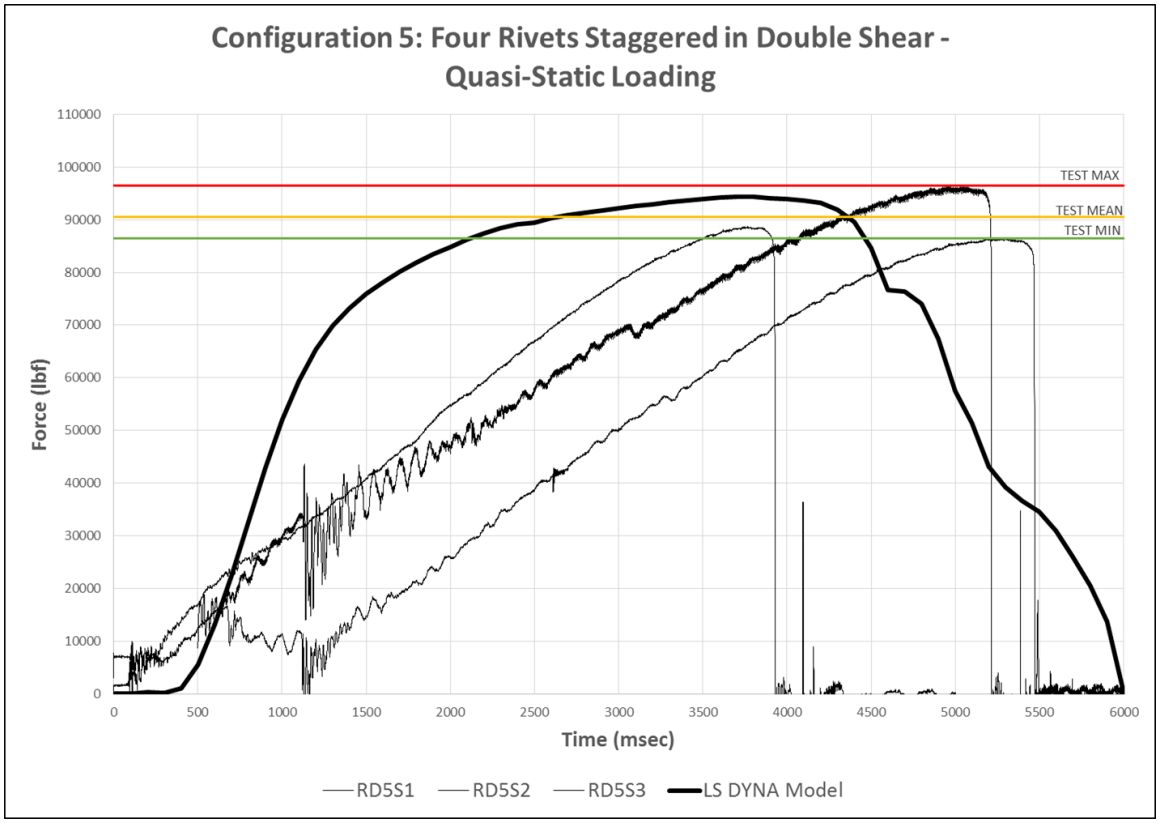


Fig. A-10: Configuration 5, Double Shear, Quasi-Static

# Appendix B: Bounding Dynamic Simulations versus Experimental Results

Appendix B provides the load versus time output from five riveted connection configurations in single- and double-shear (10 total figures) under dynamic loading. Dashed lines represent predicted rivet behavior from LS-DYNA (2013) using the original Cowper Symonds (1957) parameters ($C$ = 40.4 $s^{-1}$ and $q$ = 5). Bold solid lines represent predicted rivet behavior from LS-DYNA (2013) using Abramowicz and Jones (1986) parameters ($C$ = 6884 $s^{-1}$ and $q$ = 3.91). Light (unbold) lines represent experimental test data (Rabalais, 2015). In addition, there are red, yellow, and green lines on each plot that indicate the experimental maximum load, mean load, and minimum load, respectively. Above each load versus time plot is a LS-DYNA (2013) illustration of the applicable figure. Details regarding the development of these plots and an analysis of their significance are found in Sections 4.2 and 4.3.

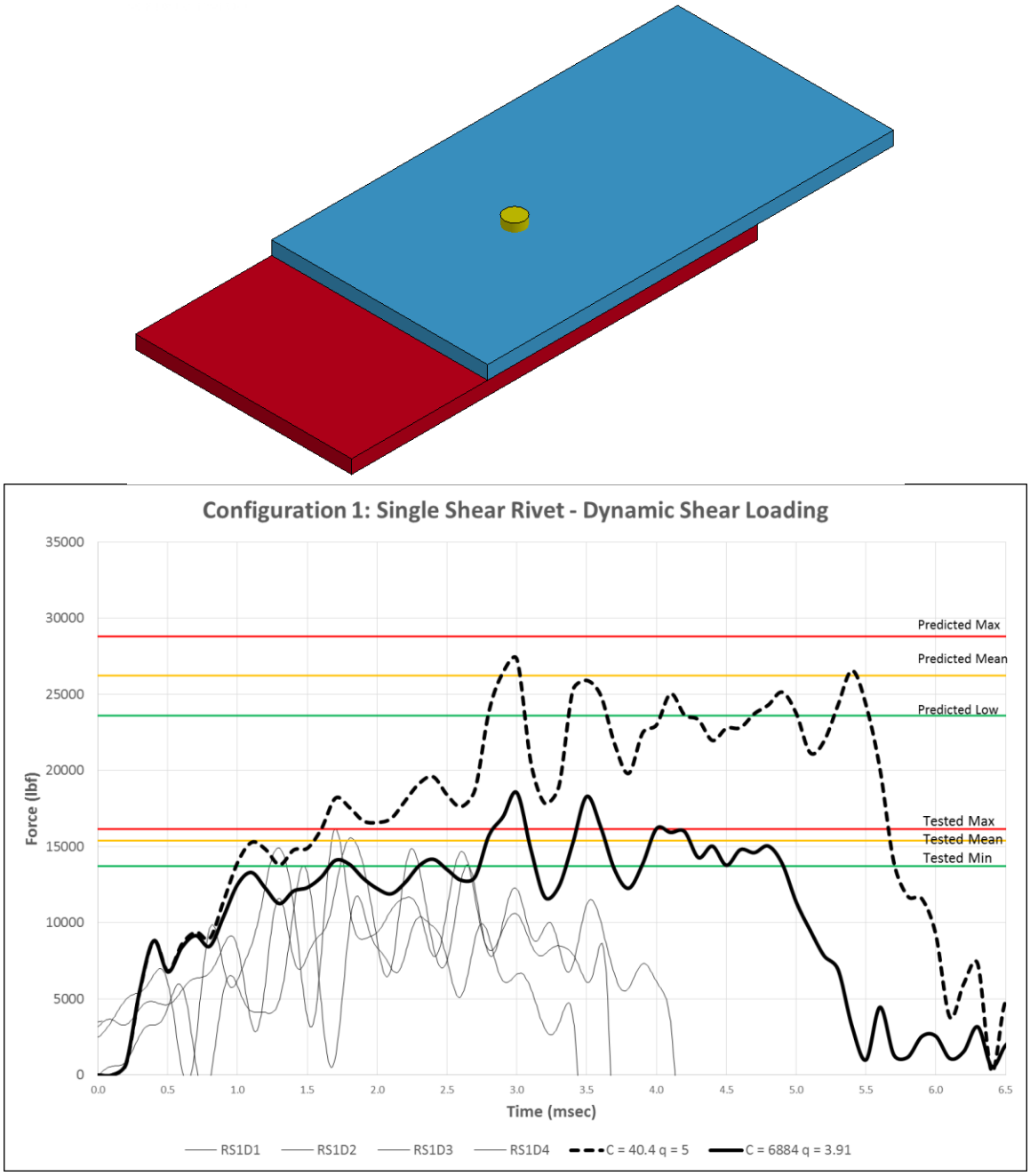


Fig. B-1: Bounding Results, Configuration 1, Single Shear, Dynamic

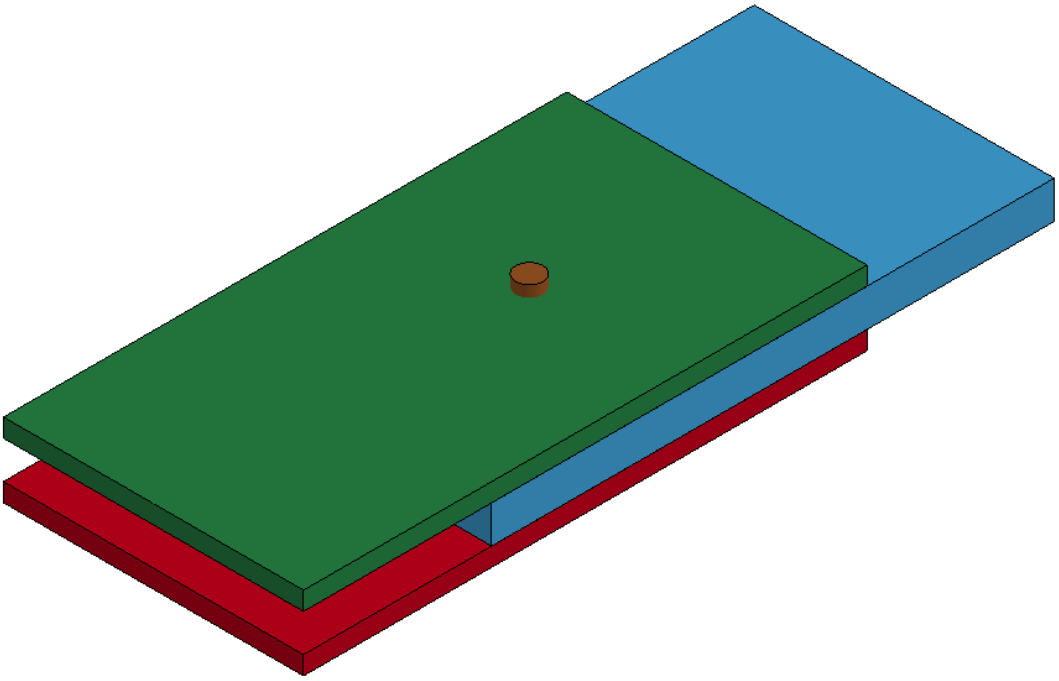

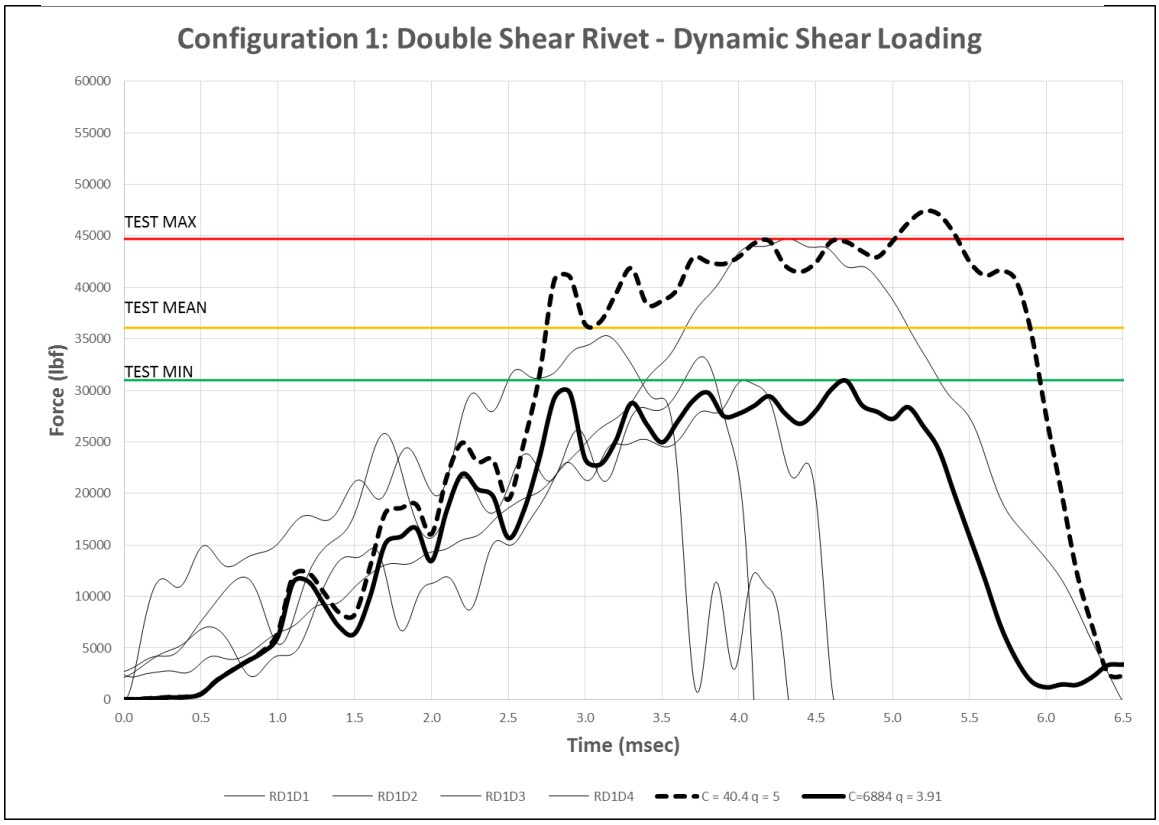


Fig. B-2: Bounding Results, Configuration 1, Double Shear, Dynamic

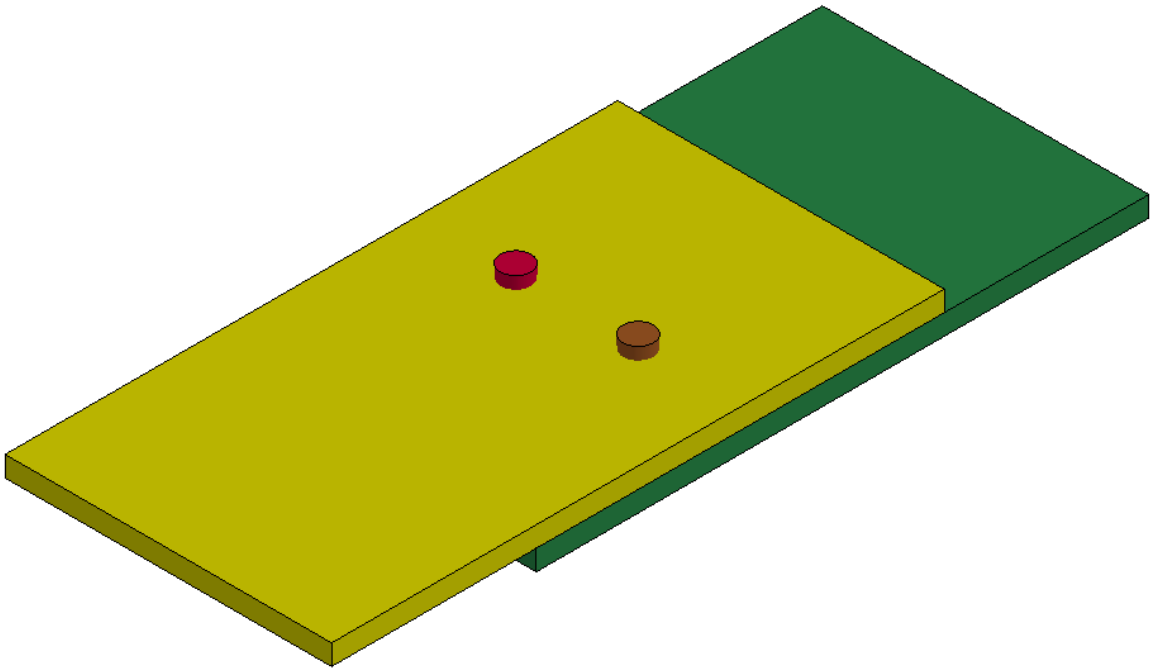

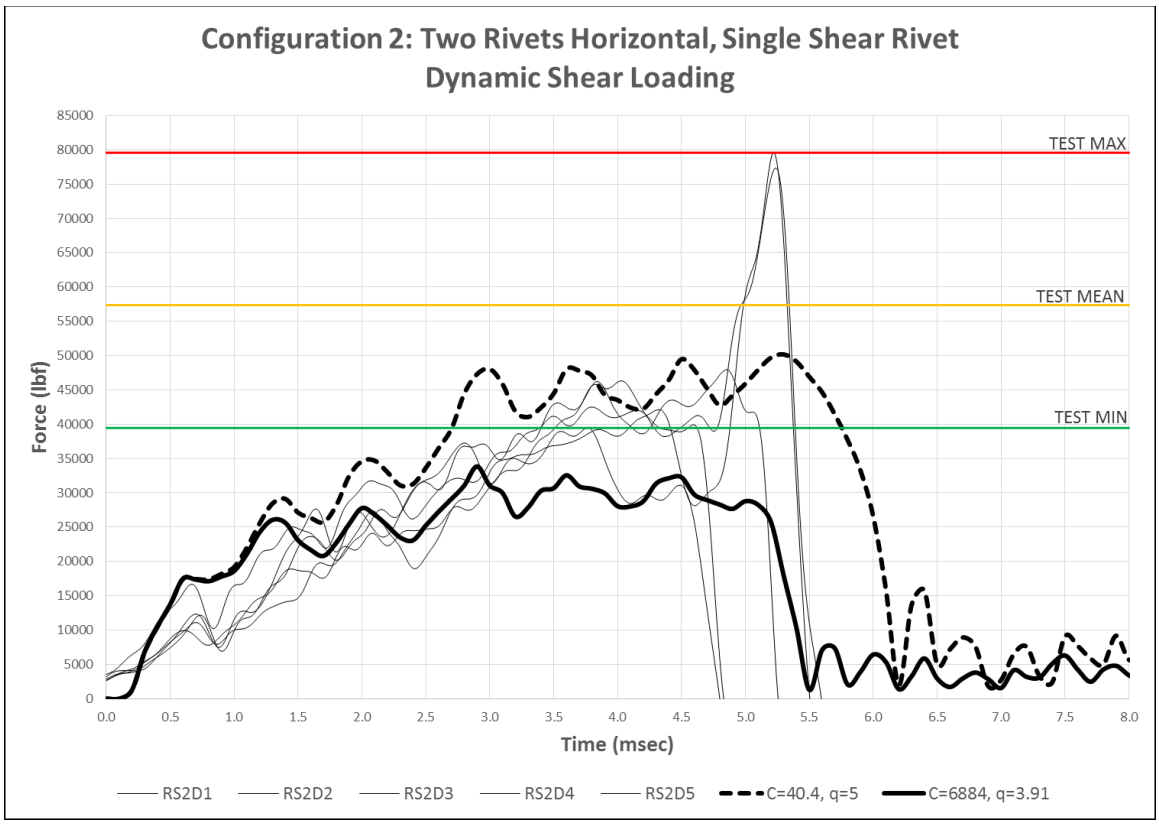


Fig. B-3: Bounding Results, Configuration 2, Single Shear, Dynamic

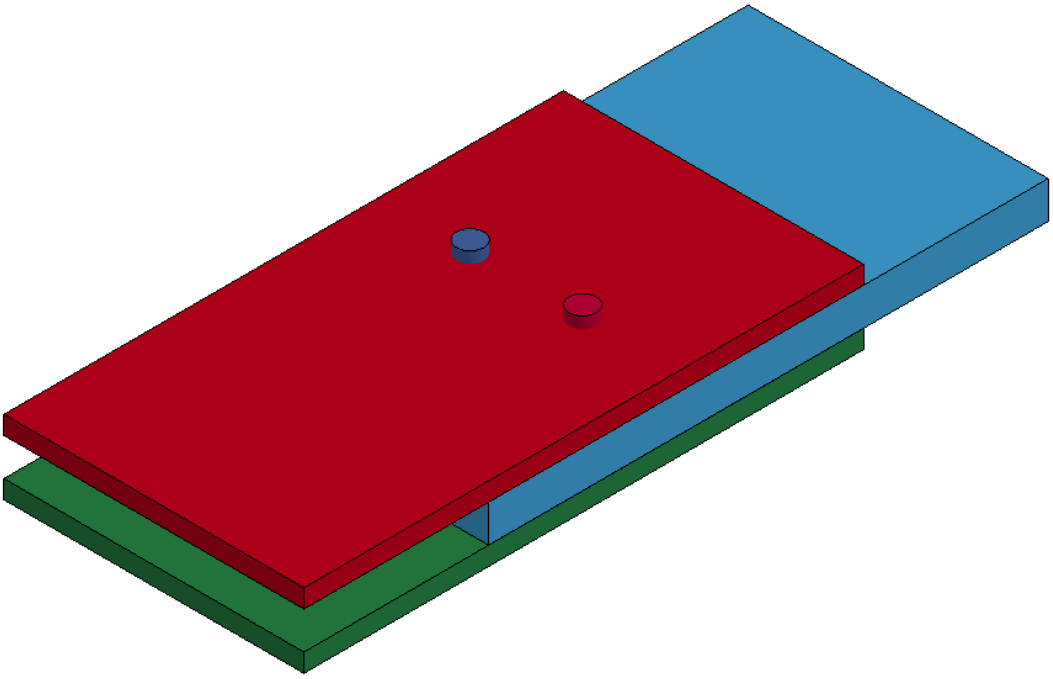

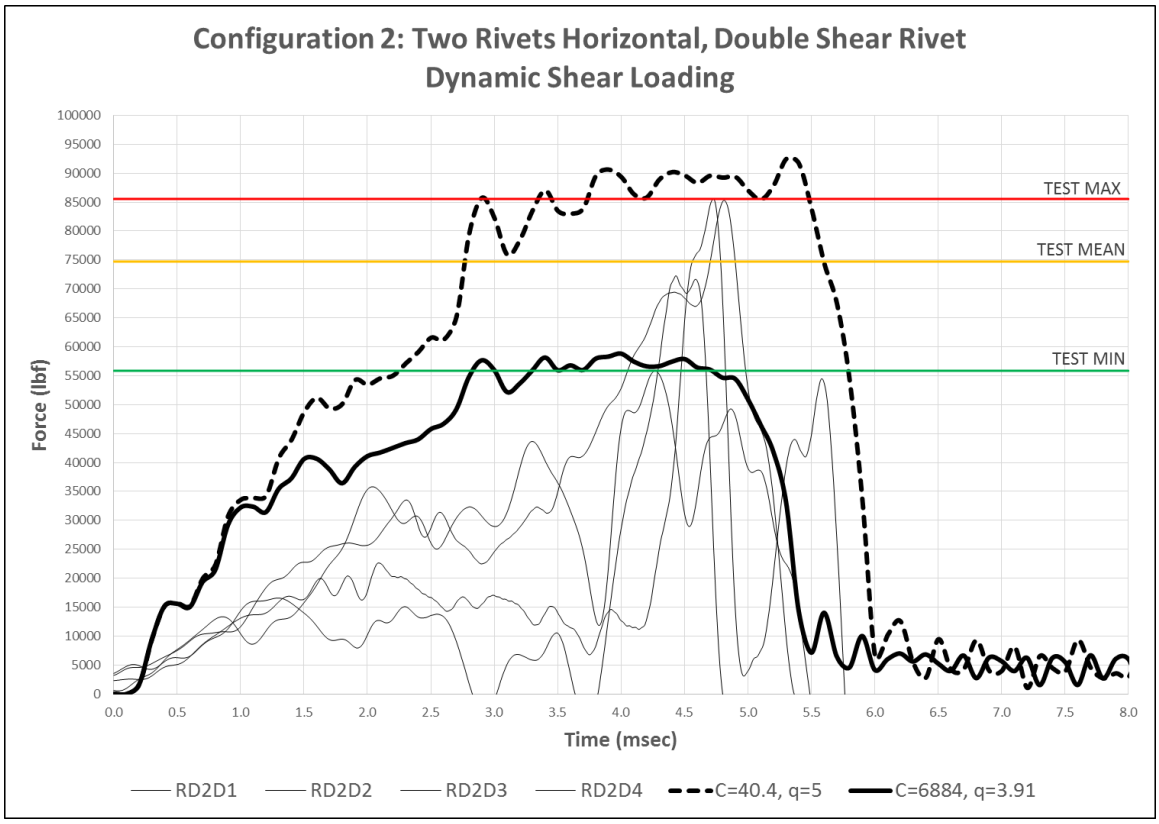


Fig. B-4: Bounding Results, Configuration 2, Double Shear, Dynamic

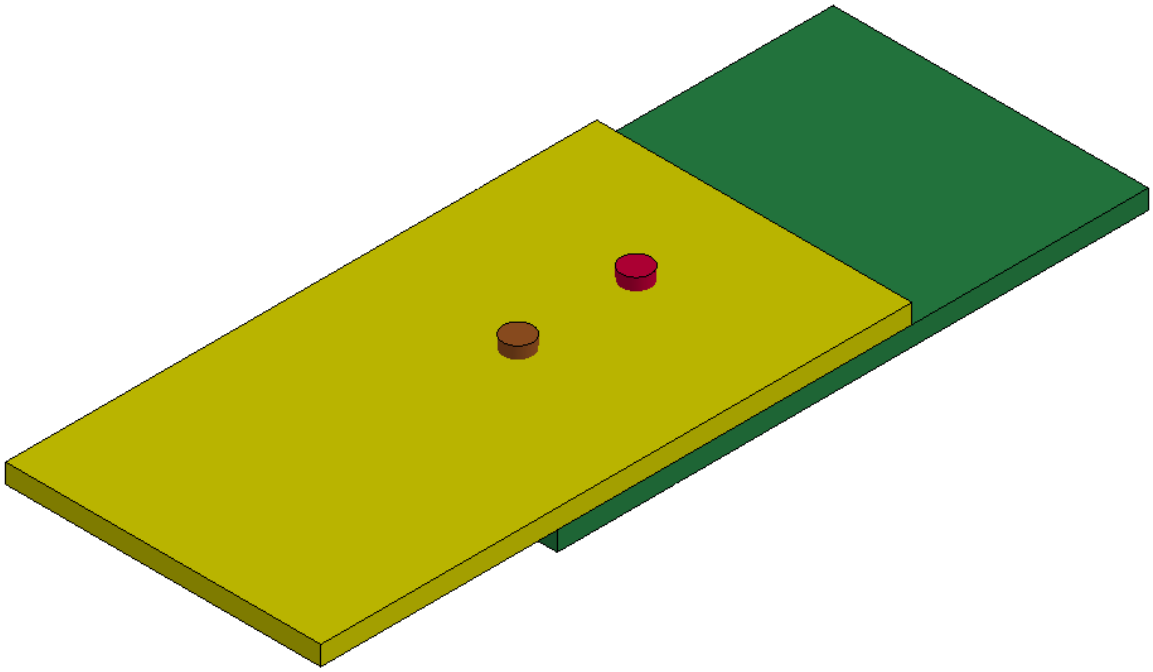

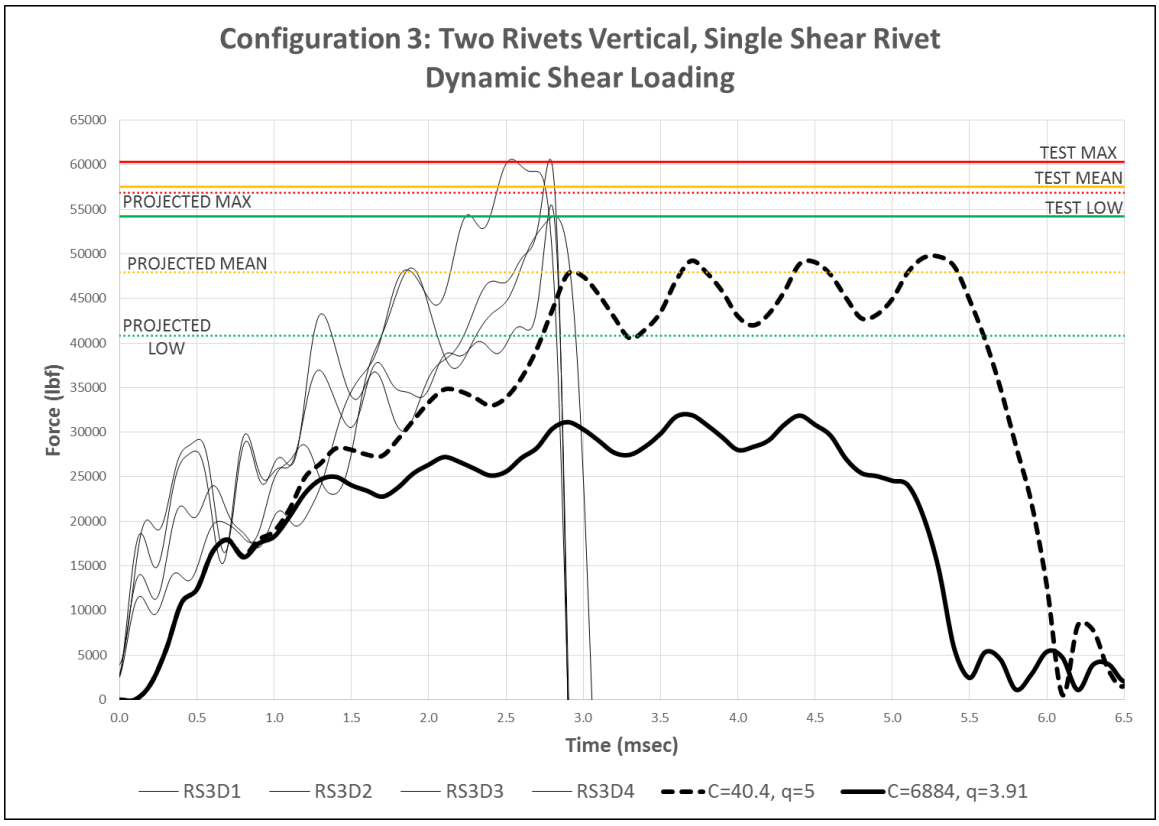


Fig. B-5: Bounding Results, Configuration 3, Single Shear, Dynamic

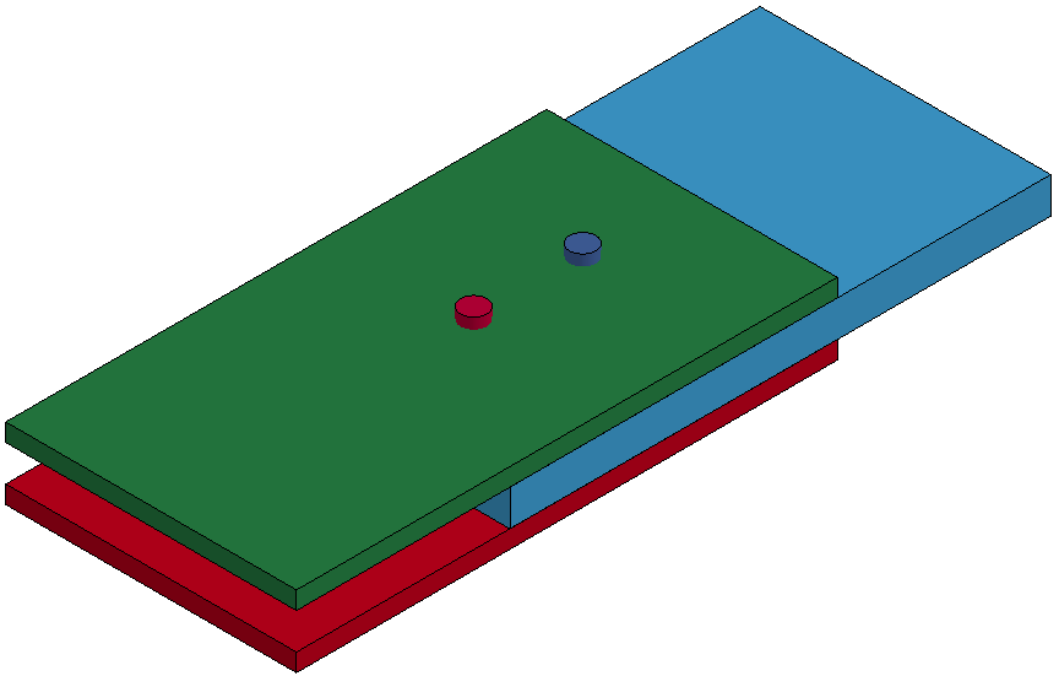

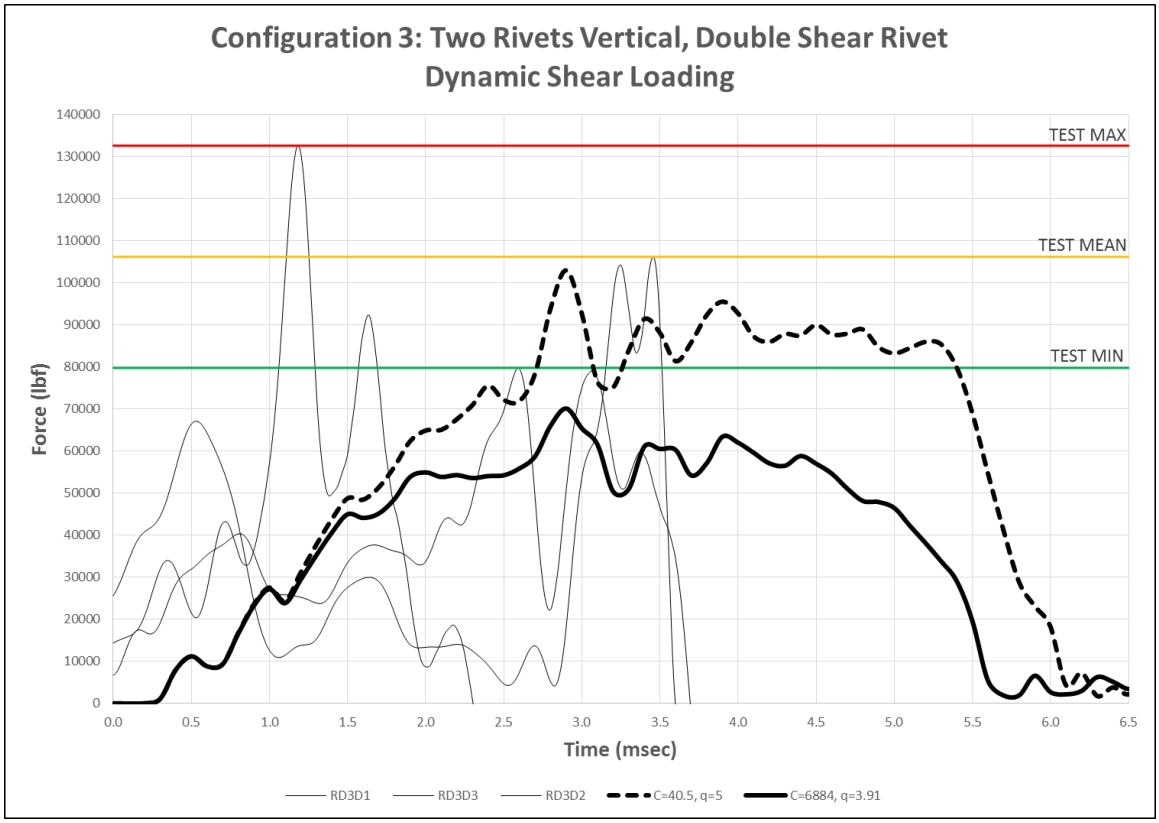


Fig. B-6: Bounding Results, Configuration 3, Double Shear, Dynamic

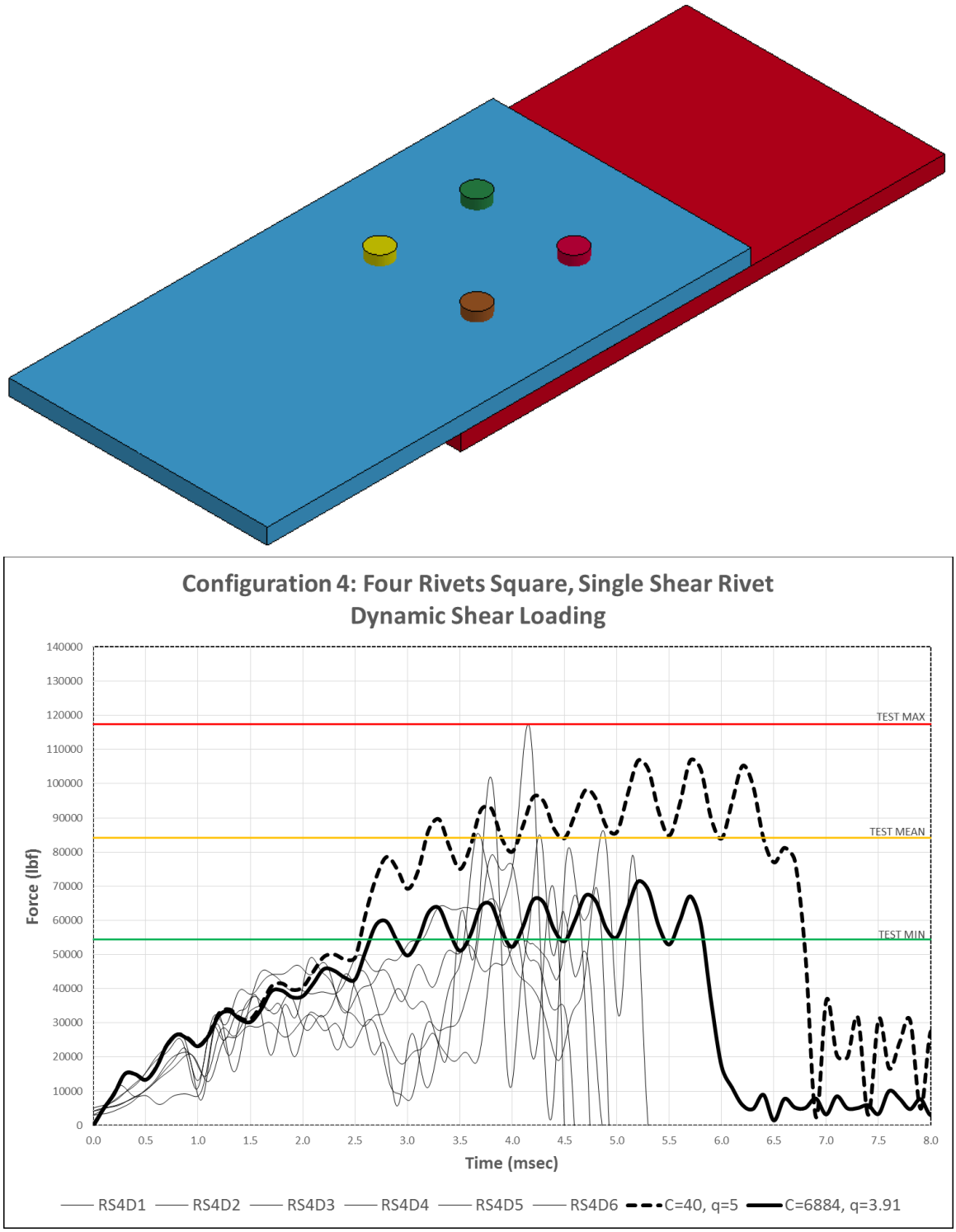


Fig. B-7: Bounding Results, Configuration 4, Single Shear, Dynamic

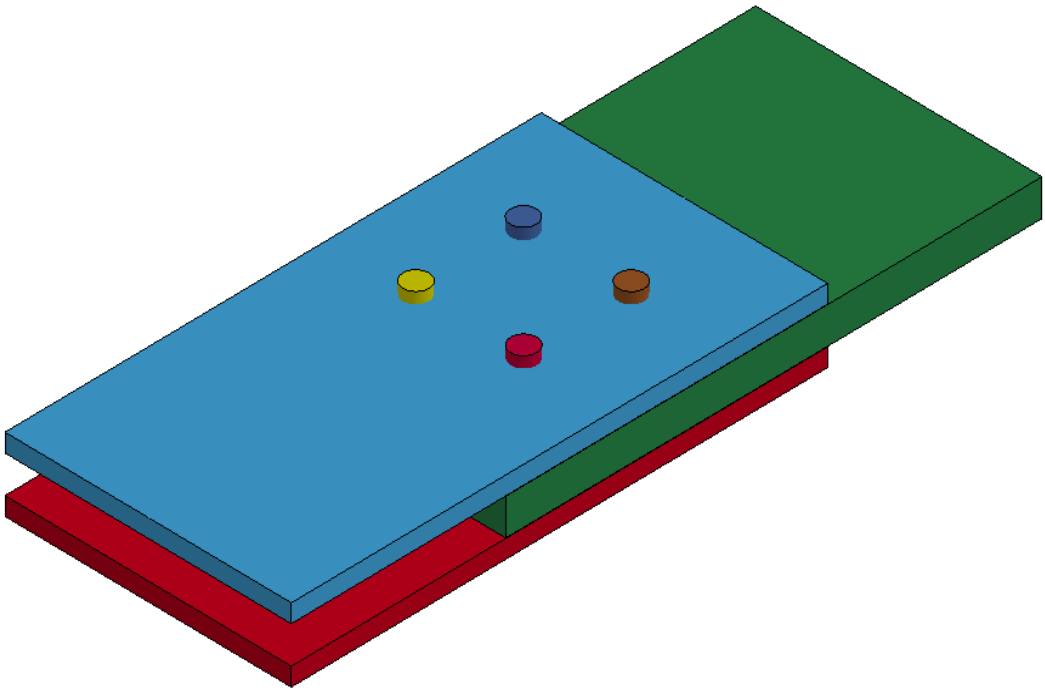

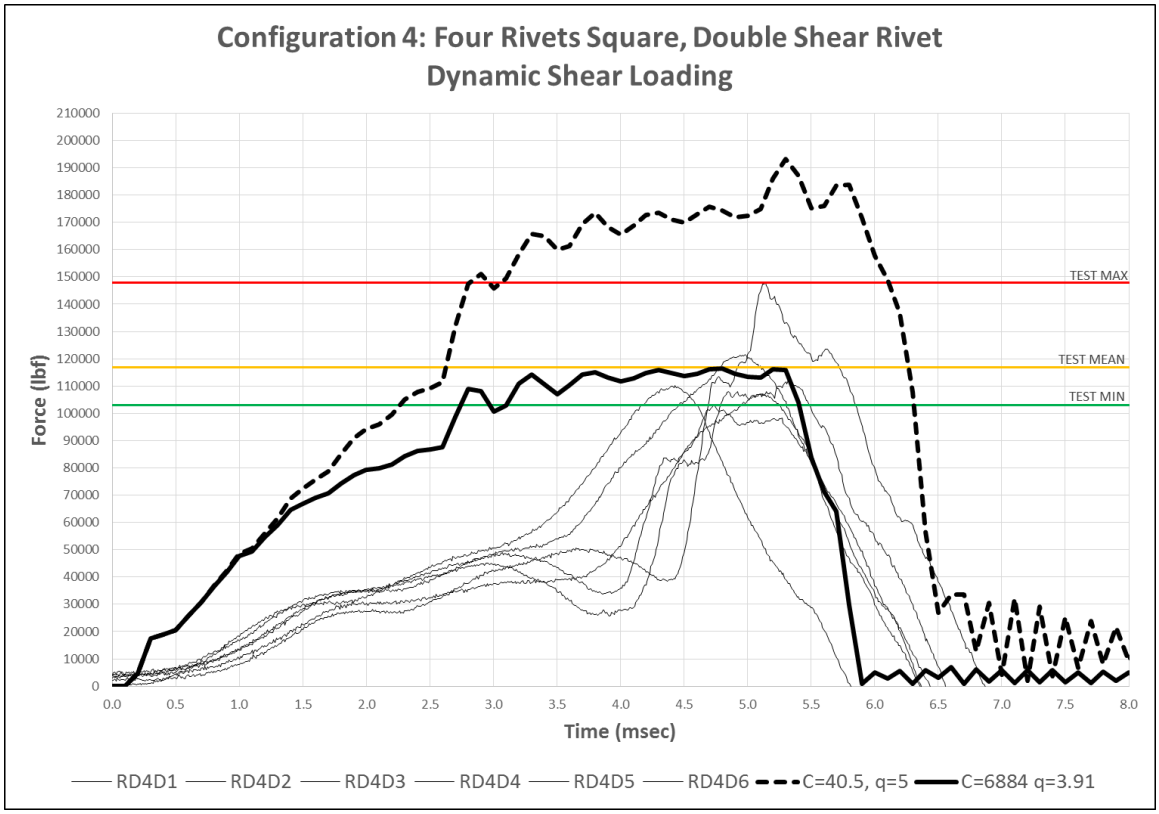


Fig. B-8: Bounding Results, Configuration 4, Double Shear, Dynamic

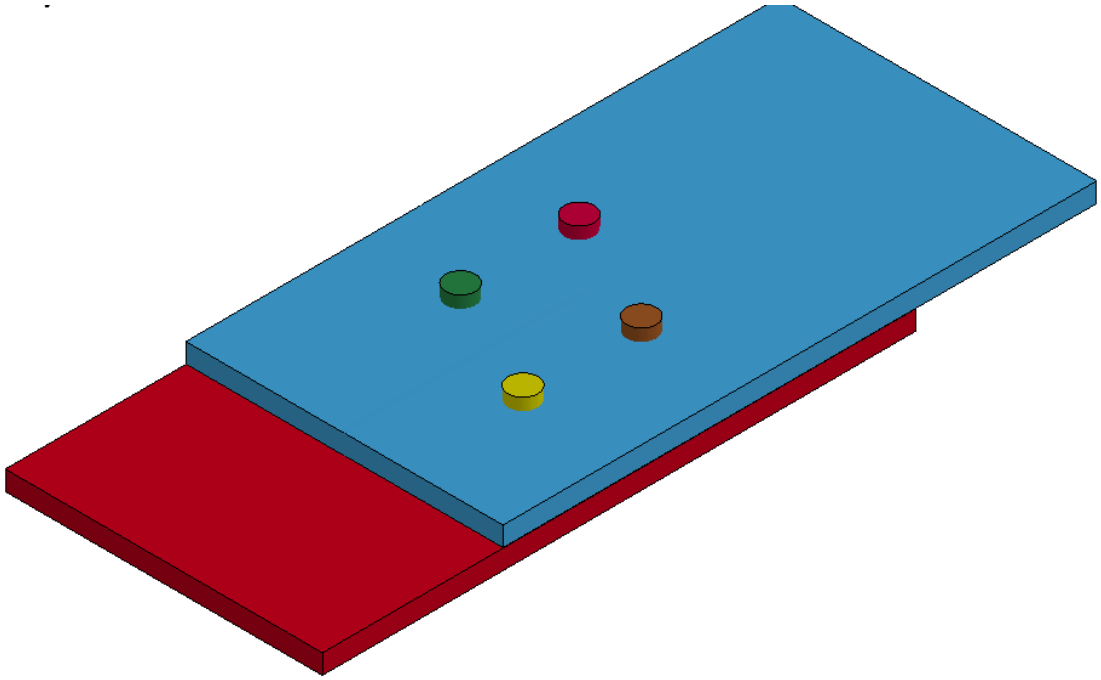

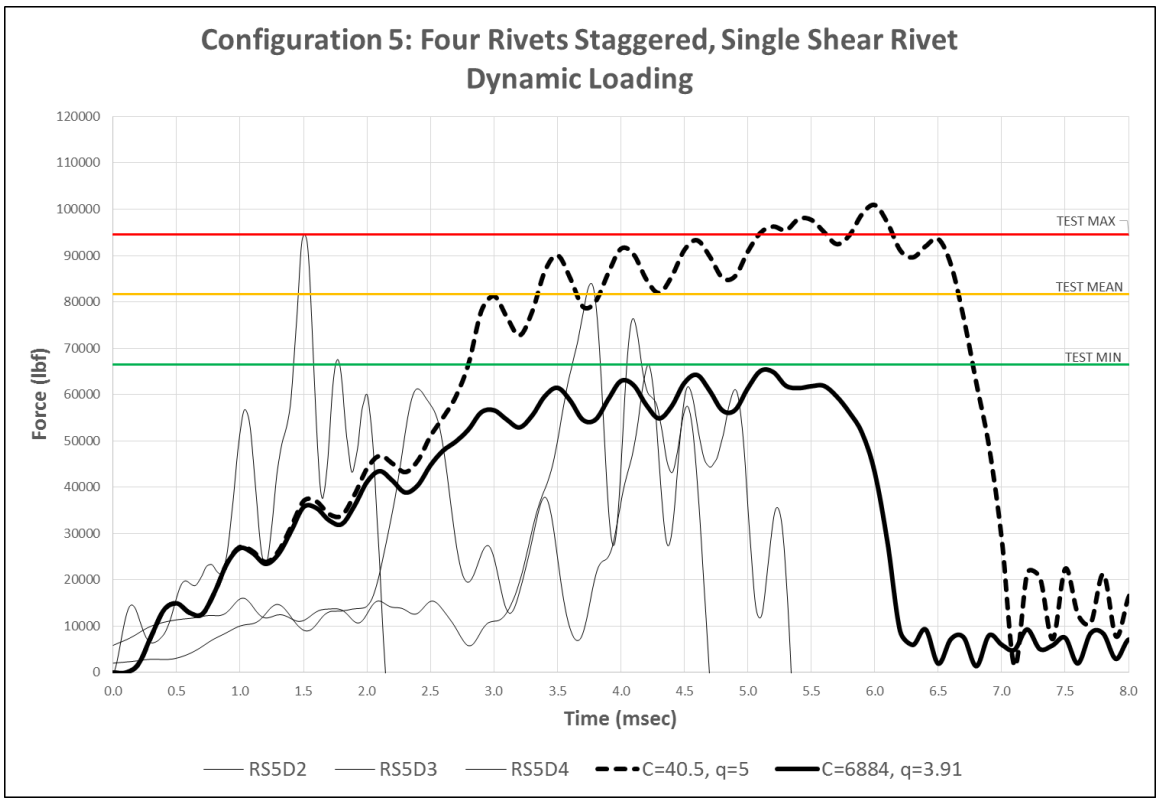


Fig. B-9: Bounding Results, Configuration 5, Single Shear, Dynamic

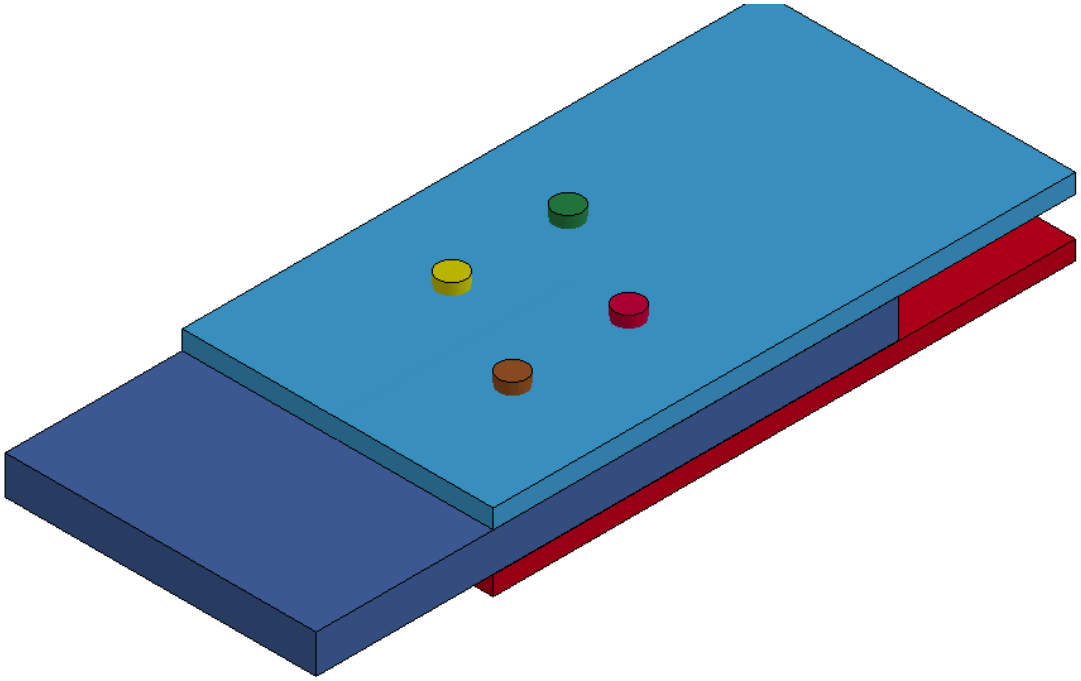

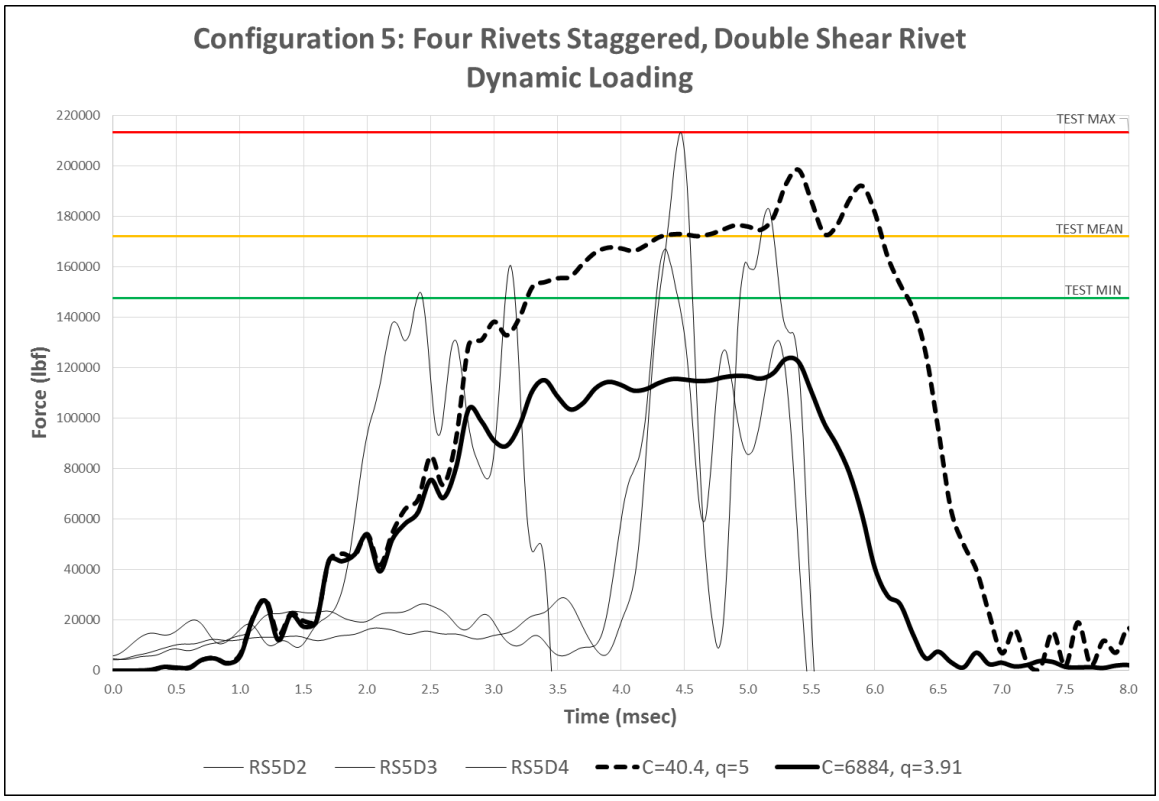


Fig. B-10: Bounding Results, Configuration 5, Double Shear, Dynamic

# Appendix C: Dynamic Simulations with Recommended Cowper Symonds Coefficients versus Experimental Results

Appendix C provides the load versus time output from five riveted connection configurations in single- and double-shear (10 total figures) under dynamic loading. Solid, bolt lines represent predicted rivet behavior from LS-DYNA (2013) using the University of Liverpool recommended parameters ($C$ = 802 $s^{-1}$ and $q$ = 3.585). Light (unbold) lines represent experimental test data (Rabalais, 2015). In addition, there are red, yellow, and green lines on each plot that indicate the experimental maximum load, mean load, and minimum load, respectively. Above each load versus time plot is a LS-DYNA (2013) illustration of the applicable figure. Details regarding the development of these plots and an analysis of their significance are found in Section 4.3.

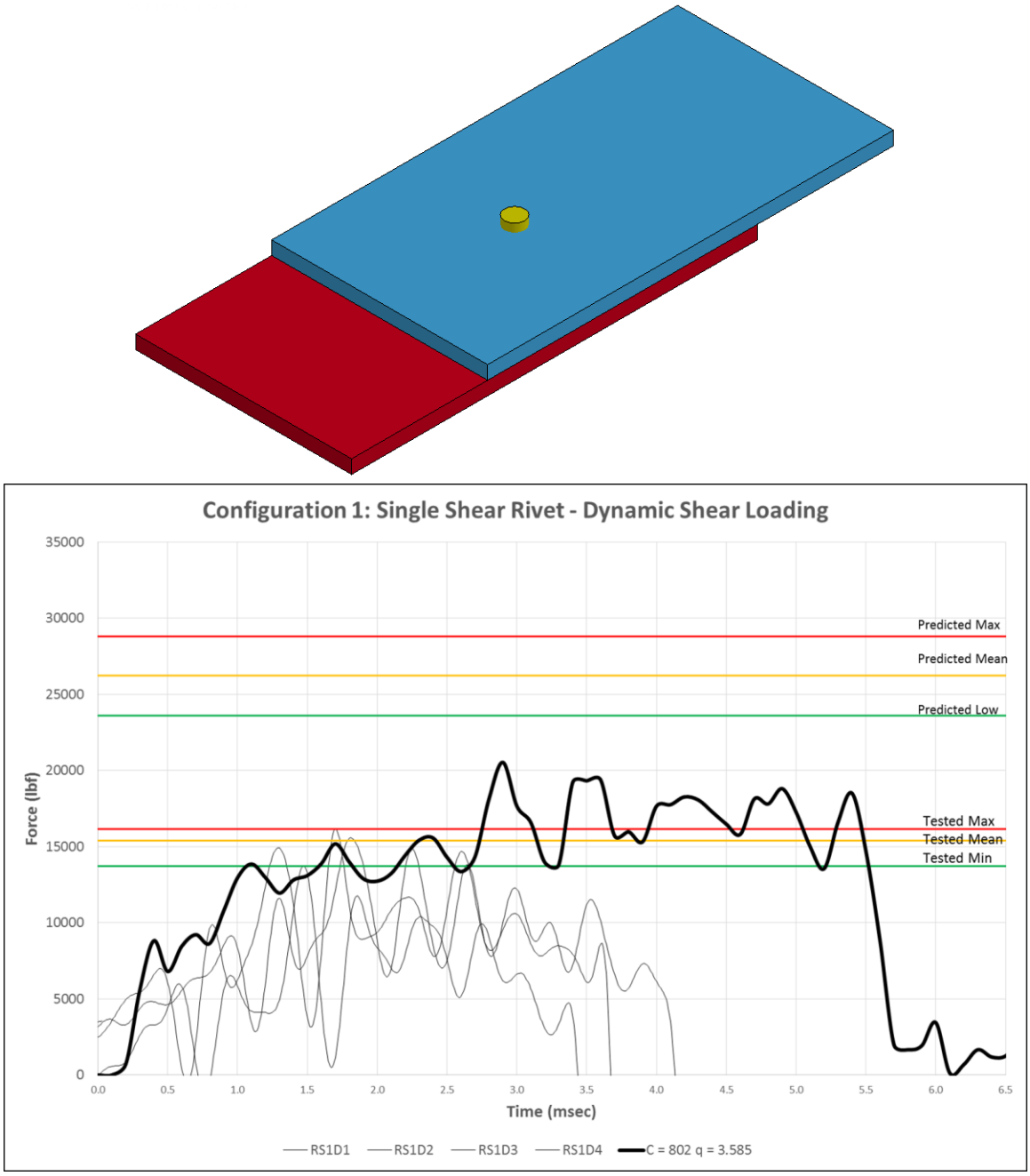


Fig. C-1: Configuration 1, Single Shear, Dynamic with Recommended CS Parameters

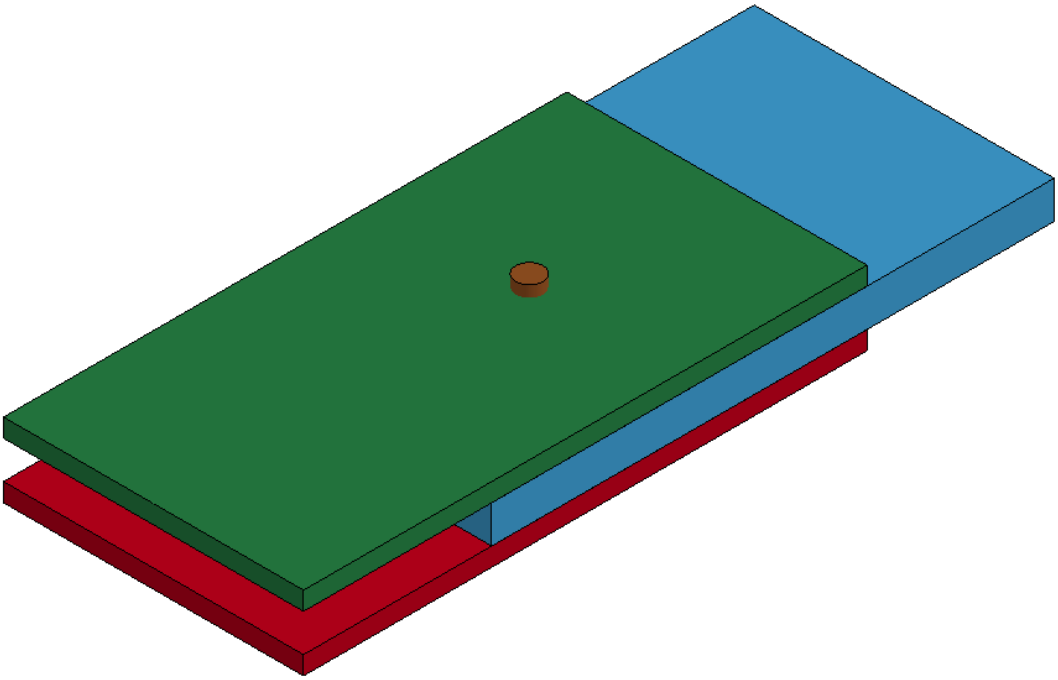

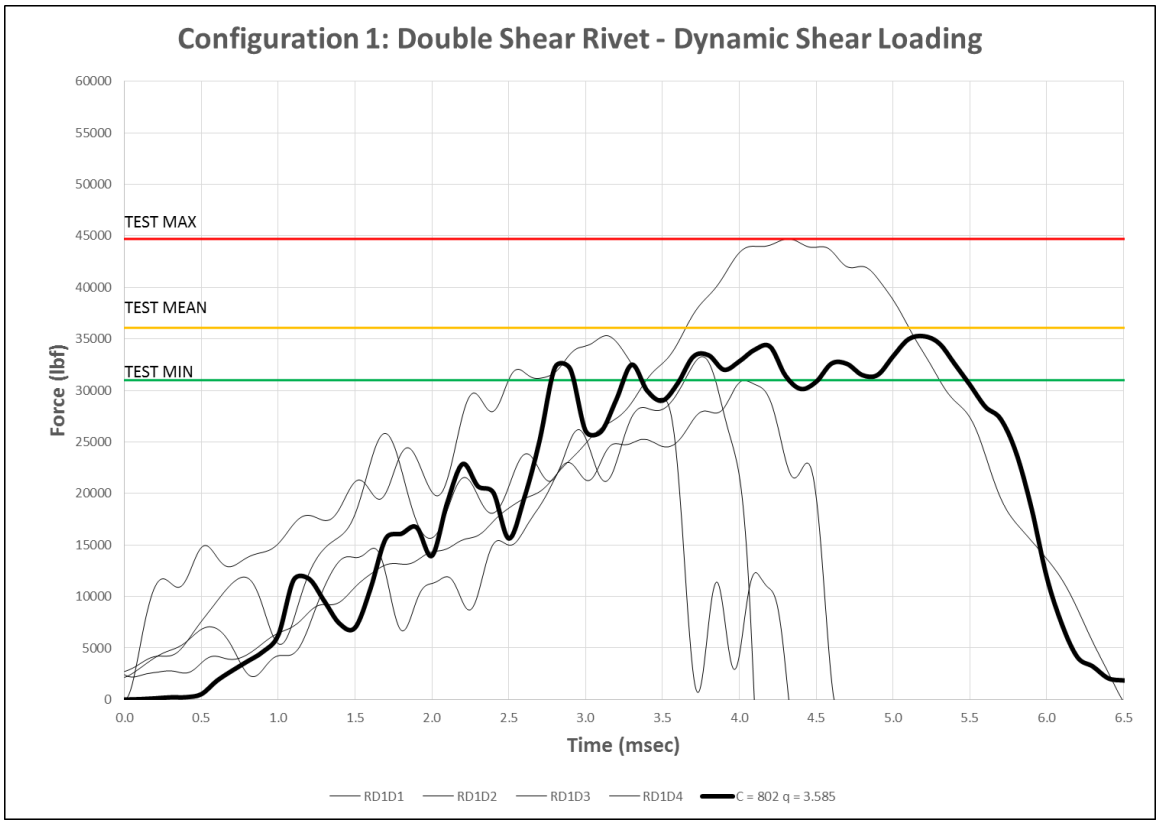


Fig. C-2: Configuration 1, Double Shear, Dynamic with Recommended CS Parameters

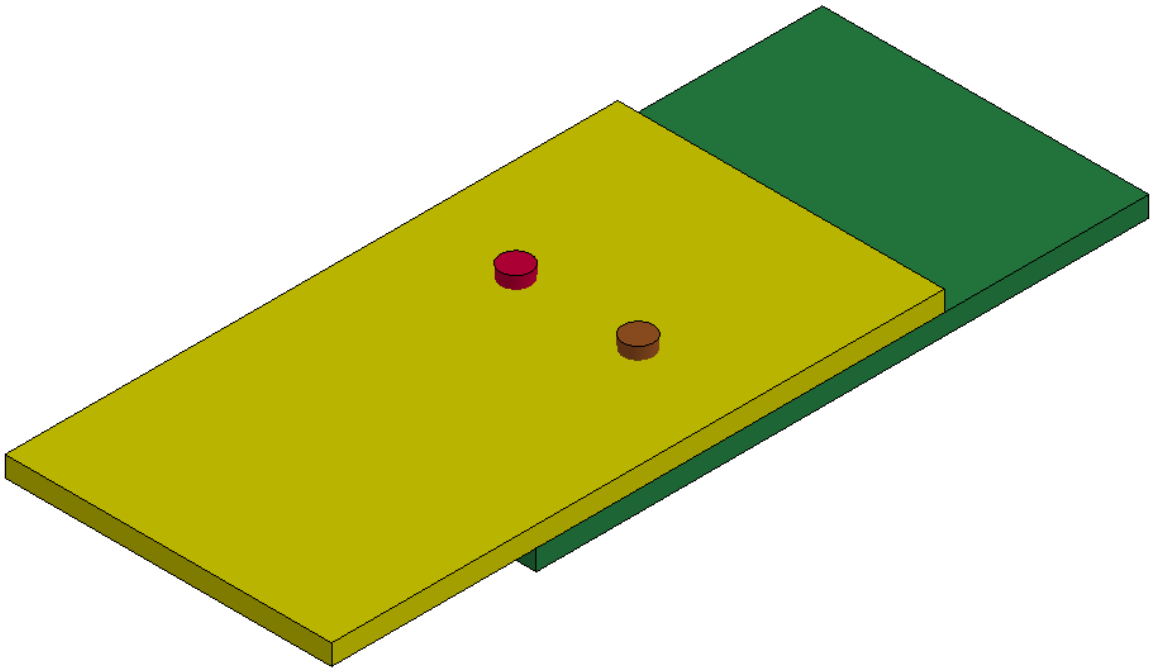

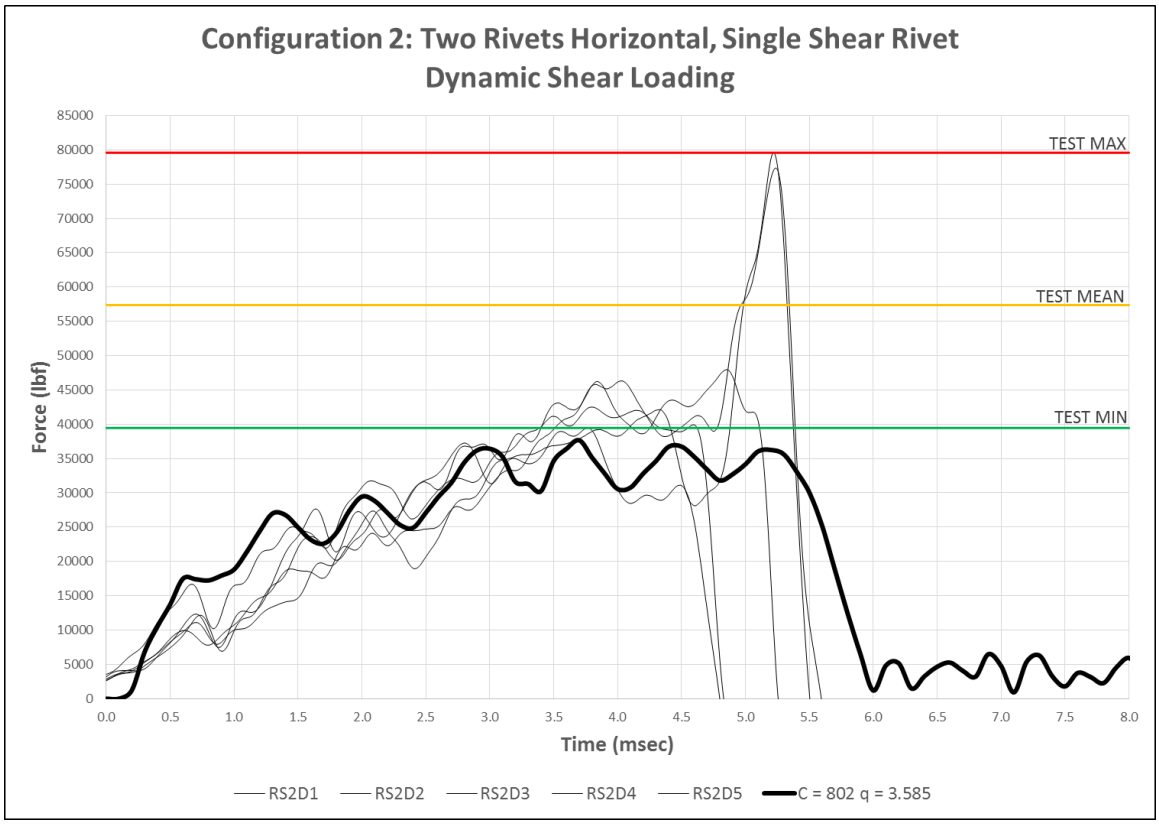


Fig. C-3: Configuration 2, Single Shear, Dynamic with Recommended CS Parameters

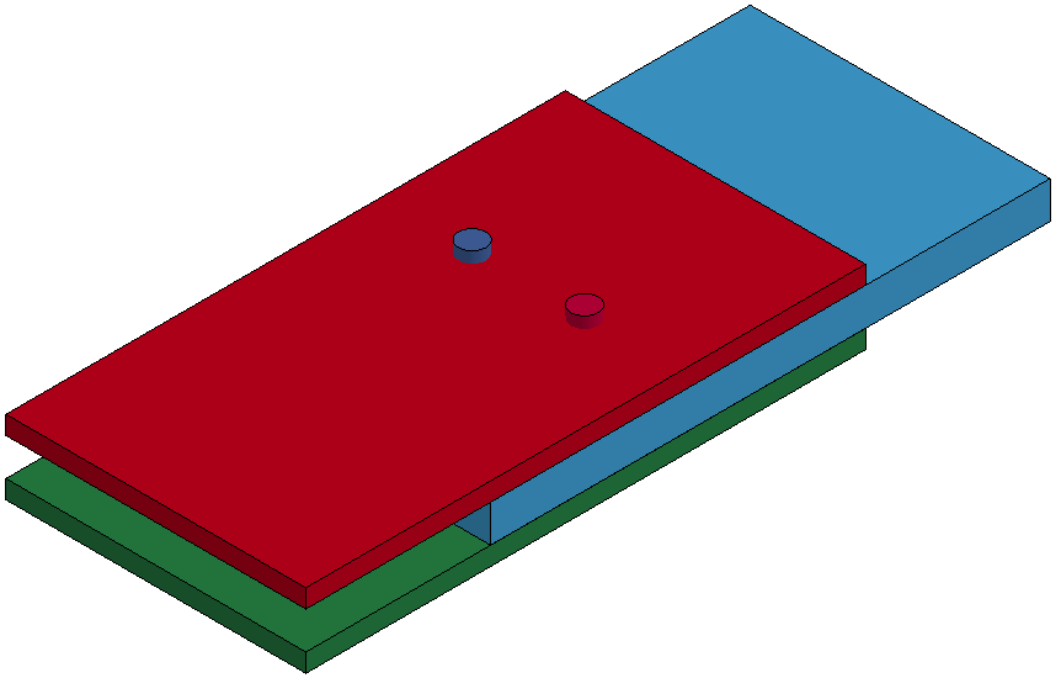

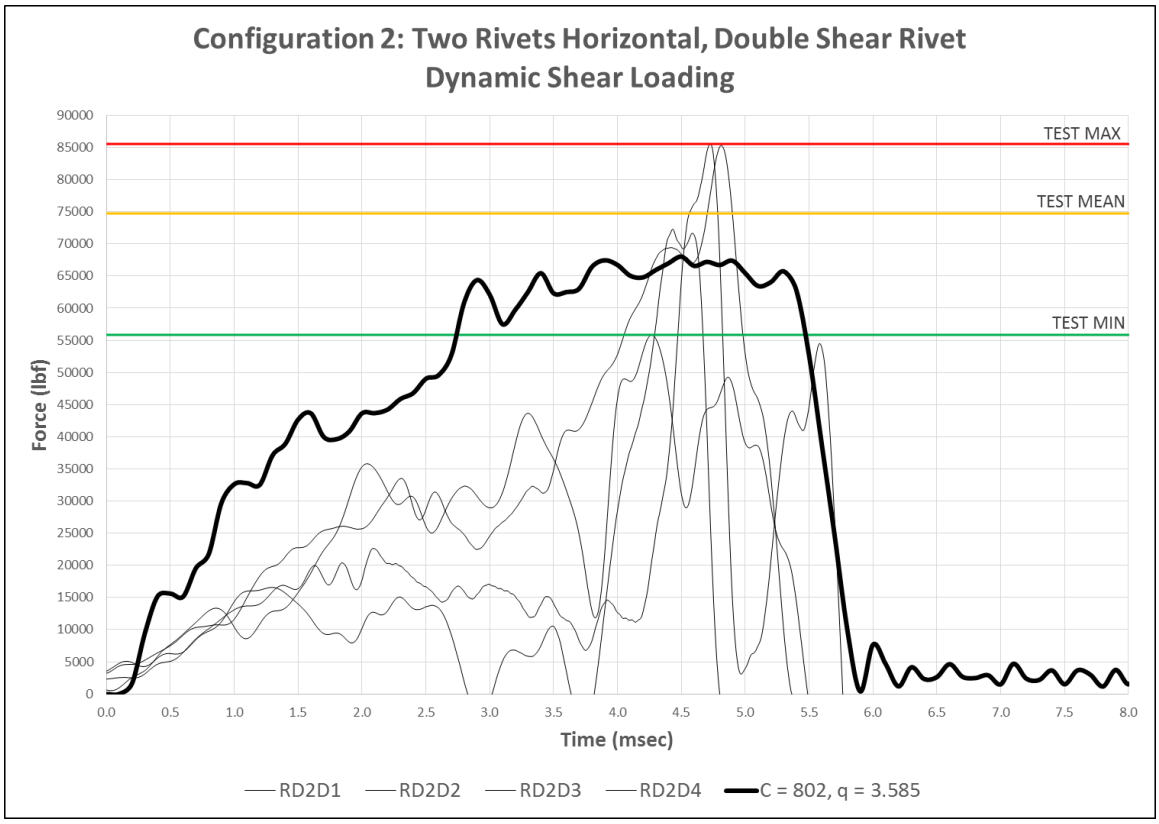


Fig. C-4: Configuration 2, Double Shear, Dynamic with Recommended CS Parameters

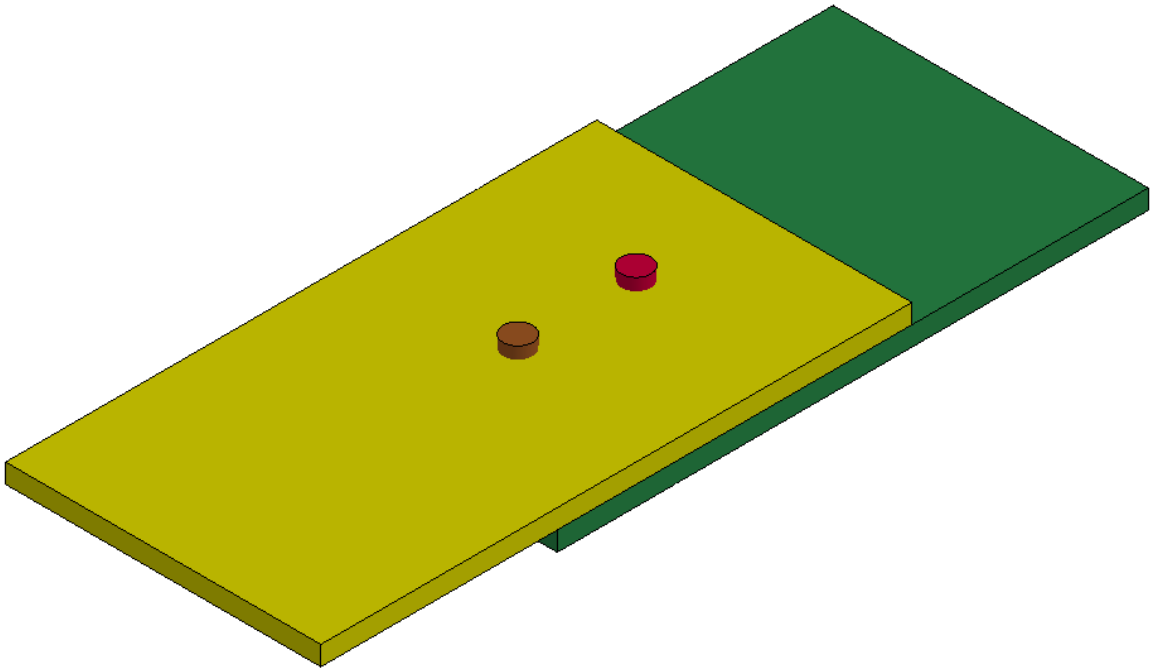

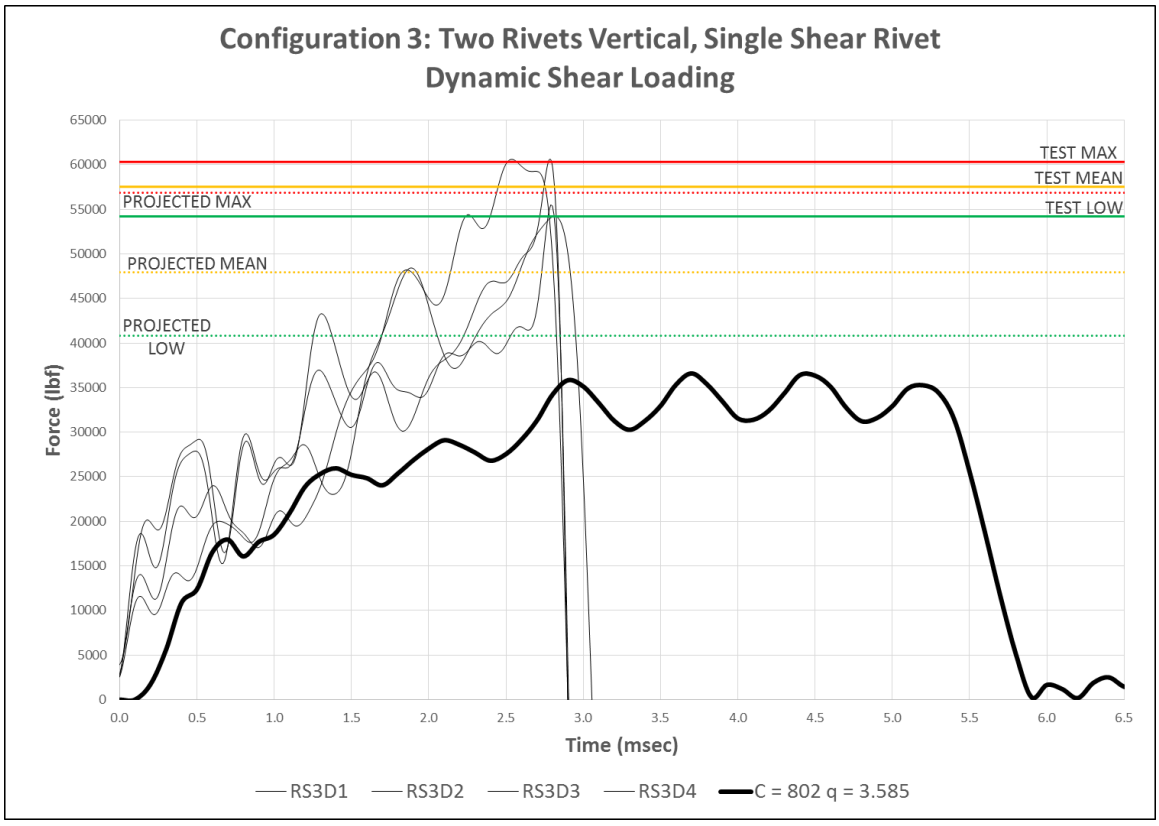


Fig. C-5: Configuration 3, Single Shear, Dynamic with Recommended CS Parameters

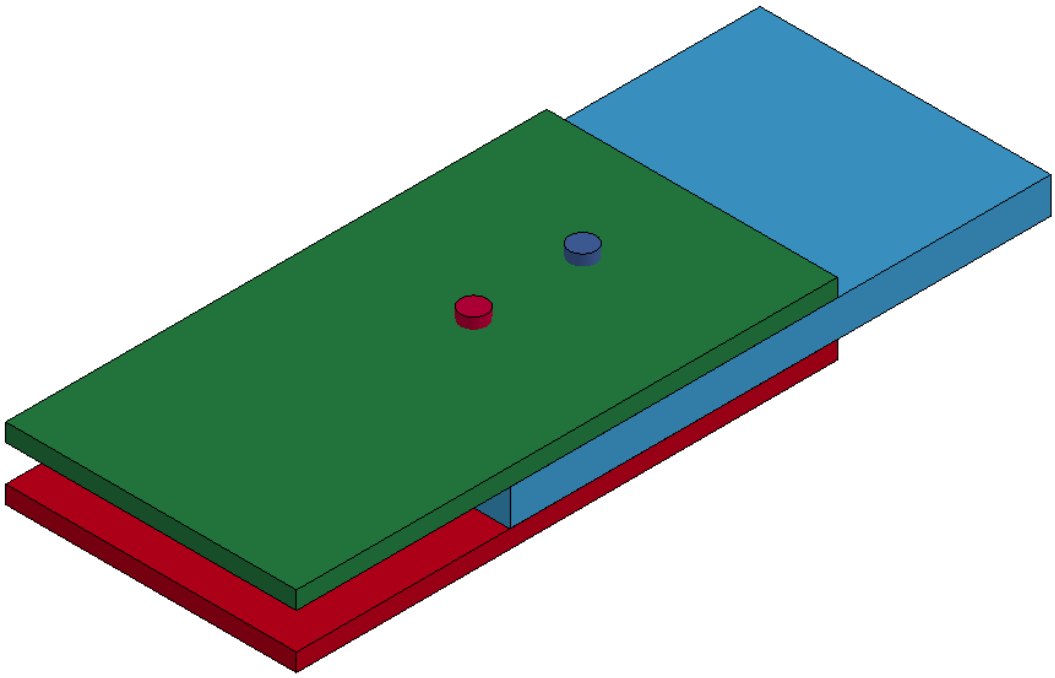

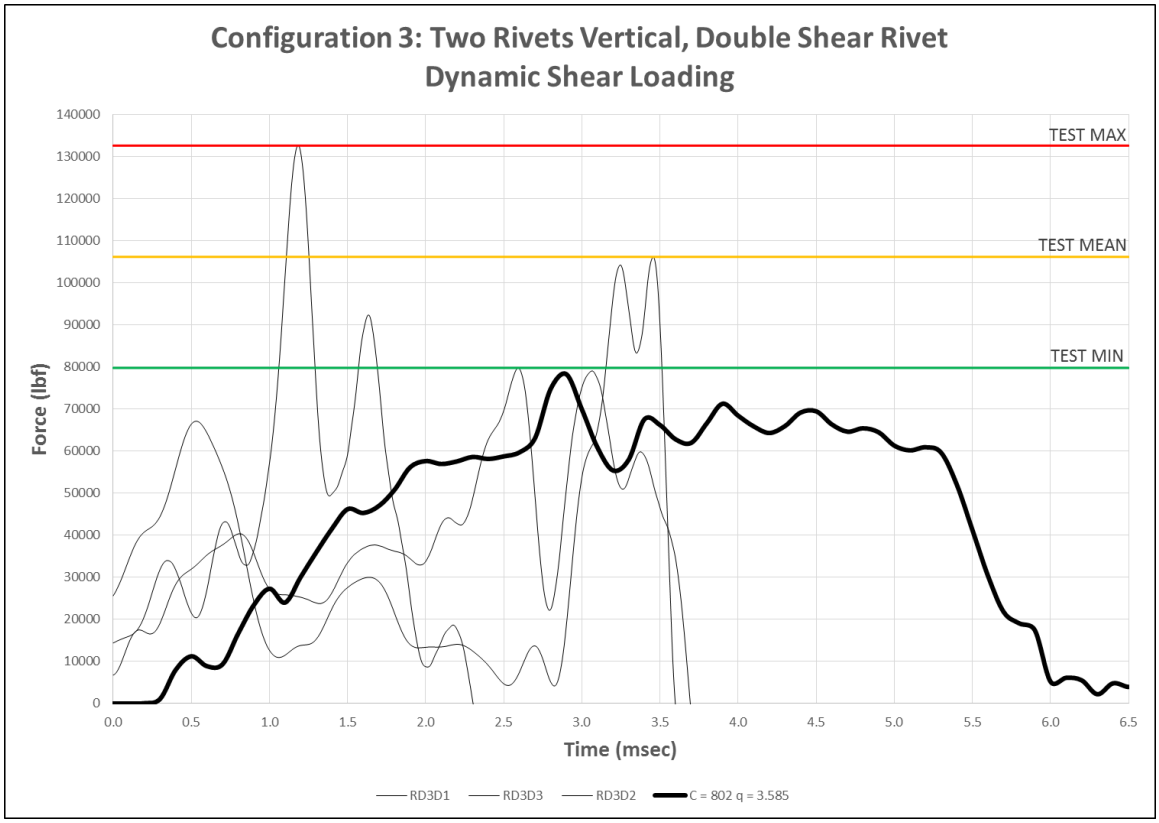


Fig. C-6: Configuration 3, Double Shear, Dynamic with Recommended CS Parameters

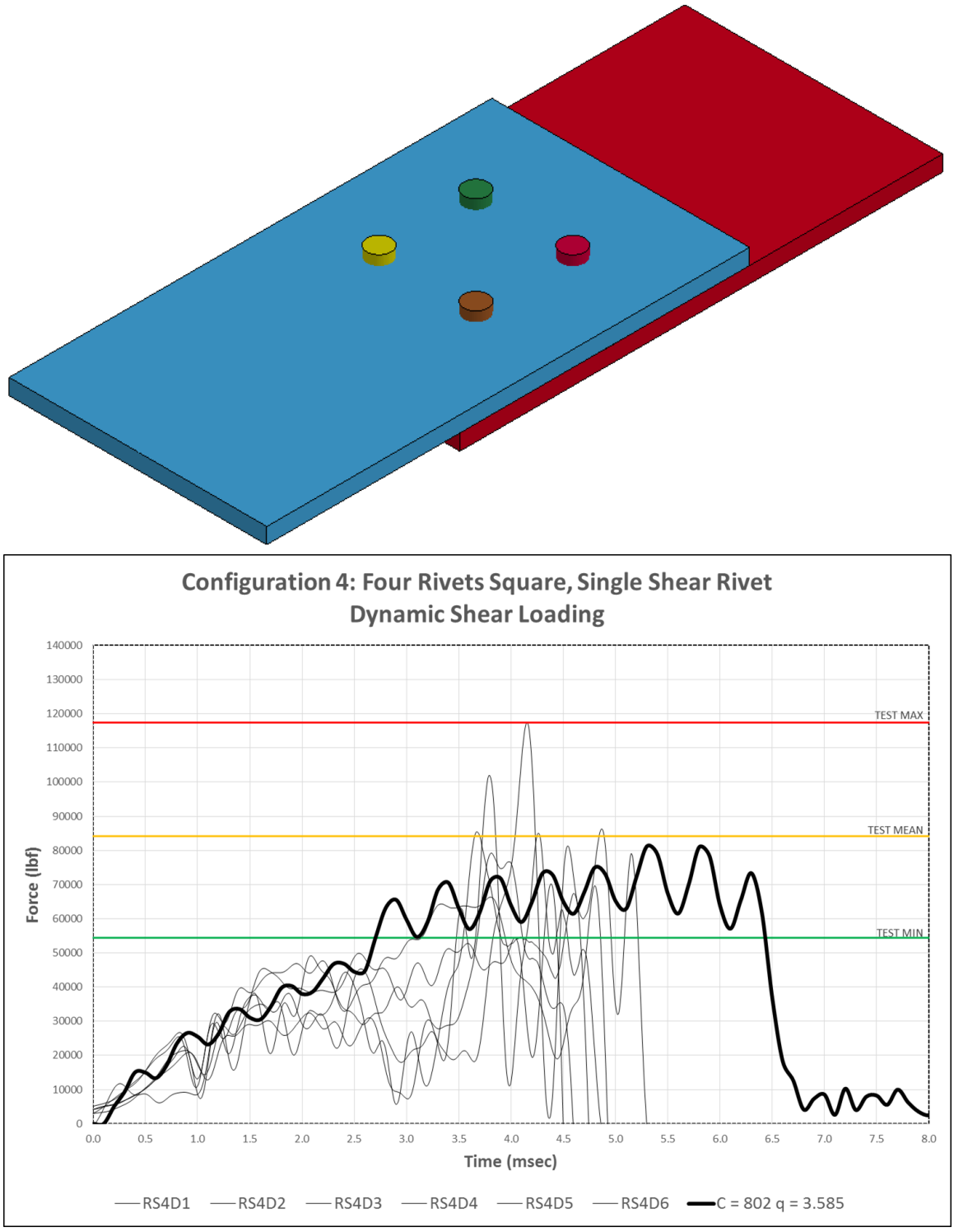


Fig. C-7: Configuration 4, Single Shear, Dynamic with Recommended CS Parameters

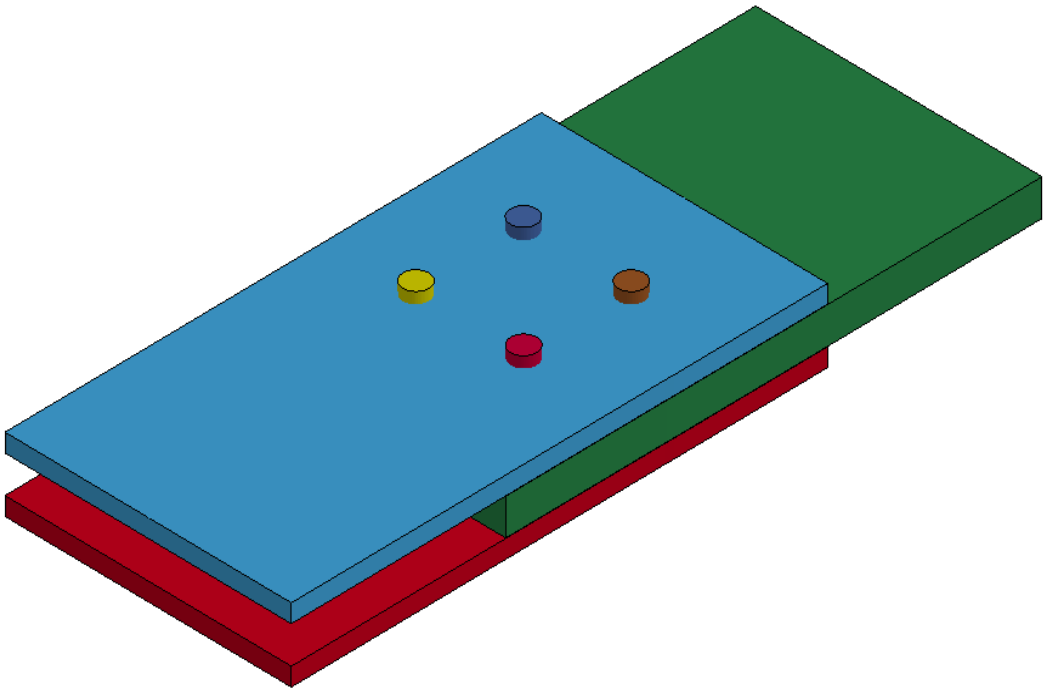

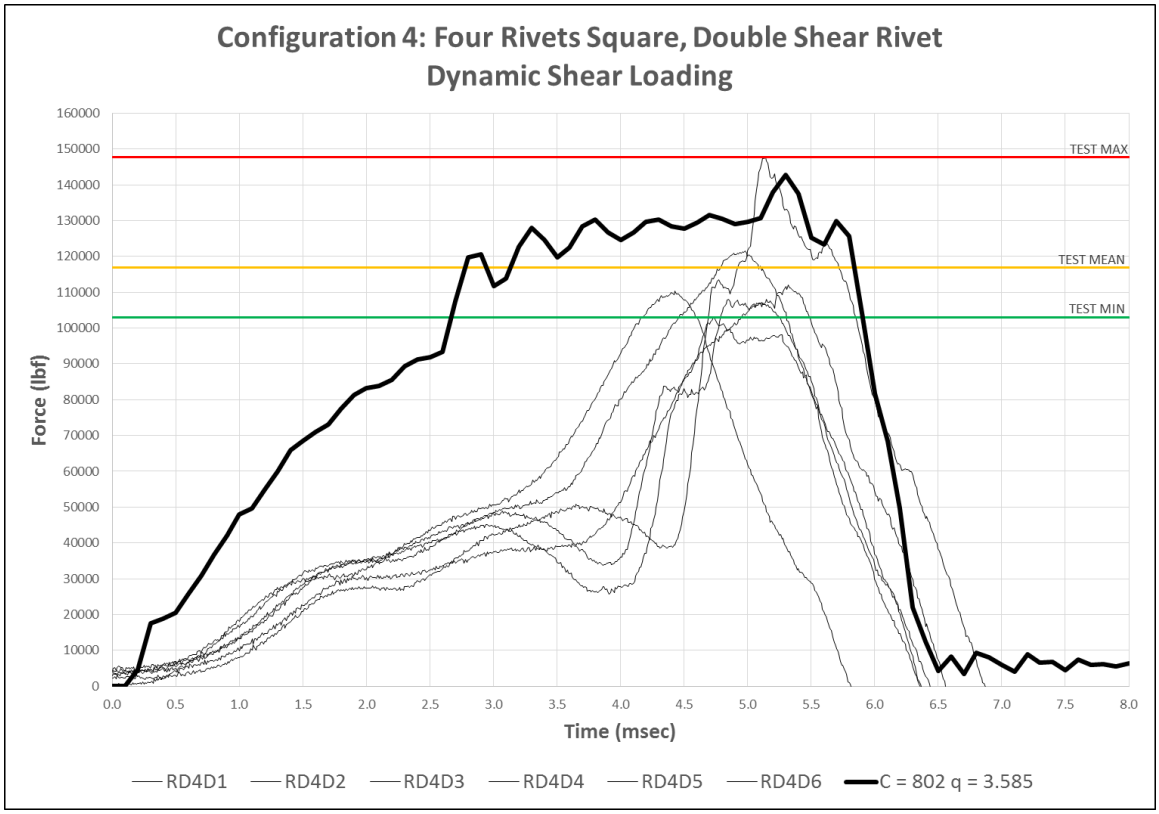


Fig. C-8: Configuration 4, Double Shear, Dynamic with Recommended CS Parameters

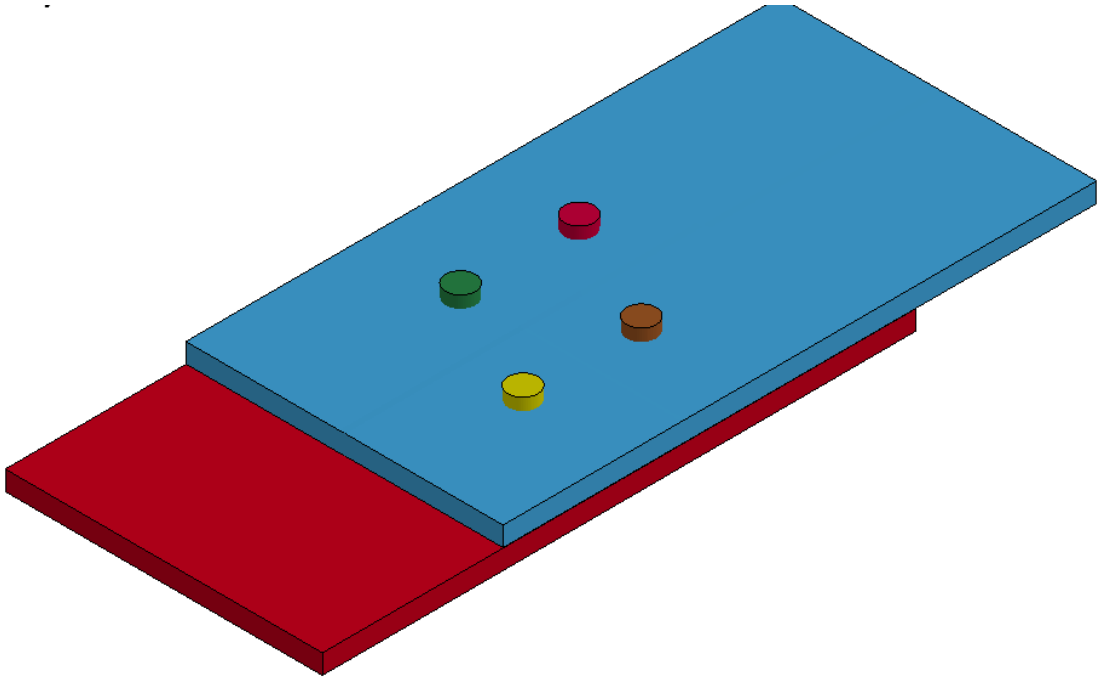

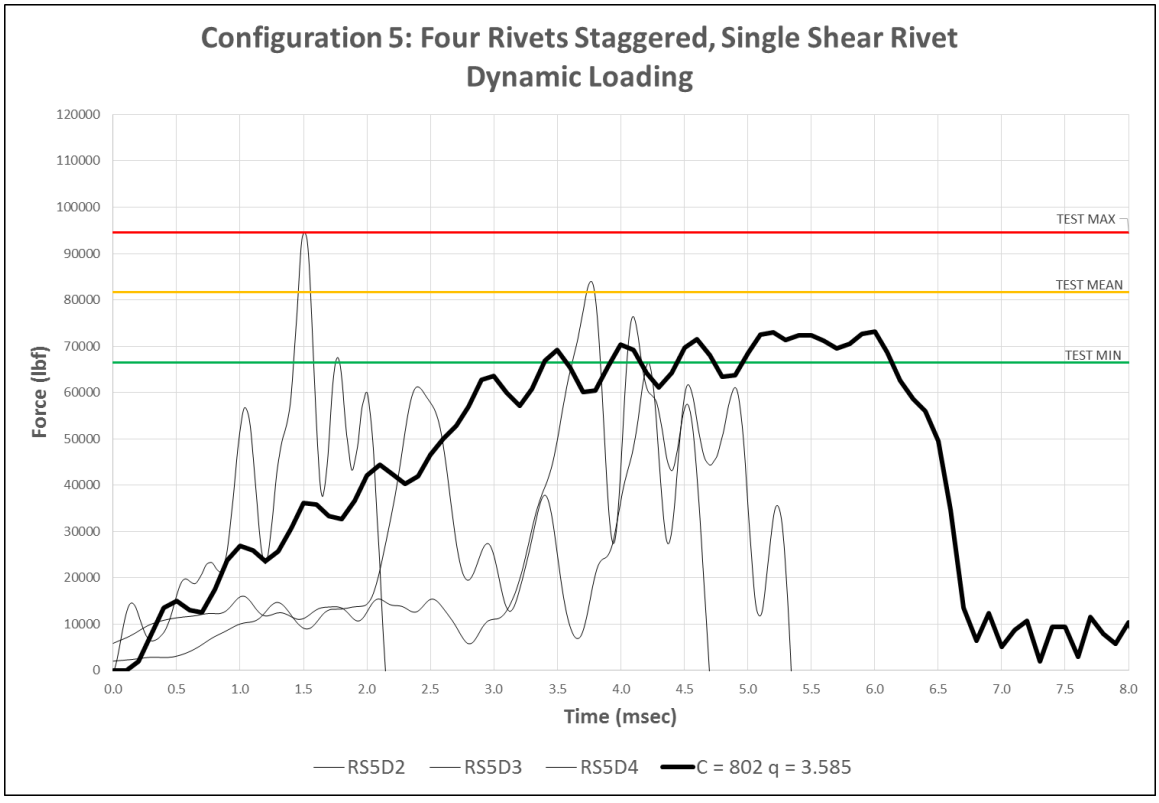


Fig. C-9: Configuration 5, Single Shear, Dynamic with Recommended CS Parameters

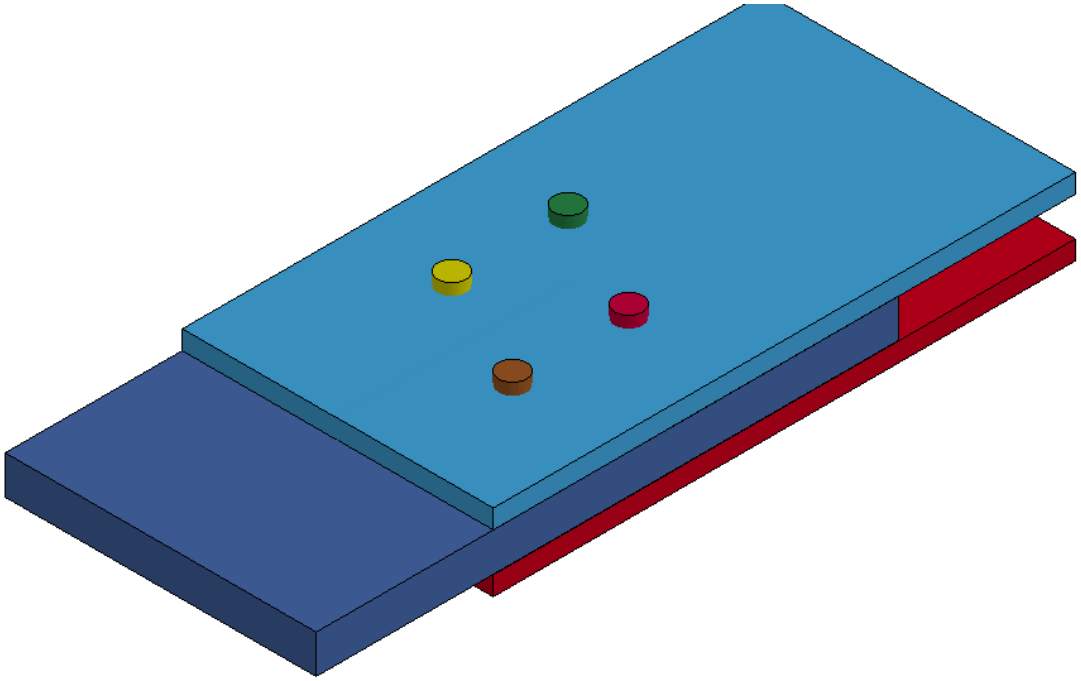

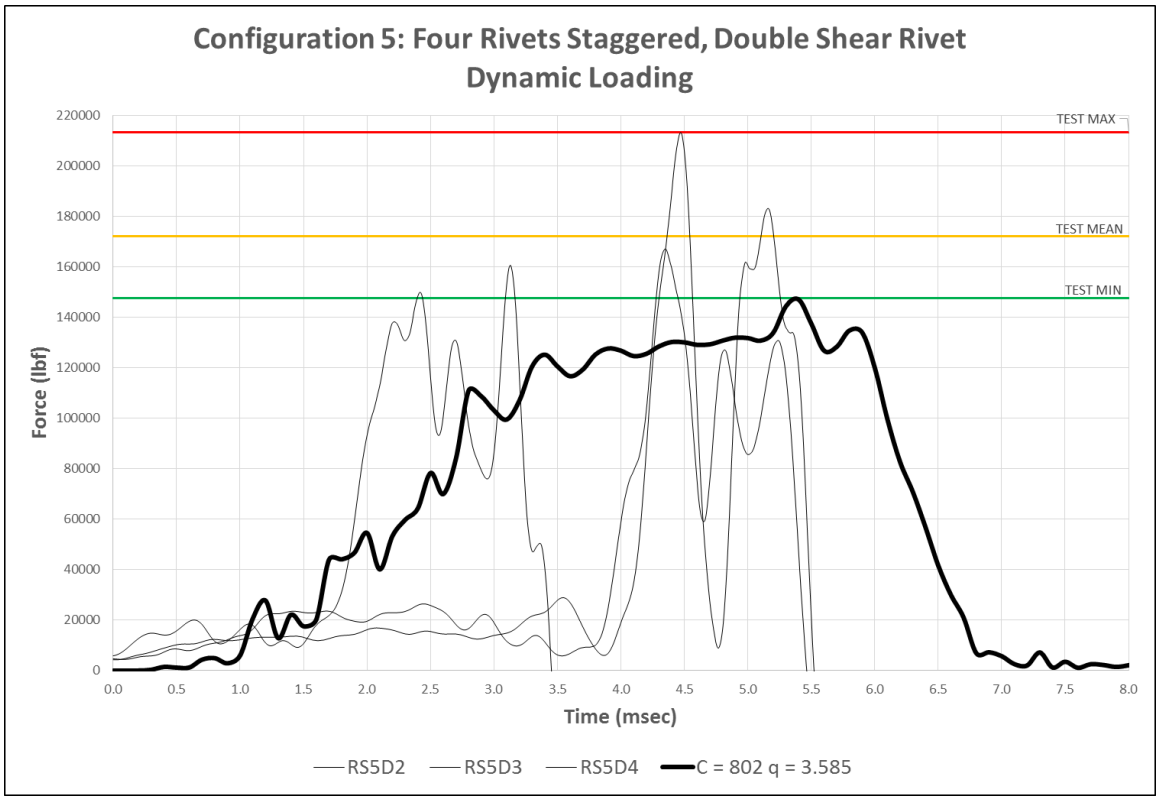


Fig. C-10: Configuration 5, Double Shear, Dynamic with Recommended CS Parameters

# References


Livermore Software Technology Corporation. LS-DYNA. Computer software. Version Smp S R7.0.0. 2013.

AutoCAD Civil 3D. Computer software. Version G.55.0.1. 2013.

Livermore Software Technology Corporation. LS-Prepost. Computer software. Version 4.1. 2014.

*2011 Interim Revisions to the Manual for Bridge Evaluation, Second Edition, 2010*.

*A Manual for the Prediction of Blast and Fragment Loadings on Structures*. Amarillo, TX: U.S. Dept. of Energy, 1980.

*AASHTO LRFD Bridge Design Specifications (5th Edition)*. 2010.

*ASCE* | 2013 Report Card for America's Infrastructure. ASCE | 2013 Report Card for America's Infrastructure. Accessed July 14, 2015. http://www.infrastructurereportcard.org/a/#e/welcome.

*ASTM A307 - 14 Standard Specification for Carbon Steel Bolts, Studs, and Threaded Rod 60000 PSI Tensile Strength*. Accessed January 5, 2015. http://www.astm.org/Standards/A307.htm.

*ASTM A307-83a, Carbon Steel Externally Threaded Standard Fasteners*. Philadelphia, PA, 1983.

*ASTM A325-84, High-Strength Bolts for Structural Steel Joints*. Philadelphia, PA, 1985.

*ASTM A36/A36M-14, Standard Specification for Carbon Structural Steel*. West Conshohocken, PA: ASTM International, 2014.

*ASTM A490-84, Heat-Treated Steel Structural Bolts, 150 Ksi Minimum Tensile Strength*. Philadelphia, PA, 1985.

*ASTM A502 - 03 Standard Specification for Rivets, Steel, Structural*. Accessed January 5, 2015. http://www.astm.org/DATABASE.CART/HISTORICAL/A502-03.htm.

*ASTM A992/A992M-11, Standard Specification for Carbon Structural Steel Shapes*. West Conshohocken, PA: ASTM International, 2011.

*ASTM E8 / E8M - 15a Standard Test Methods for Tension Testing of Metallic Materials*. Accessed March 20, 2016. http://www.astm.org/Standards/E8.htm.

Abramowicz, W., and N. Jones. "Dynamic Progressive Buckling of Circular and Square Tubes." *International Journal of Impact Engineering* 4, no. 4 (1986): 243-70.

Allison, Paul. "Fractured Samples." E-mail message to author. May 26, 2015.

Baier, Bret. "Intel Chief Says 2014 Deadliest Year for Terror Ever Recorded, in Counter to Upbeat Kerry | Fox News." Fox News. February 26, 2015. Accessed March 10, 2015. http://www.foxnews.com/politics/2015/02/26/top-intel-official-2014-deadliest-year-for-terror-ever-recorded.html.

Batho, Cyril. "The Partition of the Load in Riveted Joints." *Journal of the Franklin Institute* 182, no. 5 (1916): 553-604.

Belytschko, Ted, and Lee P. Bindeman. "Assumed Strain Stabilization of the Eight Node Hexahedral Element." *Computer Methods in Applied Mechanics and Engineering* 105, no. 2 (1993): 225-60.

Bendigo, R. A., and R. M. Hansen. "Long Bolted Joints." *Journal of the Structural*

*Division, ASCE* 89, no. ST6 (December 1963): 187.

Bendigo, R. A., R. M. Hansen, and J. L. Rumpf. "Long Bolted Joints." *Journal of the Structural Division, ASCE* 89, no. ST6 (1963).

Benson, Pam. "New Terrorist Plot to Attack Plane Foiled." CNN. May 7, 2012. Accessed June 19, 2015. http://www.cnn.com/2012/05/07/world/meast/yemen-qaeda-plot/.

Boyd, A., and J. P. Sullivan. "Emergency Preparedness for Transit Terrorism (TR News Version)." Emergency Preparedness for Transit Terrorism (TR News Version). May 2008. Accessed June 19, 2015. https://www.academia.edu/4192503/Emergency_Preparedness_for_Transit_Terrorism_TR_News_Version_.

Broad, William J. "In Weak Rivets, a Possible Key to Titanic's Doom." The New York Times. April 14, 2008. Accessed May 25, 2015. http://www.nytimes.com/2008/04/15/science/15titanic.html?_r=0.

Campbell, J. D., and W. G. Ferguson. "The Temperature and Strain-rate Dependence of the Shear Strength of Mild Steel." *Philosophical Magazine* 21, no. 169 (1970): 63-82.

Collette, Q., I. Wouters, and L. Lauriks. "Evolution of Historical Riveted Connections: Joining Typologies, Installation Techniques and Calculation Methods." *WIT Transactions on The Built Environment*, 2011, 295-306.

Collette, Q., I. Wouters, and L. Lauriks. "Evolution of Historical Riveted Connections: Joining Typologies, Installation Techniques and Calculation Methods." *WIT*

*Transactions on The Built Environment*, 2011. www.witpress.com, ISSN 1743-3509.

Conrath, Edward J. *Structural Design for Physical Security: State of the Practice*. Reston, VA: SEI, 1999.

Cowper, G. R., and P. S. Symonds. *Strain-hardening and Strain-rate Effects in the Impact Loading of Cantilever Beams*. Report no. 28. Brown University: Division of Applied Mathematics, 1957.

Crane, C. Kennan, Christopher P. Rabalais, and Vincent P. Chiarito. *Blast Loading of Steel Bridge Towers Constructed with New and Vintage Materials*. Report. Vicksburg: U.S. Army Research and Development Center, 2015.

Davis, R. E., G. B. Woodruff, and H. E. Davis. "Tension Tests of Large Riveted Joints." *Transactions of ASCE* 105 (1940): 1193.

Dlugosz, Stanley E. *Static Tension Tests of Long Riveted Joints*. Master's thesis, Lehigh University, 1962.

Dusenberry, Donald O. *Handbook for Blast-resistant Design of Buildings*. Hoboken, NJ: J. Wiley, 2010.

D'Aniello, M., F. Portioli, L. Fiorino, and R. Landolfo. "Experimental Investigation on Shear Behaviour of Riveted Connections in Steel Structures." *Engineering Structures* 33, no. 2 (February 2011): 516-31.

Edwards, Julia, and Mark Hosenball. "FBI Says It Thwarted Islamic State-inspired July 4 Attacks." FBI Says It Thwarted Islamic State-inspired July 4 Attacks. July 9,

2015. Accessed July 10, 2015. http://www.msn.com/en-us/news/us/fbi-says-it-thwarted-islamic-state-inspired-july-4-attacks/ar-AAcLwOv.

Engelhardt, Michael D. "Course Notes from CE382L: Plastic Design of Metals." Lecture, Department of Civil, Architectural, and Environmental Engineering, Austin, TX, 2015.

Erhart, Tobias. "Review of Solid Element Formulations in LS-DYNA." —. October 12, 2011. Accessed October 5, 2013. http://www.dynamore.de/de/download/papers/forum11/entwicklerforum-2011/erhart.pdf.

Eversley, Melanie. "Vulnerable NYC Bridges Make Tempting Terror Targets." USA Today. September 08, 2014. Accessed July 16, 2015. http://www.usatoday.com/story/news/nation/2014/09/07/nyc-bridges-security-terrorism/14801559/.

The Blue Ribbon Panel on Bridge and Tunnel Security. "Recommendations for Bridge and Tunnel Security." FHWA. September 2003. http://www.fhwa.dot.gov/bridge/security/brp.pdf.

Fisher, John, Geoffrey Kulak, and Lynn Beedle. "The Behavior of Large Bolted Joints." *Fritz Engineering Laboratory Report* 288.31A (1965).

Fisher, John W., and John H. A. Struik. *Guide to Design Criteria for Bolted and Riveted Joints*. New York: Wiley, 1974.

Foecke, Tim. *Metallurgy of the RMS Titanic*. Gaithersburg, MD: U.S. Dept. of

Commerce, Technology Administration, National Institute of Standards and Technology, Materials Science and Engineering Laboratory, 1998.

Forsberg, Jimmy. "Short Introduction to LS-DYNA and LS-PrePost." DYNAMORE Nordic. September 9, 2013. Accessed November 5, 2014. http://www.solidmechanics.iei.liu.se/Examiners/Courses/Master_Level/TMHL19/intro_lsdyna_lsprepost.pdf.

Friedman, Donald. *Historical Building Construction: Design, Materials and Technology*. New York: Norton, 2010.

*Fundamentals of Protective Design for Conventional Weapons (TM 5-855-1).* Washington, D.C.: Headquarters, Dept. of the Army, 1986.

Gardner, L., and D. A. Nethercot. *Designers' Guide to Eurocode 3: Design of Steel Buildings EN 1993-1-1, -1-3 and -1-8*. London: ICE, 2011.

"Information on More than 140,000 Terrorist Attacks." Global Terrorism Database. Accessed July 14, 2015. http://www.start.umd.edu/gtd/.

Hagmann, Douglas, and Judi McCleod. "A Detailed Overview of the 2006 New York Tunnel Bombing Plot." A Detailed Overview of the 2006 New York Tunnel Bombing Plot. July 11, 2006. Accessed July 16, 2015. http://canadafreepress.com/2006/hagmann071106.htm.

Hallquist, John O. *LS-DYNA Theory Manual*. Livermore: Livermore Software Technology Corporation, 2006.

Hayashi, T., and Y. Tanaka. "Impact Engineering." *Nikkan Kogyo Simunsha (Daily*

*Engineering Newspaper Company)*, 1988.

Higgins, T. R., and E. J. Ruble. "Structural Uses of High-Strength Bolts." *Transactions* 120:1389-398, 1955.

Higgins, T. R., and W. H. Munse. "How Much Combined Stress Can a Rivet Take?" *Structural Research Series 45, University of Illinois*, 1952.

Holth, Nathan. "Historic Bridges .org." Historic Bridges .org. Accessed March 17, 2016. http://historicbridges.org/.

Hooper, J. J., T. Foecke, L. Graham, and T. P. Weihs. "The Metallurgical Analysis of Wrought Iron from the RMS Titanic." *Measurement Science and Technology Meas. Sci. Technol.* 14, no. 9 (2003): 1556-563.

Hryciów, Zdzisław, Wacław Borkowski, Piotr Rybak, and Józef Wysocki. "Influence Of The Shape Of The Explosive Charge On Blast Profile." *Journal of KONES. Powertrain and Transport* 21, no. 4 (2014): 169-76.

"Chemical Explosions." HySafe Wiki. Accessed October 5, 2015. http://www.hysafe.net/wiki/BRHS/ChemicalExplosions.

"Induction Heating Equipment, Systems and Services for Industrial Applications - EFD Induction." Induction Heating Equipment, Systems and Services for Industrial Applications - EFD Induction. Accessed July 23, 2015. http://www.efd-induction.com/.

Inserra, David. "Terrorist Plot 72: Congress Needs to Address Rising Islamist Terrorism at Home." The Heritage Foundation. July 22, 2015. Accessed August 5, 2015.

http://www.heritage.org/research/reports/2015/07/terrorist-plot-72-congress-needs-to-address-rising-islamist-terrorism-at-home.

Jama, H.h., G.n. Nurick, M.r. Bambach, R.h. Grzebieta, and X.l. Zhao. "Steel Square Hollow Sections Subjected to Transverse Blast Loads." *Thin-Walled Structures* 53 (2012): 109-22.

Jenkins, Brian Michael. "Long-Term Trends in Attacks on Public Surface Transportation in Europe and North America." Mineta Transportation Institute. January 25, 2016. Accessed February 1, 2016. http://transweb.sjsu.edu/.

Jewish Virtual Library. Accessed May 1, 2015. https://www.jewishvirtuallibrary.org/.

Johnson, F. R., and W. H. Cook. "A Constitutive Model and Data for Metals Subjected to Large Strains, High Strain Rates and High Temperatures." *Proceedings of the 7th International Symposium on Ballistics, The Hague, The Netherlands*, April 1983.

Johnson, Gordon R., and William H. Cook. "Fracture Characteristics of Three Metals Subjected to Various Strains, Strain Rates, Temperatures and Pressures." *Engineering Fracture Mechanics* 21, no. 1 (1985): 31-48.

Jonge, A. E. Richard De. *Riveted Joints; a Critical Review of the Literature Covering Their Development*. New York: Published by the American Society of Mechanical Engineers, 1945.

Kane, Will, Ellen Huet, and Kevin Fagan. "Golden Gate Bridge Climber in Custody." SFGate. August 4, 2012. Accessed June 17, 2015. http://www.sfgate.com/bayarea/article/Golden-Gate-bridge-climber-in-custody-

3760235.php.

Kaplan, S. "Double Shear Tests of High Strength Bolts." *Fritz Laboratory Reports*, 1959.

Krauthammer, Theodor. *Modern Protective Structures*. Boca Raton, FL: CRC Press, 2008.

Kulak, Geoffrey L., John W. Fisher, John H. A. Struik, and John W. Fisher. *Guide to Design Criteria for Bolted and Riveted Joints*. New York: Wiley, 1987.

"Hourglass." LS-DYNA Examples. Accessed November 3, 2014. http://www.dynaexamples.com/process_simulation/hourglass.

"Contact Modeling in LS-DYNA." LS-DYNA Support. Accessed October 3, 2014. http://www.dynasupport.com/tutorial/ls-dyna-users-guide/contact-modeling-in-ls-dyna.

Lindeburg, Michael R. *Civil Engineering Reference Manual for the PE Exam*. Belmont, CA: Professional Publications, 2003.

Livermore Software Technology Corporation (LSTC). 2012. Accessed December 10, 2014. http://ftp.lstc.com/anonymous/outgoing/jday/hourglass.pdf.

Lobo, Hubert. "Methodology for Selection of Material Models for Plastics Impact Simulation." Methodology for Selection of Material Models for Plastics Impact Simulation. Accessed March 20, 2016. http://www.datapointlabs.com/testpaks/LS-Dyna07/LS-Dyna07_paper.htm.

"Mackinac.com Home." Mackinac.com. Accessed February 1, 2016. http://www.mackinac.com/.

Manzarpour, Mohammad. "Canada Foils 'al-Qaeda Linked' Terror Attack on Train - BBC News." BBC News. April 23, 2013. Accessed March 7, 2016. http://www.bbc.com/news/world-us-canada-22258191.

Marais, S. T., R. B. Tait, and T. J. Cloete. "Material Testing at High Strain Rate Using the Split Hopkinson Pressure Bar." *Latin American Journal of Solids and Structures* 1 (2004): 319-39.

McCarty, J.J. Hooper, and T. Foecke. "Microscopic Analysis of Metal Recovered from the Wreck of RMS Titanic." *Microscopy Today* 15, no. 2 (March 2007): 6.

Mehta, Aaron. "Odierno: ISIS Fight Will Last '10 To 20 Years'" Defense News. July 17, 2015. Accessed August 17, 2015. http://www.defensenews.com/story/defense/2015/07/17/odierno-isis-fight-last-10-20-years/30295949/.

Metal Industry Product Profile. Accessed August 1, 2015. http://metalpass.com.

Muhlhausen, David, and Jena Baker McNeill. "Terror Trends: 40 Years' Data on International and Domestic Terrorism." The Heritage Foundation. May 20, 2011. Accessed May 1, 2015. http://www.heritage.org/research/reports/2011/05/terror-trends-40-years-data-on-international-and-domestic-terrorism.

Muir, Larry, and Cynthia J. Duncan. "The AISC 2010 Specification and the 14th Edition Steel Construction Manual." *Structures Congress 2011*, 2011.

Mulcahy, Marty. "The Building Tradesman Newspaper." Mackinac Bridge Workers Recall the Highs and the Lows... and Tell Tall Tales. October 26, 2007. Accessed

February 1, 2016. http://www.michiganbuildingtrades.org/newspaper/mackinac-bridge-workers-recall-the-highs-and-the-lows-and-tell-tall-tales.

Mulrine, Anna. "US Is No Safer after 13 Years of War, a Top Pentagon Official Says." The Christian Science Monitor. July 28, 2014. Accessed July 29, 2014. http://www.csmonitor.com/USA/Military/2014/0728/US-is-no-safer-after-13-years-of-war-a-top-Pentagon-official-says.

Munse, W. H., D. T. Wright, and N. M. Newmark. "Laboratory Tests of Bolted Joints." *Transactions* 120:1299-318, 1952.

Munse, W. E., and E. L. Cox. "The Static Strength of Rivets Subjected to Combined Tension and Shear." *Bulletin No. 437. Engineering Experiment Station, University of Illinois*, 1956. https://www.ideals.illinois.edu/bitstream/handle/2142/4323/engineeringexperv00000i00437.pdf?sequence=3.

Ocel, Justin. *Guidelines for the Load and Resistance Factor Design and Rating of Riveted and Bolted Gusset-Plate Connections for Steel Bridge*. PDF. McLean: NCHRP, February 2013.

Olson, Aaron W. *Triage Evaluation of Gusset Plates in Steel Truss Bridges*. Master's thesis, University of Washington, 2010.

Paik, J. K., and J. Y. Chung. "A Basic Study on Static and Dynamic Crushing Behavior of a Stiffened Tube." *KSAE Transactions* 7, no. 1 (1999): 219-38.

"Canada Terrorist Attack Tactics Against Bridges and Tunnels: January 2002 –

December 2008 | Public Intelligence." Public Intelligence. June 17, 2009. Accessed June 1, 2015. https://publicintelligence.net/terrorist-attack-methodology-and-tactics-against-bridges-and-tunnels-january-2002-–-december-2008/.

Select Committee on Intelligence United States Senate. "Publications." Publications. Accessed October 19, 2015. http://www.intelligence.senate.gov/publications/report-attempted-terrorist-attack-northwest-airlines-flight-253-may-24-2010.

"RAND Database of Worldwide Terrorism Incidents." RDWTI. Accessed May 19, 2015. http://www.rand.org/nsrd/projects/terrorism-incidents.html.

"REL Inc." REL Inc. Accessed December 15, 2015. http://www.relinc.net/.

Rabalais, Christopher. "Analysis of Bolt and Rivet Structural Fasteners Subjected to Dynamic and Quasi-Static Shear Loadings." *Master's thesis. Texas A&M University*, 2015.

Rabalais, Christopher. "Question." E-mail message to author. November 10, 2015.

Ray, James C. "Risk-Based Prioritization of Terrorist Threat Mitigation Measures on Bridges." *J. Bridge Eng. Journal of Bridge Engineering* 12, no. 2 (2007): 140-46.

Ray, James, R. E. Walker, J. T. Baylot, and C. Charman. "Validation of Numerical Modeling and Analysis of Steel Bridge Towers Subjected to Blast Loadings." *US Army ERDC Report 5. Vicksburg, MS*, 2012.

"Rivets & Fasteners." Rivets. Accessed August 31, 2015.

http://www.valleyfastener.com/.

Schwer, Len. "Optional Strain-Rate Forms for the Johnson Cook Constitutive Model and the Role of the Parameter Epsilon_0 1." *6th European LS-DYNA Users' Conference*. Accessed August 1, 2015. http://www.dynalook.com/european-conf-2007/optional-strain-rate-forms-for-the-johnson-cook.pdf.

Scott, Eugene. "FBI Director: U.S. at Greatest Threat from Terrorist Groups since 9/11." CNN. December 9, 2015. Accessed March 21, 2016. http://www.cnn.com/2015/12/09/politics/terrorist-threats-fbi-director-9-11/.

*Seismic Provisions for Structural Steel Buildings*. Chicago, IL: American Institute of Steel Construction, 2010.

"Sixth Street Bridge." Sixth Street Bridge. Accessed May 24, 2015. http://www.brooklineconnection.com/history/Facts/SixthStreetBridge.html.

*Specifications for Assembly of Structural Joints Using High Strength Steel Bolts*. New York: Institute, 1954.

Starr, Kevin. *Golden Gate: The Life and times of America's Greatest Bridge*. New York: Bloomsbury Press, 2010.

Steinman, D. B., and John T. Nevill. *Miracle Bridge at Mackinac*. Grand Rapids: Eerdmans, 1957.

Sterling, G. H., and J. W. Fisher. "A440 Steel Joints Connected by A490 Bolts." *Proceedings of ASCE*, 304th ser., 92, no. ST3 (1966).

"Teaching Aids for Structural Steel Design Courses." Teaching Aids for Structural Steel

Design Courses. Accessed May 5, 2015. https://www.aisc.org/content.aspx?id=24858.

"39 Terror Plots Foiled Since 9/11: Examining Counterterrorism's Success Stories." The Heritage Foundation. May 20, 2011. Accessed July 28, 2014. http://www.heritage.org/research/reports/2011/05/39-terror-plots-foiled-since-911-examining-counterterrorisms-success-stories.

"Anti-Terrorist Security Network Almost Done on Bay Area Bridges and Tunnels." *The San Jose Mercury News*, March 25, 2003.

*The Manual for Bridge Evaluation: 2011 Interim Revisions*. Washington, DC: American Association of State Highway and Transportation Officials, 2011.

"National Consortium for the Study of Terrorism and Responses to Terrorism: Annex of Statistical Information." U.S. Department of State. 2013. Accessed July 10, 2015. http://www.state.gov/j/ct/rls/crt/2012/210017.htm.

"National Consortium for the Study of Terrorism and Responses to Terrorism: Annex of Statistical Information." U.S. Department of State. 2014. Accessed July 10, 2015. http://www.state.gov/j/ct/rls/crt/2014/239416.htm.

*UFC 3-340-02 Structures to Resist the Effects of Accidental Explosions*. Washington, D.C.: Depts. of the Army, the Navy, and the Air Force, 2008.

"Varmint Al's Engineering Page - Finite Element Analysis of Structures." Varmint Al's Engineering Page - Finite Element Analysis of Structures. Accessed March 1, 2016. http://www.varmintal.com/aengr.htm.

Vermes, William. "'Design and Performance of Riveted Bridge Connections." *ISPC Conference Newsletter*, October 24, 2007. Accessed January 01, 2015. http://www.dot.state.oh.us/engineering/OTEC/2007 Presentations/Wednesday Sessions/Session 58 - 2-15 pm C111 - C112/Performance of Rivets - OTEC W Vermes.pdf.

Volz, Dustin. "FBI Director Warns Lawmakers ISIS Is Using Encryption To Order Killings." Defense One. July 8, 2015. Accessed June 2, 2015. http://www.defenseone.com/technology/2015/07/fbi-director-warns-lawmakers-isis-using-encryption-order-killings/117247/.

Walker, R. E., J. C. Ray, L. A. Walker, and J. K. Minor. "Validation of Numerical Modeling and Analysis of Steel Bridge Towers Subjected to Blast Loadings: Series 1 Report." *ERDC/GSL Technical Report 11-11*, 2011a.

Walker, R. E., J. C. Ray, L. A. Walker, and J. K. Minor. "Validation of Numerical Modeling and Analysis of Steel Bridge Towers Subjected to Blast Loadings: Series 2 Report." *ERDC/GSL Technical Report 11-11*, 2011b.

Walker, R. E., J. C. Ray, L. A. Walker, and J. K. Minor. "Validation of Numerical Modeling and Analysis of Steel Bridge Towers Subjected to Blast Loadings: Series 3 Report." *ERDC/GSL Technical Report 11-11*, 2011c.

Walker, R. E., J. C. Ray, L. A. Walker, and J. K. Minor. "Validation of Numerical Modeling and Analysis of Steel Bridge Towers Subjected to Blast Loadings: Series 4 Report." *ERDC/GSL Technical Report 11-11*, 2011d.

Wallaert, James J., and John W. Fisher. "Shear Strength of High-Strength Bolts." *Fritz Laboratory Reports* 1822 (1962). http://preserve.lehigh.edu/engr-civil-environmental-fritz-lab-reports/1822.

Walters, Riley. "The 75th Terrorist Plot on the United States." The Heritage Foundation. December 08, 2015. Accessed January 19, 2016. http://www.heritage.org/research/reports/2015/12/the-75th-terrorist-plot-on-the-united-states.

Wang, Bo-Shiuan. *Analytical Study of Gusset Plate Joints in Steel Truss Bridges and Development of Assessment Procedures*. PhD diss., University of Washington, 2013.

Weiser, Benjamin, and Al Baker. "A Bridge Under Scrutiny, by Plotters and the Police." The New York Times. 2011. Accessed August 17, 2015. http://www.nytimes.com/2011/04/27/nyregion/brooklyn-bridge-was-terror-plot-target-documents-reveal.html?_r=0.

West, Harry. "The Ups and Downs of Suspension Bridges and the Highs and Lows Of Their Builders." Lecture, AISC Webinar, August 17, 2015.

Williamson, Eric B. *Blast-resistant Highway Bridges: Design and Detailing Guidelines*. Washington, D.C.: Transportation Research Board, 2010.

Williamson, Eric B. "Course Notes from CE 397: Blast-Resistant Structural Design." Lecture, Department of Civil, Architectural, and Environmental Engineering, Austin, TX, 2014.

Wilson, W. M., and W. A. Oliver. "Tension Tests of Rivets." *Bulletin No. 210, University of Illinois Engineering Experiment Station*, 1930.

Wilson, W. M., and F. P. Thomas. "Fatigue Tests on Riveted Joints." *Bulletin No. 302, University of Illinois Engineering Experiment Station*, 1938.

Winget, D. G., and E. B. Williamson. "Design of Critical Bridges for Security Against Terrorist Attacks." *TXDOT Project No. 0-4569, Phase 1 Report, University of Texas at Austin*, 2003.

Young, C. R., and W. B. Dunbar. "Permissible Stresses on Rivets in Tension." *Bulletin No. 8, University of Toronto Faculty of Applied Science and Engineering*, 1928.

Zee, John Van Der. *The Gate: The True Story of the Design and Construction of the Golden Gate Bridge*. New York: Simon and Schuster, 1986.

Zennie, Michael. "Al Qaeda Terror Plot Foiled after Canadian Police Arrest Two over Plan to Blow up Train to New York as It Crossed Niagara Falls." Mail Online. April 22, 2013. Accessed March 7, 2016. http://www.dailymail.co.uk/news/article-2313125/Canada-terror-plot-Authorities-thwart-al-Qaeda-backed-attack-trains-Toronto.html.

# VITA

Aaron T. Hill, Jr. grew up as part of an Army family with his parents, Aaron and Tina Hill, and his brother and sister, Ahmond and Alisha. After graduating from Bethel High School in 1993, he attended the United States Military Academy at West Point, NY, and received a Bachelor's of Science in Civil Engineering in 1997. To date, he has served worldwide as an Engineer officer in the United States Army for almost 19 years to include assignments in Bosnia, Croatia, the Sinai Peninsula, and Afghanistan. While serving in the Army, Aaron earned Master's of Science degrees from the University of Missouri-Rolla in Engineering Management (2001) and from Virginia Tech in Civil Engineering (2006). While serving as a faculty member at the United States Military Academy from 2006-2009, Aaron earned the academic rank of Assistant Professor and received the ASCE 2009 ExCEEd New Faculty Excellence in Teaching Award. In 2013, Aaron was recognized as a Via Department of Civil and Environmental Engineering Virginia Tech Outstanding Young Alumni. As part of his selection to return to the United States Military Academy as an Academy Professor, Aaron started his Ph.D. at The University of Texas at Austin in 2013. His Ph.D. was completed in 2016. Aaron is a Professional Engineer (Virginia) and a Project Management Professional. Aaron is married to Diana Lynn Hill and is blessed with three children: Aaron III, Alyssa, and Amaya.

Permanent e-mail: aaron_dianahill@hotmail.com

This dissertation was typed by the author.